PB92-192988

REPORT NO.
UCB/EERC-90/03
OCTOBER 1990

EARTHQUAKE ENGINEERING RESEARCH CENTER

EARTHQUAKE SIMULATOR TESTING AND ANALYTICAL STUDIES OF TWO ENERGY-ABSORBING SYSTEMS FOR MULTISTORY STRUCTURES

by

IAN D. AIKEN
JAMES M. KELLY

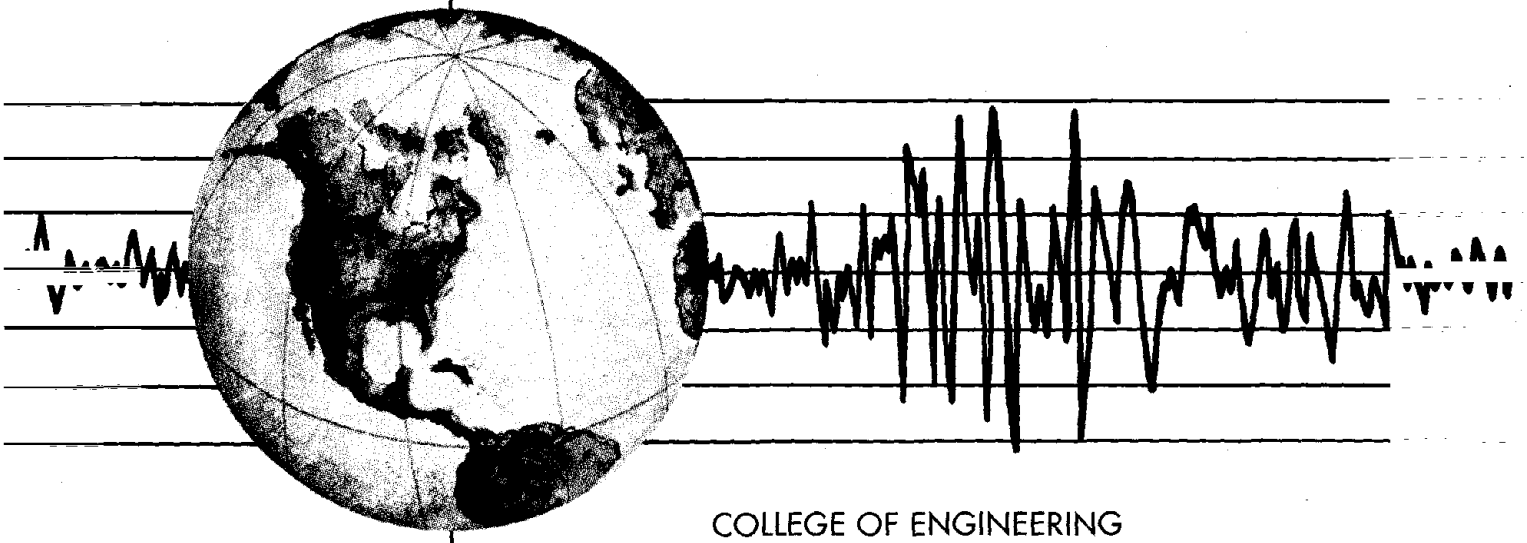

COLLEGE OF ENGINEERING

UNIVERSITY OF CALIFORNIA AT BERKELEY

For sale by the National Technical Information Service, U.S. Department of Commerce, Springfield, Virginia 22161

See back of report for up to date listing of EERC reports.

DISCLAIMER

5027-10

REPORT DOCUMENTATION PAGE	1. REPORT NO. NSF/ENG-90003	2.	3. PB92-192988

4. Title and Subtitle
Earthquake Simulator Testing and Analytical Studies of Two Energy-Absorbing Systems for Multistory Structures

5. Report Date
October 1990

6.

7. Author(s)
Ian D. Aiken and James M. Kelly

8. Performing Organization Rept. No.
UCB/EERC-90/03

9. Performing Organization Name and Address
Earthquake Engineering Research Center
University of California, Berkeley
1301 So. 46th Street
Richmond, Calif. 94804

10. Project/Task/Work Unit No.

11. Contract(C) or Grant(G) No.
(C)* Award no. 86-3025
(G)

12. Sponsoring Organization Name and Address
National Science Foundation
*Subcontract through NCEER-SUNY
1800 G Street
Washington, D.C. 20550

3M Company
3M Center
St. Paul, MN
55144

Sumitomo Metal Indus.
Osaka Steel Works
1-109, 5-chome,
Shimaya, Konohana-ku
Osaka, 554 Japan

13. Type of Report & Period Covered

14.

15. Supplementary Notes

16. Abstract (Limit: 200 words)

This study used two different types of energy-absorbing devices to improve the seismic behavior of a large-scale, multistory steel frame building: a viscoelastic shear damper designed using an energy approach, and a friction device with almost perfectly rectangular hysteresis behavior for which an iterative nonlinear analysis design method was adopted. A 9-story, moment-resisting steel frame representing the basic structure of the study was tested with both types of energy absorbers installed and also in moment-resisting and concentrically-braced configurations. The large number of tests permitted numerous comparisons of the four structural systems. The damped structures were found to have base shears similar to the moment-resisting frame while reducing drifts to the level of those of the concentrically-braced frame. Analytical methods suitable for predicting the response of the two damped structures were studied. A linear analysis incorporating damping on a modal basis produced very good results for the viscoelastically-damped system. Furthermore, the use of linear elastic response spectra with high damping gave good results for story shears and displacements. A nonlinear analysis of the friction-damped structure was necessary to predict the response accurately.

17. Document Analysis a. Descriptors

b. Identifiers/Open-Ended Terms

c. COSATI Field/Group

18. Availability Statement:	19. Security Class (This Report)	21. No. of Pages
Release Unlimited	unclassified	293
	20. Security Class (This Page) unclassified	22. Price

EARTHQUAKE SIMULATOR TESTING AND ANALYTICAL STUDIES OF TWO ENERGY-ABSORBING SYSTEMS FOR MULTISTORY STRUCTURES

by

Ian D. Aiken

and

James M. Kelly

Report No. UCB/EERC-90/03
Earthquake Engineering Research Center
College of Engineering
University of California at Berkeley

October 1990

ABSTRACT

This combined experimental and analytical study focusses on the use of two different types of energy-absorbing devices to improve the seismic behavior of a large-scale, multistory steel frame building. The energy-absorbing devices studied are a viscoelastic shear damper designed using an energy approach, and a friction device with almost perfectly rectangular hysteretic behavior for which an iterative nonlinear analysis design method was adopted.

Extensive earthquake simulator testing of both systems was carried out. A nine-story, moment-resisting steel frame represented the basic structure of the study. The structure was tested with both types of energy absorbers installed and also in moment-resisting and concentrically-braced configurations. The large number of tests performed permitted numerous different comparisons of the four structural systems. The damped structures were found to have base shears similar to the moment-resisting frame while reducing drifts to the level of those of the concentrically-braced frame.

Analytical methods suitable for predicting the response of the two damped structures were studied. It was found that a linear analysis incorporating damping on a modal basis produced very good results for the viscoelastically-damped system. Furthermore, the use of linear elastic response spectra with high values of damping gave good results for story shears and displacements. A nonlinear analysis of the friction-damped structure was necessary to predict the response accurately. A previously developed and extensively used nonlinear time-history analysis program was used and the friction devices modeled using existing elements. The analyses produced good results.

ACKNOWLEDGEMENTS

The research reported herein was supported by the National Science Foundation and was conducted at the Earthquake Simulator Laboratory of the Earthquake Engineering Research Center of the University of California at Berkeley. The dampers used in the experimental program were supplied by 3M Company and Sumitomo Metal Industries Ltd., Japan. Financial assistance was also provided by Sumitomo.

The authors would like to express their thanks to Messrs. D. Clyde, W. Neighbour, I. Van Asten, and J. McNab of the Earthquake Simulator Laboratory for their assistance during the experimental phase of the project. Thanks also are due to Dr. Beverley Bolt for her assistance in the editing and preparation of this report.

Table of Contents

List of Tables

List of Figures

CHAPTER 1

INTRODUCTION

Conventional seismic design practice permits the reduction of forces for design below the elastic level on the premise that inelastic action in a suitably designed structure will provide that structure with significant energy dissipation potential and enable it to survive a severe earthquake without collapse. This inelastic action is typically intended to occur in especially detailed critical regions of the structure, usually in the beams near or adjacent to the beam-column joints. Inelastic behavior in these regions, while able to dissipate substantial energy, also results in often significant damage to the structural member, and although the regions may be well detailed, their hysteretic behavior will degrade with repeated inelastic cycling. The interstory drifts required to achieve significant hysteretic energy dissipation in critical regions are large and would usually result in substantial damage to non-structural elements such as in-fill walls, partitions, doorways, and ceilings.

1.1 Innovative Approaches to Seismic Design

As a response to the shortcomings inherent in the philosophy of conventional seismic design a number of innovative approaches have been developed. Some of these approaches are discussed in the following sections, with brief mention made of existing structural applications (if they exist) and current research activity. An overview of the field of innovative seismic design is presented in Fig. 1.1. The notation that has been adopted in this research and a brief discussion of the terminology used throughout are given in Appendix A. The following sections are limited to a discussion of passive systems, energy-absorbing devices and base isolation, with no mention made of active control systems. This is a rapidly developing area with much current research activity, and is beyond the scope of the present research.

1.1.1 Base Isolation

Base isolation is a seismic design strategy which reduces the level of ground motion that a structure experiences during an earthquake by moving the period of the structure away from the predominant period of the ground motion [1]. This is achieved by introducing a flexible connection, usually at the foundation level, between the structure and the ground.

The most common technique that has been used to achieve the flexible foundation is the elastomeric bearing system [2]. This approach uses elastomeric bearings, which consist of multiple bonded layers of elastomer and steel shims, to carry the gravity load of the isolated structure and, simultaneously, to provide the horizontal flexibility necessary to reduce the level of seismic forces transmitted to the superstructure. Other systems that have been utilized in practice include elastomeric bearings coupled with devices to provide additional energy dissipation (these devices which are many and varied, include lead inserts in the bearings themselves, lead extrusion dampers, flexural lead dampers, flexural and torsional mild steel dampers, hydraulic viscous dampers, and friction dampers), elastomeric bearing-slider bearing systems, and sleeved-pile systems to provide horizontal flexibility, coupled with mechanical energy dissipating devices [3,4]. The number of base isolation applications has grown considerably over the last decade. The list of buildings and other structures incorporating base isolation is now extensive (approximately 140 structures worldwide at the end of 1989 [1,5]).

1.1.2 Eccentrically-Braced Frame

Steel moment-resisting frames (MRFs) have long been recognized as having stable and repeatable inelastic behavior under cyclic loading conditions. Often, however, their flexibility can prove detrimental to the overall seismic performance of the building. Excessive flexibility allows displacements that may well be in excess of those permitted by code, displacements that will result in substantial damage to nonstructural components of the building. Until recently, cross bracing or chevron bracing (X- or K-bracing) was the main way of increasing the stiffness of steel MRFs, and bracing or wall systems for non-ductile reinforced-concrete struc-

tures. However, the inelastic behavior of such bracing under cyclic loading conditions degrades rapidly, and is not desirable.

The eccentrically-braced frame (EBF) was developed as an alternative to the conventional concentrically-braced frame (CBF). Hysteretic behavior is concentrated in especially designed regions (shear links) of the EBF and other structural elements are designed according to capacity design principles and intended to remain elastic under all but the most severe excitations. Extensive research has been devoted to the EBF [6,7,8] and the concept has seen rapid recognition and acceptance by the structural engineering profession, aided significantly by the inclusion of design rules into seismic codes of practice.

Energy dissipation, while concentrated in the especially designed and detailed shear links of the EBF, nonetheless still occurs in primary structural elements. This means that structural and non-structural damage to the building is likely to be significant in a severe earthquake.

1.1.3 Yielding Steel Elements in Bracing

The concept of utilizing the bracing system of a structure to dissipate energy has been explored by Henry and subsequently by Tyler [9,10,11,12]. An energy-absorbing device in the form of a round mild steel rod in a rectangular shape (geometrically similar to the structural bay in which it is included) is introduced at the intersection of cross bracing. The nature of the devices ensures that, unlike conventional cross bracing, buckling of the braces and, hence, pinched hysteretic behavior do not occur. Experimental tests of the devices have been conducted, and they have been incorporated in a number of buildings in New Zealand.

This idea of using the bracing system of a structure for the purpose of energy absorption (through geometric changes in the structure caused by the earthquake loading) is the fundamental concept of all the recently developed energy-absorbing devices. The types of devices discussed in this and the following sections, while their specific details may differ, all function in the same basic way.

Recently another type of yielding steel energy absorber has been the subject of experimental studies. The device, called an "ADAS" element, an acronym for "added damping and stiffness", was included in a three-story steel MRF and subjected to simulated earthquake motions [13]. An ADAS element consists of multiple X-shaped steel plates and develops plastic flexure uniformly over the height of the X-plates when deformed. Although recently patented by another party, it is conceptually the same as devices developed by Tyler et al. in the mid 1970s [14] and identical to devices tested by Stiemer, Godden, and Kelly (and others) in the early 1980s [15,16,17]. Triangular plate devices that function on the same principle of distributed plastic bending were incorporated in the isolation system of a base-isolated building constructed in New Zealand in 1983 [18]. ADAS elements have not yet been incorporated in any structure.

1.1.4 Viscous Dampers

A number of types of viscous dampers have been developed in Japan in recent years for use in base isolation systems [5], and several types of viscous damping systems for fixed-base buildings have also been developed there. Sumitomo Construction Company, Ltd., and the Building Research Institute have investigated the use of "viscous damping" walls [19], consisting of a plate hanging from the floor above into a case (the wall) of highly viscous fluid. Earthquake simulator tests of a 5-story, reduced-scale building model and a 4-story, full-scale steel frame building containing such walls have been carried out. Reductions in acceleration of the order of those seen in a base-isolated structure were observed. A 4-story prototype reinforced-concrete building with viscous walls was completed in 1987. It has been monitored for earthquake response and six large earthquakes (magnitude 4.1 — 6.7) have been recorded. The walls provide 19 to 29 % damping to the stories of the building, and increase its stiffness by a factor of 1.7. The observed accelerations were 25 — 70 % lower than those of the building without the viscous walls.

Viscoelastic dampers similar to those of the present research have also been proposed by

Sumitomo.

1.1.5 Friction-Damped Braced Frames

Various types of friction devices have been proposed for seismic energy absorption in structures. Pall [20,21] developed a device that is incorporated at the intersection of cross bracing in the same way as the Henry device (Sec. 1.1.3). The device prevents buckling of the bracing from occurring and possesses semi-rectangular hysteretic behavior that is achieved by brake pad-steel sliding interfaces. It has been tested in two series of earthquake simulator tests of model structures incorporating such devices [22,23], and devices of this type have been incorporated in a building in Canada [24], and studied for the retrofit of a building in Mexico [25].

An experimental study of a friction device that uses brake pad material has been conducted by Tyler [26]. Another type of friction device that consists of a brake pad-steel pad friction interface and which can be included in concentric or eccentric bracing, has been developed by Aktan et al. [27]. Earthquake simulator tests of a six-story structure incorporating the devices have been performed. More recently, the behavior of a small-scale three-story model outfitted with friction devices with self-centering characteristics has been studied in an extensive series of shake table tests [28]. An active friction device has been the subject of another recent analytical study [29] and an experimental program is planned. The device is capable of regulating the slip load to control energy dissipation under any level of seismic action. Several friction systems that do not involve special devices, but which are based on allowing slip at bolted connections of bracing have been proposed and tested [30,31].

1.2 Energy-Absorbing Devices Studied

Two types of energy-absorbing devices were considered in this study. The devices are introduced here, and mention made of existing seismic and non-seismic applications of these devices to building structures. A more detailed description of the devices follows in Chapter 2.

1.2.1 Viscoelastic Dampers

A range of acrylic co-polymer materials for damping applications has been developed by 3M Company. There have been extensive applications of these materials in the aerospace industry and to vibration problems in the field of electromechanics, but the number of applications to building structures is still small.

All of the applications of viscoelastic (VE) dampers in buildings to date have been wind vibration applications. The first, and most notable of these, was in the twin towers of the World Trade Center in New York City, where the dampers have been for about twenty years. The towers, each 110 stories in height, have 100 VE dampers installed at each level. The dampers are placed on the perimeter of the building and are located in the bottom chord of the trusses of the floor system. Small deformations in the dampers as a result of wind-induced motions are sufficient to achieve the desired increase in damping. More recent wind vibration applications have been the 73-story Columbia SeaFirst Building and the 60-story Number Two Union Square Building, both in Seattle. The Columbia SeaFirst Building has 260 double-layer sandwich dampers mounted in parallel on multistory diagonal bracing and the elastic axial deformations of the braces are exploited to cause shear displacements in the dampers [32,33]. The dampers weigh about 600 lb each. In the Number Two Union Square Building, 16 multilayer dampers with heat transfer fins are mounted in series with secondary columns and are deformed by wind-induced column axial loads. The dampers consist of six VE layers and weigh about 200 lbs each. VE dampers have also been used on the Sears Tower antenna and on four spires of the AT&T Building, both in Chicago.

Viscoelastic dampers have proved to offer a good solution to the problem of wind-induced vibrations in tall buildings. They are able to provide significant increases in structure damping and in the existing applications have shown good performance for at least twenty years' service.

There are several significant differences associated with the extension of VE dampers to the seismic environment. The levels of damping necessary for seismic loading conditions are

considerably greater than those necessary to be effective for wind vibration control. The greater severity of the earthquake loading imposes significantly larger deformations on the dampers, which means that VE material shear strain demands are much larger than those due to wind loading. Recent work by Bergman and Hanson [34] has demonstrated desirable behavior of VE dampers under seismic-type loading conditions and shake table tests of a small-scale model building containing VE dampers have shown the improvements in response possible [35]. The current research has been aimed at investigating the suitability of VE dampers for enhancing the earthquake resistance of a structure by designing and testing a large-scale VE-damped building.

1.2.2 Friction Dampers

For many years, Sumitomo Metal Industries Ltd., Japan, has developed and manufactured friction damping devices for shock absorption applications in railway rolling stock bogie trucks. These devices have very high performance characteristics, with their behavior negligibly affected by amplitude, frequency, temperature or the number of applied loading cycles. It is only since the mid 1980s that the friction dampers have been extended to the field of structural and seismic engineering. Nikken Sekkei, working in conjunction with Sumitomo, has designed three buildings that incorporate Sumitomo friction dampers.

The Sonic City Office Building, completed in 1988, is located in Omiya City. It is a 31-story steel frame structure with precast concrete infill panels. There are eight 22 kip dampers (maximum displacement ± 2.36 inches) at each level, with four dampers located in each of the two main plan directions. The dampers are incorporated in the structural system at the connections of the infill panels to the steel frame. The Asahi Beer Azumabashi Building in Tokyo was completed in 1989. It is a 22-story braced steel frame structure that contains four 22 kip dampers (maximum displacement ± 2.36 inches) at each level. Two dampers are oriented in each of the two main plan directions at each level and they are installed on 20 floors of the building. The dampers are connected between the bracing and the structural frame. The

design of a base-isolated, six-story reinforced concrete building in Tokyo has recently been completed that incorporates Sumitomo friction dampers as the energy-absorbing elements of the isolation system. The building is currently under construction and is expected to be completed in 1991. It contains twelve 22 kip dampers, each with a displacement range of ± 9 inches.

The basis of the design of the dampers for the Sonic City Office Building and the Azumabashi Building was to reduce the building response to ground-borne vibrations, microtremors, and small earthquakes. The potential of the dampers to substantially improve the behavior of the buildings in a major earthquake was not a primary consideration in the design and selection of the dampers. The objective of the current research, however, was to use the dampers to improve the behavior of a nine-story, large-scale steel MRF to severe earthquake inputs. In this respect, the research represents the first such application of Sumitomo friction dampers for this purpose.

The primary objective of incorporating energy-absorbing devices in a structure is to concentrate the absorption of seismic energy in devices designed specifically for this, and to minimize inelastic yielding action in the gravity load-carrying elements of the structural system. To do this requires limiting structural drifts, while at the same time maximizing the energy dissipation that is achieved within these displacement limits. Thus; since all the proposed devices absorb energy only when they are caused to deform, while it is desired to limit structure deformations, these same deformations are necessary to cause the devices to function. Therefore, for any device to be effective, it must be able to provide sufficient energy absorption (and stiffness) to the structure while at the same time operating within the displacement limits imposed on the structure. It is recognized that, while avoiding yielding in the primary structural elements is an ideal objective, it is unlikely to be achievable in practice unless the stiffness and strength of the primary structure are designed from the outset with this objective in mind. In most cases the devices (and added bracing) themselves are unlikely to be able to prevent yielding of the primary structural system under severe earthquake loads.

1.3 Objectives and Scope

1.3.1 Objectives

The aims of this research program were to

(i) Perform earthquake simulator tests of a large-scale, multistory steel structure incorporating two different types of energy-absorbing devices, a viscoelastic device and a friction device;

(ii) Evaluate the effectiveness of both types of devices by comparing the results with those obtained for the "undamped" structure in moment-resisting and concentrically-braced configurations; and

(iii) Investigate analytical methods suitable for the computer modeling of the structure incorporating the energy-absorbing devices.

1.3.2 Scope

To achieve the above-stated objectives the following tasks were undertaken:

(i) Selection and design of the devices for the test structure. This entailed the development of suitable procedures for the design of the two types of energy dissipation systems.

(ii) Design of the bracing systems necessary to incorporate the devices in the test structure.

(iii) Diagnostic testing of the damped structures to determine their dynamic characteristics.

(iv) Earthquake testing of the damped structures using a selection of recorded and synthesized earthquake ground motions.

(v) Diagnostic and earthquake testing of the model structure in "undamped" moment-resisting and concentrically-braced configurations. Schematic diagrams of the four structural systems tested are shown in Fig. 1.2.

(vi) A comparison of the experimental results obtained for the structure in the damped and "undamped" configurations.

(vii) A study of the suitability of current analytical methods for predicting the response of the damped structures to earthquake inputs. The results of these analyses were compared with the experimental results.

(viii) A review of the applicability of the design methods used at the outset of the research program in light of the experimental and analytical results.

1.4 Organization of Text

In Chapter 1 an overview of conventional design philosophy and a description of some new and innovative approaches to seismic design are presented, followed by a description of the energy-absorbing devices that are the subject of the current study and mention of existing applications of these devices. The objectives and scope of the research are also presented. Chapter 2 describes the two types of energy-absorbing devices studied and the approaches used to design the two damped structural systems. In Chapter 3 the earthquake simulator test programs for the two damped systems are outlined. The test facility, input signals used, and various aspects of data reduction and analysis are also described. Chapter 4 presents the results of the diagnostic and earthquake tests of the various configurations of the test structure. Comparisons of the different structural systems are made. Numerical analyses of the damped structures are described in Chapter 5, and the results are compared with the experimental results. Various other results obtained from the analyses are also presented. Conclusions from the research and recommendations for future work are presented in Chapter 6.

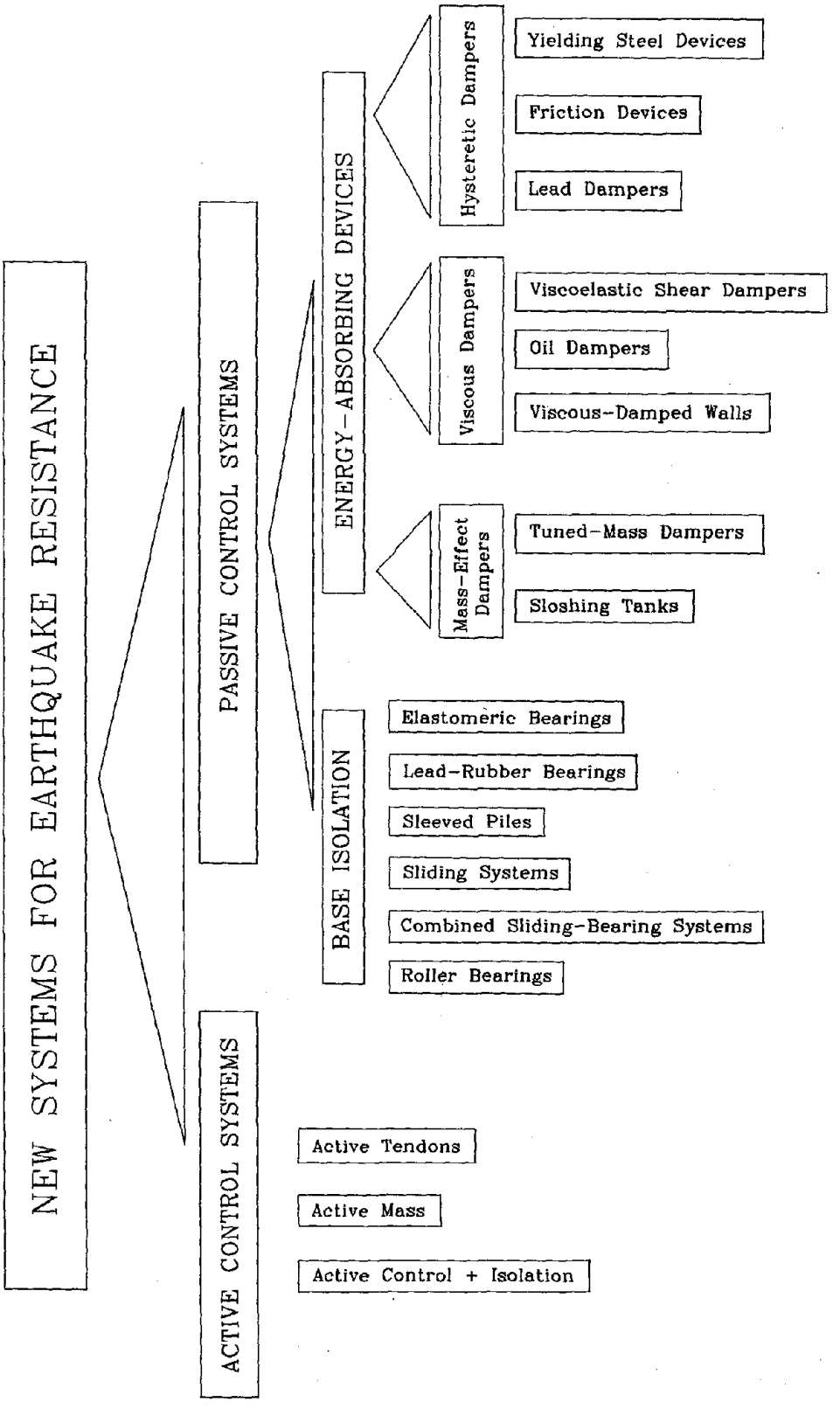

Fig. 1.1 New Systems for Improved Earthquake Resistance of Structures

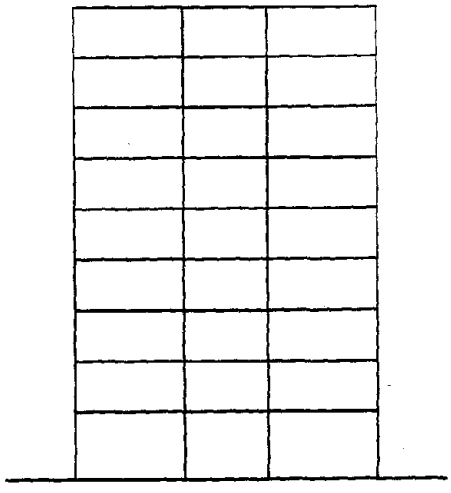

(a) MRF

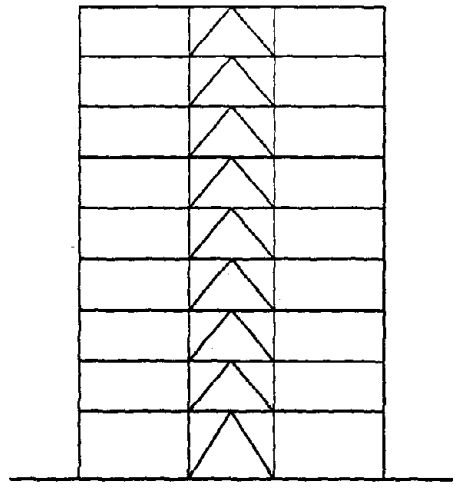

(b) CBF

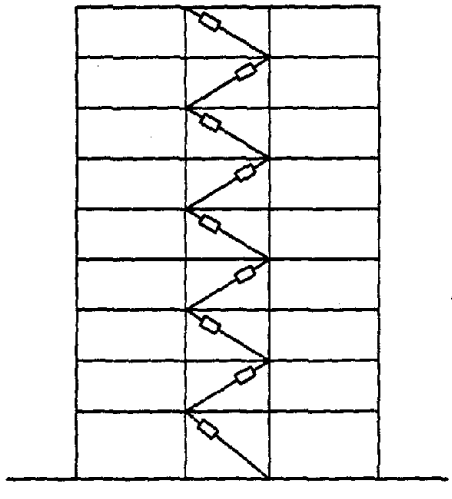

(c) VD

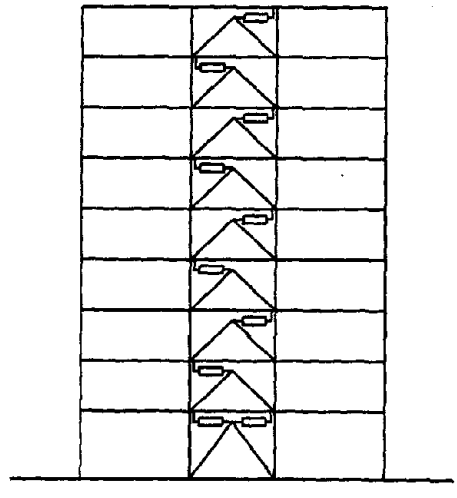

(d) FD

Fig. 1.2 Test Configurations of Model Structure

CHAPTER 2

DESIGN OF ENERGY DISSIPATION SYSTEMS FOR TEST STRUCTURE

2.1 Introduction

This chapter describes the methods used for the design of the viscoelastic and friction energy dissipation systems for the test structure. A description of the VE material used in the test program and the basis of the theory of the behavior of the material are followed by an outline of the procedure used to design the VE dampers for the test structure. The second part of the chapter describes the friction devices used in the test program and the approach used to design the friction devices for the test structure. The chapter concludes with a description of the nine-story MRF test structure.

2.2 Viscoelastic Material Used in Test Program

2.2.1 Material Description

The viscoelastic material used in the test program belongs to a class of acrylic copolymers that have been developed by the Minnesota Mining and Manufacturing (3M) Company. The materials have stable dynamic characteristics, are chemically inert, and have good aging properties. They are resistant to environmental pollutants. Four types of the material are currently available from 3M.

The behavior of the material is influenced by three important material properties. These are the shear loss modulus, G'', the shear storage modulus, G', and their ratio, which is the material loss factor $= \eta = \frac{G''}{G'}$. The shear loss modulus controls the specific energy dissipation capacity of the material; a high G'' means high energy dissipation per unit volume. All three of these material properties are sensitive to frequency, temperature, and strain.

The variation of G'' and η with temperature, frequency, and strain is the same for all four of the material types. Thus, the general relationship for one type can be used to predict that for the others, provided that data points at a certain temperature, frequency, and strain are available [36]. This is the basis of material property charts that have been developed by the manufacturer.

The materials all exhibit a large variation in shear moduli in the small strain range (< 10 %). However, the variation over the range from about 20 — 150 % strain is not great, and if the material is designed for operation in this strain range quite linear response can be achieved.

2.2.2 Governing Equations

A linear theory of viscoelasticity can be used to describe the behavior of a constrained layer VE shear damper subjected to sinusoidal deformation [37]. If the applied displacement is of the form

$$X = X_o \sin\omega t \tag{2.1}$$

then the resulting force in the VE layer is

$$F = F_o \sin(\omega t + \delta) \tag{2.2}$$

where X_o = deformation amplitude
F_o = load amplitude
ω = loading frequency (rad/s)
δ = (leading) phase angle

If the dimensions of the viscoelastic layer are taken into account, then Eqs. 2.1 and 2.2 can be expressed in terms of strain and stress, respectively:

$$\gamma_o = \frac{X_o}{t} \tag{2.3}$$

$$\sigma_o = \frac{F_o}{A} \tag{2.4}$$

and then

$$\gamma = \gamma_o \sin\omega t \tag{2.5}$$

$$\sigma = \sigma_o \sin(\omega t + \delta) \tag{2.6}$$

where t = thickness of viscoelastic layer
A = shear area of viscoelastic layer

Stress and strain are related by what has commonly become called in industry practice [37] the complex modulus, G^*,

$$\sigma = G^* \gamma_o \sin(\omega t + \delta) \tag{2.7}$$

$$= \gamma_o (G' \sin\omega t + G'' \cos\omega t) \tag{2.8}$$

$$\text{where} \quad G^* = \frac{\sigma_o}{\gamma_o} = \left[G'^2 + G''^2 \right]^{1/2} \tag{2.9}$$

$$G' = G^* \cos\delta = \text{shear storage modulus} \tag{2.10}$$

$$G'' = G^* \sin\delta = \text{shear loss modulus} \tag{2.11}$$

G' is a measure of the stiffness capacity (or energy stored and recovered per cycle) of the material, while G'' is a measure of the damping capacity (energy dissipated or lost per cycle).

The loss factor of the material, η, is defined as

$$\eta = \frac{G''}{G'} = \tan\delta \tag{2.12}$$

The amount of energy dissipated in one cycle is

$$W_D = \pi G'' \gamma_o^2 V \tag{2.13}$$

W_D represents the area enclosed by a plot of force versus deformation for one cycle of loading. This type of plot is frequently referred to as a hysteresis loop. Thus, the size or area of the hysteresis loop is a direct measure of the energy dissipated by the damper. It is seen that W_D is a function of the volume of material (V), the square of the strain amplitude (γ_o^2), and the shear loss modulus (G''), which in turn is a function of the loading frequency, the temperature,

and the amplitude of deformation. Thus, by changing one, all, or a combination of these variables it is possible to change the amount of energy dissipated by a damper.

2.3 Design of Viscoelastic Dampers for Test Structure

The method used for the design of the VE dampers for the test structure was a simplified first-mode procedure aimed at providing the structure with a specified level of damping. Since the VE damping system was being designed for an existing structure, no criteria were laid down for the design of the MRF itself. The stiffness and strength properties of the MRF model were simply taken as input values for the damper design process.

The design philosophy was simple; to provide a specified level of damping to the structure at a nominal maximum structure displacement using VE dampers. It was assumed that the response of the structure at this maximum displacement would be in the elastic range. Notably, the philosophy says nothing about the maximum input earthquake or the degree of inelastic response acceptable in the structure, but since the strength and stiffness of the structure were predetermined (and changing these properties was beyond the scope of the experimental program) these factors were not considered. Of course, it was recognized that the addition of the VE dampers and the diagonal braces would add somewhat to the stiffness (and strength) of the structure, but the effect of these contributions on the seismic response of the structure was expected to be significantly less than that of increasing the structure damping.

The fundamental frequency and associated mode shape of the nine-story MRF model were known from previous experimental tests and numerical analyses. This frequency and mode shape are denoted by f_1 and ϕ^1, respectively. The maximum displacement at which the target damping ratio, ξ_t, was to be achieved is d_{max}, and in the case of the test structure this corresponded to a drift of approximately 0.7%.

The design procedure then followed these steps and employed the following relationships:

1. $$X = d_{max}\, \phi^1$$

2. Calculate the elastic strain energy in the structure at d_{max}

$$W_S = \frac{1}{2} X^T K X$$

where $K = M\omega_1^2$, M is a diagonal matrix of story masses, and $\omega_1 = 2\pi f_1$. Thus, the elastic strain energy can be readily calculated from

$$W_S = \frac{1}{2} \omega_1^2 X^T M X$$

3. Calculate the energy dissipation, W_D, that will be required to achieve ξ_t

$$\xi_t = \frac{W_D}{4\pi W_S}$$

thus $W_D = 4\pi W_S \xi_t$, where ξ_t is specified.

4. Select the VE material best suited to the temperature range appropriate for the application.

5. Decide on the operating displacement of the damper, and thus the strain range for the material; this will dictate the thickness and number of VE layers.

6. With the temperature and operating frequency known (approximately), the material G'' and η can be determined. These are found from manufacturer's data sheets or from the results of tests of individual dampers under controlled conditions.

7. Calculate the total volume, V, of VE material required to supply the structure with the desired damping of ξ_t,

$$W_D = \pi G'' \gamma_o^2 V$$

$$V = \frac{W_D}{\pi G'' \gamma_o^2}$$

8. Decide on the distribution of this volume of VE material throughout the structure, and on the size of the individual dampers.

For the design of the dampers for the test structure, it was assumed that

(i) the operating strain was $\approx$ 100%

(ii) the ambient temperature was 65 $^{\circ}$ F

(iii) the distribution of VE material throughout the structure would be uniform; that is, all of the dampers would be of one design and there would be an equal number of dampers at each level of the structure.

This method and the associated assumptions led to a simple and workable design procedure which was felt to be suitable considering all of the nonlinearities and variables contributing to the design problem. The important assumptions were the "linear" material properties used for the dampers (in reality being functions of frequency, strain amplitude, and temperature) and that of primarily first-mode behavior. The first-mode properties themselves were known from previous experiments, and thus did not represent any significant approximation. On the basis of the first vibrational frequency of the MRF and an estimate of the stiffness contribution of the VE dampers, an estimate of the frequency of the viscoelastically-damped frame was obtained. The VE material design properties were determined for this estimated frequency.

Existing wind vibration applications of VE dampers have typically involved levels of structure damping less than about 4 % of critical. For VE dampers to be useful in the seismic environment it is felt that they should provide at least 10 % damping to a structure. Simple analyses suggest that 15 — 20 % damping is an optimum level of damping to provide to a structure from the point of view of enhancing its energy dissipation capacity and reducing response. The target damping ratio, ξ_t, was selected as 10 % for the design of the VD structure.

The final VE damper design is shown in Fig. 2.1. The dampers consisted of two 0.15-inch thick layers of ISD 110 material with a shear area of 3 inches by 5 inches.

Installation of Devices in Test Structure

Details of the installation of the VE dampers in the test structure are shown in Fig. 2.2. The dampers were installed in series with single-diagonal, double t-section bracing that was connected by simple pinned (bolted) connections to the frame. An elevation of the 9-story structure with the VE dampers installed is shown in Fig. 2.3. The staggered formation of the

dampers was in order to minimize the fabrication work necessary to install the dampers and bracing for the friction damped frame tests, which were performed prior to the VE damper tests. As illustrated in Fig. 2.10, the friction dampers were also installed in a staggered formation, for the same reason.

2.4 Description of Friction Dampers

Longitudinal and cross-sections of a typical Sumitomo friction damper are shown in Fig. 2.4. The dampers consist of a series of wedges, which acting against each other under the load from a compressed spring, apply a normal force to the friction pads. The friction pads slide directly on the inner surface of the steel casing of the device. The friction pads are copper alloy with graphite plug inserts which provide dry lubrication to the unit, ensuring a stable friction force and reducing noise during movement.

2.5 Design of Friction Dampers for Test Structure

The size of the dampers (that is, their slip force) and their layout in the test structure was determined using a nonlinear time history analysis approach. A simplified stick-model of the structure was adopted for the design analyses (Fig. 2.5). The model consisted of elements with bilinear stiffness characteristics, which represented the summation of an elastic stiffness component for the MRF and a bilinear elastic-perfectly-plastic stiffness component for the brace-damper assemblage. A series of analyses were performed for a number of different earthquakes, each at several different intensity levels. The earthquakes and peak ground acceleration (PGA) levels used for the design analyses are listed in Table 2.1.

The choice of the initial distribution of slip loads was based closely on the results of previous work on the nine-story model containing another type of friction damper [23]. This distribution was assumed as the starting point of the analyses for the design of the Sumitomo friction dampers. Each set of analyses was performed for slip load distributions equal to one-quarter, one-half, three-quarters, and one times the distribution that was used in [23]. A

detailed study of displacement and shear force response quantities obtained from the analyses indicated that the same distribution of slip load within the structure as that used in [23] provided most improvement in the response of the structure. In fact, the final slip load distribution chosen [38,39], being influenced by practical design dimensions of the friction devices and installation requirements, differed somewhat from that in [23].

The nominal distribution of slip loads selected for the test program is shown in Fig. 2.6. The actual slip forces of the dampers in their as-installed configuration are also shown in the figure. Plan and dimension views of one of the friction dampers are shown in Fig. 2.7. All the dampers for the test structure were the same as the one shown in the figure, with the exception of the overall diameter of the device. The diameters of the three different types of devices are given in Fig. 2.7.

Component Tests

Each of the friction devices manufactured for the test program was subjected to proof tests prior to shipment to EERC. These tests were intended to confirm the correct setting of the slip load and to identify any dependence of the force-displacement behavior on the variables of loading frequency, amplitude, temperature, or number of loading cycles. The matrix of component tests performed is shown in Table 2.2. All of the dampers performed as intended, and the effect of these factors was found to be negligible [40].

Installation of Devices in Test Structure

Details of the installation of the friction dampers in the test structure are shown in Fig. 2.8. In the upper levels (2 — 9) of the structure a single device was installed in the middle bay of each frame, as shown in Fig. 2.8(a). To achieve the required slip load at the bottom level, two devices were mounted in each frame (at total of four at each level), as shown in Fig. 2.8(b). The dampers were fitted to mounting beams which were bolted to the undersides of the floor beams. A chevron brace arrangement fabricated from 2 1/4 × 2 1/4 × 3/16 SHS with all-welded end connections was attached to one end — the free end — of the damper, and the

other end was attached to the outer end of the mounting beam. In this way, any interstory deformation occurring was imposed on the damper, assuming of course that the brace assemblage was rigid (or nearly so). The bracing was designed such that the deformations occurring in it under a lateral load equal to the slip load of the attached device would be negligible. At the brace-damper connection, a stainless steel-teflon guide plate arrangement ensured that the only deformation imposed on the damper would be along its longitudinal axis. A cross-section of the guide plate arrangement is shown in Fig. 2.9.

An elevation of the nine-story structure with the friction dampers installed is shown in Fig. 2.10. The staggered formation of the dampers in levels 2 — 9 was in order to minimize the fabrication work necessary to install the dampers and bracing for the VD model tests, which were performed upon completion of the friction damper tests. As illustrated in Fig. 2.3, the VE bracing was also installed in a staggered formation, for the same reason.

2.6 Description of Nine-Story MRF Test Structure

A nine-story, moment-resisting steel frame model represented the basic structure for the test program. This frame was modified in turn, to include concentric bracing, then viscoelastically-damped braces, and then friction devices. Figure 1.2 shows sketches of these four different structural configurations.

The nine-story steel MRF was first constructed and tested in 1976-77 for a study investigating the behavior of a multistory structure with column uplift permitted at its foundation [41]. For the present series of tests, the structure was fixed at its base. The model has been used in a number of different research programs [42,43]. The design and construction details of the model are described in detail in [41]. The MRF model is shown in Figs. 2.11 and 2.12. The model is intended to represent a typical section in the weak direction of a steel MRF building at 1/4 scale. Primary connections are all welded, while the connections for the out-of-plane bracing are bolted. The model is approximately 29 ft high and 18 ft wide, giving a height-to-width aspect ratio in the direction of testing of 1.56. The model comprises three bays

in the direction of testing and is one bay wide in the lateral direction. The response of the model in the out-of-plane direction was of no interest since the dynamic loads applied by the shake table were to be in one direction only, so additional bracing was provided (in the plane of the floors and also at the ends of the model, see Fig. 2.11) to increase the lateral and torsional stiffness sufficiently that unwanted modes of vibration would be suppressed. Additional mass was necessary to satisfy similitude requirements. This was provided by a combination of large concrete blocks (2 or 4 kips in size) and lead ballast in the form of 100 lb billets connected together in 500 lb packets. The mass distribution was the same for all four configurations of the test structure, and consisted of 10 kips added mass at each level. This loading is shown in Fig. 2.11.

The concentrically-braced (CBF) configuration of the test structure is shown in Fig. 2.12. The bracing consisted of 1 1/2 × 1 1/2 × 1/4 double-angles at the bottom level and 1 × 1 × 1/4 double-angles at levels 2 — 9 which were bolted into the MRF. The slenderness ratios of the bracing were l/r_1 = 78.1 and $l/r_{2\text{-}9}$ = 89.6.

TABLE 2.1 Earthquake Signals Used for FD Design Analyses

EARTHQUAKE	SIGNAL	TIME SCALE	PGA [g]
Imperial Valley May 18, 1940	El Centro NS	$\frac{1}{2}$	0.304 0.422 0.552 0.716 0.838
Kern County July 21, 1952	Taft Lincoln School Tunnel EW	$\frac{1}{2}$	0.409 0.642 0.777
Tohoku Univ. (1F) June 12, 1978	Sendai Miyagi-Ken-Oki NS	$\frac{1}{2}$	0.170 0.206 0.307 0.447
Michoacan September 19, 1985	SCT Mexico City EW	$\frac{1}{5}$	0.115 0.249 0.426 0.687
Michoacan September 19, 1985	CDAF Mexico City EW	$\frac{1}{5}$	0.115 0.249 0.426 0.687

TABLE 2.2 Matrix of Component Tests of Friction Dampers

Characteristic Studied	LOADING			Test Performed		
				Damper [kips]		
	Frequency [Hz]	Amplitude [± inch]	No. of Cycles	2.42	2.87	4.85
Frequency	0.5—10	0.08	-	•	•	•
	0.33—2	0.39	-	•	•	•
Amplitude	5	0.02—2	-	•	•	•
	2	0.04—0.39	-	•	•	•
	0.5	0.04—0.79	-	•	•	•
Durability	0.5	0.39	4000†	○	•	•

Notes:

1. all tests consisted of sinusoidal displacement cycles.
2. • = test performed; ○ = test not performed
3. † = data recorded for first cycle, then subsequently every 1000 cycles.
4. upper limit of damper casing temperature was 302 °F (150 °C).

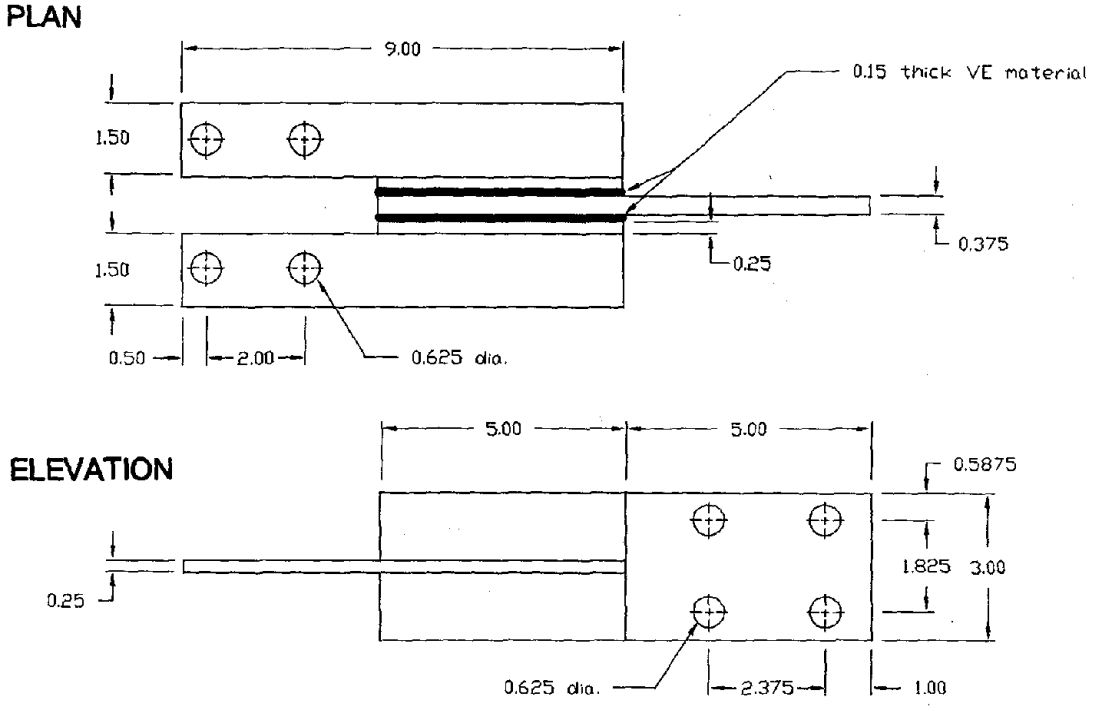

All dimensions in inches

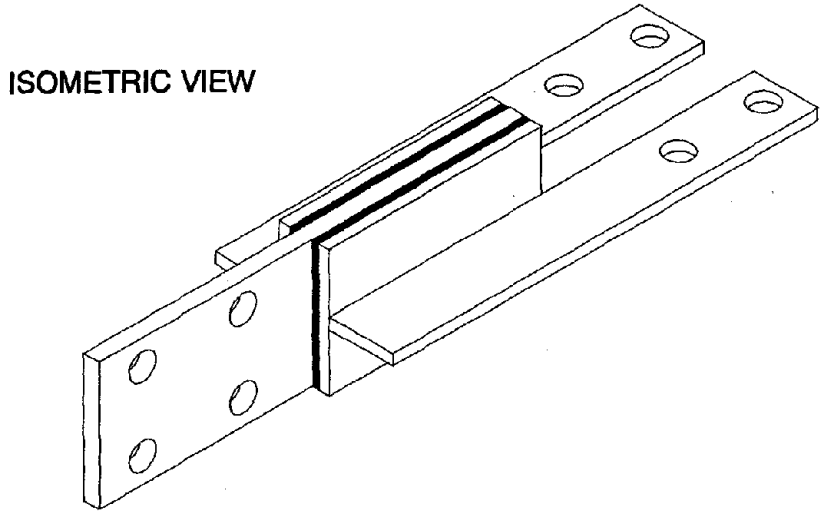

Fig. 2.1 VE Damper Design for Test Program

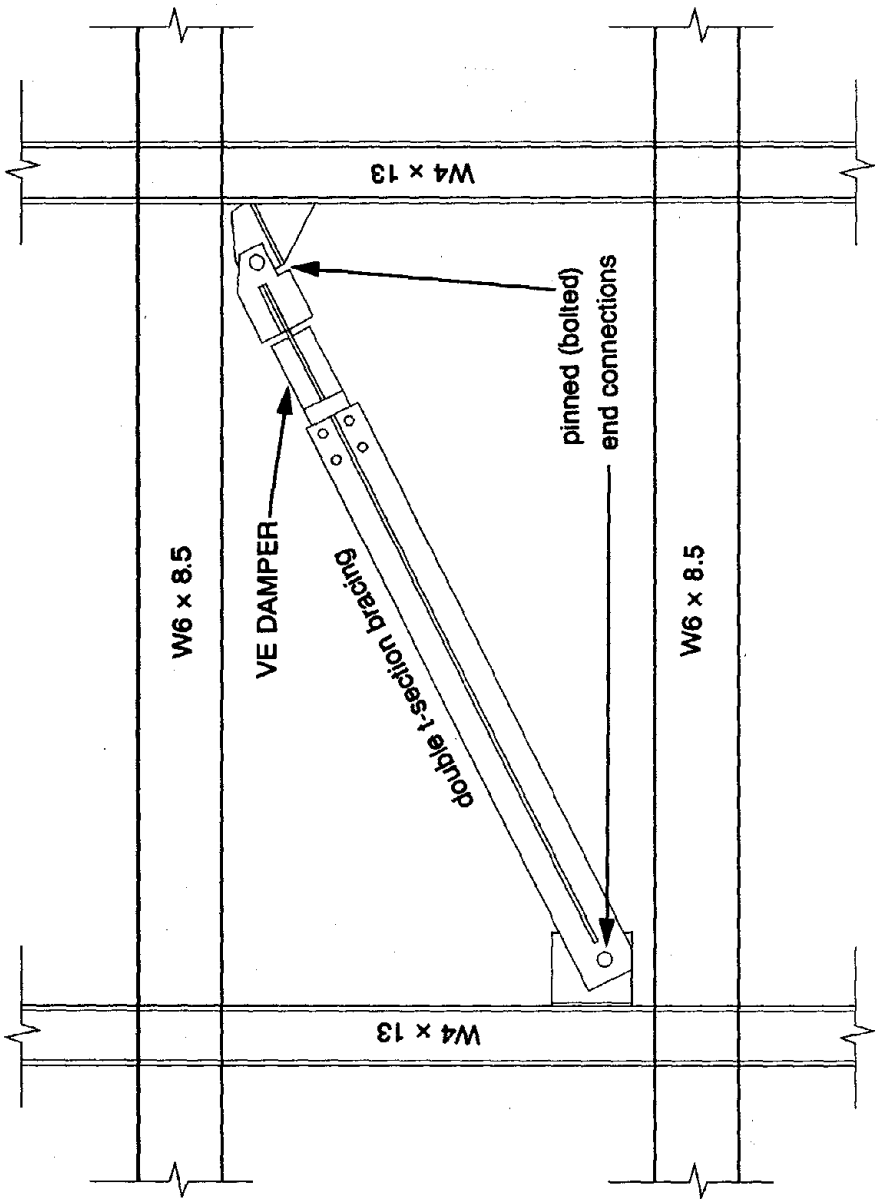

Fig. 2.2 Installation of VE Dampers in Model

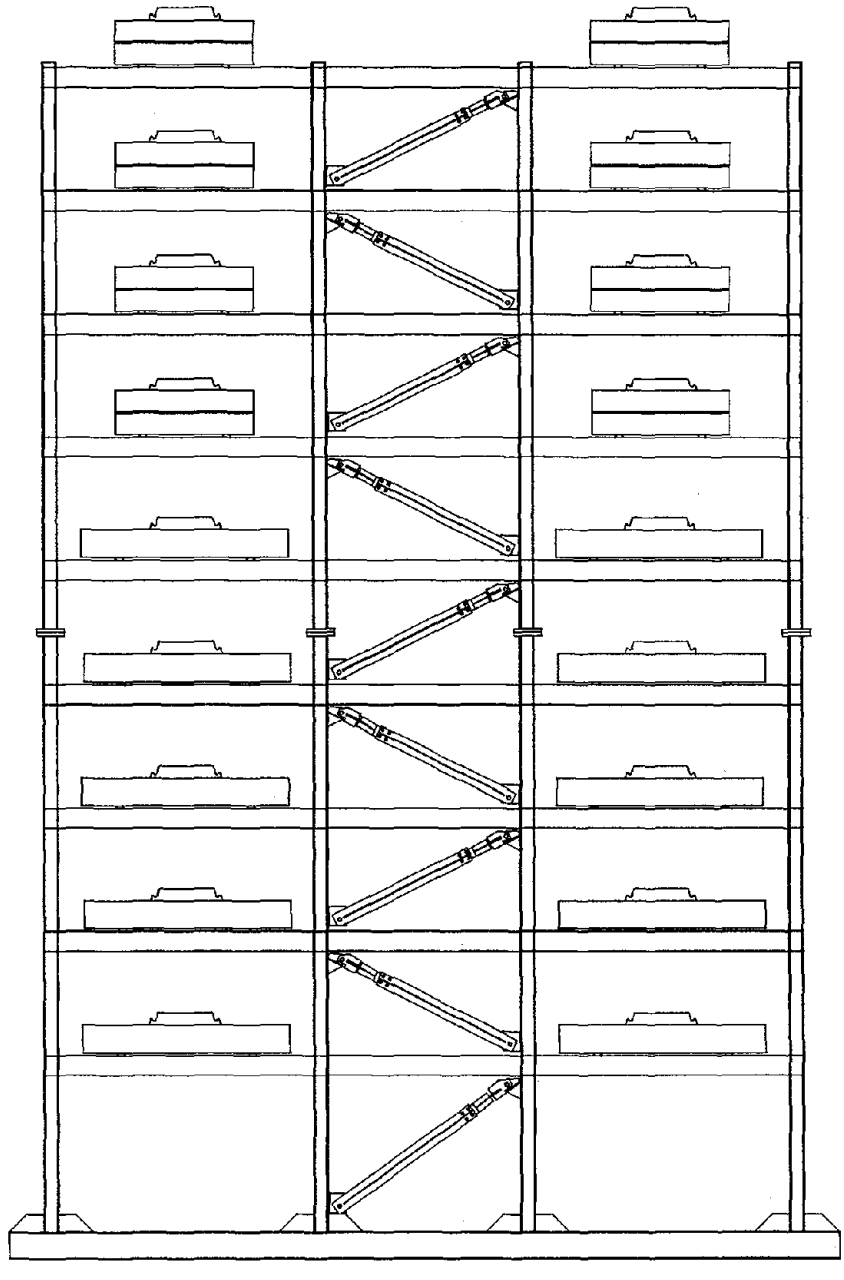

Fig. 2.3 Nine-Story Viscoelastically-Damped Model

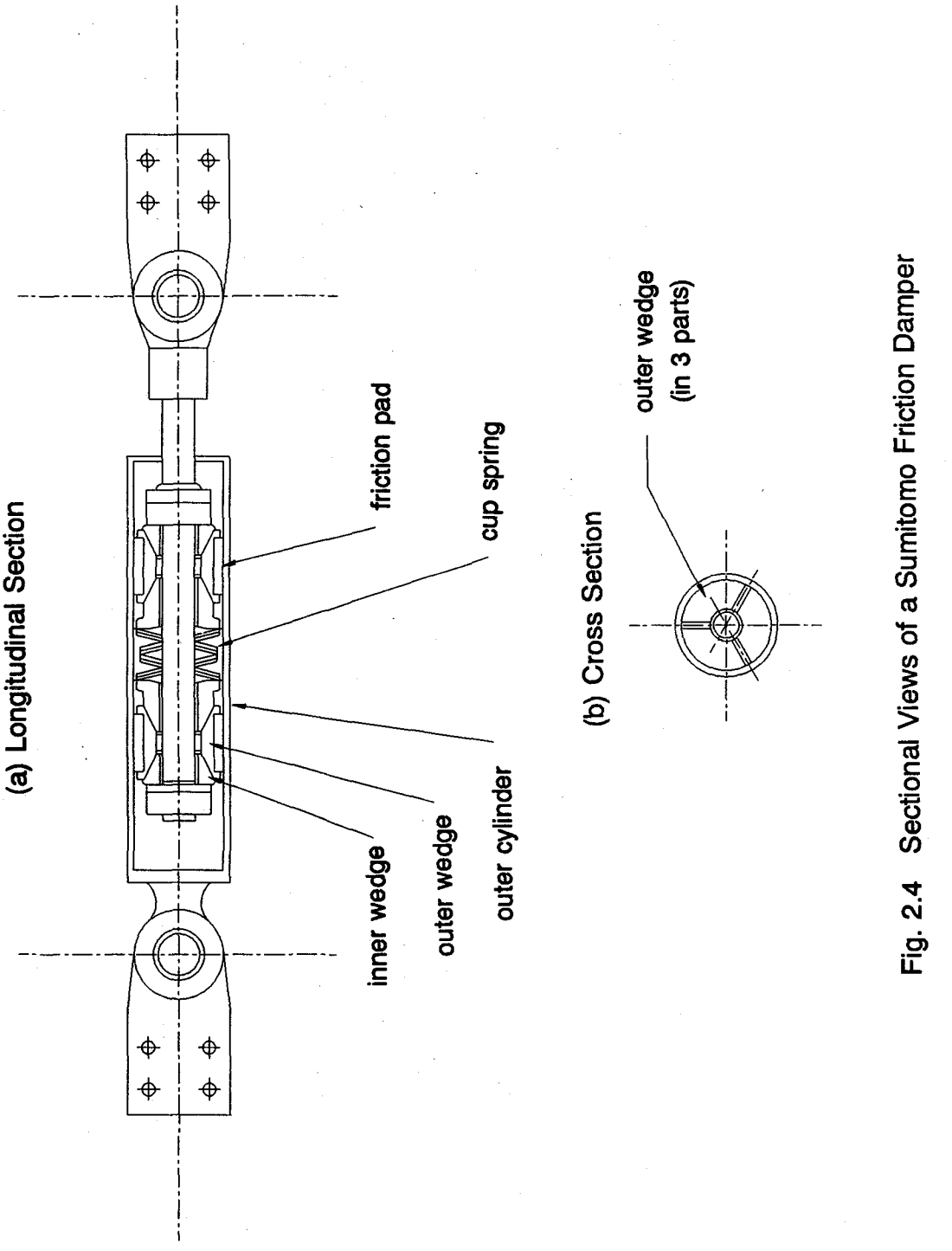

Fig. 2.4 Sectional Views of a Sumitomo Friction Damper

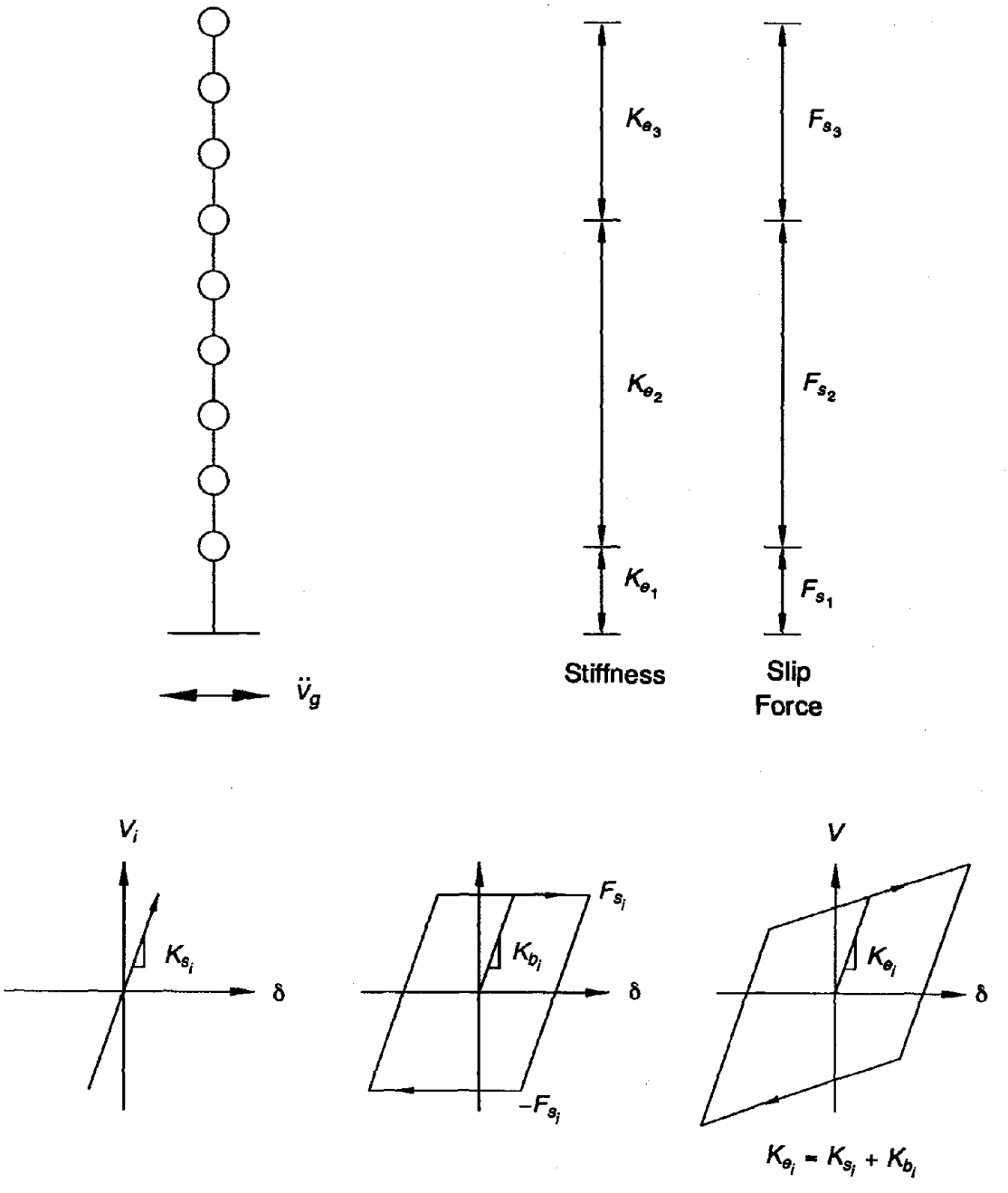

(a) MRF Elastic Story Force-Deformation Relationship

(b) Bilinear (EPP) Damper + Brace Force-Deformation Relationship

(c) Combined Effective Story Force-Deformation Relationship

Fig. 2.5 Schematic of Computer Model Used for Design Analyses of FD Structure

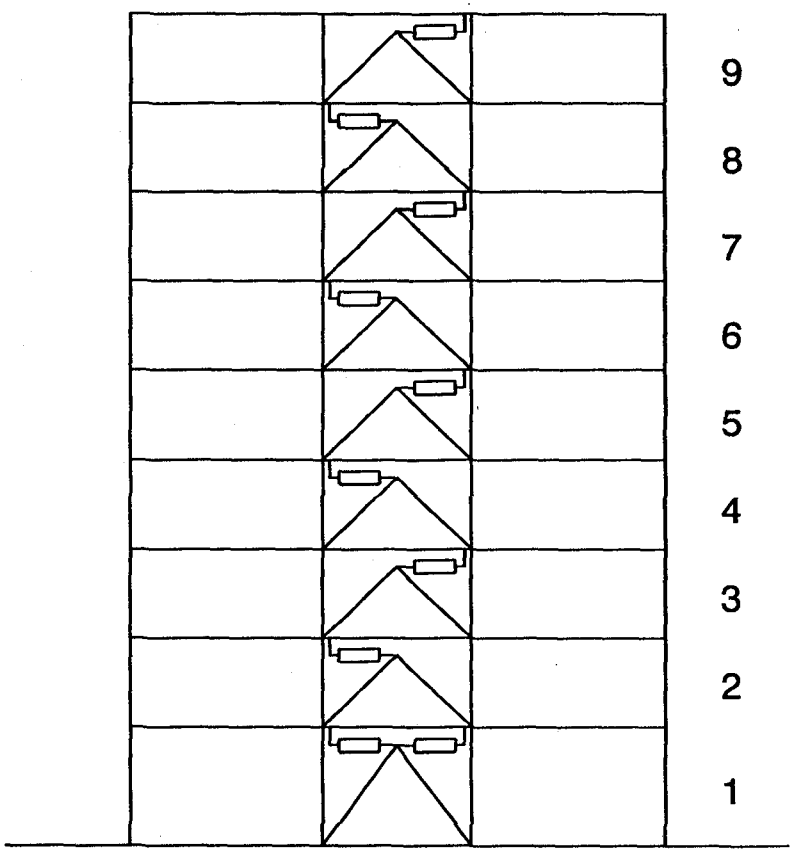

LEVEL	DESIGNED [kips]	ACTUAL [kips]
9	4.84	4.8
8	4.84	4.8
7	4.84	5.2
6	9.70	9.8
5	9.70	10.0
4	9.70	9.6
3	9.70	9.6
2	9.70	9.8
1	11.48	11.6

Fig. 2.6 Distribution of Friction Forces in FD Model

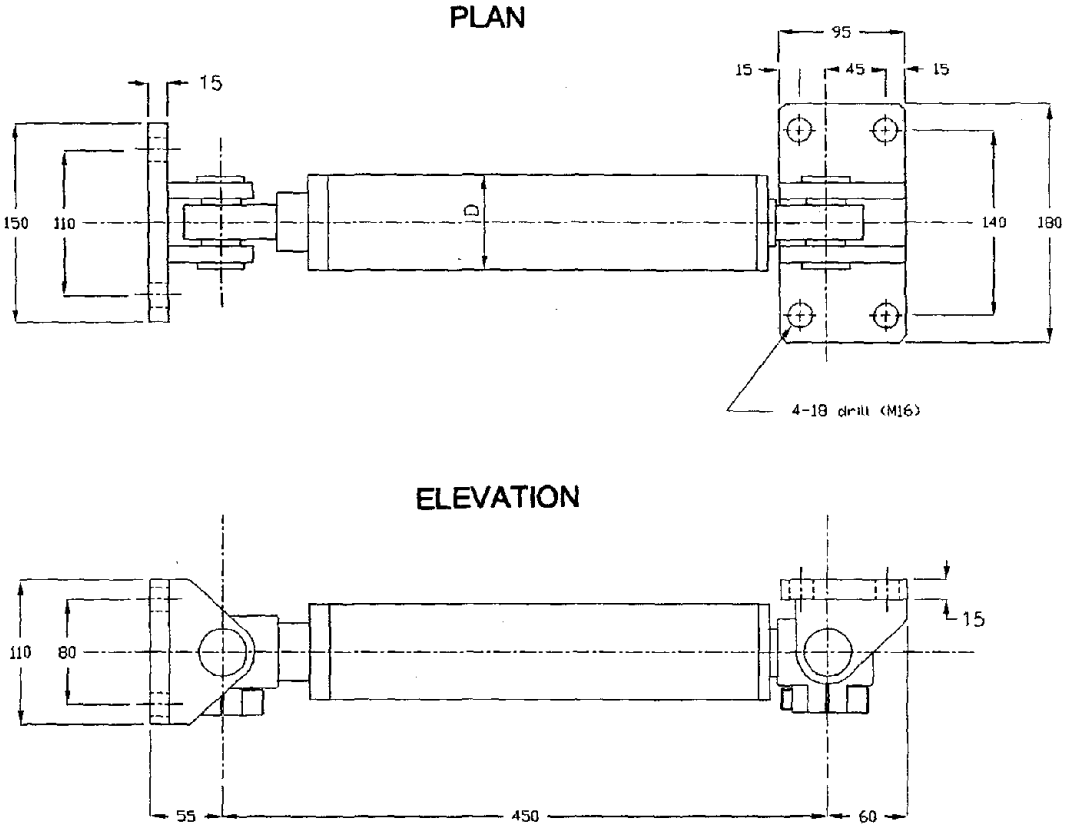

All dimensions in millimeters

damper type	levels installed	friction force [kips]	diameter [mm]
1	1	2.87	76.3
2-6	2	4.85	95
7-9	3	2.42	76.3

Fig. 2.7 Friction Damper Designs for Test Program

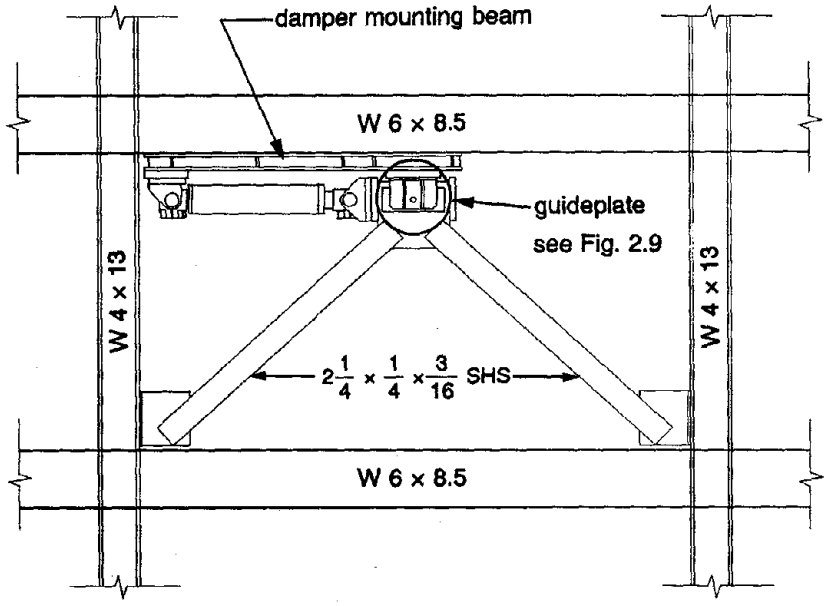

(a) Upper Floors (2 — 9), Dampers staggered at alternate levels

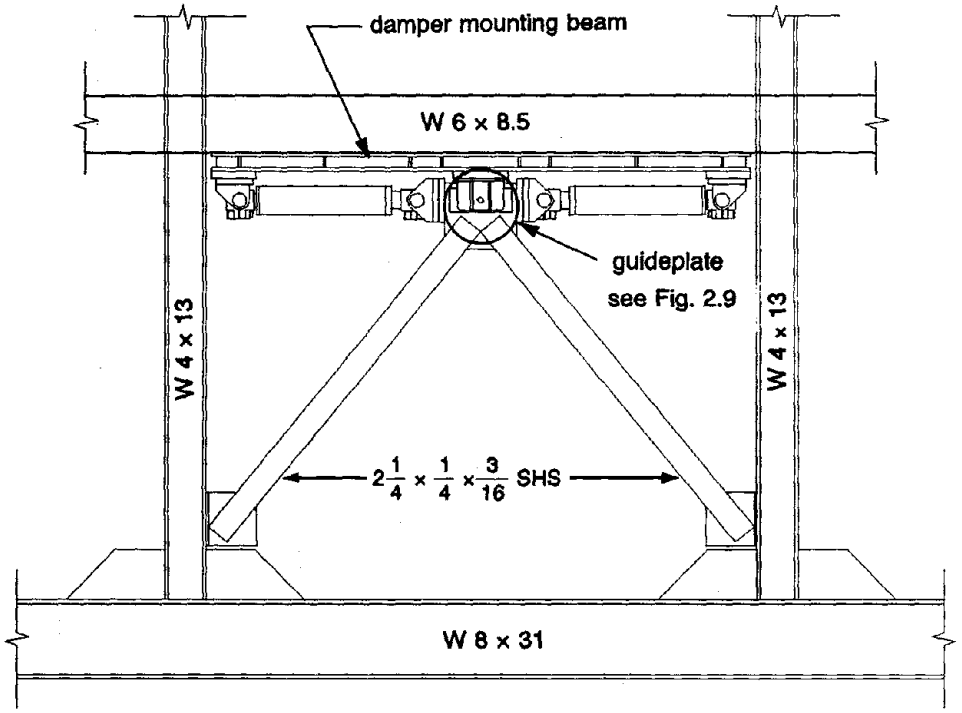

(b) Bottom Floor

Fig. 2.8 Installation of Friction Dampers in Model

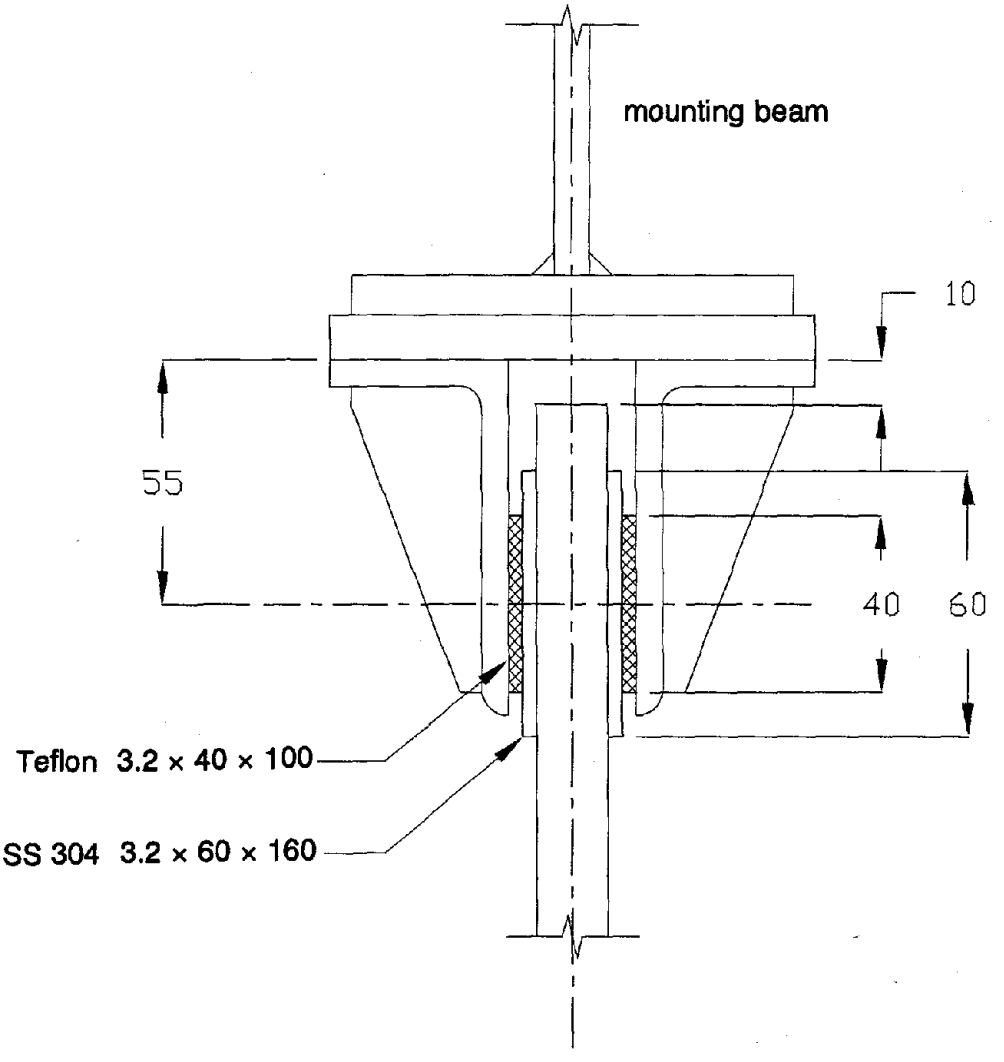

All dimensions in millimeters

Fig. 2.9 Cross-Section of Guide Plate

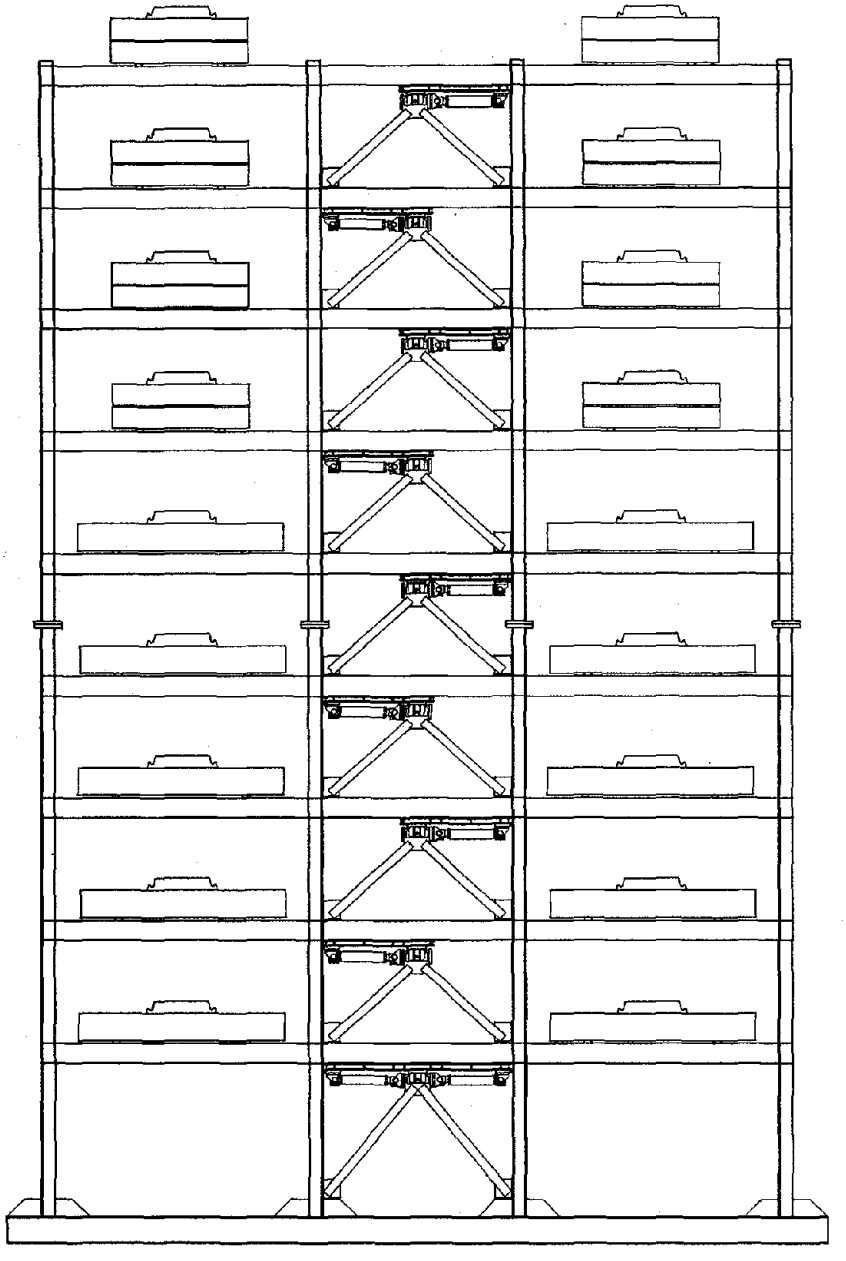

Fig. 2.10 Nine-Story Friction-Damped Model

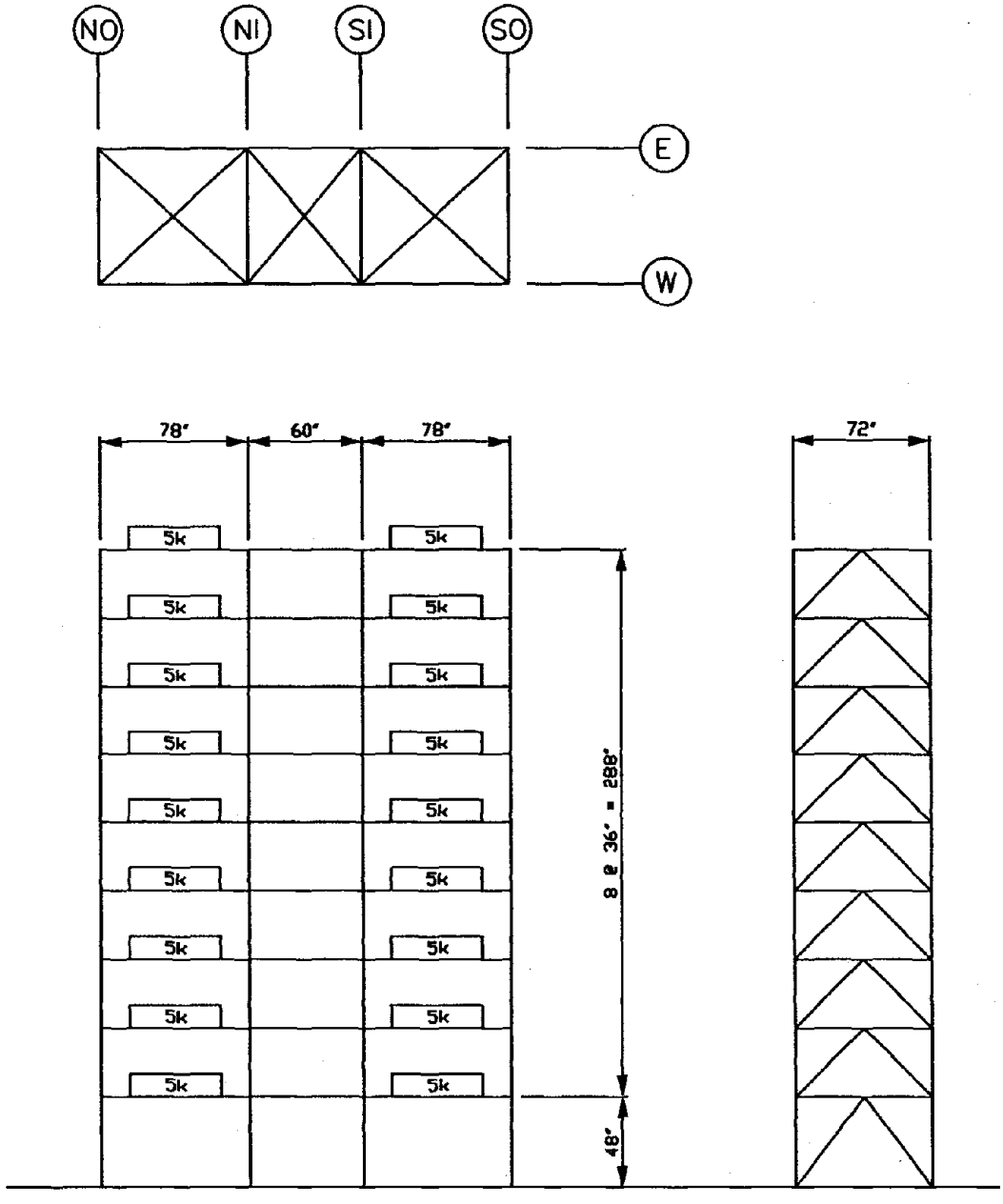

Fig. 2.11 Nine-Story MRF Model with Loading Distribution

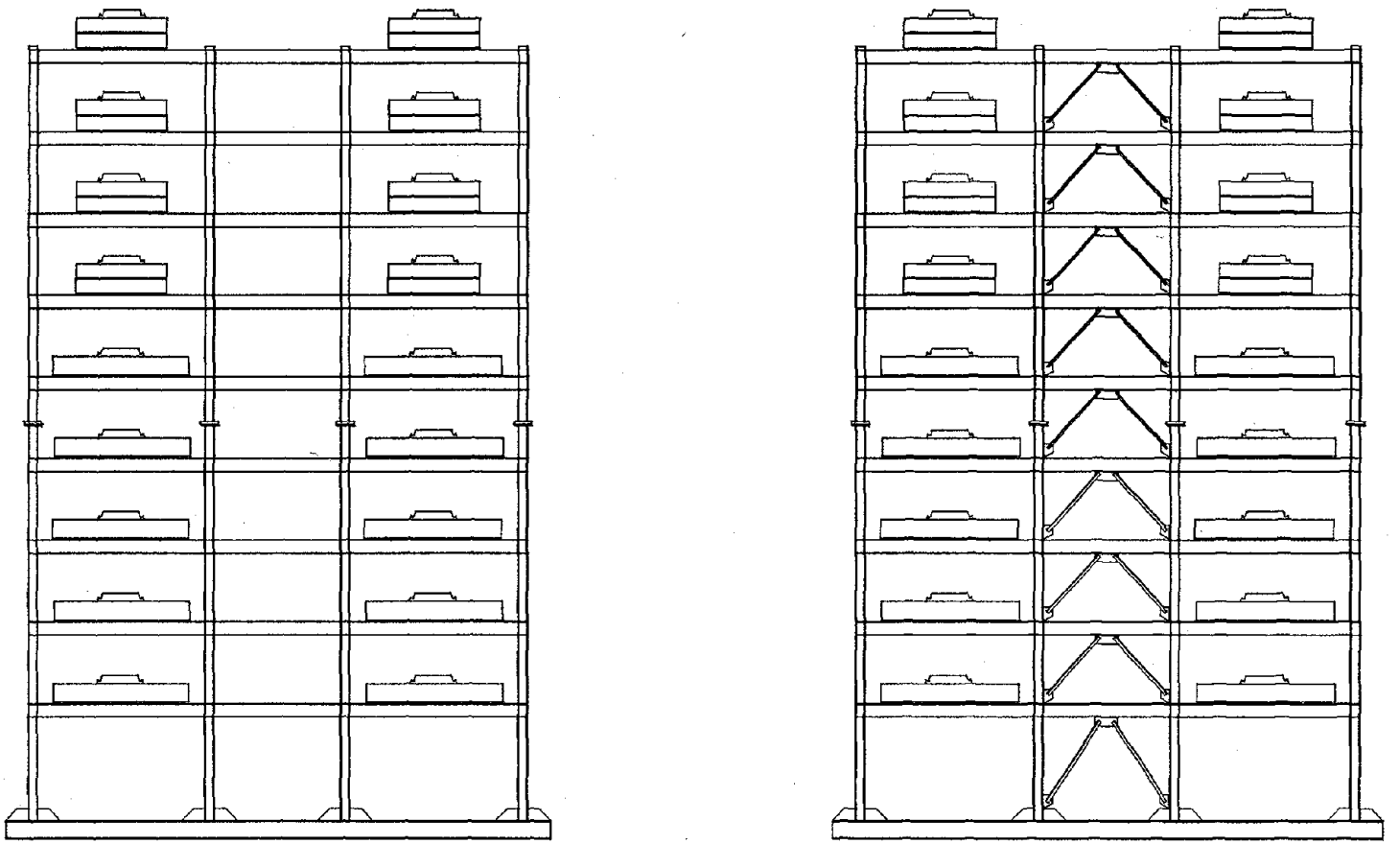

(a) MRF

(b) CBF

Fig. 2.12 MRF and CBF Configurations of Test Model

CHAPTER 3

EARTHQUAKE SIMULATOR TESTS

3.1 Introduction

This chapter describes the tests performed on the damped and undamped test structures. The earthquake simulator facilities of the Earthquake Engineering Research Center (EERC) of the University of California are also described. The instrumentation of the test structures is detailed and the earthquake motions used for the tests are presented. The chapter concludes with discussion of some of the computational methods used to analyze the experimental data.

3.2 Earthquake Simulator Test Facility

The central feature of the Earthquake Simulator Laboratory at EERC is the 20 ft by 20 ft earthquake simulator, or "shake table." At the time of testing the table was capable of producing two translational components of motion, one horizontal and one vertical, and is currently undergoing an upgrade to six degrees of freedom. These degrees of freedom can be programmed to reproduce any form of generalized dynamic motion, within the force, velocity, displacement, and frequency limits of the system.

The concrete table is heavily reinforced both with ordinary reinforcement and post-tensioning tendons. It is 12 inches thick and weighs 100,000 lb. The maximum test structure weight is approximately 130,000 lb. The shake table is driven by three 70 kip hydraulic actuators in the horizontal direction and four 25 kip actuators vertically. A passive stabilizing system is provided to control the pitching of the table caused by overturning moments generated in the test structure during excitation. The design and performance of the shake table are described by Rea and Penzien in [44], and its physical characteristics and performance specifications are summarized in Appendix B.

During operation, the hydraulics pit beneath the table is pressurized so that the self-weight of the table and test structure are carried by air pressure. Thus, the force demands on the vertical actuator system are only those necessary to cause the dynamic vertical motions. A 12-inch gap between the table and the surrounding foundation walls permits horizontal movement of the table. This gap is sealed by a 24-inch wide strip of reinforced nylon fabric. The table is supported by screw jacks in the pit when it is not pressurized.

3.3 Similitude and Scaling

The earthquake simulator experiments were performed using an existing model structure. The model was designed and built in 1976 for studies of the behavior of a building with column uplift permitted at the foundation level [41]. For the present series of tests a geometric scale factor of 1:4 was assumed, and scaling performed accordingly to satisfy geometric and loading parameters. To satisfy mass density requirements, additional concrete blocks and lead ballast were added to the model. The scaling relationships for artificial mass similitude are presented in Table 3.1. In addition to length and mass similitude requirements, scaling must also be performed in time. This requires that the excitation signals used be scaled by $\frac{1}{\sqrt{\text{geometric scale factor}}} = 1/2$; that is, the time-base of the scaled input signals must be halved. This halves the duration of the input signals and doubles the frequency content.

3.4 Data Acquisition and Analysis

A VAX 11-750 computer is the basis of the earthquake simulator data acquisition system, a block diagram of which is presented in Fig. 3.1. Pacific Signal Conditioners provide the excitation voltage to the transducers and amplify and filter the output signals. A Preston Multiplexer scans the output from the signal conditioners at a burst rate of 500 kHz. The scanning rate for the individual transducers is controlled by the data acquisition software and is variable to approximately 450 Hz per channel. For the tests described here, the sampling rate was 200 Hz for all channels and all tests. A Preston A/D Converter converts the analog output from

the multiplexer to digital form and the data is then stored on the hard disk of the VAX 11-750. The data acquisition system is configured to monitor 128 channels, but can be expanded to a maximum of approximately 170 channels by providing additional signal conditioners.

Data reduction and analysis are performed on the VAX 11-750 and a SUN 3/50 workstation network using an interactive data analysis and programming language [45]. This software provides an environment for graphics and has been expanded by a number of users to include bandpass filters, FFT routines, numerical integration and differentiation, response spectrum analysis and other signal analysis tools.

3.5 Instrumentation of Test Structure

3.5.1 MRF and CBF Configurations

Instrumentation for the MRF tests comprised a total of 42 channels, 9 of which monitored the response of the shake table (Table 3.2). The table channels measured table horizontal displacement, horizontal and vertical translational accelerations, pitch and roll rotational accelerations, and vertical displacements of three of the vertical actuators. Accelerometers were located at each floor of the test structure to record absolute accelerations. One accelerometer was located at each of floors 1 — 8, with two positioned at level 9. Two accelerometers were placed at the top of the structure oriented transversely to the axis of testing (the long plan dimension of the model). These accelerometers measured any out-of-plane accelerations associated with torsional response of the model. Linear potentiometer displacement transducers (LPs) measured the absolute displacement of each floor level from a fixed reference frame located off the shake table. Relative displacements were subsequently obtained by subtracting the table displacement from the absolute floor displacements. Two LPs were placed at each of levels 1 and 9, located on each side of the model on frames W and E, and a single LP was placed at each of levels 2 — 8. The primary instrumentation on the MRF for acceleration and displacement measurements is shown in Fig. 3.2. This instrumentation was the same for all configurations of the test structure. In addition to the acceleration and displacement response

instruments, strain gauge stations were located at the base of each of the columns on frame line W to measure the local behavior of the columns. This instrumentation was in place for the MRF, VD, and FD tests, and is shown in Fig. 3.3.

The instrumentation layout for the test structure in the CBF configuration was the same as that for the MRF, with the exclusion of the strain gauges at the column bases of frame line W. The CBF instrumentation is listed in Table 3.3.

3.5.2 Viscoelastically-Damped Configuration

A total of 72 channels was used for the tests of the VD model. The complete channel list for the VD model is presented in Table 3.4. The nine channels that monitored the behavior of the shake table were the same as those for the MRF tests (described in the previous section). The floor acceleration, floor displacement and column base force measurements are also as described for the MRF and shown in Fig. 3.2.

The behavior of the VE-damped braces was recorded at levels 1, 2, 3, 4, 6, and 8 of the VD model. At level 1 the braces on both frame lines W and E were instrumented, while at the upper levels only those on frame line W were instrumented. At each of these levels the brace instrumentation comprised two direct current differential transformers (DCDTs), one placed above and one below the VE damper to measure the shear deformations that occurred in the VE layers, and strain gauge bridges on each brace t-section calibrated to record the dynamic axial loads in the braces. The instrumentation for the VD model is shown in Fig. 3.3(a). The brace instrumentation permitted shear force versus shear deformation plots (hysteresis loops) to be obtained for the VE dampers.

In addition to the instrumentation described above, the temperature of one of the VE dampers was monitored throughout the earthquake test program. A thermocouple embedded in the one of the VE layers of the level 1E damper coupled with a digital display provided dynamic readout of temperature variation during tests.

3.5.3 Friction-Damped Configuration

A total of 72 channels (extended to 83 part-way through the FD test program) was used for the tests of the FD model (Table 3.5). The instrumentation layout was the same as for the VD tests, with the exception of the channels associated with the response of the friction dampers. All of the friction devices on frame line W were monitored during the tests, with the addition of the level 1 devices on frame line E. At each of these locations the instrumentation comprised one DCDT to measure the slip displacement of the friction device and 4-gauge strain bridges on the chevron brace SHS tube to measure the axial loads in the bracing. The instrumentation for the FD model is shown in Fig. 3.3(b). The forces in the friction devices were obtained by taking the appropriate components of the brace forces. Force-displacement relationships were obtained by plotting these resolved forces against the DCDT slip displacements.

After some of the tests were completed an additional 11 instrument channels were added to the model. Nine of these channels were DCDTs to measure displacements of the brace-damper connection assemblage, and the remaining two channels were accelerometers added at level 6 to investigate apparently faulty readings coming from the accelerometer at the floor. Inspection of the test data and visual observations during testing indicated that there was some slight elastic deformation of the chevron brace assemblage occurring. The additional instrumentation was included to quantify these observations. Eight of the DCDTs were added to measure vertical displacements (subsequently giving rotations) of the brace-damper connection assemblage at levels 1, 2, and 3. The remaining DCDT was placed to measure the relative displacement between the first floor of the model and the top of the brace-damper connection assemblage at that level.

3.6 Types of Tests Performed and Signals Used

3.6.1 Diagnostic Tests

Diagnostic tests were performed on each test structure to evaluate its dynamic properties prior to the earthquake tests. The different types of diagnostic tests are described in the following sections.

Pull-Back Free Vibration Tests

Free vibration tests of the model in the various test configurations were conducted by applying a (static) lateral load to the structure and then rapidly releasing the load. This was achieved in practice using a wire cable and chain block arrangement. A short length of approximately 5/8-inch diameter steel rod was connected in-line with the cable adjacent to the chain block. Once the required lateral load was applied, bolt cutters were used to sever the rod and initiate the free vibration. A schematic diagram of the test set up is shown in Fig. 3.4. This procedure was undertaken with the load applied at level 3 and level 5. Practical constraints prevented pulling the model any higher than at level 5, nonetheless, it was hoped that by pulling at at least two different levels free vibration response would be induced in at least the first two or three modes of the model. All of the instrument channels were monitored during the free vibration decay.

The shake table was inactive during the free vibration tests, with motion prevented by locking it against the surrounding foundation. The dynamic properties of any test structure on the shake table are influenced by table-structure interaction effects. Thus, with the table locked and inactive for the pull-back free vibration tests the dynamic properties determined for the test structure will vary somewhat from those obtained from tests conducted when the table is active. This is discussed further, and results indicating this are presented in Sec. 4.2.

Random Excitation Tests

A random excitation (or white noise) input was used to achieve low-level excitation of the first few modes of the test structure. The random excitation signal has an approximately flat

FFT spectrum in the frequency range 0–10 Hz, and thus excited the test structure strongly in those modes with frequencies below 10 Hz. The MRF model has its first three frequencies below 10 Hz and strong response was seen in these modes, while for the CBF, VD, and FD configurations only two frequencies were in this range and response in the third mode was not well defined by this signal. The table acceleration, acceleration FFT, and linear elastic response spectra for the random-800 signal are presented in Fig. 3.5. The frequency, mode shape, and damping properties determined from the random excitation tests were obtained with the shake table active, and thus included the effects of table-structure interaction.

Pulse Free Vibration Tests

To evaluate any change in the dynamic characteristics of the test structure due to damage, free vibration tests of the models were performed periodically throughout the course of the earthquake test programs. These tests consisted of inputting a small amplitude displacement square-wave (pulse) to the shake table. The table displacement and acceleration signals for a typical pulse test are shown in Fig. 3.6. The free vibration decays were recorded and analyzed to determine the natural frequencies and damping ratios of the test structures. This type of test differs from the pull-back type of free vibration test in that the dynamic properties obtained are representative of the model on the active or soft foundation provided by the shake table. The frequencies determined from this type of test will be lower than those found from the pull-back test, while the damping ratios will be higher because of the damping contribution of the hydraulic actuators. The pulse tests also provided useful information on the dynamic characteristics of the table-model system for use in the dynamic analyses (see Sec. 5.3).

3.6.2 Earthquake Tests

Details of the earthquakes in which the records used for testing were obtained are presented in Table 3.6. Included in the table is a column headed "EERC Name", which lists the abbreviated notation used throughout this report (and at EERC) to refer to each of the test signals. Table 3.7 provides expanded information on each of the test signals. The earthquake or

record name, time scale, scaled duration, and the time interval of the input signal (dt) for each test signal are also listed.

The command signal for the shake table is a displacement signal, the maximum value of which is referred to as the "span" of the input. The maximum horizontal displacement of the table is 5 inches, which corresponds to a span of 1000. Thus, a span of 200 refers to an input signal with a maximum displacement of 1 inch, and a span of 500 to a maximum displacement of 2.5 inches. Throughout the remainder of this research the individual tests performed are referred to using the EERC name of the signal, and the horizontal span setting for that particular test. For example, the abbreviation ec-300 refers to the El Centro input at a horizontal span of 300, and zaca-750 refers to the Zacatula signal input at a horizontal span of 750. A suffix of "1" on the EERC name indicates that no filtering has been applied to the signal, while a suffix of "2" indicates that the signal has been highpass filtered at 0.07 — 0.1 Hz. The numerical suffixes (and the ".al" suffix on unio.al and zaca.al) on the various signals have been dropped to simplify notation.

The following comments provide a brief description of the frequency and energy content characteristics of the time-scaled signals. All of the test signals contain an initial one second of zero motion and wherever reference is made in the following descriptions to the time-base of the signal, it is with respect to the time-scaled test signal including the one-second lead-in; not to the original, unscaled record.

El Centro S00E, 18 May 1940 — the frequency content is strongest between 1 and 3 Hz, and most of the energy is concentrated between 2.5 and 4 seconds into the signal.

Taft S69E, 21 July 1952 — the frequency content is broadly spread between 1 and 6 Hz, and most of the energy is contained in the first 6 seconds of the signal, with one short burst at approximately 5.5 seconds.

San Francisco S80E, 22 March 1957 — this is a particularly high-frequency motion, with the frequency content strongest between 3 and 10 Hz. Almost the entire energy content is

contained between 2 and 3.5 seconds into the signal.

Parkfield N65E, 27 June 1966 — the frequency content is strongest between 1 and 4 Hz and almost all of the energy is contained between 3 and 5 seconds into the motion.

Pacoima Dam S14W, 9 February 1971 — the frequency content is strongest between 1 and 2 Hz, being dominated by a large pulse at the 3 second mark. Most of the energy of the signal is also associated with this pulse.

Bucharest EW, 7 March 1977 — this is a low-frequency motion with the frequency content concentrated between 0.5 and 2 Hz and most of the energy contained between 3 and 5 seconds into the motion.

Miyagi-Ken-Oki N00E, 12 June 1978 — the frequency content is strongest at and around 2 Hz, and the energy is broadly contained throughout the signal with distinct bursts between 5 and 8 seconds and 9 and 10 seconds.

Two versions of the Llolleo N10E record were used in the study: "chile.s", an unscaled 36 second signal containing the strong motion portion of the record, and "chile.u", the same signal but with time scaling applied to approximately double the frequency of the signal, thus reducing the duration to 15 seconds.

Llolleo N10E, 3 March 1985 (chile.s) — the frequency content is broadly contained between 0.5 and 9.5 Hz and 11 and 14 Hz, being strongest between 0.5 and 3 Hz. The energy is broadly contained over the 10 to 28 second portion of the signal.

Llolleo N10E, 3 March 1985 (chile.u) — the frequency content is broadly contained between 1 and 8 Hz, while the energy is almost evenly contained throughout the duration of the signal, particularly between 2 and 5 seconds, and 7 and 12 seconds.

Mexico City SCT E00W, 19 September 1985 — this is a low-frequency motion, with the frequency concentrated almost entirely at 1 Hz. The energy is broad, although mostly contained

between the 19 and 23 second marks of the signal.

La Union N00E, 19 September 1985 — the frequency content is broad, being strongest between 0.5 and 6 Hz. The energy content is also broad, with bursts at 8 to 10 seconds and 13 to 15 seconds.

Zacatula S00E, 19 September 1985 — the frequency content is broad, between 0.5 and 9 Hz, although strongest between 2 and 2.5 Hz. The energy is concentrated in two bursts, between 3 and 10 seconds, and 20 and 23 seconds.

The following two signals are synthesized motions intended to match the soil-type S1 spectrum specified by ATC 3-06 [46] :

ATC-S1, El Centro-based — the frequency content is broadly contained between 0.5 and 7 Hz, being strongest between 1 and 3 Hz. The energy content is also broad, although mostly between 3 and 9 seconds.

ATC-S1, Taft-based — the frequency content is strongest between 0.5 and 3.5 Hz, and the energy content is broadly spread between the 7 and 16 second marks of the signal.

Representative acceleration and displacement time histories and linear elastic response spectra for all of these motions are presented in Figs. 3.7 — 3.20. These figures are plotted for actual shake table response signals obtained in the test program.

3.7 Test Programs

The tests for each model are presented in the following sections in terms of the various test signals and ordered by increasing input, rather than in the original chronological sequence.

3.7.1 MRF Model

The tests performed on the MRF are listed in Table 3.8. A brief description of the tests is presented below.

Diagnostic Tests

The MRF model was subjected to two random input signals and also to a total of five pulse tests during the course of the earthquake tests.

Earthquake Tests

Six different earthquake motions were used to test the MRF model. The El Centro signal was input at four different intensity levels, while the remaining five signals (Taft, Miyagi, Chile.u, La Union and Zacatula) were each input at two different intensity levels.

3.7.2 CBF Model

The tests performed on the CBF are listed in Table 3.9. These tests were conducted as part of a previous research program, in which only a few tests were performed on the model in a CBF configuration. It was not possible to perform further tests of the CBF during the current investigation.

Diagnostic Tests

The diagnostic tests performed on the CBF consisted of a random input signal and a pulse test.

Earthquake Tests

Three earthquake motions were used to test the CBF model. The El Centro and Miyagi signals were each input at three different intensity levels and the Mexico City signal was input at one intensity level.

3.7.3 Viscoelastically-Damped Model

The tests performed on the VD model are listed in Table 3.10. A brief description of the tests is presented below.

Diagnostic Tests

A total of thirteen diagnostic tests were performed on the VD model. Pull-back tests were performed for applied loading at levels 3 and 5 (two tests at each level). Two random input signals and seven pulse tests were also performed. The pulse tests were performed throughout the course of the earthquake test program.

Earthquake Tests

Eight different earthquake motions were used to test the VD model. The input intensities for the different signals are listed in Table 3.10. The El Centro, Taft, and Miyagi signals were each input at eight different intensity levels, Bucharest was input at three intensity levels, San Francisco at only one intensity level, and the remaining three signals, Pacoima Dam, Parkfield, and Mexico City were each input at two different intensity levels.

El Centro Control Tests

Throughout the course of the earthquake test program six ec-150 tests were performed to investigate any degradation or change in the performance of the VE dampers, typically at the start and end of the daily test schedule.

3.7.4 Friction-Damped Model

The tests performed on the FD model are listed in Table 3.11. A brief description of the tests follows.

Diagnostic Tests

Free-vibration, random excitation, and pulse tests were performed on the FD model. The very first tests of the FD model consisted of four pull-back free vibration tests. These comprised two tests with the applied load at level 3 and two tests with the applied load at level 5. At the very conclusion of the entire FD test program, a further two pull-back tests were performed, with applied loads at level 3 and level 5. Four random excitation tests (at increasing input level) were performed immediately following the pull-back tests at the start of the

test program, two were performed midway through the test program, and a further two were performed at the conclusion of the test program. Throughout the course of the earthquake tests a total of ten pulse tests were performed.

Earthquake Tests

Fourteen different earthquake motions were used to test the FD model; the eight motions used to test the VD model plus an additional six motions. These were two versions of the Llolleo N10E record (chile.s and chile.u) from the 1985 Chile earthquake, the La Union and Zacatula records from the 1985 Michoacan earthquake, and two synthesized signals, ecatc.s1 and taftatc.s1. The different input intensities for each of the earthquake motions are presented in Table 3.11.

3.8 Data Reduction

3.8.1 Filtering

All data channels were passed through signal conditioners that removed all frequency components of the signals above 100 Hz at the time of data acquisition. Subsequent filtering during data reduction used an Ormsby time-domain lowpass filter to remove all frequency components above 20 Hz. This filter corner was chosen for the following reasons: the first three modes of vibration of all of the test structures were contained below 20 Hz, the resonance of the oil column in the hydraulic actuators at 14-16 Hz distorts the response of the shake table above 16 Hz, and the Fourier amplitude spectra of all of the test signals (described in Sec. 2.6.2) were negligible above 20 Hz. Highpass filtering or baseline drift correction was found not to be necessary for any of the recorded data channels.

3.8.2 Computation of Various Response Quantities

(a) Story Displacements

The displacements of the floors of the test structure relative to the ground (shake table) were obtained by subtracting the table displacement from the measured absolute floor

displacements.

(b) Brace Forces/Device Forces

VD Model

The strain gauge bridges on the t-section braces were calibrated to provide brace axial force directly. The forces in the pair of t-sections attached to each VE damper were summed to obtain the damper shear force.

FD Model

The axial forces in the SHS braces were obtained from 4-gauge Poisson strain bridges calibrated to provide axial force directly. The forces in the friction devices were obtained by calculating the horizontal components of the brace forces and summing each pair connected to a device. In the case of the double-damper arrangement at the bottom level of the model, the forces in the individual dampers could not be determined, rather the resolved brace forces corresponded to the total force in both of the dampers.

(c) Story Shear Forces

The story shear force at each level of the test model was calculated by summation of the inertia forces of the floors above the level under consideration. The inertia forces were found by calculating the product of the floor acceleration and the corresponding floor mass. This approach is based on the assumption that the equation of motion can be written as

$$f_S = -f_I \tag{3.1}$$

where f_S = restoring force (story shear force)
f_I = inertial force

and that the damping force, f_D, is negligible and need not be considered. This is usually reasonable. Thus, the story shear force at level i is expressed by

$$V_{s_i} = \sum_{j=i+1}^{n} (m_j \ddot{v}_{t_j}) \tag{3.2}$$

where m_j = mass of level j

$\ddot{v}_{t_j}$ = absolute acceleration of level j

(d) Energy Input and Dissipation

The primary purpose of incorporating energy-absorbing devices in a structure is, as their name implies, to absorb energy. The behavior of the damped structures was studied to investigate the distribution and dissipation of the energy input to the structure during earthquake excitation.

The energy equations for SDOF and MDOF systems subjected to (seismic) ground motion input are developed in Appendix C. These equations and the notation adopted are consistent with those used by previous researchers [8,47]. The practical computation of the various terms in the energy equation, Eq. C.7, are described in the following sections.

Input Energy, E_I

The input energy (E_I) is the time integral of the input power

$$E_I = \int P_I dt = \int \left(\sum_{i=1}^{n} m_i \ddot{v}_{t_i} \right) dv_g$$

$$= \int \left(\sum_{i=1}^{n} m_i \ddot{v}_{t_i} \right) \dot{v}_g dt \tag{3.3}$$

where P_I is the input power, and the other terms are as described in Appendix C. From Eq. 3.3, it can be seen that E_I is equal to the product of the base shear and the ground motion velocity for the case of the base shear evaluated using the inertial force method. Strictly, the use of Eq. 3.3 to compute the input energy is conceptually incorrect, since it ignores the internal damping force. Actually,

$$V_b = \sum_{i=1}^{n} m_i \ddot{v}_{t_i} + f_D \tag{3.4}$$

and not just the term in parentheses in Eq. 3.3. However, it has been shown by other researchers [47] that f_D is negligible and that the approximation is reasonable.

Kinetic Energy, E_K

For the absolute energy formulation (as presented in Appendix C) the kinetic energy (E_K) is proportional to the square of the absolute velocity, $\dot{v}_t^2$. From Eq. C.11,

$$E_K = \frac{1}{2}\underline{\dot{v}}_t^T \underline{m}\underline{\dot{v}}_t = \frac{1}{2}\sum_{i=1}^{n} m_i(\dot{v}_{t_i})^2 \tag{3.5}$$

where the terms are as defined in Appendix C. The absolute velocity of each level was calculated by differentiating the measured absolute floor displacements.

Elastic Strain Energy, E_S

The elastic strain energy (E_S), together with the kinetic energy, is a recoverable energy quantity. E_S may be calculated as

$$E_S = \sum_{i=1}^{n} \frac{V_i^2}{2K_i} \tag{3.6}$$

where K_i is the loading stiffness of the story shear force-interstory drift relationship for the i-th level (this assuming that the story response remains elastic), and V_i is the story shear force at the i-th level. K_i was calculated as the slope of the least-squares, best-fit straight line to the story shear force-interstory drift relationship.

Dissipated Energy, E_D

The dissipated energy (E_D) is an irrecoverable energy quantity. Because the response of the undamped MRF never entered the inelastic range throughout the entire test program (see Chapter 4), the primary source of energy dissipation in the damped structures was the energy-absorbing devices. The calculation of the irrecoverable dissipated energy involved the calculation of the energy dissipated by each of the viscoelastic or friction devices in the structure.

(a) Viscoelastic Dampers

The energy dissipated by a VE damper can be calculated from

$$E_D = \int f_{vd}\, d\delta_{vd} - \frac{1}{2} K_e \delta_{vd}^2 \tag{3.7}$$

where f_{vd} = force in damper
δ_{vd} = shear deformation of damper
K_e = effective stiffness of damper

The first term represents the area of the damper shear force-deformation hysteresis loop, and the second is the recoverable elastic energy stored by the damper during excitation. If the damper returns to its initial displacement position at the end of the excitation then the elastic stored energy at the end of the motion is zero. Thus, the total energy dissipated by a VE damper during earthquake excitation is simply the damper force multiplied by the damper displacement and integrated over the duration of the motion.

(b) Friction Dampers

The friction dampers were (reasonably) assumed to be incapable of storing elastic energy. This assumption simplifies Eq. 3.7 and the energy dissipated by a friction damper can be calculated from

$$E_D = \int f_{fd}\, d\delta_{fd} \tag{3.8}$$

Since the Sumitomo friction dampers slip at an almost exactly constant friction force, Eq. 3.8 could be further simplified to

$$E_D = f_{slip} \int |d\delta_{fd}| \ ,$$

however, the more exact expression of Eq. 3.8 was used in this research.

Viscous-Damped Energy, E_ξ

The viscous-damped energy (E_ξ) is a notoriously difficult quantity to determine explicitly from shake table tests. Its computation has been addressed by other researchers [8,47] who

have not calculated it explicitly, but rather defined it as the remaining unknown in the energy equation (Eq. C.7). That is,

$$E_{\xi} = E_I - E_K - E_S - E_D \tag{3.9}$$

This relationship is not used in this research. In fact, no quantity representing the "viscous-damped" energy has been explicitly defined. Instead, the remaining unattributed energy quantity, the left-hand side of Eq. 3.9, is considered to be viscous damping *and* energy-losses due to other mechanisms present in the test structures. Some of these are discussed in Sec. 4.3.3.

TABLE 3.1 Similitude Scaling Relationships

PARAMETER	SCALING	$\frac{\text{PROTOTYPE}}{\text{1/4–SCALE MODEL}}$
length	L	4
time	$\sqrt{L}$	2
mass	L^2	16
displacement	L	4
acceleration	1	1
stress	1	1
strain	1	1
force	L^2	16
area	L^2	16
moment of inertia	L^4	256

TABLE 3.2 Instrumentation List For MRF Model

CHANNEL	INSTR.	VARIABLE	CHANNEL	INSTR.	VARIABLE
1	DCDT	table h1 displ	23	POT	level 2 displ
2	DCDT	table h2 displ	24	POT	level 3 displ
3	ACCL	table horiz accel	25	POT	level 4 displ
4	ACCL	table vert accel	26	POT	level 5 displ
5	ACCL	table pitch accel	27	POT	level 6 displ
6	ACCL	table roll accel	28	POT	level 7 displ
8	DCDT	table v1 displ	29	POT	level 8 displ
9	DCDT	table v2 displ	30	POT	level 9E displ
10	DCDT	table v4 displ	31	POT	level 9W displ
11	ACCL	level 1 accel	62	SG4	col NO shear
12	ACCL	level 2 accel	63	SG4	col NI shear
13	ACCL	level 3 accel	64	SG4	col SI shear
14	ACCL	level 4 accel	65	SG4	col SO shear
15	ACCL	level 5 accel	66	SG2	col NO moment
16	ACCL	level 6 accel	67	SG2	col NI moment
17	ACCL	level 7 accel	68	SG2	col SI moment
18	ACCL	level 8 accel	69	SG2	col SO moment
19	ACCL	level 9E accel	70	ACCL	level 6a accel
20	ACCL	level 9W accel	71	ACCL	level 6w accel
21	POT	level 1E displ	72	ACCL	9N trans accel
22	POT	level 1W displ	73	ACCL	9S trans accel

ACCL — Accelerometer

DCDT — Direct Current Differential Transformer

POT — Linear Potentiometer Displacement Transducer

SG2 — 2-gauge moment bridge

SG4 — 4-gauge axial or shear bridge

TABLE 3.3 Instrumentation List For CBF Model

CHANNEL	INSTR.	VARIABLE	CHANNEL	INSTR.	VARIABLE
1	DCDT	table avg hdispl	21	ACCL	level 9 accel
2	DCDT	table avg vdispl	22	ACCL	level 9N trans accel
3	ACCL	table horiz accel	23	ACCL	level 9S trans accel
4	ACCL	table vert accel	24	POT	level 1 displ
5	ACCL	table pitch accel	25	POT	level 2 displ
6	ACCL	table roll accel	26	POT	level 3 displ
7	ACCL	table twist accel	27	POT	level 4 displ
8	DCDT	table v1 displ	28	POT	level 5 displ
9	DCDT	table v2 displ	29	POT	level 6 displ
10	DCDT	table v3 displ	30	POT	level 7 displ
11	-	input signal	31	POT	level 8 displ
12	VT	table horiz vel	32	POT	level 9W displ
13	ACCL	level 1 accel	33	POT	level 9E displ
14	ACCL	level 2 accel	52	DCDT	table h1 displ
15	ACCL	level 3 accel	53	DCDT	table h2 displ
16	ACCL	level 4 accel	54	PTRANS	pstab1
17	ACCL	level 5 accel	55	PTRANS	pstab2
18	ACCL	level 6 accel	56	PTRANS	pstab3
19	ACCL	level 7 accel	57	PTRANS	pstab4
20	ACCL	level 8 accel			

ACCL — Accelerometer

DCDT — Direct Current Differential Transformer

POT — Linear Potentiometer Displacement Transducer

PTRANS — pressure transducer in actuator

VT — velocity transducer

TABLE 3.4 Instrumentation List for VD Model

CHANNEL	INSTR.	VARIABLE	CHANNEL	INSTR.	VARIABLE
1	DCDT	table h1 displ	37	DCDT	3Wl damper displ
2	DCDT	table h2 displ	38	DCDT	3Wu damper displ
3	ACCL	table horiz accel	39	DCDT	3Wl damper displ
4	ACCL	table vert accel	40	DCDT	4Wu damper displ
5	ACCL	table pitch accel	41	DCDT	4Wl damper displ
6	ACCL	table roll accel	42	DCDT	6Wu damper displ
8	DCDT	table v1 displ	43	DCDT	6Wl damper displ
9	DCDT	table v2 displ	46	DCDT	8Wu damper displ
10	DCDT	table v3 displ	47	DCDT	8Wl damper disp
11	ACCL	level 1 accel	48	SG4	1Wa brace force
12	ACCL	level 2 accel	49	SG4	1Wb brace force
13	ACCL	level 3 accel	50	SG4	1Ea brace force
14	ACCL	level 4 accel	51	SG4	1Eb brace force
15	ACCL	level 5 accel	52	SG4	2Wa brace force
16	ACCL	level 6 accel	53	SG4	2Wb brace force
17	ACCL	level 7 accel	54	SG4	3Wa brace force
18	ACCL	level 8 accel	55	SG4	3Wb brace force
19	ACCL	level 9E accel	56	SG4	4Wa brace force
20	ACCL	level 9W accel	57	SG4	4Wb brace force
21	POT	level 1 East	58	SG4	6Wa brace force
22	POT	level 1 West	59	SG4	6Wb brace force
23	POT	level 2 displ	60	SG4	8Wa brace force
24	POT	level 3 displ	61	SG4	8Wb brace force
25	POT	level 4 displ	62	SG4	col NO shear
26	POT	level 5 displ	63	SG4	col NI shear
27	POT	level 6 displ	64	SG4	col SI shear
28	POT	level 7 displ	65	SG4	col SO shear
29	POT	level 8 displ	66	SG4	col NO moment
30	POT	level 9E displ	67	SG4	col NI moment
31	POT	level 9W displ	68	SG2	col SI moment
32	DCDT	1Wu damper displ	69	SG2	col SO moment
33	DCDT	1Wl damper displ	70	ACCL	level 6a accel
34	DCDT	1Eu damper displ	71	ACCL	level 6w accel
35	DCDT	1El damper displ	72	ACCL	9N trans accel
36	DCDT	2Wu damper displ	73	ACCL	9S trans accel

ACCL — Accelerometer

DCDT — Direct Current Differential Transformer

POT — Linear Potentiometer Displacement Transducer

SG2 — 2-gauge moment bridge

SG4 — 4-gauge axial or shear bridge

TABLE 3.5 Instrumentation List For FD Model

CHANNEL	INSTR.	VARIABLE	CHANNEL	INSTR.	VARIABLE
1	DCDT	table h1 displ	44	SG4	1NW brace force
2	DCDT	table h2 displ	45	SG4	1SW brace force
3	ACCL	table horiz accel	46	SG4	1NE brace force
4	ACCL	table vert accel	47	SG4	1SE brace force
5	ACCL	table pitch accel	48	SG4	2N brace force
6	ACCL	table roll accel	49	SG4	2S brace force
8	DCDT	table v1 displ	50	SG4	3N brace force
9	DCDT	table v2 displ	51	SG4	3S brace force
10	DCDT	table v3 displ	52	SG4	4N brace force
11	ACCL	level 1 accel	53	SG4	4S brace force
12	ACCL	level 2 accel	54	SG4	5N brace force
13	ACCL	level 3 accel	55	SG4	5S brace force
14	ACCL	level 4 accel	56	SG4	6N brace force
15	ACCL	level 5 accel	57	SG4	6S brace force
16	ACCL	level 6 accel	58	SG4	7N brace force
17	ACCL	level 7 accel	59	SG4	7S brace force
18	ACCL	level 8 accel	60	SG4	8N brace force
19	ACCL	level 9E accel	61	SG4	8S brace force
20	ACCL	level 9W accel	62	SG4	9N brace force
21	POT	level 1E displ	63	SG4	9S brace force
22	POT	level 1W displ	64	SG4	col NO shear
23	POT	level 2 displ	65	SG4	col NI shear
24	POT	level 3 displ	66	SG4	col SI shear
25	POT	level 4 displ	67	SG4	col SO shear
26	POT	level 5 displ	68	SG2	col NO moment
27	POT	level 6 displ	69	SG2	col NI moment
28	POT	level 7 displ	70	SG2	col SI moment
29	POT	level 8 displ	71	SG2	col SO moment
30	POT	level 9E displ	72	ACCL	9N trans accel
31	POT	level 9W displ	73	ACCL	9S trans accel
32	DCDT	1NE damper displ	74 *	SG4	1NW brace force
33	DCDT	1NW damper displ	75 *	SG4	1SW brace force
34	DCDT	1SE damper displ	76 *	SG4	1NE brace force
35	DCDT	1SW damper displ	77 *	SG4	1SE brace force
36	DCDT	2 damper displ	78 *	SG4	2NW brace force
37	DCDT	3 damper displ	79 *	SG4	2SW brace force
38	DCDT	4 damper displ	80 *	SG4	3NW brace force
39	DCDT	5 damper displ	81 *	SG4	3SW brace force
40	DCDT	6 damper displ	82 *	ACCL	level 6a accel
41	DCDT	7 damper displ	83 *	ACCL	level 6w accel
42	DCDT	8 damper displ	84 *	DCDT	1W brace displ
43	DCDT	9 damper displ			

* channels added part-way through test program

Abbreviations as for Table 3.4

TABLE 3.6 Earthquake Ground Motions Used in Study

EARTHQUAKE	RECORD	EERC NAME	COMP	MAG	PGA [g]	SITE GEOLOGY	ED [km]	FD [km]
Imperial Valley May 18, 1940	El Centro	ec2	S00E	6.7	0.35	30m stiff clay volcanic rock	-	-
Kern County July 21, 1952	Taft Lincoln School Tunnel	taft2	S69E	7.7	0.18	alluvium	-	-
Daly City March 22, 1957	Golden Gate Park	sf2	S80E	5.3	0.10	-	-	8.5
Parkfield June 27, 1966	Cholame, Shandon Array No. 2	park2	N65E	5.5	0.49	-	-	-
San Fernando February 9, 1971	Pacoima Dam	pac2	S14W	6.4	1.08	jointed rock	-	8.4
Romania March 4, 1977	Bucharest, Bldg Res. Inst.	buc1	EW	7.2	0.21	12m clay over deep gravel dep.	150	110
Miyagi-Ken-Oki June 12, 1978	Tohuku Univ. Sendai	miyagi	N00E	7.4	0.25	alluvium	115	30
Chile March 3, 1985	Llolleo	chile.u chile.s	N10E	7.8	0.67	sandstone and volcanic rock	45	33
Michoacan September 19, 1985	SCT Mexico City	sct.o	E00W	8.1	0.20	very soft clay	350	18
Michoacan September 19, 1985	La Union	unio.al	N00E	8.1	0.17	rock	84	16
Michoacan September 19, 1985	Zacatula	zaca.al	S00E	8.1	0.28	alluvium	17	16

ED = Epicentral distance
FD = Focal Depth

TABLE 3.7 Input Signals for Tests

EARTHQUAKE/ RECORD	EERC NAME	TIME SCALE	DURATION [sec]	SIGNAL dt [sec]
El Centro	ec2	1/2	19	0.01
Taft	taft2	1/2	19	0.01
Golden Gate Park	sf2	1/2	12	0.01
Parkfield	park2	1/2	14	0.01
Pacoima Dam	pac2	1/2	12	0.01
Bucharest	buc1	1/2	12	0.01
Miyagi-Ken-Oki	miyagi	1/2	13	0.000905
Llolleo (Chile)	chile.u	-	15	0.0015
Llolleo (Chile)	chile.s	-	36	0.03226
Mexico City - SCT (Michoacan)	sct.o	1/2	33	0.01
La Union (Michoacan)	unio.al	1/2	23	0.005
Zacatula (Michoacan)	zaca.al	1/2	23	0.005
El Centro-based	ecatc.s1	1/2	23	0.01
Taft-based	taftatc.s1	1/2	23	0.01

Duration and Signal dt are functions of the time-scale

Sampling rate = 0.005 sec. (200 Hz) for all tests

TABLE 3.8 List of Tests Performed on MRF Model

FILE	SIGNAL	SPAN	PGA [g]	PRA [g]	PRD [in.]
890322.19	random30.d	200	-	-	-
890322.39	random30.d	200	-	-	-
890322.20	pulse	50	-	-	-
890322.27	pulse	50	-	-	-
890322.29	pulse	50	-	-	-
890322.35	pulse	50	-	-	-
890322.38	pulse	50	-	-	-
890322.21	ec2	50	0.141	0.474	0.696
890322.28	ec2	200	0.461	1.417	2.635
890322.36	ec2	300	0.604	1.480	3.102
890322.37	ec2	400	0.806	1.607	3.304
890322.22	taft2	50	0.091	0.182	0.265
890322.30	taft2	200	0.362	0.791	1.101
890322.23	miyagi	50	0.101	0.247	0.545
890322.31	miyagi	200	0.228	0.968	2.319
890322.26	chile.u	50	0.126	0.386	0.610
890322.34	chile.u	200	0.395	1.213	2.384
890322.24	unio.al	50	0.070	0.239	0.530
890322.32	unio.al	250	0.324	1.144	2.465
890322.25	zaca.al	50	0.084	0.183	0.267
890322.33	zaca.al	250	0.233	0.735	1.336

TABLE 3.9 List of Tests Performed on CBF Model

FILE	SIGNAL	SPAN	PGA [g]	PRA [g]	PRD [in.]
870618.01	random30.d	200	-	-	-
870618.02	pulse	20	-	-	-
870618.03	ec2	50	0.091	0.353	0.352
870618.05	ec2	100	0.184	0.635	0.719
870618.06	miyagi	50	0.061	0.196	0.216
870618.07	miyagi	75	0.095	0.281	0.327

PGA = Peak Ground (Table) Acceleration
PRA = Peak Roof Acceleration
PRD = Peak Roof Displacement

TABLE 3.10 List of Tests Performed on VD Model

FILE	SIGNAL	SPAN	PGA [g]	PRA [g]	PRD [in.]
890316.01	free vibration	level 3	-	-	-
890316.02	free vibration	level 3	-	-	-
890316.03	free vibration	level 5	-	-	-
890316.04	free vibration	level 5	-	-	-
890316.05	random30.d	600	-	-	-
890316.06	random30.d	800	-	-	-
890316.07	pulse	50	-	-	-
890317.07	pulse	50	-	-	-
890317.15	pulse	50	-	-	-
890317.24	pulse	50	-	-	-
890320.01	pulse	50	-	-	-
890320.08	pulse	50	-	-	-
890320.17	pulse	50	-	-	-
890317.16	ec2	150	-	-	-
890317.25	ec2	150	-	-	-
890320.02	ec2	150	-	-	-
890320.09	ec2	150	-	-	-
890320.18	ec2	150	-	-	-
890316.08	ec2	50	0.145	0.291	0.355
890316.09	ec2	100	0.227	0.490	0.712
890317.06	ec2	150	0.319	0.673	1.098
890317.08	ec2	200	0.402	1.019	1.455
890317.13	ec2	250	0.486	0.943	1.686
890317.22	ec2	300	0.561	1.084	2.038
890320.05	ec2	300	0.559	1.031	1.998
890320.14	ec2	400	0.753	1.303	2.532

TABLE 3.10 cont. List of Tests Performed on VD Model

FILE	SIGNAL	SPAN	PGA [g]	PRA [g]	PRD [in.]
890317.01	taft2	50	0.092	0.188	0.297
890317.02	taft2	100	0.190	0.459	0.586
890317.09	taft2	150	0.292	0.643	0.713
890317.10	taft2	200	0.394	0.879	0.935
890317.14	taft2	250	0.485	0.833	1.183
890317.23	taft2	300	0.586	0.952	1.286
890320.06	taft2	300	0.592	0.998	1.265
890320.15	taft2	400	0.821	1.365	1.717
890317.03	miyagi	50	0.115	0.204	0.242
890317.04	miyagi	100	0.159	0.341	0.493
890317.05	miyagi	150	0.180	0.495	0.772
890317.11	miyagi	200	0.217	0.544	1.025
890317.12	miyagi	275	0.270	0.784	1.618
890320.07	miyagi	300	0.316	0.993	2.140
890320.13	miyagi	350	0.413	1.095	2.374
890320.16	miyagi	400	0.534	1.199	2.736
890317.17	pac2	220	0.272	0.508	0.902
890320.10	pac2	350	0.461	0.835	1.590
890317.18	park2	220	0.284	0.441	0.568
890320.11	park	350	0.410	0.617	0.912
890317.19	sf2	200	0.884	1.730	1.301
890317.20	buc1	200	0.200	0.462	0.785
890320.03	buc1	200	0.225	0.462	0.809
890320.12	buc1	300	0.259	0.626	1.210
890317.21	sct.o	400	0.187	0.309	0.556
890320.04	sct.o	400	0.181	0.275	0.534

PGA = Peak Ground (Table) Acceleration
PRA = Peak Roof Acceleration
PRD = Peak Roof Displacement

TABLE 3.11 List of Tests Performed on FD Model

FILE	SIGNAL	SPAN	PGA [g]	PRA [g]	PRD [in.]
890222.01	free vibration	level 3	-	-	-
890222.02	free vibration	level 3	-	-	-
890222.03	free vibration	level 5	-	-	-
890222.04	free vibration	level 5	-	-	-
890306.17	free vibration	level 3	-	-	-
890306.18	free vibration	level 5	-	-	-
890222.07	random30.d	200	-	-	-
890222.08	random30.d	400	-	-	-
890223.01	random30.d	600	-	-	-
890223.02	random30.d	800	-	-	-
890228.01	random30.d	600	-	-	-
890228.02	random30.d	800	-	-	-
890306.15	random30.d	600	-	-	-
890306.16	random30.a	75	-	-	-
890223.04	pulse	100	-	-	-
890228.06	pulse	50	-	-	-
890228.17	pulse	50	-	-	-
890302.01	pulse	50	-	-	-
890303.08	pulse	50	-	-	-
890303.13	pulse	50	-	-	-
890303.18	pulse	50	-	-	-
890303.21	pulse	50	-	-	-
890303.24	pulse	50	-	-	-
890306.01	pulse	50	-	-	-
890228.18	h2.90	120	-	-	-
890306.02	h2.90	50	-	-	-
890306.03	h2.90	120	-	-	-
890306.04	h2.60	150	-	-	-
890306.05	h2.65	150	-	-	-
890306.06	h2.70	150	-	-	-

TABLE 3.11 cont. List of Tests Performed on FD Model

FILE	SIGNAL	SPAN	PGA [g]	PRA [g]	PRD [in.]
890306.07	h2.75	150	-	-	-
890306.08	h2.80	150	-	-	-
890306.09	h2.85	150	-	-	-
890306.10	h2.90	150	-	-	-
890306.11	h2.95	150	-	-	-
890306.12	h3.00	150	-	-	-
890306.13	h3.05	150	-	-	-
890306.14	h3.10	150	-	-	-
890228.03	ec2	50	0.134	0.326	0.391
890223.03	ec2	150	0.309	0.631	1.011
890223.05	ec2	200	0.394	0.866	1.382
890223.06	ec2	250	0.476	1.021	1.752
890223.12	ec2	300	0.555	1.105	2.137
890223.13	ec2	350	0.651	1.304	2.454
890223.14	ec2	400	0.712	1.578	2.731
890228.04	taft2	50	0.089	0.248	0.337
890223.07	taft2	200	0.406	0.637	1.106
890223.08	taft2	250	0.513	0.796	1.298
890223.15	taft2	300	0.610	1.006	1.412
890223.16	taft2	400	0.839	1.408	1.724
890228.05	miyagi	50	0.094	0.183	0.225
890223.09	miyagi	150	0.166	0.417	0.615
890223.10	miyagi	200	0.213	0.570	0.939
890223.11	miyagi	275	0.304	0.938	1.594
890223.17	miyagi	350	0.424	1.321	2.242
890223.18	miyagi	400	0.532	1.493	2.397
890228.07	pac2	220	0.290	0.532	0.801
890228.08	pac2	350	0.468	0.896	1.5391
890228.09	park2	220	0.281	0.515	0.681
890228.10	park2	350	0.419	0.657	1.094

TABLE 3.11 cont. List of Tests Performed on FD Model

FILE	SIGNAL	SPAN	PGA [g]	PRA [g]	PRD [in.]
890228.11	sf2	200	1.006	1.620	1.350
890228.12	sf2	300	1.309	2.641	2.288
890228.13	sf2	400	1.545	2.805	2.678
890228.14	buc1	200	0.200	0.480	0.732
890228.15	buc1	300	0.262	0.704	1.136
890228.16	sct	400	0.103	0.170	0.094
890303.01	chile.u	50	0.112	0.268	0.289
890303.02	chile.u	200	0.425	0.870	1.251
890303.03	chile.u	400	0.737	1.621	2.597
890303.04	chile.u	500	0.869	1.748	2.789
890303.27	chile.u	750	1.202	2.137	2.862
890303.05	chile.s	50	0.075	0.158	0.169
890303.06	chile.s	200	0.159	0.442	0.593
890303.07	chile.s	400	0.286	0.715	1.383
890303.09	unio.al	50	0.071	0.209	0.258
890303.10	unio.al	250	0.236	0.609	0.883
890303.11	unio.al	500	0.546	1.320	2.123
890303.12	unio.al	750	0.862	1.544	2.831
890303.25	unio.al	1000	1.176	1.928	3.274
890303.14	zaca.al	50	0.052	0.150	0.181
890303.15	zaca.al	250	0.219	0.527	0.864
890303.16	zaca.al	500	0.465	1.095	1.952
890303.17	zaca.al	750	0.710	1.328	2.731
890303.26	zaca.al	1000	0.900	1.596	3.110
890303.19	ecatc.s1	225	0.321	0.585	0.863
890303.20	ecatc.s1	450	0.469	1.235	1.927
890303.22	taftatc.s1	225	0.243	0.689	1.023
890303.23	taftatc.s1	450	0.528	1.176	2.067

PGA = Peak Ground (Table) Acceleration
PRA = Peak Roof Acceleration
PRD = Peak Roof Displacement

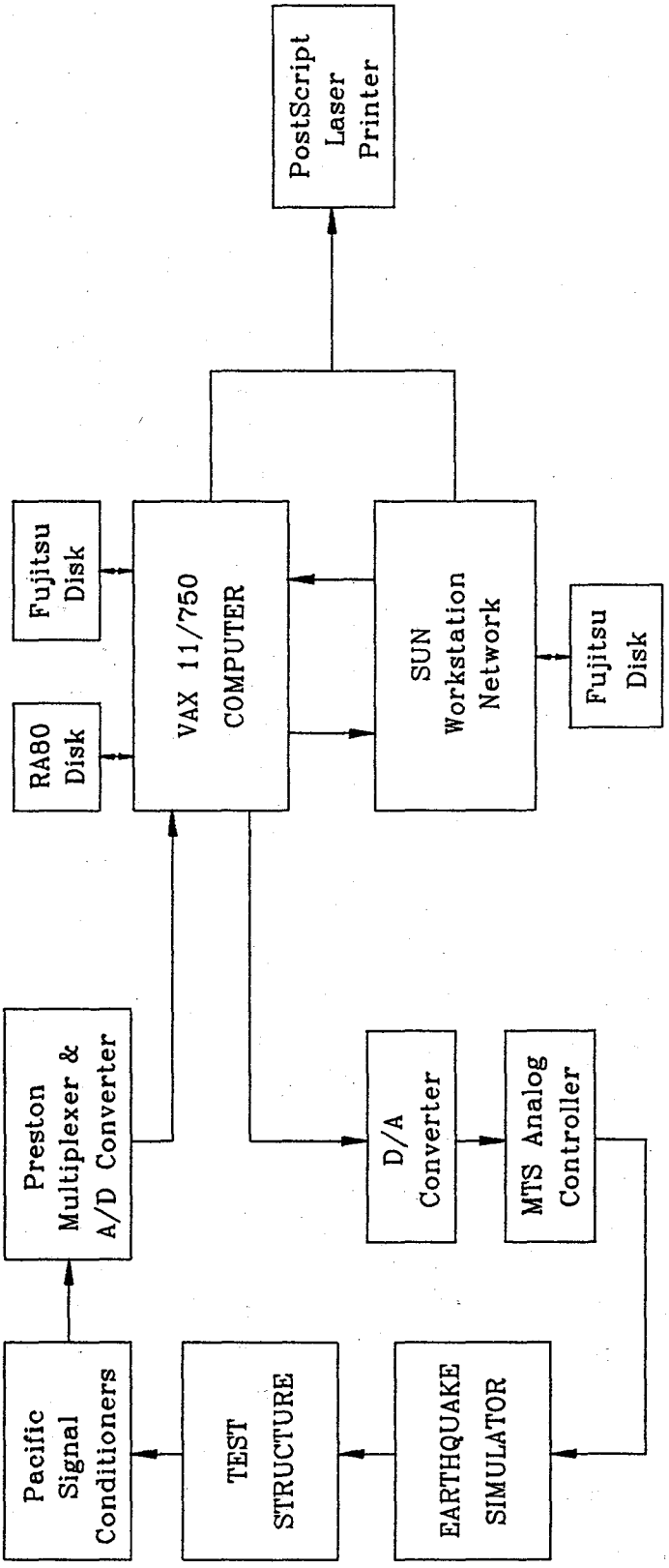

Fig. 3.1 Schematic Diagram of Earthquake Simulator Test Facility

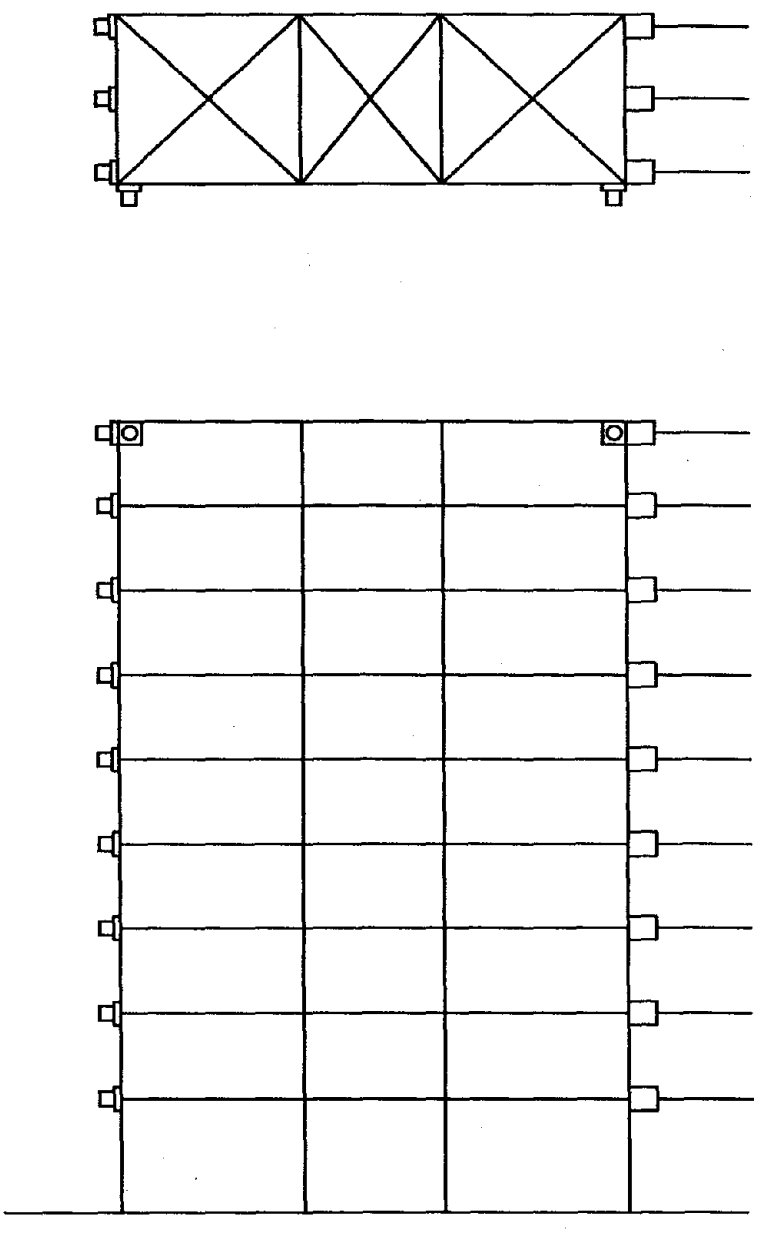

Fig. 3.2 Primary Instrumentation on MRF

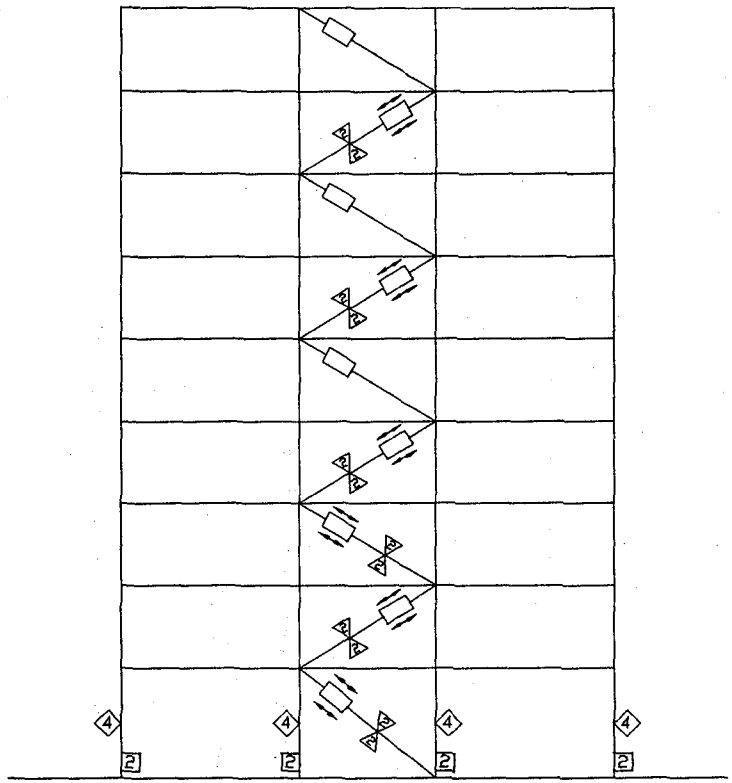

(a) VD Instrumentation

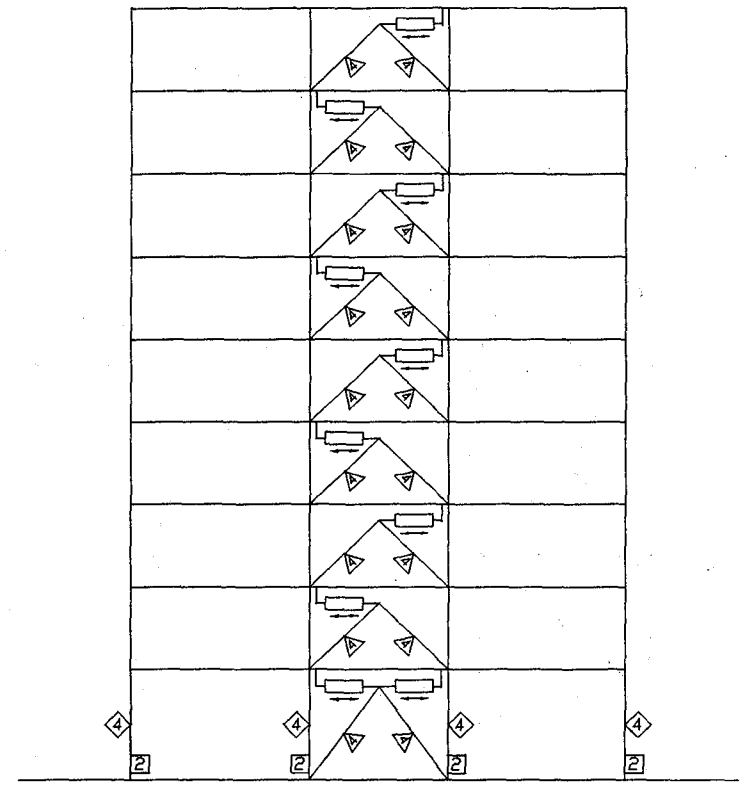

(b) FD Instrumentation

DCDT displacement

4-gauge axial bridge

4-gauge axial bridge

2-gauge moment bridge

4-gauge shear bridge

Fig. 3.3 Additional Instrumentation for Damped Structures

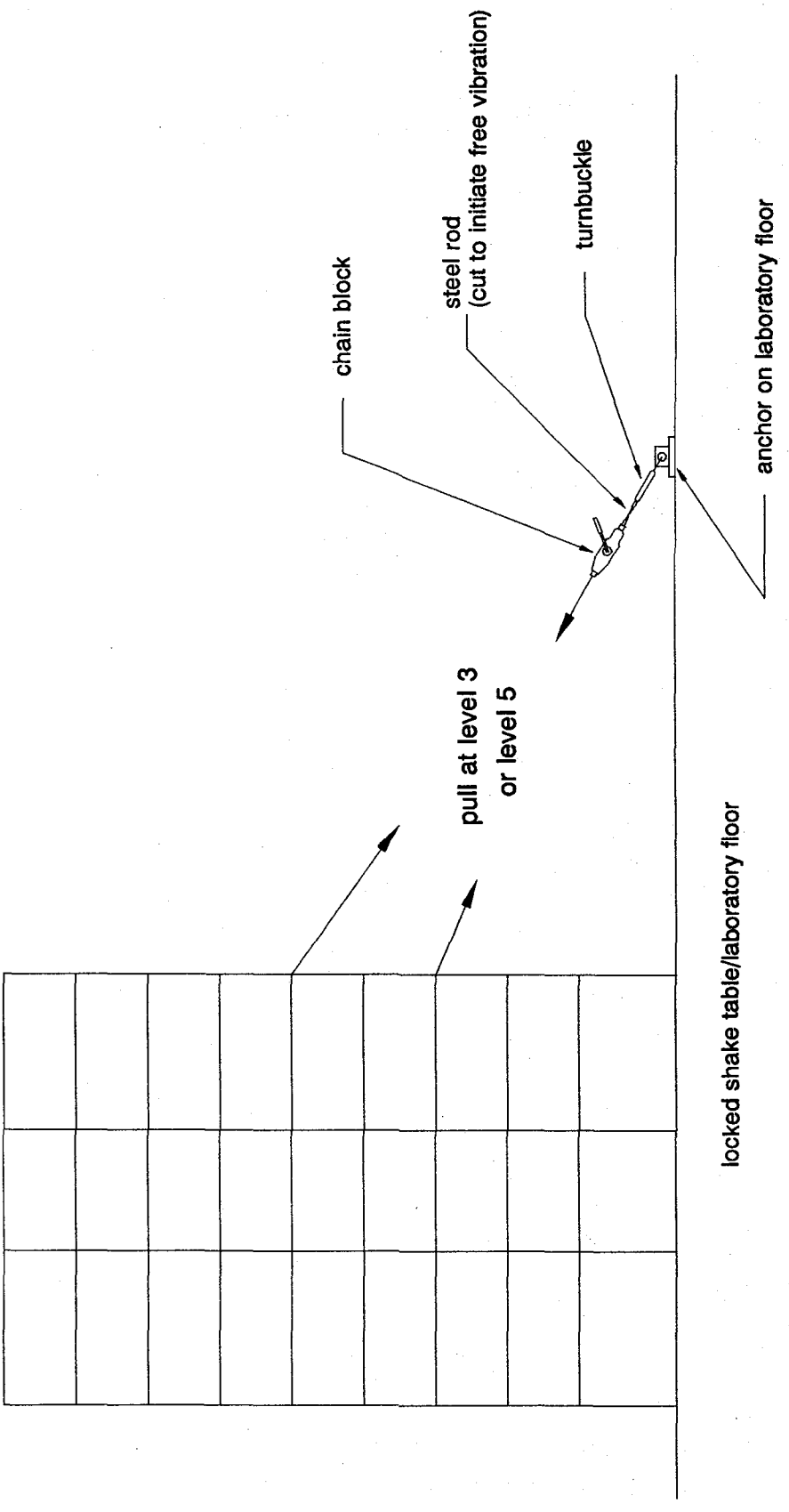

Fig. 3.4 Schematic of Pull-Back Free Vibration Test Set Up

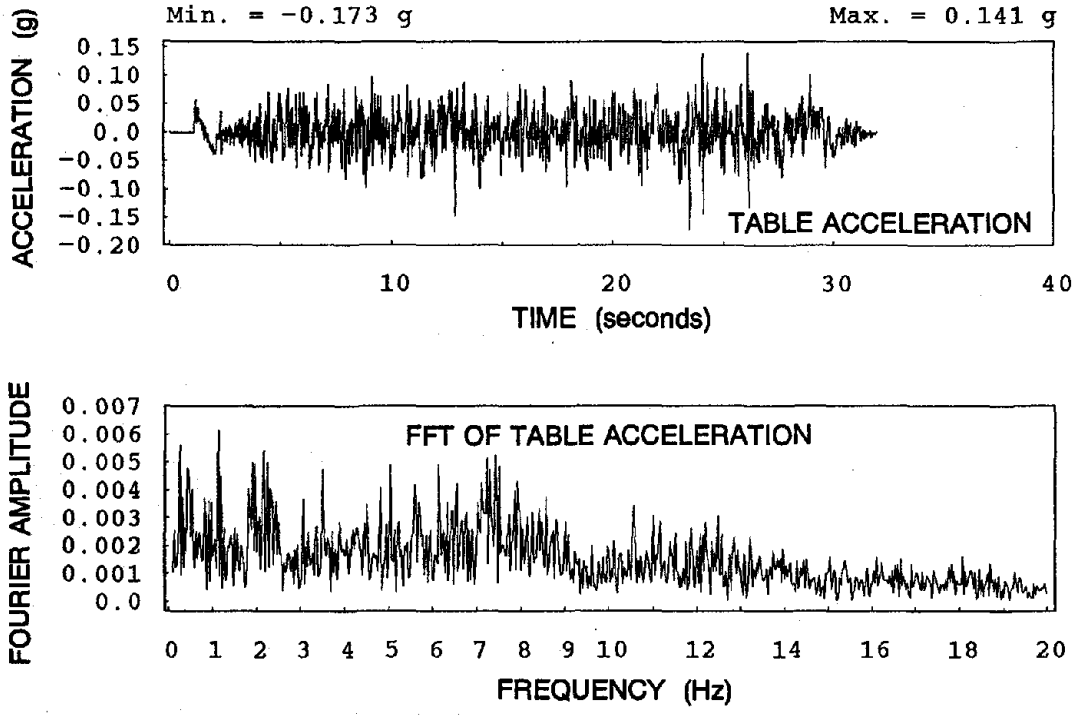

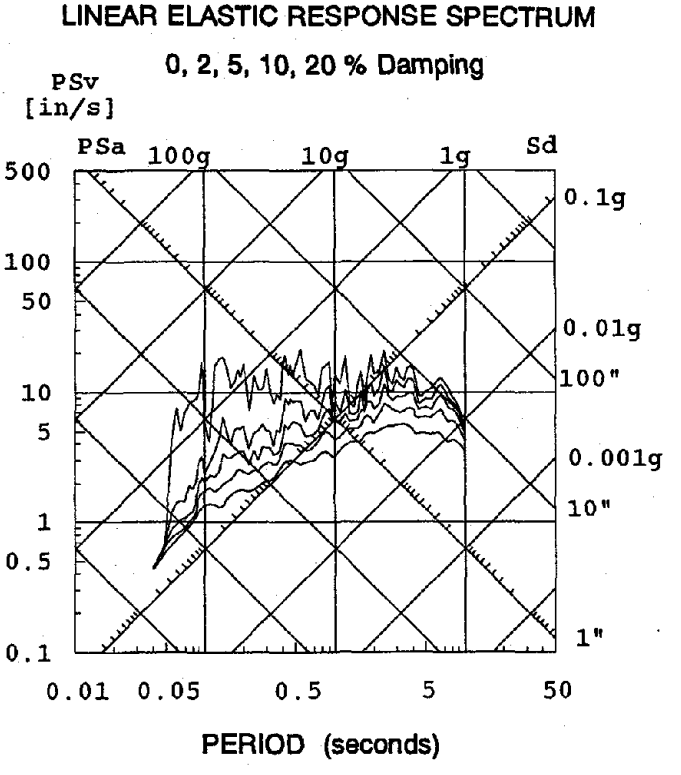

Fig. 3.5 Random Noise, Table Acceleration and Linear Elastic Response Spectrum

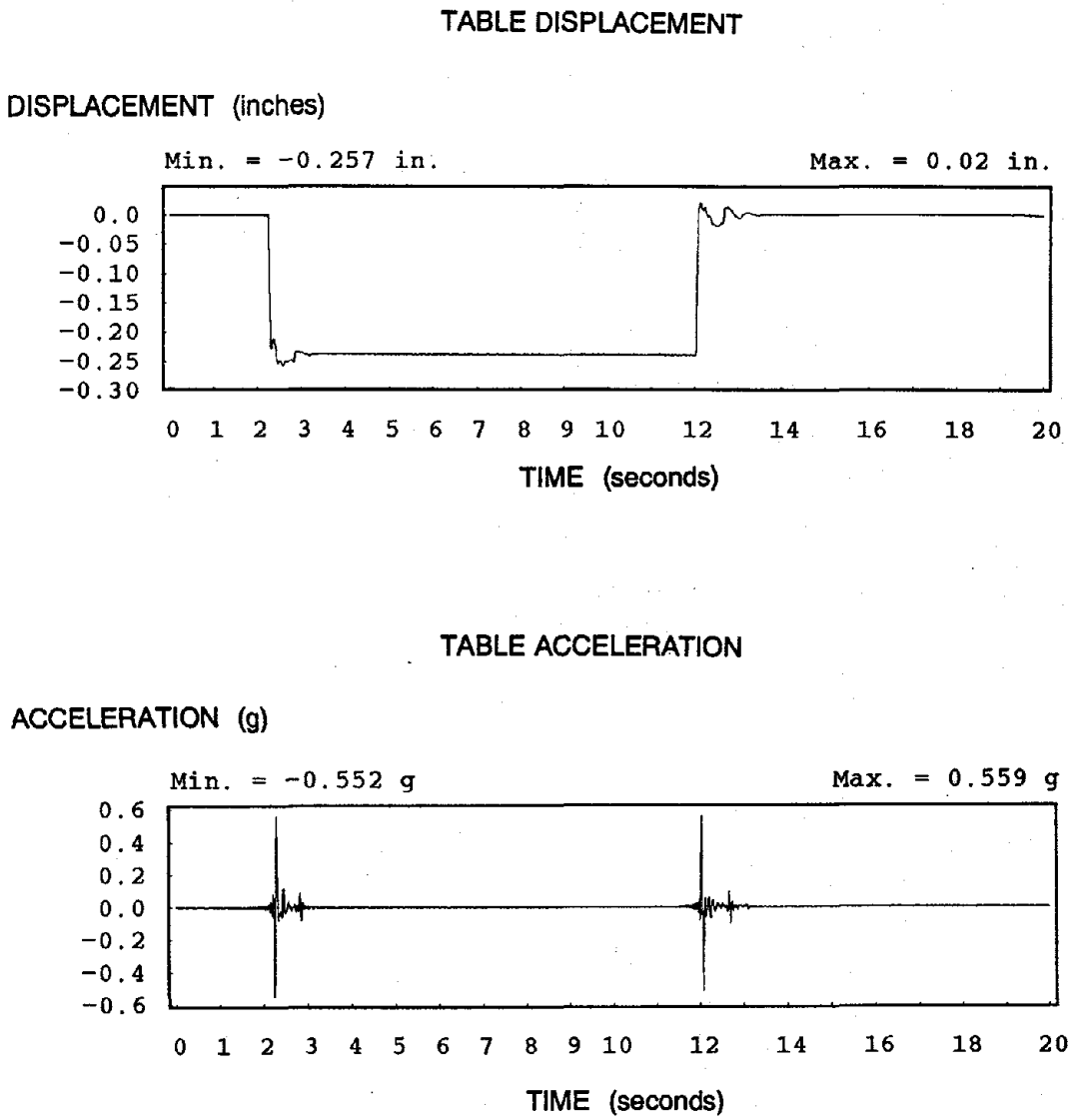

Fig. 3.6 Pulse Free Vibration Test, Table Displacement and Acceleration

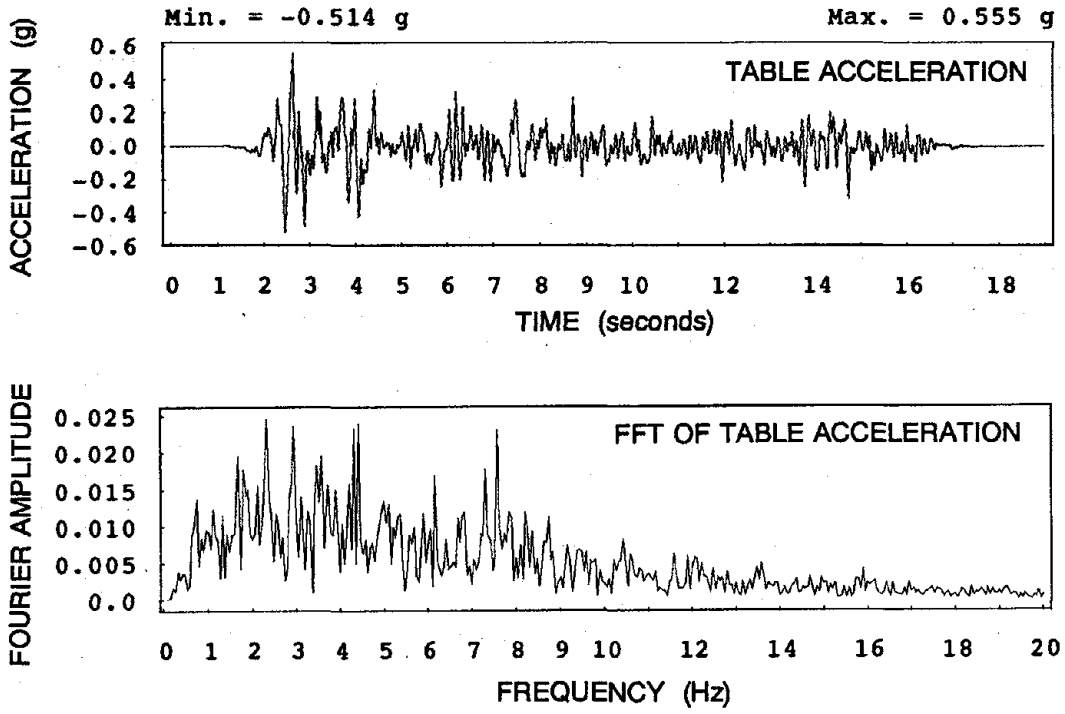

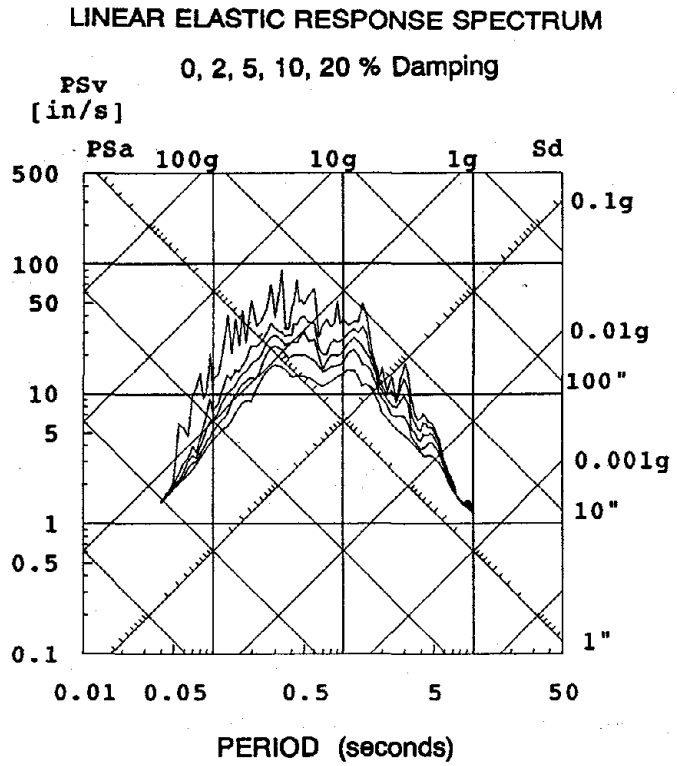

Fig. 3.7 El Centro, Table Acceleration and Linear Elastic Response Spectrum

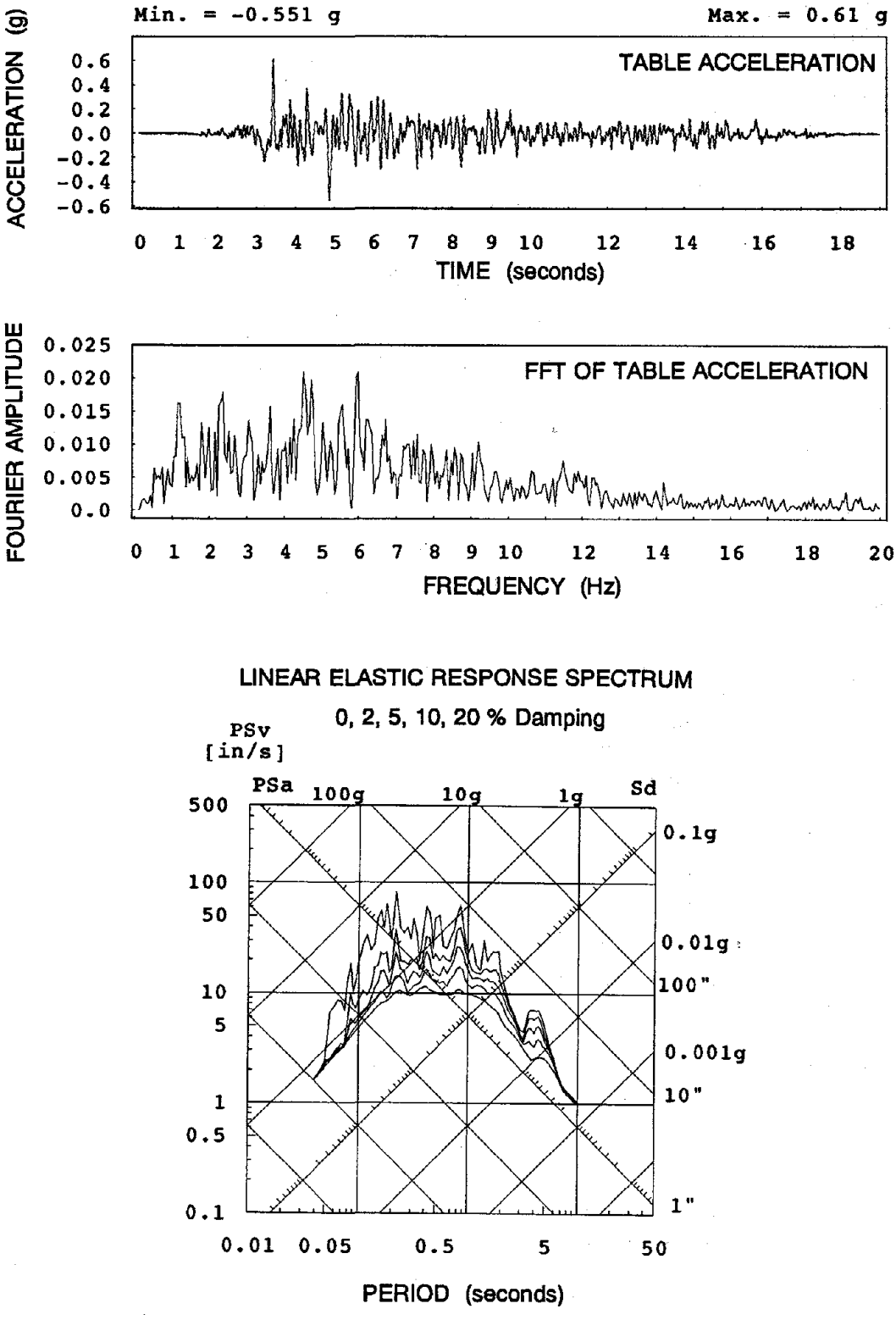

Fig. 3.8 Taft, Table Acceleration and Linear Elastic Response Spectrum

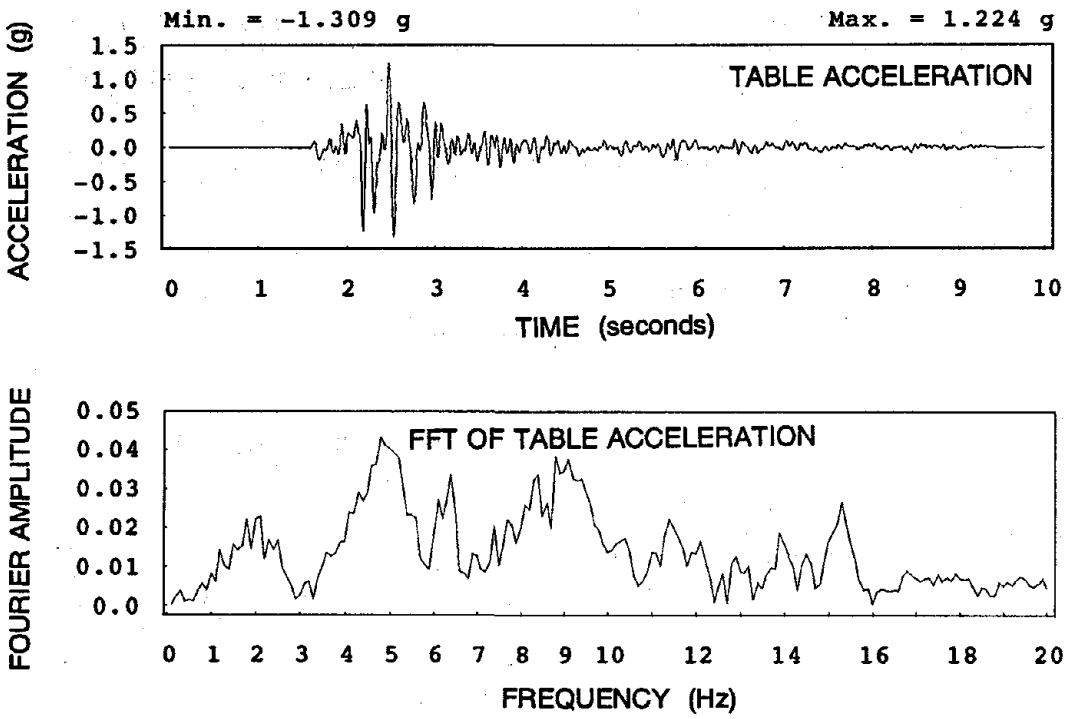

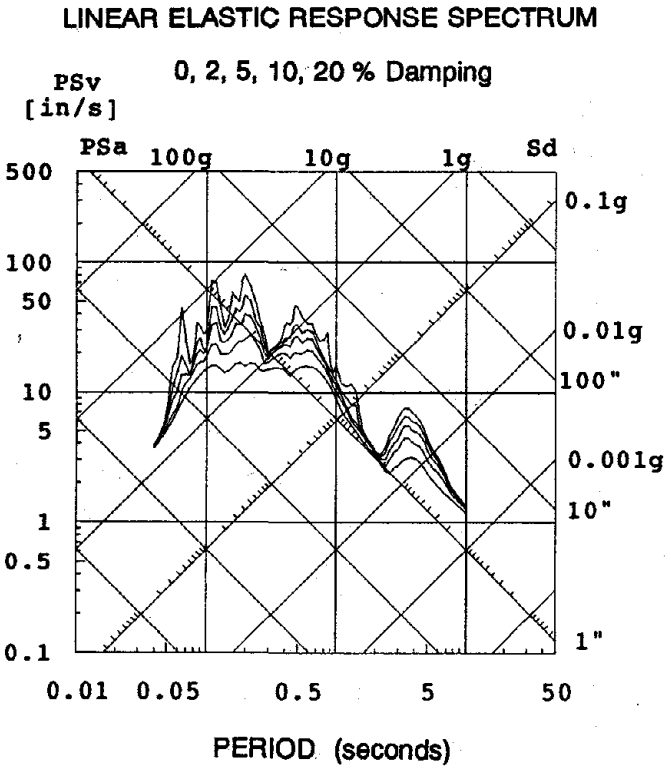

Fig. 3.9 San Francisco, Table Acceleration and Linear Elastic Response Spectrum

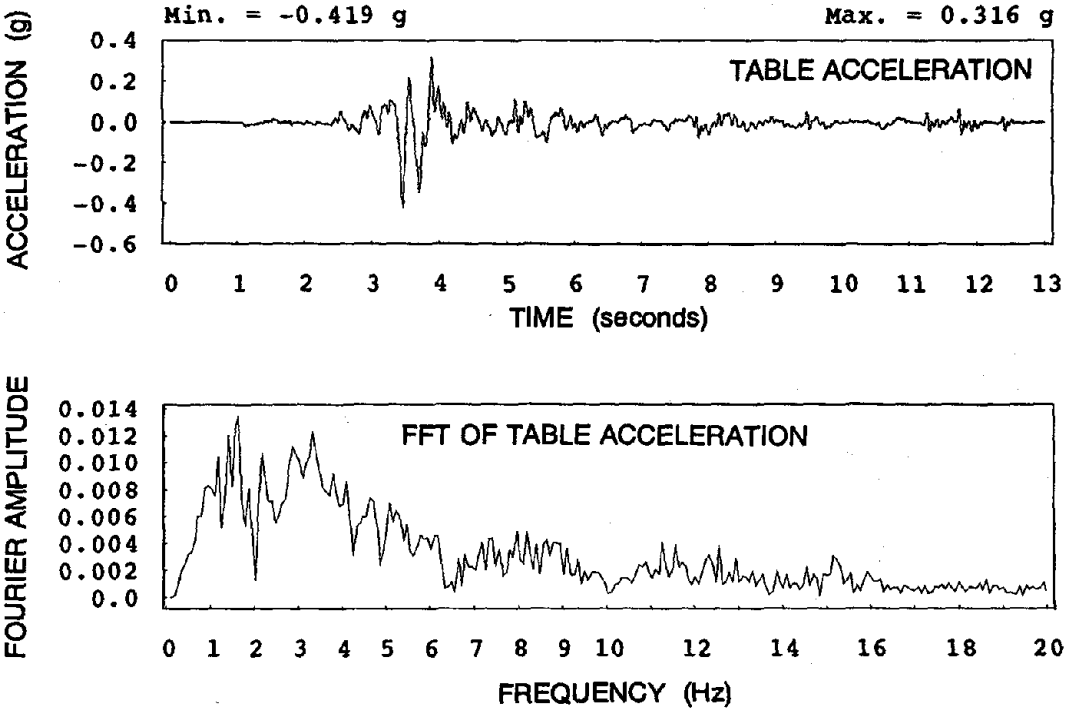

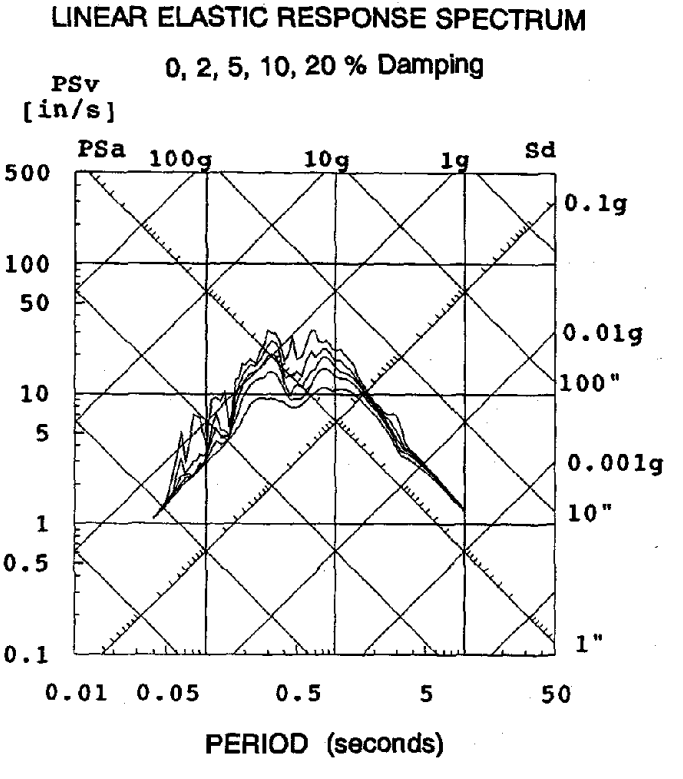

Fig. 3.10 Parkfield, Table Acceleration and Linear Elastic Response Spectrum

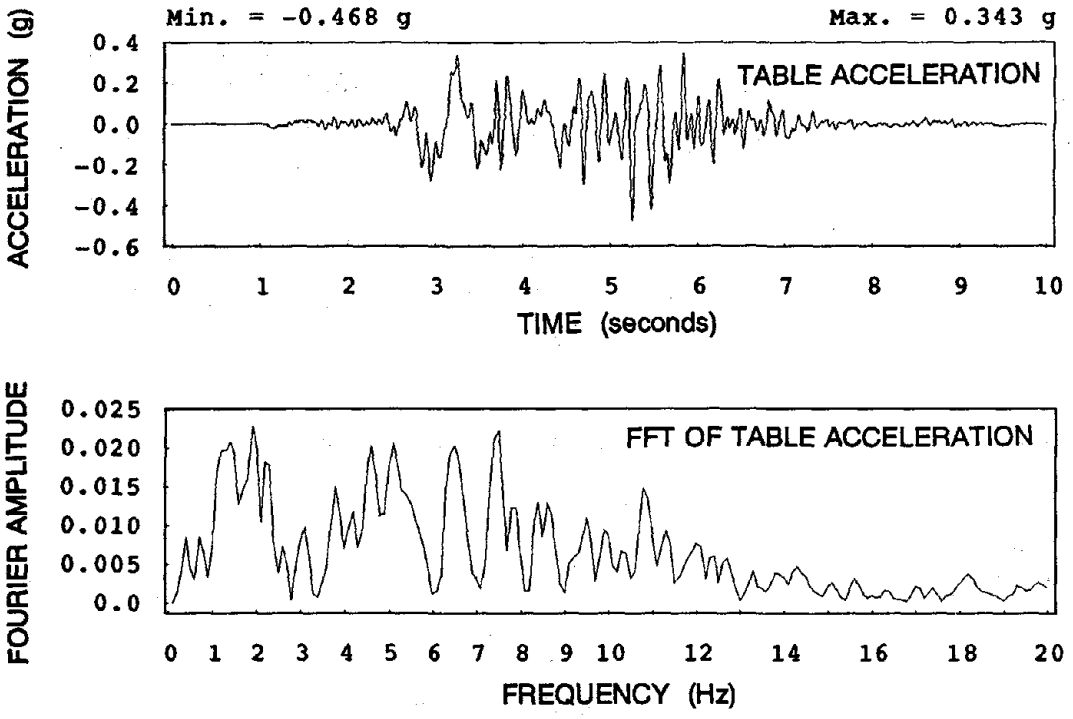

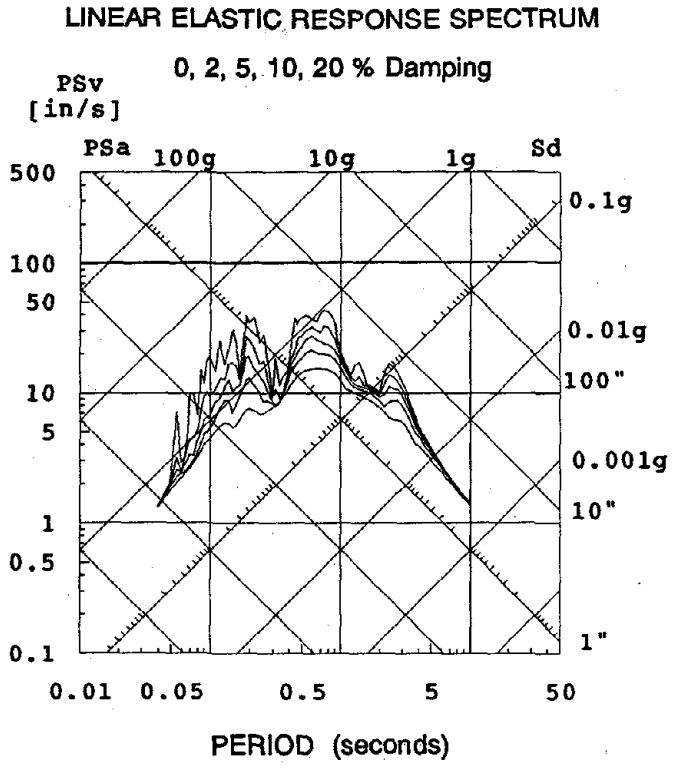

Fig. 3.11 Pacoima, Table Acceleration and Linear Elastic Response Spectrum

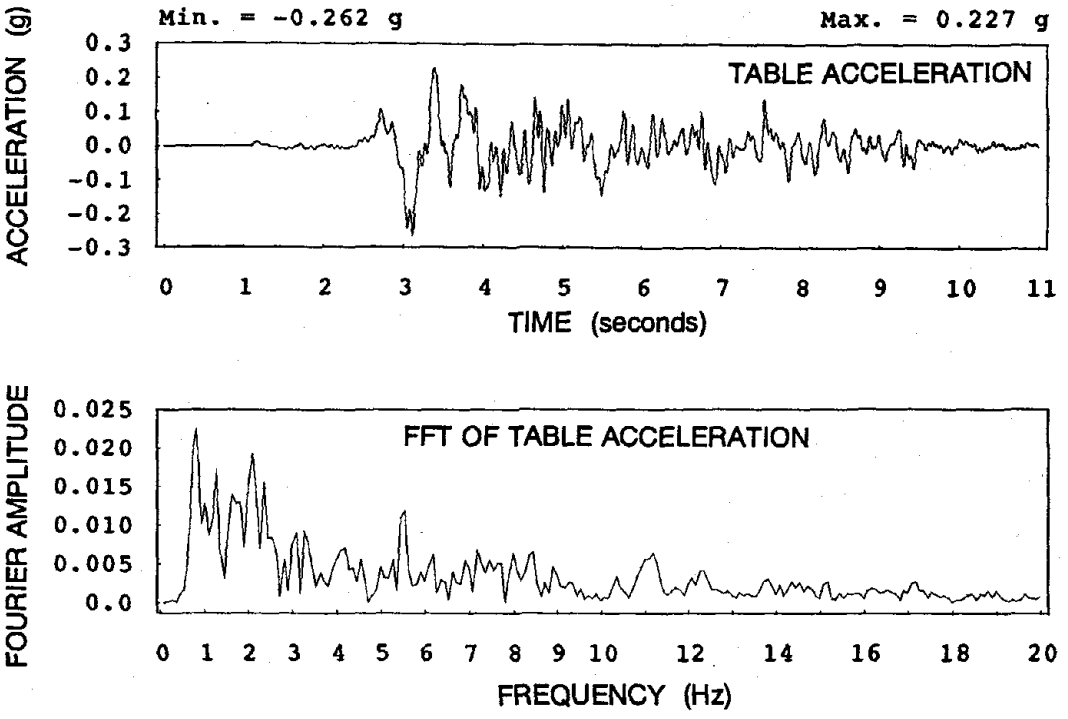

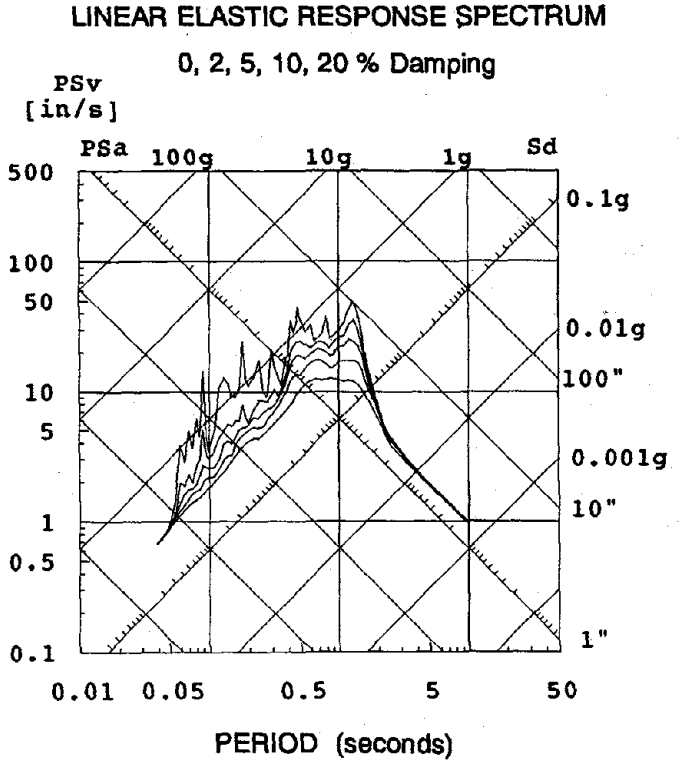

Fig. 3.12 Bucharest, Table Acceleration and Linear Elastic Response Spectrum

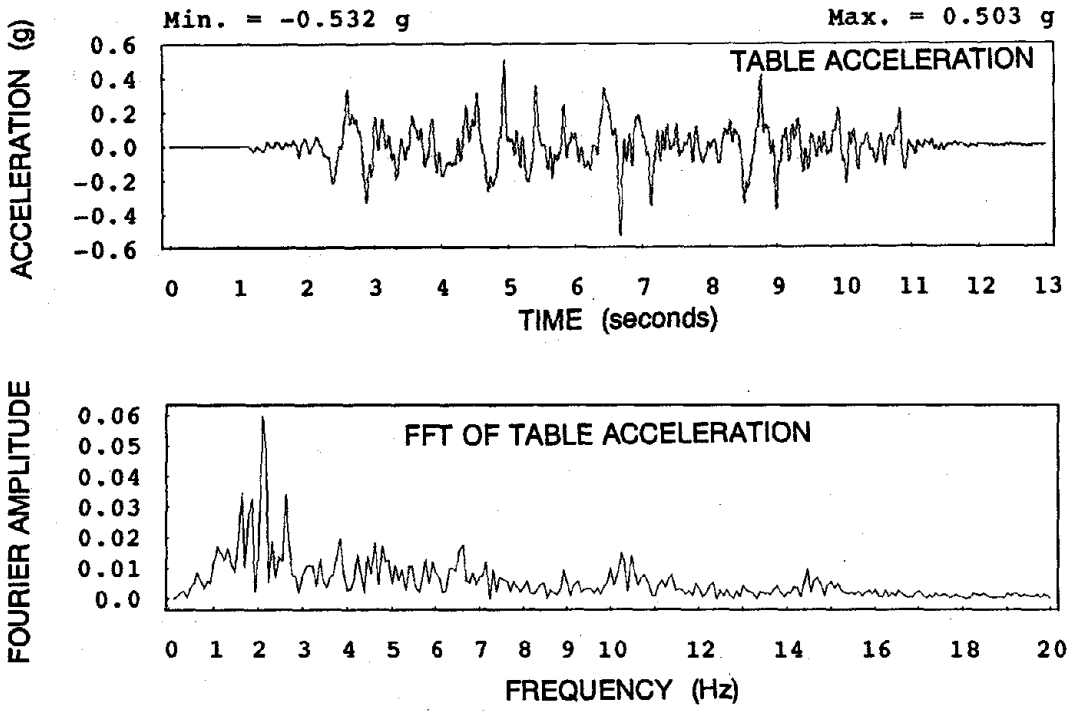

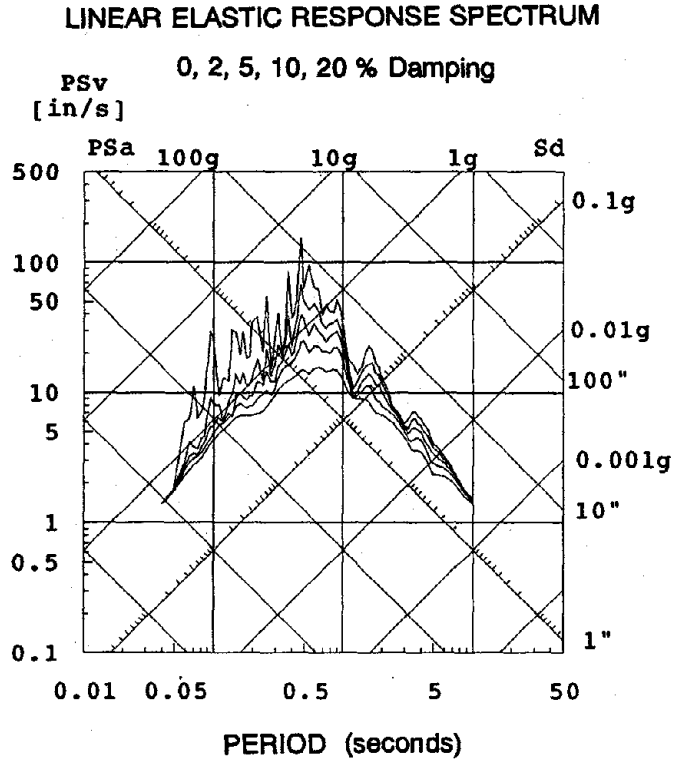

Fig. 3.13 Miyagi, Table Acceleration and Linear Elastic Response Spectrum

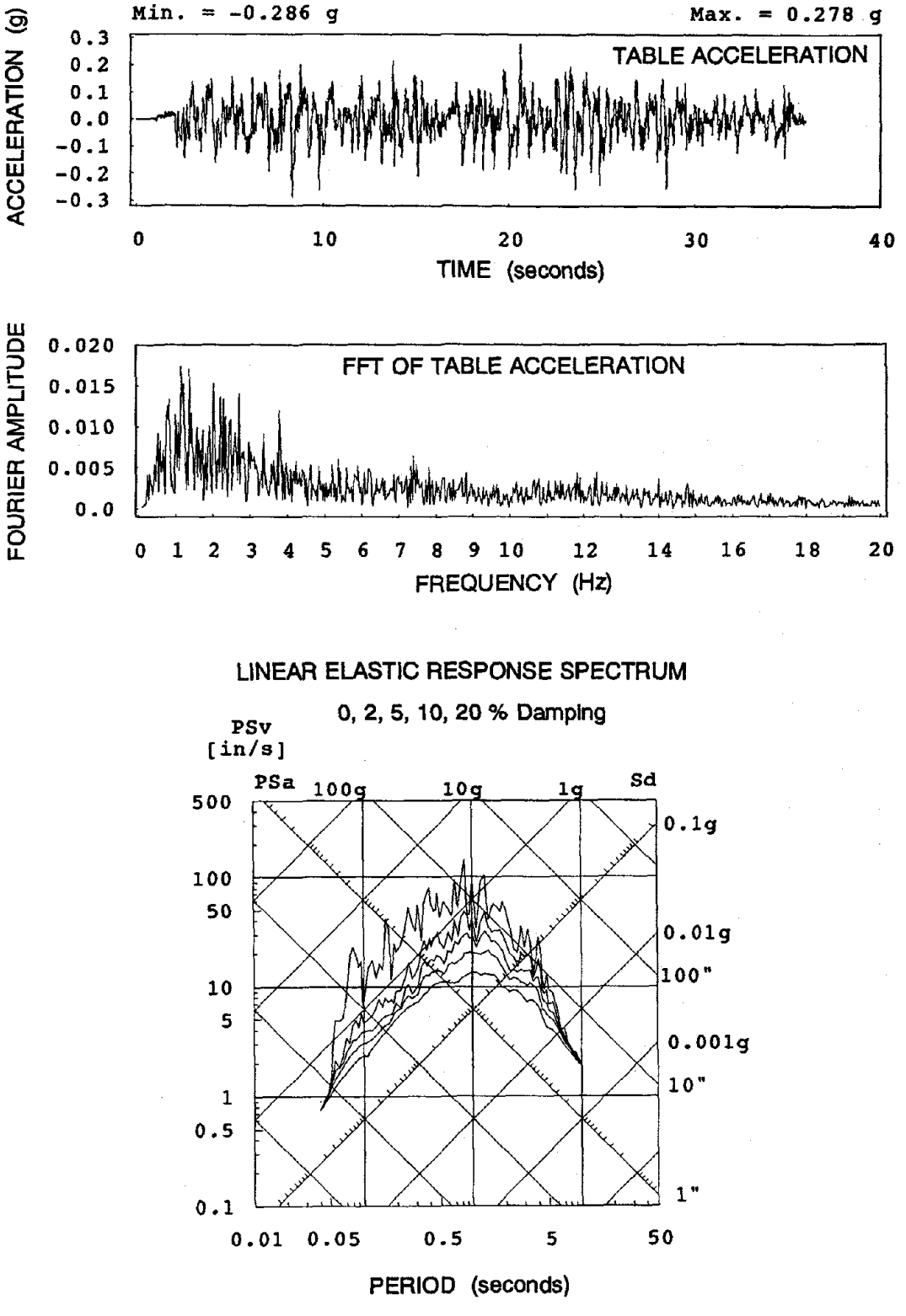

Fig. 3.14 Chile.s, Table Acceleration and Linear Elastic Response Spectrum

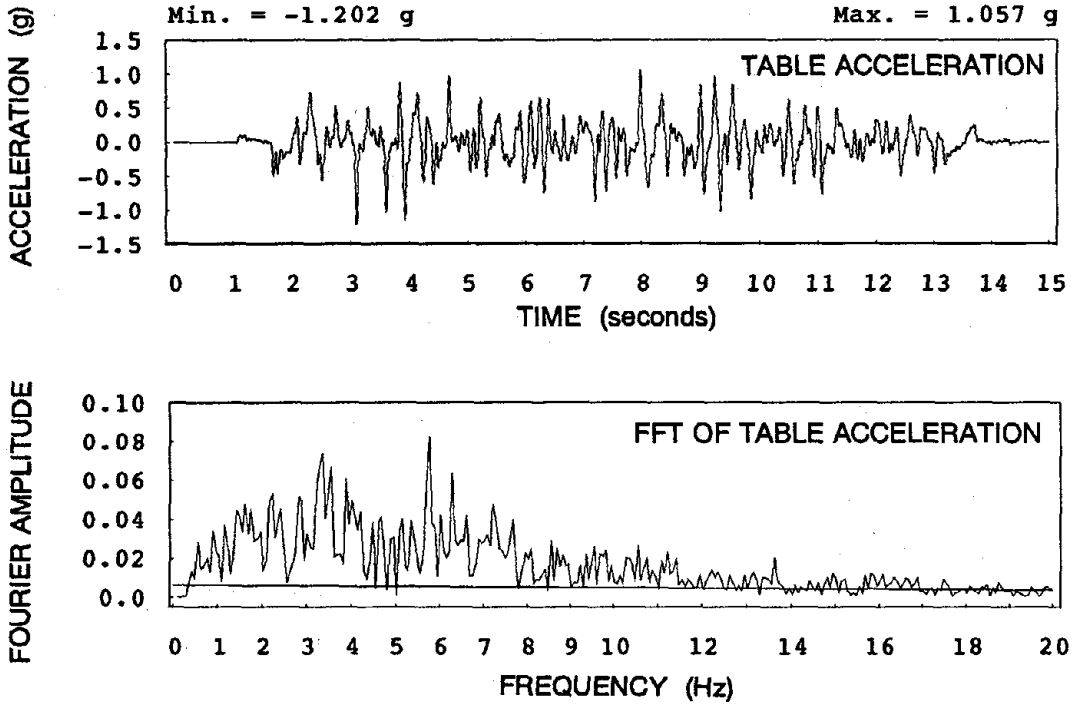

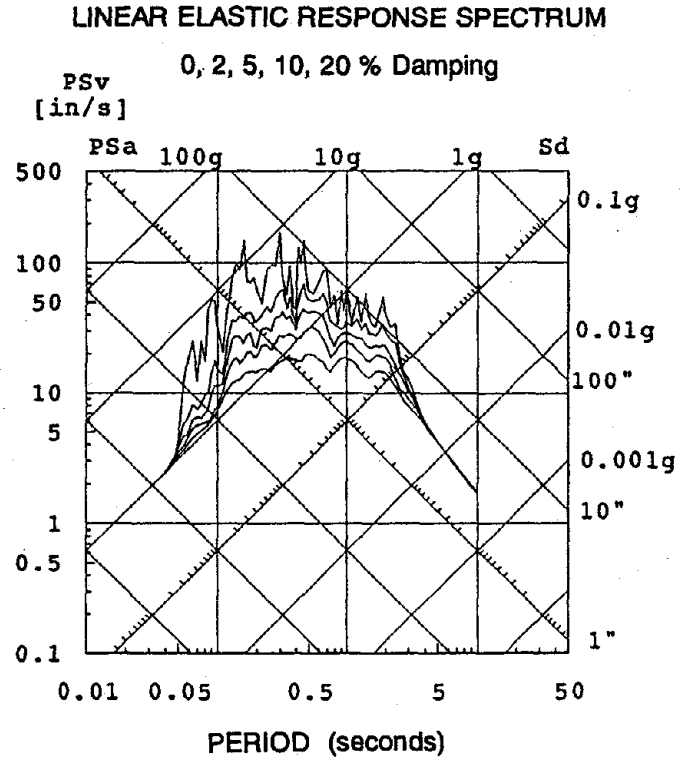

Fig. 3.15 Chile.u, Table Acceleration and Linear Elastic Response Spectrum

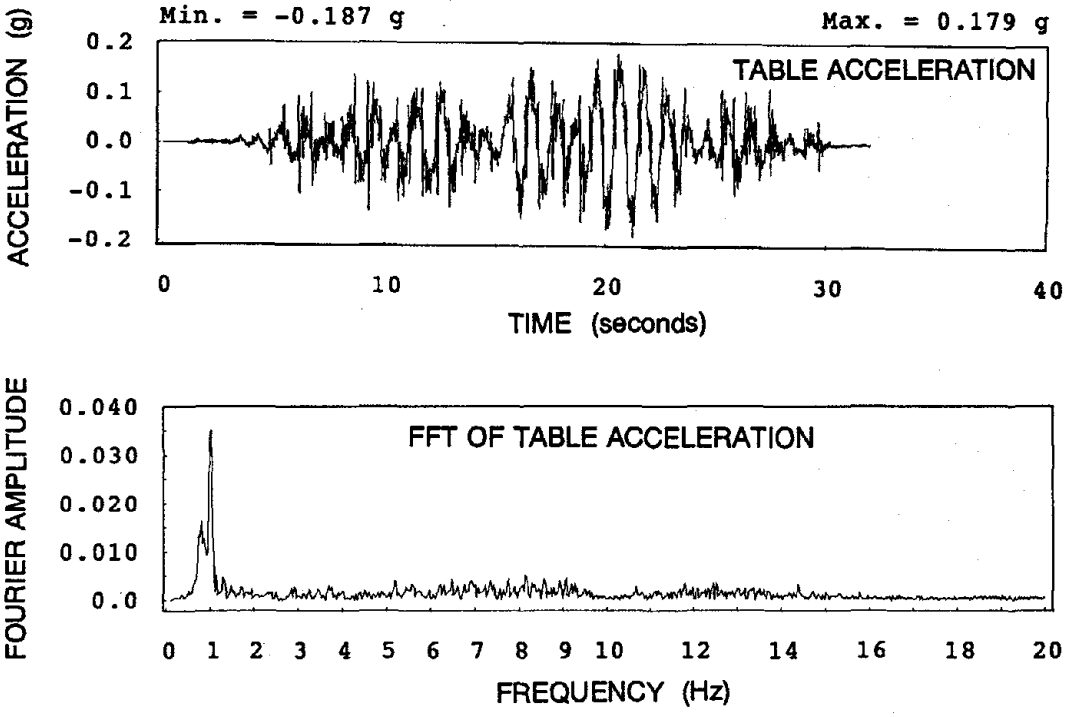

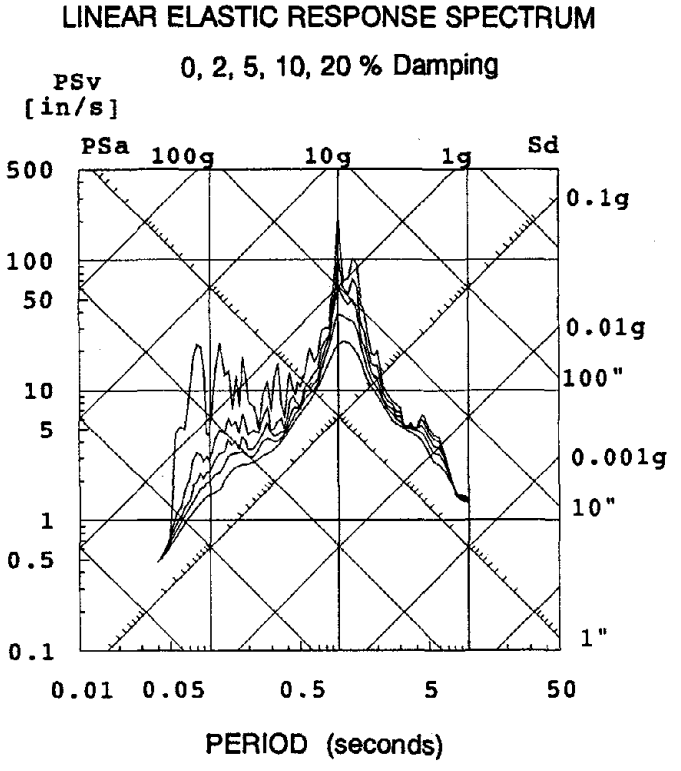

Fig. 3.16 Mexico City (SCT), Table Acceleration and Linear Elastic Response Spectrum

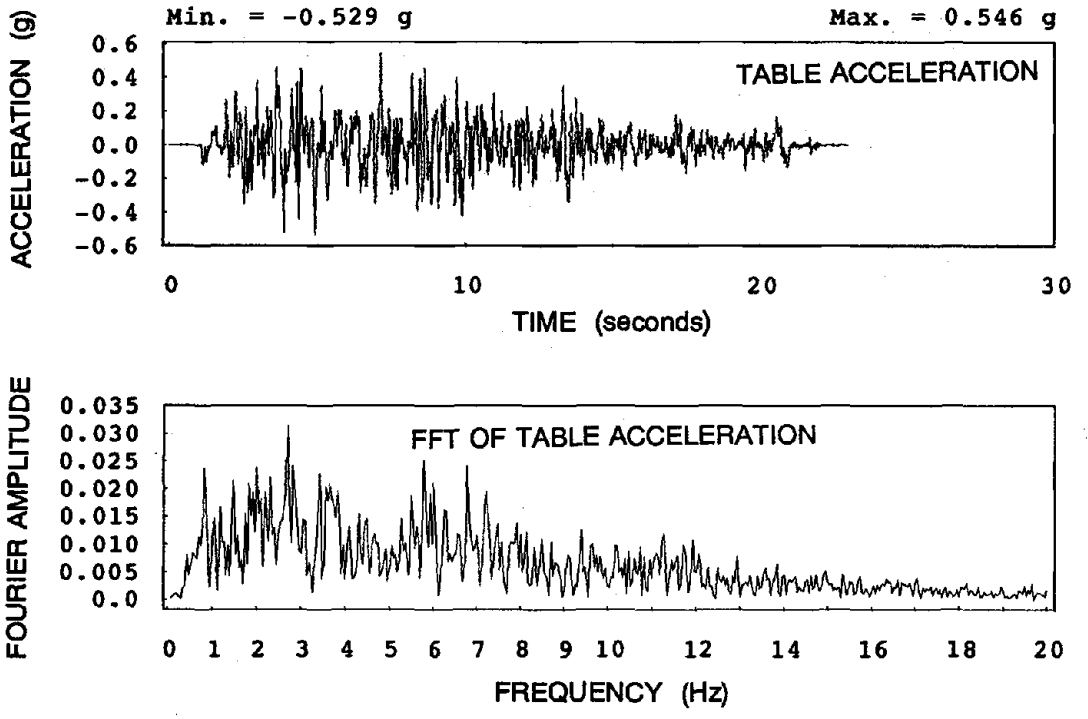

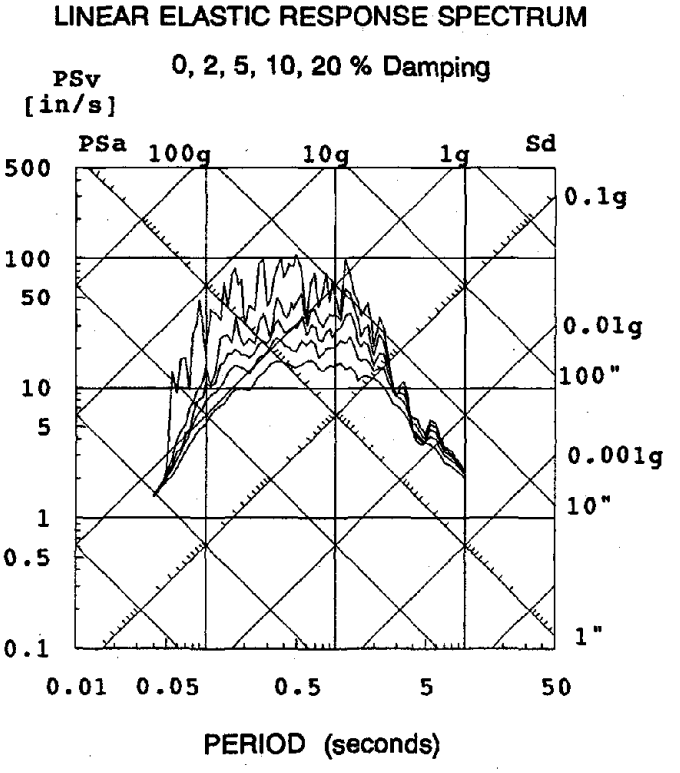

Fig. 3.17 La Union, Table Acceleration and Linear Elastic Response Spectrum

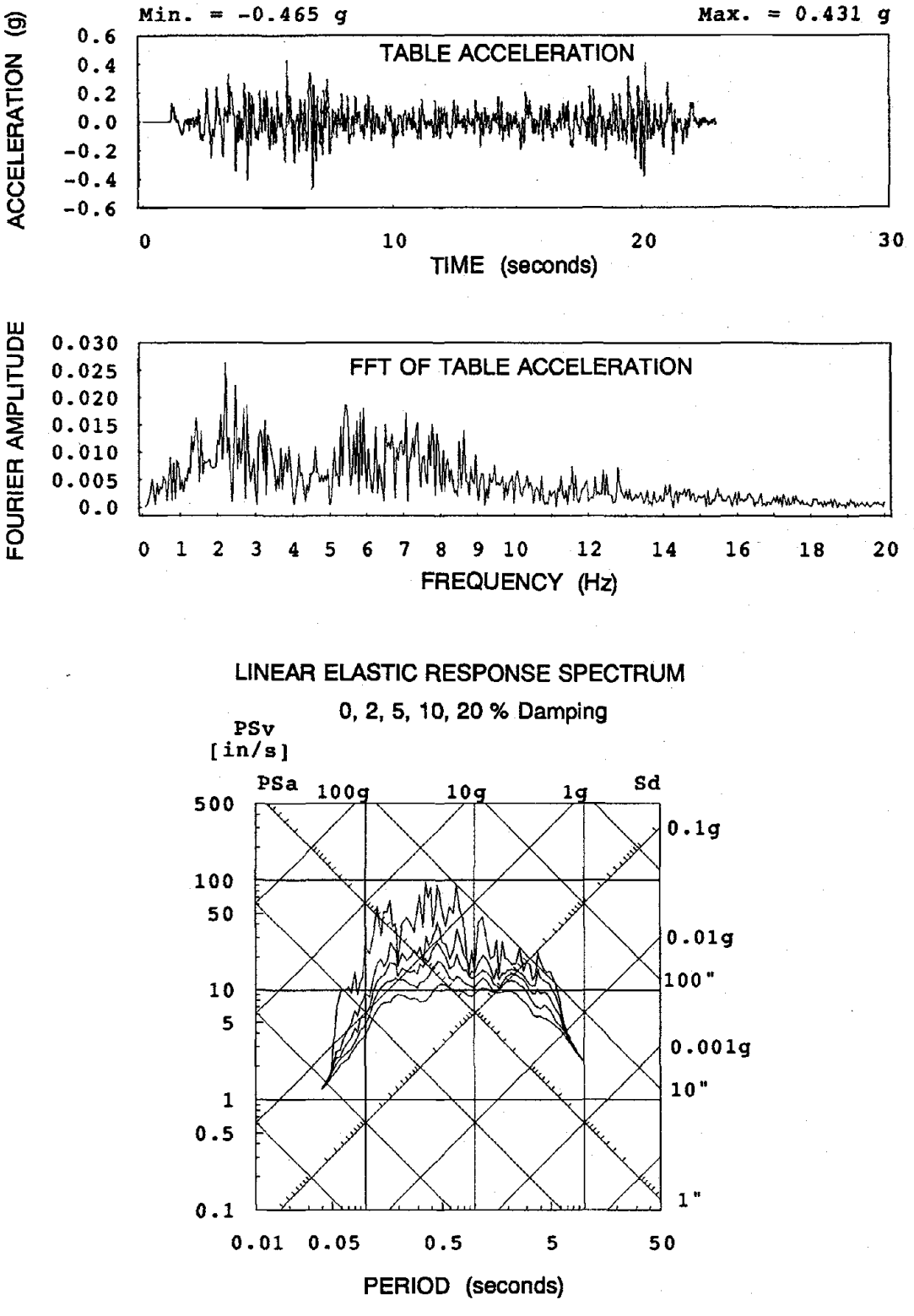

Fig. 3.18 Zacatula, Table Acceleration and Linear Elastic Response Spectrum

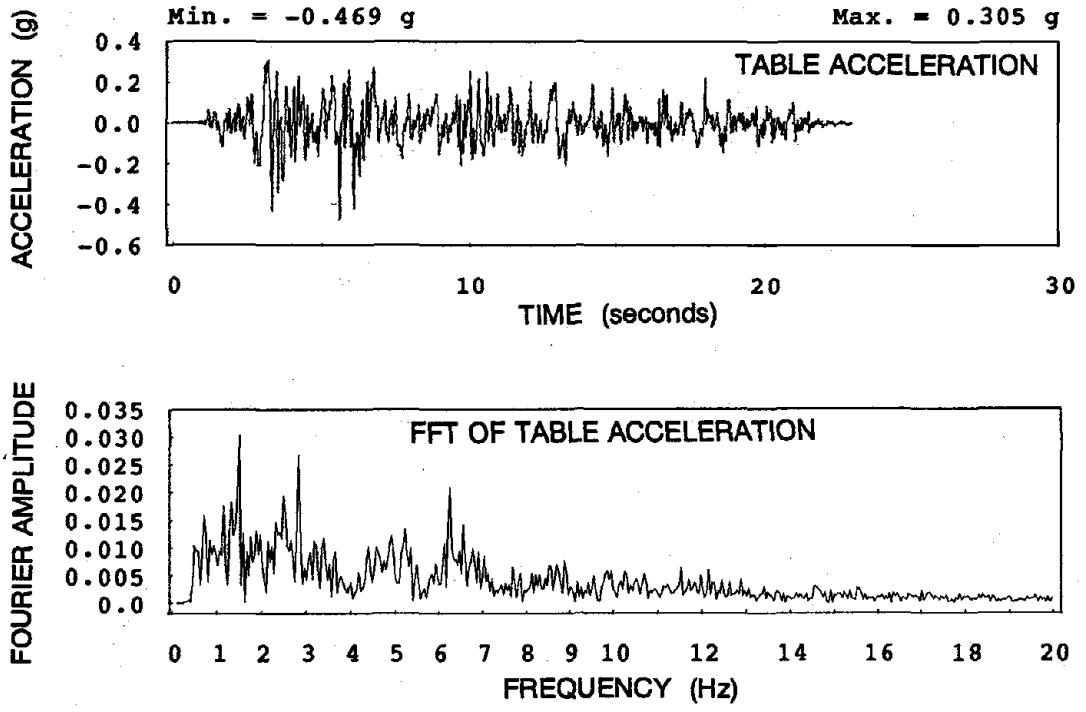

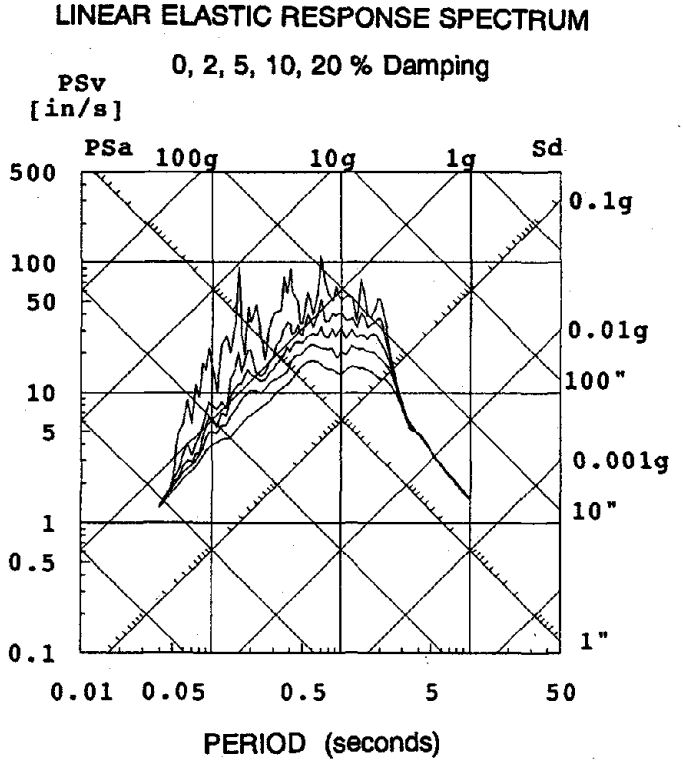

Fig. 3.19 ATC-S1 (El Centro-based), Table Acceleration and Linear Elastic Response Spectrum

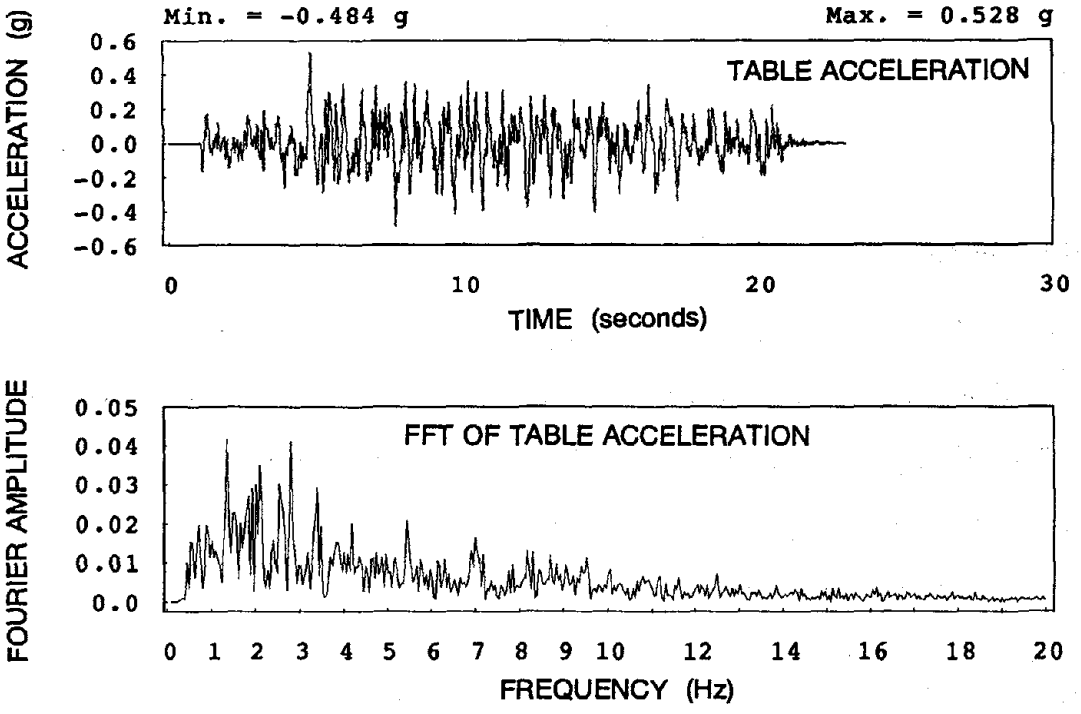

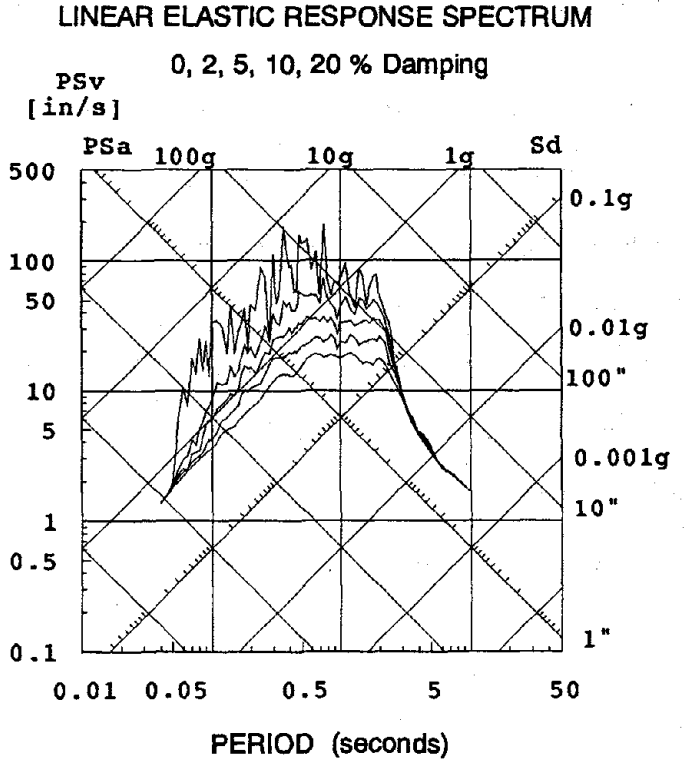

Fig. 3.20 ATC-S1 (Taft-based), Table Acceleration and Linear Elastic Response Spectrum

CHAPTER 4

TEST RESULTS

4.1 Introduction

The results of the earthquake simulator test program are presented in this chapter. Section 4.2 presents the results of the diagnostic tests of the MRF, CBF, and the two damped structures. The behavior of the VD and FD models in the earthquake tests is discussed in Sec. 4.3. Section 4.4 offers response comparisons of the various different structural systems. Conclusions from the experimental program are made in Sec. 4.5.

4.2 Diagnostic Tests

4.2.1 MRF and CBF Models

MRF — The frequencies and damping ratios of the first three modes of vibration determined from the diagnostic tests are given in Table 4.1, as well as the corresponding values determined from the earthquake tests. The dynamic properties were determined using transfer functions. The roof acceleration transfer function obtained from one of the MRF pulse tests is shown in Fig. 4.1. There is very good agreement among the frequencies for all three modes and, as expected, the damping ratios increase somewhat from the pulse tests to the earthquake tests. This is because the table is basically inactive in the pulse tests (after an initial displacement, see Fig. 3.6), whereas the active table in the earthquake tests contributes to the measured damping via the hydraulic actuator system.

CBF — Diagnostic tests of the CBF model were not performed. The dynamic properties of the first two modes of vibration of the CBF, listed in Table 4.1, have been determined from the earthquake tests only. The addition of the concentric bracing raised the first two frequencies of the MRF from 1.95 Hz and 6.58 Hz to 2.95 Hz and 11.39 Hz, respectively (as evaluated from

the earthquake test data). The damping ratios are comparable to those of the MRF for the first two modes. About half of the 4.9 % first-mode damping ratio is attributed to the damping contribution of the shake table actuator system. Fixed-base free vibration tests would be expected to show first-mode damping ratios of less than 1 % and about 2 %, respectively, for the MRF and CBF models. The increase in damping seen in the CBF is due to the addition of the bracing and the large number of bolted connections attaching it to the structural frame. (This is discussed further in Sec. 4.3.3.)

The first-mode frequencies of the MRF and CBF models are significant with respect to the VD and FD models, because they bracket the first frequency of both of these structures. This means that the damped structures can be compared with structures that are both stiffer and more flexible, and although only a few results are available for the CBF, these comparisons are more valuable than simply a MRF-damped structure comparison which cannot take into consideration the added stiffness provided by the bracing and the dampers.

4.2.2 Viscoelastically-Damped Model

The frequencies and damping ratios of the first two modes of vibration of the VD model determined from the diagnostic tests are given in Table 4.2. The frequencies from the pull-back free vibration tests were determined from FFT amplitude spectra, while the damping ratios were calculated from both the FFTs and logarithmic decrement (log-dec) analyses of displacement free vibrations. The random and pulse test dynamic properties were determined from acceleration transfer functions. The level 4 acceleration Fourier amplitude spectrum obtained from one of the pull-back tests is shown in Fig. 4.2. A typical roof acceleration transfer function obtained from one of the pulse tests is shown in Fig. 4.3.

There is good agreement among the frequencies obtained from the different tests. Small decreases in the first and second mode frequencies, 2.76 Hz to 2.30 Hz, and 9.40 Hz to 8.90 Hz, respectively, are seen between the pull-back and pulse tests. This is due to the change in foundation conditions provided by the shake table in these tests. The damping ratios from the

different tests are also consistent, with the biggest variation due to the change of the shake table foundation condition.

The variation of damping ratio found from the pull-back tests listed in Table 4.2 is detailed in Table 4.3. The static displacement of the roof prior to load release varied for each of the tests (listed in the table), and while it might be expected that the damping be related to maximum displacement, the variation of damping ratio with maximum initial displacement shows that this is not the case. For these displacement levels the deformations in the dampers were small (only a few percent shear strain) and not large enough to reflect any variation in material properties.

A comparison of the MRF and VD damping ratios determined from the pulse tests indicates the additional damping provided to the structure by the VE dampers. The MRF first-mode damping ratio of 2.9 % is increased to 11.8 %, while the second-mode damping ratio is increased from 0.3 % to 10.5 %. The pulse tests performed throughout the course of the earthquake test program did not reveal any significant changes in the VD model frequencies. Each of the pulse tests consisted of two pulses (Fig. 3.6), and the first and second frequencies found from the individual pulses are listed in Table 4.4. There is very little variation of the observed frequencies. Significant factors associated with some of the tests are as follows:

(i) Test 890317.24 : The level 1E damper failed in this test. Delamination of the VE layers had been progressive during the preceding earthquake tests.

(ii) Test 890320.01 : Prior to this test the failed level 1E damper was replaced and all brace-to-damper connection bolts were tightened after those at level 3W were found to be loose. No other loose bolts were found.

(iii) Test 890320.17 : The level 1W damper had failed prior to this test. Delamination had been progressive during the preceding earthquake tests. This was both visually apparent and identifiable from the reduced brace forces at level 1W recorded during shaking.

It is noted that although two dampers failed during the course of testing, the effect of these failures on the response of the VD model and its dynamic properties was not significant. The failure of the two dampers was related to the way in which the VE dampers had been manufactured. The 0.15-inch viscoelastic layers were actually multi-layer laminations of 0.005-inch thick sheets of VE material and, in each case, separation of these layers led to eventual failure of the damper.

4.2.3 Friction-Damped Model

The frequencies and damping ratios of the first two modes of vibration of the FD model determined from the diagnostic tests are given in Table 4.2. The frequencies from the pull-back tests were determined from FFT amplitude spectra, while the damping ratios were calculated from both the FFTs and log-dec analyses of displacement free vibrations. The random and pulse test dynamic properties were determined from acceleration transfer functions. The level 4 acceleration Fourier amplitude spectrum obtained from one of the pull-back tests is shown in Fig. 4.4. A typical roof acceleration transfer function obtained from one of the pulse tests is shown in Fig. 4.5.

The frequencies determined from the different tests agree well. As observed for the VD model, there is a decrease in frequency between the pull-back and the pulse tests due to the change from inactive to active foundation condition. First mode frequencies of 3.00 Hz and 2.60 Hz and second mode frequencies of 10.10 and 9.70 Hz were determined from the pull-back and pulse tests, respectively. With only one or two exceptions, none of the friction dampers were activated during any of the diagnostic tests. The damping ratios presented in Table 4.2 thus represent those of a braced frame and do not reflect the presence of the friction dampers in the structure. The first-mode damping ratio, ξ_1, of the FD model compares favorably with that of the CBF. In particular, ξ_1 = 4.8 % determined from the pulse tests compares closely with ξ_1 = 4.9 % for the CBF (obtained from the earthquake tests).

Throughout the course of the earthquake tests of the FD model ten pulse tests were per-

formed. Analyses of the modal frequencies and damping ratios obtained from these tests revealed that there was no appreciable change of the dynamic properties of the FD model and no indication of damage to the structure caused by any of the earthquake inputs.

The transfer functions obtained from the random tests were not sufficiently well defined to allow damping ratios to be determined.

Stiffness Ratios

As the MRF, CBF, VD, and FD models all had the same total mass and mass distributions, the relative stiffnesses of the structures can be determined from their natural frequencies. Using the frequencies determined from the pulse tests (earthquake tests for the CBF) listed in Tables 4.1 and 4.2, the following stiffness ratios with respect to the MRF are calculated:

$$\frac{K_{CBF}}{K_{MRF}} = \left[\frac{2.95}{1.95}\right]^2 = 2.29 \tag{4.1}$$

$$\frac{K_{VD}}{K_{MRF}} = \left[\frac{2.30}{1.95}\right]^2 = 1.39 \tag{4.2}$$

$$\frac{K_{FD}}{K_{MRF}} = \left[\frac{2.60}{1.95}\right]^2 = 1.78 \tag{4.3}$$

As seen from the fundamental frequencies, the MRF and CBF models bound the VD and FD structures in terms of relative stiffness. The increase in stiffness (over the MRF) due to the concentric bracing of the CBF, although substantial (2.29) is not nearly as large as described in [8,47] where CBF and EBF models had stiffness ratios of 3.9 and 4.5, respectively, over an equivalent unbraced MRF model.

4.3 Earthquake Tests

4.3.1 Introduction

This section presents the results of the earthquake tests of the VD and FD models. Given

the very large number of earthquake tests performed on the VD and FD models (40 and 50, respectively) it is not feasible to discuss the response of the structures in detail for every test. In presenting and discussing the results of the earthquake test programs, the approach has been to make observations on the basis of a number of tests and to describe the behavior of the systems in terms of global response characteristics. An in-depth and detailed evaluation of the response of the various structures to selected individual earthquakes has not been undertaken. Instead, the experimental phase of the research program has been devoted to achieving an overall appreciation of the type of response to be expected from the two damped structural systems subject to earthquake inputs of varying levels and representing a wide range of different ground motions.

In Secs. 4.3.2 and 4.3.3 the VD and FD systems are discussed separately. Global response quantities of acceleration, displacement, interstory drift, story shear, base shear, and energy dissipation are presented. The force deformation behavior of the individual dampers is presented for a number of tests. The response of the MRF and CBF models in the earthquake tests is not separately discussed. However, these structures are mentioned in Sec. 4.4, where comparisons between their response and the responses of the damped structures are presented. For those tests performed on more than one configuration of the test structure it was possible to make the following comparisons:

(i) VD-MRF-CBF

(ii) FD-MRF-CBF

(iii) VD-FD-MRF

(iv) FD-MRF

(v) VD-FD

The comparisons are made in terms of acceleration, displacement, interstory drift, story shear, and base shear for the different structural systems.

4.3.2 Viscoelastically-Damped Model

The earthquake tests performed on the VD model are listed in Table 3.10. The peak roof displacement and acceleration responses are included in the table. Envelopes of peak story accelerations, displacements and interstory drifts for the El Centro, Taft, and Miyagi series of tests are presented in Fig. 4.6.

(a) Damper Behavior

The measured force-deformation behavior of the VE dampers for the ec-400, taft-400, miyagi-50, miyagi-300, miyagi-400, park-350, and buc-300 tests is presented in Figs. 4.7 — 4.13. The following observations are made:

- In general, the figures indicate that the behavior of the VE dampers is stable and repeatable. For repeated cycling at large strains (for example, miyagi-300 and miyagi-400, Figs. 4.10 and 4.11), some stiffness degradation is apparent. This occurred mainly in the dampers at the lower levels where the largest damper strains were developed.

- All the dampers were activated in all the tests. Even for low-level excitations, for example, the miyagi-50 test with a PGA of 0.115g (Fig. 4.9), all the dampers are deformed and absorb energy, albeit sustaining very small shear deformations in the upper levels.

- The general shape of the hysteresis loops is typical of the force-deformation relationship for a material with velocity-dependent properties. The park-350 and buc-300 loops (Figs. 4.12 and 4.13) are good examples, showing that the loop area grows in both the minor and major axes dimensions with increasing displacement. Hysteretic behavior, on the other hand, possesses only displacement-dependent energy dissipation (loop area).

- Peak displacement demands on the VE dampers occurred in the miyagi-400 test, in which the maximum level 1 device displacement was 0.31 inch. This displacement corresponds to a VE material peak shear strain of 208 %. This contrasts with the peak strains of only 6 % developed at level 1 in the miyagi-50 test.

- The distorted shape of the level 3W damper force-deformation loop in the miyagi-50 test (Fig. 4.9) was a consequence of loose bolts connecting the damper to the bracing. This resulted in a short range of slip displacement with almost zero force before the bolts contacted the edges of the bolt holes, at which stage the force in the bracing, and thus in the damper began to increase.

- Some of the loss of stiffness that is apparent in the level 1W and 1E dampers for the ec-400, taft-400 and miyagi-400 tests (Figs. 4.7, 4.8, and 4.11) was due to progressive delamination of these dampers during these tests.

The distribution of damper deformations in the structure is in direct proportion to the interstory deformations of the VD model. Figure 4.6 shows that the interstory drift (ISD) distribution is quite uniform up the structure for all but the largest input level for each earthquake motion. The bottom floor ISD is larger than that of the upper stories in all cases, but this is because the first story is one-third taller (48"/36") than the upper stories, while the column sections are the same for all stories. Plotting drift index (interstory drift/story height) would have produced drift profiles of a more uniform appearance, but ISD is a more meaningful quantity in relation to damper displacements and so drift index was not used. The damper deformations are related to ISD by

$$d_1 = \frac{ISD_{0\text{-}1}}{\cos 38.6^o} \tag{4.4}$$

for the first floor, and

$$d_2 = \frac{ISD_{1\text{-}2}}{\cos 31^o}$$

$$d_3 = \frac{ISD_{2\text{-}3}}{\cos 31^o} \quad \text{, etc., for the upper floors.} \tag{4.5}$$

The force-deformation loops presented in Figs. 4.7 — 4.13 were plotted using the measured damper deformations and not the resolved ISDs as expressed in Eqs. 4.4 and 4.5, however, the latter relationships were used in the energy calculations for the un-instrumented dampers at lev-

els 5, 7, and 9.

(b) Device Stiffness versus Shear Strain

An effective stiffness quantity was determined for each of the instrumented dampers for all of the earthquake tests of the VD model. This stiffness was defined to be the slope of the least-squares, best-fit straight line to the hysteresis loop for all portions of the loop between $\pm d_{max}/2$ and $\pm d_{max}$. An example of these stiffnesses, shown plotted directly on the hysteresis loops for the ec-250 test, is given in Fig. 4.14. The maximum shear strain in the VE material (γ_{max}) was identified for each damper in all of the tests. The relationship between device stiffness and γ_{max} is shown in Fig. 4.15 for the El Centro, Taft, and Miyagi series of tests. Each point in the figures represents a value of stiffness and strain evaluated for an individual damper. The general trend of decreasing stiffness with increasing γ_{max} is clear. The most substantial stiffness decrease occurs over the 0 — 50 % shear strain range in each case, and for strains in excess of about 50 % the stiffness assumes a relatively constant value.

(c) Effect of Dampers on Structure Frequency

For the El Centro, Taft, and Miyagi tests for which results have been plotted in Fig. 4.15, the fundamental frequency of the test structure was determined by a transfer function evaluation of the story accelerations. The fundamental frequencies obtained are plotted against PGA for each test in Fig. 4.16. The spread of values reflects the influence of damper stiffness on the frequency characteristics of the VD model. The fundamental frequency decreased by as much as 0.43 Hz, from 2.43 Hz to 2.00 Hz (18 %), with increased excitation intensity.

(d) Story Shears

Peak story shears and peak damper forces are shown in Fig. 4.17 for the ec-100, ec-200, and ec-400 tests. Similar plots for the miyagi-100, miyagi-200, and miyagi-400 tests are shown in Fig. 4.18. The story shear ratio, SSR, is defined as

$$SSR_i = \frac{\text{horiz. component of peak damper force at level } i}{\text{peak story shear at level } i} \qquad (4.6)$$

SSRs for every level of the VD model and all of the earthquake tests performed are given in Table 4.5. With the exception of SSR_9, which is consistently greater than 0.5 (about 0.7 to 0.8) the level 1 — 8 SSRs follow a uniform pattern. For the small intensity inputs, the SSRs are about 0.45 — 0.5, and decrease to about 0.25 — 0.3 as the input intensity increases. There is very little variation of SSR up the structure for a single test. Given the uniform story stiffness of the MRF and the fact that all of the VE dampers are of the same design, it is expected that the SSRs be approximately the same for all levels (and SSR_1 slightly lower that $SSR_{>1}$). The consistently higher values of SSR_9 are explained by the fact that the dampers at this level were barely activated in any of the earthquake tests, and when they were the damper strains were small. The damper stiffness at small strains was much higher than at large strains (Fig. 4.15), and thus the portion of total story shear carried by the dampers (that is, the SSR) was greater than that for the larger strain conditions that existed in the lower levels.

(e) Energy Dissipation

Representative energy time histories for the VD model are shown in Figs. 4.19 — 4.24, for the ec-150, ec-250, miyagi-300, pac-350, sf-200, and buc-300 tests. The energy quantities plotted are input energy, elastic strain energy, kinetic energy, energy dissipated by the VE dampers, and energy dissipated by other loss mechanisms. The computational approaches used to determine these various quantities are outlined in Sec. 3.8.2. For levels 5, 7, and 9 where the dampers were not instrumented, the force-deformation relationships were estimated from those measured at the adjacent floors. For levels 5 and 7, the mean of the forces in the dampers in the floors above and below was calculated and ISD resolved to obtain the damper displacement (Eq. 4.5). For level 9, the level 8 damper force was extrapolated on the basis of the ratio of the respective ISDs, and the resolved level 9 ISD used as the damper displacement (Eq. 4.5). With these approximations, the energy dissipated at every level of the VD model could be either calculated directly or estimated reasonably.

The energy dissipation ratio, EDR, is defined as

$$EDR = \frac{\text{total dissipated energy}}{\text{total input energy}} \ \% \tag{4.7}$$

where the total dissipated energy is assumed only to be that dissipated by the dampers.

The El Centro time histories (Figs. 4.19 and 4.20) show a significant increase in energy dissipated with the increase in input motion intensity. The EDRs for the ec-150 and ec-250 tests are 45.1 % and 74.6 %, respectively, while the corresponding PGAs were 0.319g and 0.486g. The pac-350 time histories (Fig. 4.22) show the response of the VD model to an impulsive type of ground motion. In this test the dampers dissipated 74.1 % of the input energy. The results for the sf-200 and buc-300 tests show the response of the VD model to a high-frequency and a low-frequency ground motion, respectively (Figs. 4.23 and 4.24). In both cases the dampers absorbed a significant amount of the energy input to the structure, 73.4 % in the case of the sf-200 test and 72.4 % in the case of the buc-300 test.

EDR is plotted against PGA for the El Centro, Taft, and Miyagi series of tests in Fig. 4.25. One readily apparent feature of these relationships is that there are two distinct ranges of energy dissipation. For the El Centro and Taft tests these ranges are approximately 0 — 0.5g PGA, in which the $EDR \approx 50$ %, and 0.5g PGA and above, in which the EDR gets as high as 75 %. For the Miyagi tests the two ranges are approximately 0 — 0.25g and 0.25 — 0.5g PGA. The following explanation is one possible reason for this phenomenon.

In the smaller intensity tests the excitation was not sufficient to cause significant deformations in the VE material of the dampers. The dampers were loaded through only a few small amplitude cycles. However, once the excitation reached a certain level, it caused large deformations in the dampers, these led to a gradual softening of the VE material as the earthquake motion progressed, and as the dampers softened the force required to induce continued large deformations decreased. Thus, the dampers continued to be deformed through more large cycles, even though the intensity of the input reduced with time toward the end of the motion. This increase in the amount of deformation induced in the dampers corresponds to significant

energy dissipation, and results in a significant increase in EDR for the larger intensity tests, as seen in Fig. 4.25.

The distribution of energy dissipation in the VD model is investigated by studying the story dissipation ratio, SDR, defined as

$$SDR_i = \frac{\text{total energy dissipated by dampers at level } i}{\text{total energy dissipated by dampers}} \tag{4.8}$$

SDRs for every level of the VD model and all of the earthquake tests performed are given in Table 4.6. The SDRs listed in the table indicate that there is no dependence of SDR on the intensity of the input motion. The bottom level dampers dissipated the largest amount of the total dissipated energy, with SDR_1 typically about 0.25. The upper level dissipation ratios are approximately 0.2, 0.15, 0.13, 0.13, 0.08, 0.06, 0.02, and ≈ 0 for levels 2 through 9, respectively. Given that all of the VE dampers are of the same design and the strong dependence of the energy dissipated by a damper on the VE layer shear strain (Eq. 2.13) this trend in SDRs is expected. The negligible energy dissipation of the level 8 and 9 dampers is offset by the level 1 and 2 dampers each dissipating in excess of 20 % of the total dissipated energy.

The SSR and SDR results indicate that there are no detrimental aspects of the uniform damper distribution chosen in the design of the VD structure. The damper design preserved the relative stiffnesses of the stories and led to uniform ISDs while dissipating significant amounts of earthquake energy input to the VD structure.

(f) Temperature Increases in VE Layers Under Earthquake Loading

As described in Sec. 4.5.2, the level 1W damper contained a thermocouple in one of its layers to permit temperature observations during earthquake tests. The temperature increases were typically only 4 — 6 °F at most for all of the tests monitored. The changes in the VE material properties due to such increases are small, and not enough to cause appreciable changes in the dynamic properties of the VD model. Earthquake loadings can be regarded as short duration in this regard, and the temperature increases due to this type of loading are not

large.

Temperature increases under large-strain, steady-state loading conditions are more significant. For twenty-cycle tests at a frequency of 1 Hz, Bergman and Hanson [48] report temperature increases of 14 °F for 100 % shear strain and 24 °F for 200 % shear strain. The changes in material properties, particularly stiffness reduction, are significant for these temperature increases, which are much larger than those observed in the current earthquake tests. To minimize temperature effects on the material properties, it is usual to separate the (individual) laminations of multilayer dampers with heat transfer fins. These fins are thin stainless steel plates that extend beyond the edges of the VE layers and assist with heat transfer from within the layers.

4.3.3 Friction-Damped Model

The earthquake tests performed on the FD model are listed in Table 3.11. The peak roof displacements and accelerations are included in the table. Profiles of peak story acceleration, displacement, and interstory drift for selected earthquakes are shown in Fig. 4.26. Results for the complete sequences of tests at increasing span are shown for the El Centro, Taft, Miyagi, Chile.u, La Union, and Zacatula motions. As seen for the VD model ISD profiles (Fig. 4.6), the first floor ISD is larger than those of the upper floors, except for the particularly low-level excitations. The ISDs of the intermediate floors (2 — 8) are quite uniform, showing a gradual decrease with height.

(a) Damper Behavior

The measured force-deformation behavior of the friction dampers for the ec-400, miyagi-400, chile.u-50, chile.u-750, unio-1000, and zaca-1000 tests is presented in Figs. 4.27 — 4.32. The following are some general observations on the hysteresis loops:

- The behavior of the Sumitomo friction dampers is extremely regular and repeatable. This is clearly evident from the hysteresis loops presented. The slip force of the devices is well-defined and the devices exhibit almost no variation of slip force during earthquake

excitation. For the 50 earthquake tests performed on the FD model no degradation of performance was observed for any of the friction devices in the structure.

- The rectangular shape of the hysteresis loops achieves maximum energy dissipation for a given displacement.

- Peak displacement demands on the devices occurred during the ec-400, chile.u-750, and unio-1000 tests. The maximum displacements recorded for the level 1 devices were 0.34, 0.33, and 0.37 inch, respectively, for these tests.

- The chile.u-50 and chile.u-750 tests illustrate the response of the dampers to small and large excitations. The chile.u-50 test with PGA = 0.112g was too small to activate the dampers, and the force-deformation plots in Fig. 4.29 show that the dampers did not slide. The rather jagged appearance of these loops is due to the extremely small displacements being measured, which are almost of the order of accuracy of the DCDTs (± 0.001 inch). It is possible to obtain an estimate of the elastic stiffness of the friction dampers from these plots, and this estimate was used to calculate the appropriate element elastic properties for the analyses of the FD model presented in Chapter 5. The dampers were fully activated by the large chile.u-750 test, with PGA = 1.202g (Fig. 4.30).

- The distribution of damper deformations is in direct proportion to the interstory deformations of the FD model. As already noted above, the interstory deformations of the intermediate levels (2 — 8) of the FD model were quite uniform, indicating that the selection of and distribution of device slip forces in the structure represented a good design.

- The cause of the very slight distortions of the level 6W hysteresis loops (Figs. 4.27, 4.28, 4.30 — 4.32) is not known. The DCDTs mounted on the friction dampers measured only the damper slip deformation and not any of the deformations that may have occurred in the swivel bearings at the ends of the dampers. This suggests that the distortion was a result of free travel inside the friction damper occurring upon load reversal. This is not known for

certain. Nonetheless, of the ten dampers instrumented and for the 50 earthquake tests performed this was the only indication of unusual behavior and is a very minor aspect of the overall behavior of the dampers.

- The hysteresis loops indicate no amplitude or velocity dependencies in the force-displacement behavior of the devices. Similar observations have been made during numerous earlier component tests of the dampers performed by Sumitomo [40].

(b) Effect of Dampers on Structure Frequency

The influence of the nonlinear behavior of the friction dampers on the frequency of the FD model was investigated by evaluating the first-mode frequency of the structure from the earthquake test data. The low-level earthquake tests (in which no device slip occurred) revealed a first-mode frequency (f_1) of 2.67 Hz. This is slightly higher than f_1 identified from the pulse or random excitation tests, and close to f_1 of the CBF (2.95 Hz). For the moderate to large earthquake tests it was not easy to identify the structure frequencies from transfer functions; however, for two for which it was possible the results are presented below. (It is possible that a moving-window (in time) transfer function analysis might better reveal the changing frequency of the FD model during excitation, however, this approach was not pursued.)

The roof acceleration transfer functions for the ec-50 and ec-400 tests are shown in Fig. 4.33. These show a reduction in f_1 from 2.63 Hz to 2.47 Hz. In the case of no device slip (ec-50) the resonant frequency is well defined, whereas when substantial slip occurred in the devices (ec-400) the transfer function is poorly defined in the region of f_1 and there is no readily identifiable first frequency. The frequency corresponding to the peak of the transfer function is 2.47 Hz, but there is considerable response in frequencies as low as about 2 Hz. The roof acceleration transfer functions for the unio-50 and unio-1000 tests are shown in Fig. 4.34. The general reduction in f_1 is even more clear in these tests than for the El Centro tests. The unio-50 transfer function is well defined in the region of f_1 = 2.65 Hz. The peak of the unio-1000 transfer function corresponds to a frequency of 2.35 Hz, but again, there is considerable

response in frequencies as low as about 1.9 Hz.

These results indicate that prior to slip of the friction devices the structure responds strongly in its first mode of vibration, but with the onset of device slip the frequency associated with the first mode becomes less well-defined and there is appreciable response in a band of frequencies below the pre-slip f_1. On the basis of the frequencies associated with the peaks of the respective transfer functions, the f_1 reductions are 2.63 Hz to 2.47 Hz and 2.61 Hz to 2.35 Hz for the El Centro and La Union tests, respectively. These are not big changes, but the frequencies identified from the ec-400 and unio-1000 tests are not properly representative of the post-slip transfer functions and this comparison should be made with caution.

(c) Story Shears

Peak story shears and peak device forces are shown in Fig. 4.35 for the ec-50, ec-200, and ec-400 tests. Similar plots for the miyagi-50, miyagi-200, and miyagi-400 tests are shown in Fig. 4.36, and for the unio-50, unio-250, unio-500, and unio-1000 tests in Fig. 4.37. No devices slipped during the miyagi-50 or unio-50 tests, and in the ec-50 test only the devices up to (and including) level 3 slipped. This explains the uniform reduction of peak device forces with height in the model for each of these tests.

The story shear ratio, SSR, for the FD model is defined in a similar fashion to Eq. 4.6,

$$\text{SSR}_i = \frac{\text{total device slip force at level } i}{\text{peak story shear at level } i} \tag{4.9}$$

SSRs for every level of the FD model and all of the earthquake tests performed are given in Table 4.7. For the small intensity inputs (span = 50) the SSRs are typically about 0.75 at the first level, reducing to about 0.55 in the top levels. The ec-50 SSRs are a little lower, ranging from about 0.6 at the bottom level to about 0.5 at the top of the structure. The SSR at each level decreases considerably as the earthquake motion intensity increases. This is for the simple reason that the maximum force that can develop in a friction device is the device slip force, and even though increases in input intensity cause larger story shears, the maximum forces in

the devices remain unchanged and thus the SSRs decrease. This contrasts with the VE dampers, which do not have a defined maximum force capacity. SSR_1 reduces from about 0.75 for small intensity inputs to about 0.17 — 0.25 for large inputs. The reductions in the upper levels are not quite as dramatic, being about 0.5 — 0.6 down to 0.2 — 0.3. At the top level the friction devices were only occasionally activated, and SSR_9 does not show large variations with input intensity, being about 0.4 — 0.55 for most tests.

(d) Energy Dissipation

Representative energy time histories for the FD model are shown in Figs. 4.38 — 4.48 for the ec-50, ec-250, miyagi-350, pac-350, sf-300, buc-300, unio-50, unio-250, unio-500, unio-750, and unio-1000 tests. Unlike the VD tests, the dampers at every level of the FD were instrumented, and no approximations were necessary to calculate the energy dissipated by all of the dampers.

The El Centro time histories (Figs. 4.38 and 4.39) show a significant increase in EDR (Eq. 4.7) with the increase in input intensity. The ec-50 and ec-250 tests showed EDRs of 29.9 % and 63.4 %, respectively, with PGAs of 0.134g and 0.476g. A similar variation of EDR with PGA is seen in Figs. 4.44 — 4.48 for the La Union sequence of tests. The EDR varies from 21.1 % to a maximum of 92.9 % for these tests. The pac-350 time histories (Fig. 4.41) show the response of the FD model to an impulsive type of ground motion. In this test the dampers dissipated 69.5 % of the input energy. The results for the sf-300 and buc-300 tests show the response of the FD model to a high-frequency and a low-frequency ground motion, respectively (Figs. 4.42 and 4.43). In both cases the dampers absorbed a significant amount of the energy input to the structure, 77.4 % in the case of the sf-300 test and 60.8 % in the case of the buc-300 test.

EDR is plotted against PGA for the El Centro, Taft, and Miyagi series of tests in Fig. 4.49(a) and for the Chile.s, Chile.u, La Union, and Zacatula tests in Fig. 4.49(b). The two plots show different trends for the two groups of earthquake signals. In Fig. 4.49(a), EDR increases

sharply from an initial value of about 20 % for small input intensities, to reach a relatively constant value of about 70 % for accelerations beyond 0.3g. Fig. 4.49(b) shows the same general initial shape but reaches a peak EDR in excess of 90 % and then drops slightly for accelerations greater than about 0.7g. The very large EDRs for the FD system subjected to large inputs show the friction dampers to be extremely effective at dissipating energy.

The shapes of these curves are related to the characteristics of the various ground motions. The earthquake motions of Fig. 4.49(b) (Chile, La Union, and Zacatula) are all long duration motions that have their energy contained broadly over the entire duration of the signal. For moderate to severe input intensities they are able to drive the friction dampers through many large cycles of displacement over most of their duration. In contrast, the El Centro, Taft, and to a lesser extent Miyagi, motions contain most of their energy over the initial portion of the signal. Thus, they induce a number of large displacement cycles in the early part of the motion, but are not able to sustain sliding of the dampers over the latter portion of the motion. Over the latter portion of the motion the other energy-loss mechanisms (following section) must dissipate the energy not absorbed by the inactive dampers.

The distribution of energy dissipation in the FD model was investigated by studying the story dissipation ratio (SDR) defined in Eq. 4.8. SDRs for every level of the FD model and all of the earthquake tests performed are given in Table 4.8. From the table, it can be seen that there is no strong relationship between input intensity and SDR. Level 1 dissipated the most energy, with SDR_1 being typically about 0.3–0.4. SDR_2 is about 0.2, while the intermediate levels (3 — 6) have SDRs of about 0.1 — 0.2. The top three levels contributed very little, typically less that 5 — 10 %, to the total energy dissipated in the FD model. The friction dampers at these levels (particularly 8 and 9) were not often activated, and thus did not dissipate much energy. This contrasts with the VE dampers at these levels, which although subject to similarly small forces, were able to dissipate energy for the small input excitations. For moderate to large inputs, the (percentage) contribution of the upper level dampers to the total energy dissi-

pation was about the same for both the VD and FD structures.

(e) Other Energy-Loss Mechanisms

The unaccounted-for energy in the energy time histories is attributed to a number of factors that are not readily evaluated. They have been denoted "other energy-loss mechanisms". No explicit energy quantity has been defined or calculated to represent viscous damping. As noted in Sec. 4.8.2, other researchers [8,47] have defined the viscous-damped energy in the energy equation (Eq. C.7) to be the remaining unknown term when all of the other quantities are accounted for. This approach is felt to over-estimate the likely viscous, or internal damping of the test structure unreasonably and not to consider other possible sources of damping.

Among the other energy-loss mechanisms in the test structure, the most significant are the bolted connections. For the otherwise identical MRF and CBF models, ξ_1 increases from 4.1 % to 4.9 % with the introduction of the bracing (see Table 4.1, earthquake test results). This increase is attributed to the additional bolted connections present in the CBF (more than 300). The FD model contains even more bolted connections than the CBF (about 450) associated with the attachment of the friction dampers and the bracing in the structure. The attachment of the lead billets to the concrete blocks and the concrete blocks to the structural frame are also bolted connections. While every effort was made throughout the test program to ensure that all bolted connections remained tight, it is nonetheless likely that slip occurred at a few locations at least. For very large lateral accelerations in the test structure (approaching or in excess of 1g) the complete fixity of the large concrete blocks was questionable. Even very small slip displacements of the blocks could absorb an appreciable amount of energy.

In the energy time histories presented, the "other energy-loss mechanisms" quantity is assumed to be the internal (or viscous) damping of the test structure and also the contribution of the factors discussed above.

4.4 Comparisons of Structural Systems

4.4.1 Introduction

In this section the behavior of the four configurations of the test structure is compared. The responses of the VD, MRF, and CBF models are compared for the El Centro, Taft, and Miyagi tests common to the three systems in Sec. 4.4.2. Similar comparisons are made of the FD, MRF, and CBF models in Sec. 4.4.3. In Sec. 4.4.4 the responses of the VD, FD, and MRF models are compared for the tests common to these structural systems. Finally, in Sec. 4.4.5, direct comparisons of the VD and FD models are made for a selection of tests common to these systems.

4.4.2 VD-MRF-CBF Systems

Profiles of peak story acceleration, displacement, and interstory drift for the VD, MRF, and CBF models are compared in Figs. 4.50 and 4.51 for the ec-100, ec-200, ec-300, ec-400, and miyagi-200 tests. Each of these tests was performed on the VD and MRF models (except that the MRF ec-100 results are taken to be twice the measured ec-50 results), but the CBF profiles represent scaled results. The only test results available for the CBF are listed in Table 3.9, and of these, the ec-100 and miyagi-75 results were used and scaled accordingly to obtain the profiles in Figs. 4.50 and 4.51. Elastic response has been assumed in each case. (The assumption of linear behavior for the CBF under the ec-400 signal is supported by the non-linear analyses presented in Sec. 5.3.3, where it was found that there was no yielding in the CBF under this signal — with the exception of minor buckling of only one brace). Recognizing the variability of the shake table in reproducing the same PGA (typically about ± 10 %) for a given signal and span, the profiles presented in the figures have all been scaled according to the largest PGA for each set of tests. That is,

$$\text{plotted profile} = \text{profile } i \times \left[\frac{\text{PGA}_{\max}}{\text{PGA}_i} \right] \tag{4.10}$$

so that each set of data is scaled to a single PGA. The relative displacement (with respect to

the shake table) and the ISD profiles are self-explanatory, the acceleration profiles have been normalized to PGA_{max} in each case.

The acceleration and displacement plots in Figs. 4.50 and 4.51 show that the VD model generally behaves in the same way as the CBF with regard to displacements and in the same way as the MRF with regard to accelerations. For example, in the ec-200 test the MRF peak roof displacement is 2.64 inches, while those of the VD and CBF are 1.67 inches and 1.79 inches, respectively. The peak roof accelerations are 1.42g, 1.17g, and 1.59g for the MRF, VD, and CBF, respectively. The miyagi-200 results compare somewhat differently. The peak roof displacements are 2.57 inches, 1.20 inches, and 0.87 inch and the peak roof accelerations are 1.07g, 0.63g, and 0.75g for the MRF, VD, and CBF, respectively.

Story shear profiles for the VD, MRF, and CBF models are compared for the ec-100, ec-200, ec-300, and miyagi-200 tests in Fig. 4.52. These further illustrate the "best of both" response of the VD model seen in the acceleration and displacement comparisons. For the El Centro tests, the story shears in the VD are approximately the same as the MRF, and about 30 % less than the CBF. The miyagi-200 profile shows that the VD and CBF story shears are comparable, and about 30 % less than those of the MRF.

4.4.3 FD-MRF-CBF Systems

Profiles of peak story acceleration, displacement, and interstory drift for the FD, MRF, and CBF models are compared in Figs. 4.53 and 4.54 for the ec-100, ec-200, ec-300, ec-400, and miyagi-200 tests. The results plotted for the MRF and CBF models are the same as in Figs. 4.50 and 4.51. As was done for the VD-MRF-CBF profiles, the acceleration profiles have been normalized to PGA_{max} in each case.

The acceleration and displacement profiles indicate that the FD model behaves in the same way as the CBF in terms of displacements and in the same way as the MRF in terms of accelerations. (This observation was also made for the VD model.) For example, in the ec-200 test, the MRF peak roof displacement is 2.64 inches, while those of the FD and CBF are 1.62

inches and 1.79 inches, respectively. The peak roof accelerations are 1.42g, 1.01g, and 1.59g for the MRF, FD, and CBF, respectively. The miyagi-200 results compare somewhat differently. The peak roof displacements are 2.57 inches, 1.30 inches, and 0.87 inch and the peak roof accelerations are 1.07g, 0.68g, and 0.75g for the MRF, FD, and CBF, respectively.

Story shear profiles for the FD, MRF, and CBF models are compared for the ec-100, ec-200, ec-300, and miyagi-200 tests in Fig. 4.55. These further illustrate the "best of both" response of the FD model seen in the acceleration and displacement comparisons. The ec-100 story shear profile shows the difference in response for the FD and VD models under low-level excitations. For the ec-100 test, the FD shear profile is almost the same as that of the CBF. This is because the friction devices were barely activated in this small test. The VD shear profile for the ec-100 test (Fig. 4.52), on the other hand, is about the same as that of the MRF and about 30 % less than that of the CBF. For the larger El Centro tests the FD story shears are comparable to those of the MRF, which are typically about 30 % less than the CBF story shears. The miyagi-200 profile shows that the FD and CBF story shears are comparable, and are about 30 % less than those of the MRF.

Direct comparisons of the VD and FD models for a range of earthquake motions are made in Sec. 4.4.5.

4.4.4 MRF and Damped Models

The response of the MRF model is compared with those of the VD and FD models in this section. The tests presented were not performed on the CBF.

Peak acceleration, displacement, and interstory drift profiles for the El Centro (ec-50, ec-200, ec-300, ec-400), Taft (taft-50, taft-200), and Miyagi (miyagi-50, miyagi-200) series of tests are presented in Figs. 4.56 — 4.58. The scaling of Eq. 4.10 has been applied to these results. The following general observations are made for each set of tests:

El Centro : The displacements of the VD are 25 — 50 % less than those of the MRF, while the FD displacements range between those of the VD and the MRF. The

accelerations of the VD are typically less than those of the MRF (by up to 50 %), while the FD accelerations are intermediate between those of the VD and the MRF.

Taft : Both the VD and FD displacements are higher than the MRF displacements for the taft-50 test. However, all of the displacements in this test were very small. The results for the taft-200 test show the VD displacements to be about 20 % less than those of the MRF, and the FD displacements to be about 10 % less than those of the MRF. The irregular acceleration profiles are not readily described, although all of the FD accelerations, and all of the VD accelerations with the exception of the top two levels, are less than the corresponding MRF accelerations.

Miyagi : The VD and FD displacements are almost identical for both the miyagi-50 and miyagi-200 tests, and about 60 % less than those of the MRF. The VD accelerations are about 60 % less than those of the MRF in the miyagi-50 test and about 50 % less than those of the MRF in the miyagi-200 test. The FD accelerations are about 50 % less than those of the MRF in both tests.

Base Shears

Peak base shear ($V_{b_{max}}$) is plotted against PGA for the El Centro, Taft, and Miyagi test series of the MRF, VD, and FD models in Fig. 4.59. There is very little difference between the $V_{b_{max}}$ developed in the VD and FD models for these motions, and they are typically the same (or less in the case of El Centro) as the base shears developed in the MRF.

A number of further tests were performed on only the FD and MRF models. Comparisons of these two structural systems for the chile.u-50, chile.u-200, unio-50, unio-250, zaca-50, and zaca-250 tests are presented in Figs. 4.60 — 4.62. The scaling of Eq. 4.10 has been applied to these results. The following general observations are made for each set of tests:

Chile.u : The FD displacements are about one-half those of the MRF in both tests. The FD accelerations for the chile.u-50 test are about the same as those of the MRF (devices not activated) and about one-half those of the MRF for the chile.u-200 test when the devices were activated (although not activated at level 9 and only for a few cycles at level 8).

La Union : The FD displacements and accelerations are about one-half those of the MRF in both tests. The devices were not activated in the unio-50 test, and were activated up to level 8 (although for only a few cycles at levels 5-8) in the unio-250 test.

Zacatula : The FD displacements are about the same as those of the MRF for the zaca-50 test and about 30 % less than those of the MRF for the zaca-250 test. The FD accelerations are about 30 % larger than those of the MRF in the zaca-50 test (devices not activated). In the zaca-250 test the FD accelerations are about the same as those of the MRF in the lower six stories and about 30 % less in the top three stories. The friction devices were activated up to (and including) level 7 in the zaca-250 test.

Base Shears

$V_{b_{max}}$ is plotted against PGA for the Chile.u, La Union, and Zacatula series of tests of the MRF and FD models in Fig. 4.63. The FD $V_{b_{max}}$ are about the same, or less in the case of the Chile.u (chile.u-200) and La Union (unio-250) tests, as those of the MRF. The three plots of Fig. 4.63 are summarized in Fig. 4.64. The FD $V_{b_{max}}$— PGA relationships for the three earthquake motions are seen to be very similar, in each case reaching a peak of about 80 kips at approximately 0.8g which is not exceeded for larger inputs. The FD base shear is about the same or less than that of the MRF.

4.4.5 VD and FD Models

A number of tests were performed on only the VD and FD models. These tests are compared in this section.

Response profiles of peak acceleration, displacement, and interstory drift are compared for the El Centro, Taft, Miyagi, Pacoima, Parkfield, San Francisco, Bucharest, and Mexico City motions at various spans in Figs. 4.65 — 4.70. Apart from small differences in a few cases (park-220 and park-350, buc-200, and sct-400), the most striking aspect of all of these results is the great similarity between the responses of the VD and FD systems. In general, there is less than about a 10 % difference in displacements, and less than about a 20 % difference in accelerations. There are some local exceptions to these values, but they are few in comparison with the overall results. Profiles of peak story shear have not been computed for these tests, but given the great similarity between the VD and FD story accelerations the story shears would be expected to be very similar.

The stick-slip behavior of friction systems will, to some extent, increase higher frequency responses in a structure containing such devices. This aspect is investigated by studying floor response spectra for the FD, VD, and MRF models. Because of its strong components of response in the second and third modes of vibration, the level 3 acceleration was chosen for the floor spectra comparisons.

Two percent-damped spectra for the FD, VD, and MRF are presented in Figs. 4.71 — 4.73 for the El Centro, Taft, and Miyagi tests, respectively. The El Centro spectra (Fig. 4.71) show that the FD and VD system responses up to about 10 Hz (in the first and second modes) are very similar and are considerably reduced from the MRF response. In the frequency range above about 12 Hz there are some variations. The VD spectral accelerations are less than those of the MRF in all cases, while for the ec-200 and ec-400 tests the FD spectral accelerations exceed those of the MRF and are about 50 % to 100 % higher than those of the VD. The VD and FD spectra for the Taft tests are less than the MRF spectrum over the entire frequency range, while the FD spectrum is slightly higher than that of the VD for frequencies greater

than about 10 Hz. The Miyagi spectra show variations that are similar to those noted above. There is a considerable reduction of second-mode response for both damped systems for the miyagi-200 and miyagi-400 tests. The VD accelerations are less than those of the MRF over the entire frequency range for these tests. The FD accelerations are also generally reduced, although less so in the higher frequencies. From about 15 to 25 Hz, the FD accelerations are about 50 % to 100 % larger than those of the VD. The stiffness increases provided by the dampers, particularly in the second mode, are clearly seen in the miyagi-50 spectra. The acceleration reductions achieved by both damped systems are negligible for this small test.

VD and FD level 3 floor response spectra are compared for the Pacoima, Parkfield, Bucharest, San Francisco, and Mexico City (SCT) motions at various input levels in Figs. 4.74 — 4.77. In general, the spectra for both systems are very similar up to about 5 Hz, above which the FD accelerations are higher than those of the FD.

4.5 Conclusions

The following general comments are made:

- Both types of energy absorbers worked well and considerably improved the response of the test frame in the earthquake tests performed.
- For those tests common to both damped systems, their responses were very similar.
- The FD system was subjected to larger inputs than was the VD system. The friction dampers absorbed very large amounts of the input energy for large excitations.
- The friction dampers are characterized by outstanding performance.
- Comparisons of floor response spectra for the FD, VD, and MRF showed that the friction devices did not significantly amplify higher frequencies of the model.
- Several delamination failures of VE dampers occurred throughout the test program. These failures occurred at the interfaces of the thin VE laminations that comprised the damper layers. It is believed that the failures were initiated by the development of tensile stresses in the VE layers due to spreading of the steel plates to which the VE material was bonded,

that occurred at large deformations. A practical solution to this problem is discussed below.

The design details of the VE dampers for the VD model tests were somewhat simplified from those of a prototype damper. In a prototype damper "shoulder bolts" would be used to prevent spreading of the steel plates and the development of tensile stresses in the VE layers. These bolts pass right through the damper, and a slotted hole in the middle steel plate permits the damper to deform in shear. The inner portion of the bolt is of a larger diameter than its threaded ends, and the step in diameter is called the "shoulder", hence giving the bolt its name. Nuts are tightened down onto the outer plates which sit down on the shoulders of the bolts. This arrangement prevents any separation of the steel plates and ensures that undesirable tensile stresses cannot develop. This detail, had it been used in the model dampers, would have likely prevented the delamination failures from occurring.

Both sets of dampers were subjected to a very large number of earthquake motions. In reality, it is likely that a building in a region of moderate to high seismic risk would experience only one or maybe two earthquakes of these intensities in its lifetime. The performance of the VD and FD systems demonstrated that they are both more than capable of surviving any number of severe seismic events. The following questions relate to the long-term performance of the dampers.

(i) What are the aging characteristics of the VE material? Observations of VE dampers in the World Trade Center have been going on for twenty years and have so far indicated that changes in material properties with age are not significant.

(ii) Will the friction dampers slip at their original friction force if they are not activated over a long period of time? The phenomenon of long-term stick remains one of the main issues related to the performance of friction systems of all kinds.

The two damping systems showed different variations of Story Shear Ratio (SSR) with input intensity. The VD system showed SSRs of about 0.45 — 0.5 for small inputs and these decreased to about 0.25 — 0.3 for large inputs. The FD system SSRs were about 0.5 — 0.75

for small inputs, decreasing to about 0.2 — 0.3 for large inputs. The differences relate to the fact that the VE dampers do not have a threshold or activation force level and the damper force continues to increase with increasing deformation, whereas the friction dampers have a clearly-defined activation force (the friction force), and once activated cannot resist larger forces.

The Story Energy Dissipation Ratios (SDRs) for both damped systems showed that the distribution of energy dissipation throughout the structure was quite uniform, with the exception of the top two levels where the dampers did not contribute significantly to the total energy dissipation. The results suggest that the uniform VE damper design was successful. The small contribution of the upper level dampers indicates that the VD system would have been improved if the dampers at these levels had been smaller than those at the lower levels. Nonetheless, the overall response of the VD system was not compromised by the uniform design. The three different levels of friction force designed for the FD model (Fig. 2.6) were necessary to achieve good performance. The activation-level characteristic of the friction system requires that the distribution of damper forces in the structure be more graduated than that necessary for the VD system to achieve good behavior.

A study of floor response spectra for the FD, VD, and MRF for various input motions showed that both types of energy absorbers produced significant acceleration reductions for frequencies up to about 10 Hz. The VD accelerations for frequencies greater than 10 Hz were also less than those of the MRF, while the FD accelerations were about the same as those of the MRF. The nature of the viscoelastic damping is beneficial over a wide range of frequencies. The FD system, while not offering the level of acceleration reductions of the VD system over such a wide frequency range, nonetheless does not produce significant amplifications over the MRF, and for a somewhat more limited range (about 0 to 10 or 12 Hz) is still able to offer significant improvements. From the point of view of equipment and non-structural component response, the floor spectra results show that the friction dampers do not pose any more of a response amplification problem than that already typical of moment-resisting frames.

TABLE 4.1 MRF and CBF Dynamic Properties

		RANDOM	PULSE	EARTHQUAKE
MRF	f_1	1.94	1.95	1.95
	f_2	6.59	6.60	6.58
	f_3	11.13	11.09	11.26
	ξ_1	3.3	2.9	4.1
	ξ_2	0.4	0.3	0.4
	ξ_3	1.1	0.9	1.2
CBF	f_1	•	•	2.95
	f_2	•	•	11.39
	ξ_1	•	•	4.9
	ξ_2	•	•	1.0

• = test not performed

TABLE 4.2 VD and FD Dynamic Properties From Diagnostic Tests

		PULLBACK	RANDOM	PULSE
VD	f_1	2.76	2.44	2.30†
	f_2	9.40	9.50	8.90†
	ξ_1	8.6 - 10.4 *	8.5	11.8
	ξ_2	6.4 - 8.3 *	6.5	10.5
FD	f_1	3.00	2.60	2.60
	f_2	10.10	10.00	9.70
	ξ_1	3.9	•	4.8
	ξ_2	4.1	•	3.3

* see Table 4.3

† see Table 4.4

• unable to evaluate from test data

TABLE 4.3 VD Model Damping Ratios From Pull-Back Tests

TEST	PULL AT LEVEL	d_o [in.]	DAMPING RATIOS [%]	
			ξ_1	ξ_2
890316.01	3	0.10	9.0	7.9
890316.02	3	0.27	8.6	8.3
890316.03	5	0.37	8.6	6.4
890316.04	5	0.47	10.4	7.5

d_o = maximum static roof displacement prior to load release and free vibration

TABLE 4.4 VD Model Frequencies From Pulse Tests

TEST	f_1 [Hz]		f_2 [Hz]		COMMENTS
	Pulse 1	Pulse 2	Pulse 1	Pulse 2	
890316.07	-	-	-	-	test not evaluated
890317.07	2.30	2.35	8.75	8.85	
890317.15	2.35	2.35	9.10	9.15	
890317.24	2.30	2.25	8.95	8.95	Level 1E failure
890320.01	2.40	2.45	8.95	9.05	replaced damper tightened bolts
890320.08	2.20	2.15	8.50	8.50	
890320.17	2.15	2.15	8.25	8.20	Level 1W failure

TABLE 4.5 VD Model Story Shear Ratios

TEST	STORY SHEAR RATIO AT LEVEL								
	1	2	3	4	5	6	7	8	9
ec-50	0.52	0.57	0.39	0.39	0.42	0.47	0.42	0.36	0.66
ec-100	0.48	0.45	0.41	0.37	0.41	0.46	0.42	0.38	0.70
ec-150	0.44	0.46	0.39	0.36	0.39	0.43	0.41	0.38	0.73
ec-200	0.41	0.43	0.39	0.36	0.38	0.43	0.41	0.40	0.73
ec-250	0.37	0.41	0.40	0.35	0.38	0.44	0.44	0.43	0.83
ec-300	0.25	0.41	0.40	0.32	0.35	0.40	0.41	0.42	0.81
ec-300 †	0.31	0.36	0.36	0.30	0.33	0.37	0.37	0.38	0.74
ec-400	0.21	0.30	0.31	0.26	0.27	0.29	0.31	0.37	0.72
taft-50	0.46	0.44	0.32	0.36	0.39	0.45	0.36	0.19	0.37
taft-100	0.51	0.47	0.40	0.38	0.42	0.49	0.37	0.19	0.36
taft-150	0.44	0.40	0.30	0.30	0.35	0.39	0.37	0.39	0.69
taft-200	0.44	0.41	0.34	0.33	0.36	0.38	0.37	0.39	0.70
taft-250	0.34	0.41	0.40	0.37	0.40	0.47	0.43	0.42	0.80
taft-300	0.31	0.44	0.38	0.33	0.36	0.41	0.39	0.39	0.76
taft-300 †	0.34	0.41	0.41	0.29	0.33	0.39	0.37	0.37	0.70
taft-400	0.29	0.42	0.41	0.31	0.33	0.37	0.36	0.38	0.72
miyagi-50	0.47	0.44	0.30	0.40	0.45	0.53	0.41	0.18	0.32
miyagi-100	0.48	0.45	0.41	0.40	0.43	0.48	0.36	0.18	0.34
miyagi-150	0.45	0.43	0.40	0.37	0.40	0.46	0.41	0.33	0.64
miyagi-200	0.41	0.42	0.42	0.38	0.41	0.46	0.43	0.40	0.81
miyagi-275	0.36	0.37	0.35	0.31	0.35	0.41	0.41	0.41	0.83
miyagi-300	0.22	0.25	0.25	0.20	0.23	0.28	0.30	0.36	0.71
miyagi-350	0.21	0.26	0.26	0.20	0.22	0.25	0.29	0.36	0.73
miyagi-400	0.16	0.26	0.26	0.20	0.22	0.25	0.29	0.39	0.76
pac-220	0.39	0.46	0.38	0.35	0.37	0.41	0.38	0.36	0.72
pac-350	0.29	0.35	0.35	0.26	0.28	0.32	0.31	0.32	0.64
park-220	0.44	0.53	0.33	0.41	0.43	0.46	0.42	0.40	0.74
park-350	0.36	0.43	0.40	0.33	0.35	0.38	0.37	0.38	0.75
sf-200	0.38	0.57	0.49	0.40	0.41	0.43	0.41	0.44	0.82
buc-200	0.36	0.52	0.41	0.41	0.42	0.44	0.40	0.36	0.72
buc-200 †	0.37	0.44	0.44	0.37	0.39	0.40	0.39	0.38	0.70
buc-300	0.31	0.39	0.40	0.30	0.31	0.34	0.33	0.34	0.67
sct-400	0.33	0.46	0.33	0.36	0.39	0.42	0.44	0.48	0.84
sct-400 †	0.37	0.41	0.40	0.31	0.32	0.33	0.34	0.38	0.75

† = test repeated

TABLE 4.6 VD Model Story Energy Dissipation Ratios

TEST	STORY ENERGY DISSIPATION RATIO AT LEVEL								
	1	2	3	4	5	6	7	8	9
ec-50	0.24	0.26	0.08	0.12	0.12	0.08	0.07	0.02	0.01
ec-100	0.25	0.23	0.11	0.11	0.12	0.09	0.07	0.01	0.01
ec-150	0.27	0.18	0.12	0.11	0.13	0.08	0.08	0.01	0.01
ec-200	0.28	0.18	0.12	0.12	0.13	0.08	0.07	0.02	0.01
ec-250	0.24	0.22	0.12	0.14	0.13	0.07	0.05	0.02	0.01
ec-300	0.19	0.23	0.14	0.14	0.13	0.08	0.05	0.02	0.01
ec-300 †	0.21	0.20	0.18	0.13	0.12	0.08	0.06	0.02	0.01
ec-400	0.17	0.21	0.19	0.14	0.11	0.09	0.05	0.03	0.01
taft-50	0.27	0.23	0.07	0.13	0.14	0.08	0.06	0.01	0.01
taft-100	0.26	0.23	0.10	0.12	0.13	0.10	0.06	0.01	0.01
taft-150	0.26	0.11	0.10	0.13	0.14	0.12	0.10	0.02	0.01
taft-200	0.26	0.14	0.11	0.13	0.15	0.11	0.08	0.02	0.01
taft-250	0.25	0.22	0.08	0.14	0.15	0.07	0.06	0.02	0.01
taft-300	0.21	0.24	0.10	0.14	0.13	0.08	0.06	0.02	0.01
taft-300 †	0.22	0.20	0.17	0.13	0.11	0.08	0.06	0.02	0.01
taft-400	0.16	0.21	0.19	0.14	0.11	0.09	0.05	0.03	0.01
miyagi-50	0.27	0.25	0.06	0.10	0.14	0.09	0.07	0.01	0.01
miyagi-100	0.26	0.21	0.12	0.12	0.14	0.09	0.06	0.01	0.0
miyagi-150	0.28	0.20	0.14	0.11	0.12	0.08	0.06	0.01	0.01
miyagi-200	0.25	0.23	0.10	0.14	0.14	0.06	0.06	0.01	0.01
miyagi-275	0.23	0.21	0.14	0.14	0.13	0.07	0.06	0.02	0.01
miyagi-300	0.19	0.19	0.18	0.13	0.13	0.08	0.07	0.02	0.01
miyagi-350	0.18	0.20	0.18	0.14	0.12	0.08	0.06	0.03	0.01
miyagi-400	0.13	0.21	0.20	0.15	0.12	0.09	0.05	0.04	0.01
pac-220	0.28	0.24	0.07	0.14	0.12	0.07	0.04	0.02	0.01
pac-350	0.23	0.21	0.18	0.12	0.10	0.07	0.05	0.02	0.01
park-220	0.25	0.22	0.05	0.14	0.16	0.07	0.07	0.02	0.01
park-350	0.22	0.20	0.17	0.13	0.13	0.07	0.05	0.02	0.01
sf-200	0.24	0.23	0.09	0.11	0.11	0.09	0.06	0.04	0.03
buc-200	0.27	0.25	0.07	0.14	0.13	0.07	0.05	0.02	0.01
buc-200	0.25	0.21	0.17	0.12	0.11	0.06	0.05	0.02	0.01
buc-300	0.24	0.22	0.18	0.13	0.11	0.07	0.05	0.02	0.01
sct-400	0.31	0.26	0.05	0.13	0.12	0.06	0.04	0.02	0.01
sct-400 †	0.29	0.22	0.17	0.11	0.09	0.06	0.04	0.02	0.01

† = test repeated

TABLE 4.7 FD Model Story Shear Ratios

TEST	STORY SHEAR RATIO AT LEVEL								
	1	2	3	4	5	6	7	8	9
ec-50	0.57	0.47	0.53	0.58	0.55	0.55	0.48	0.49	0.46
ec-150	0.37	0.32	0.36	0.44	0.53	0.49	0.37	0.49	0.41
ec-200	0.27	0.26	0.28	0.30	0.35	0.49	0.28	0.38	0.54
ec-250	0.25	0.20	0.24	0.25	0.30	0.36	0.24	0.29	0.58
ec-300	0.20	0.18	0.21	0.23	0.23	0.34	0.24	0.24	0.57
ec-350	0.18	0.17	0.20	0.19	0.22	0.28	0.18	0.23	0.38
ec-400	0.17	0.16	0.19	0.20	0.19	0.26	0.17	0.20	0.33
taft-50	0.71	0.58	0.57	0.55	0.55	0.57	0.51	0.46	0.29
taft-200	0.31	0.29	0.28	0.30	0.43	0.55	0.33	0.43	0.62
taft-250	0.28	0.23	0.26	0.28	0.39	0.48	0.27	0.40	0.60
taft-300	0.24	0.21	0.25	0.28	0.32	0.45	0.22	0.29	0.50
taft-400	0.22	0.19	0.23	0.23	0.27	0.36	0.16	0.19	0.41
miyagi-50	0.75	0.59	0.64	0.54	0.54	0.53	0.50	0.47	0.42
miyagi-150	0.44	0.41	0.33	0.50	0.58	0.53	0.45	0.43	0.47
miyagi-200	0.33	0.29	0.30	0.37	0.47	0.66	0.32	0.43	0.45
miyagi-275	0.28	0.28	0.25	0.25	0.30	0.40	0.22	0.28	0.54
miyagi-350	0.19	0.18	0.20	0.21	0.24	0.30	0.17	0.20	0.57
miyagi-400	0.18	0.16	0.21	0.21	0.21	0.26	0.15	0.21	0.38
pac-220	0.40	0.33	0.33	0.40	0.50	0.58	0.37	0.49	0.39
pac-350	0.25	0.20	0.23	0.26	0.30	0.42	0.24	0.35	0.47
park-220	0.45	0.38	0.40	0.45	0.60	0.60	0.39	0.50	0.32
park-350	0.32	0.25	0.26	0.29	0.44	0.57	0.34	0.44	0.37
sf-200	0.23	0.21	0.21	0.23	0.34	0.34	0.16	0.22	0.28
sf-300	0.17	0.14	0.20	0.18	0.20	0.26	0.12	0.15	0.25
sf-400	0.16	0.13	0.20	0.17	0.21	0.19	0.10	0.10	0.23

TABLE 4.7 cont. FD Model Story Shear Ratios

TEST	STORY SHEAR RATIO AT LEVEL								
	1	2	3	4	5	6	7	8	9
buc-200	0.39	0.31	0.37	0.43	0.70	0.53	0.42	0.45	0.33
buc-300	0.31	0.28	0.28	0.33	0.44	0.51	0.30	0.39	0.36
sct-400	0.75	0.56	0.64	0.53	0.55	0.58	0.57	0.64	0.60
chile.u-50	0.74	0.61	0.59	0.55	0.54	0.59	0.54	0.45	0.41
chile.u-200	0.32	0.24	0.23	0.36	0.43	0.53	0.25	0.37	0.50
chile.u-400	0.20	0.16	0.14	0.17	0.22	0.29	0.15	0.19	0.35
chile.u-500	0.17	0.16	0.14	0.17	0.20	0.28	0.15	0.18	0.32
chile.u-750	0.17	0.15	0.12	0.17	0.16	0.19	0.14	0.15	0.25
chile.s-50	0.74	0.60	0.59	0.61	0.55	0.53	0.57	0.59	0.51
chile.s-200	0.49	0.39	0.39	0.62	0.57	0.51	0.49	0.51	0.38
chile.s-400	0.24	0.21	0.21	0.26	0.36	0.46	0.28	0.42	0.40
unio-50	0.75	0.59	0.58	0.62	0.51	0.54	0.56	0.45	0.35
unio-250	0.36	0.28	0.28	0.40	0.52	0.59	0.40	0.54	0.38
unio-500	0.20	0.17	0.15	0.20	0.24	0.30	0.20	0.24	0.47
unio-750	0.17	0.15	0.14	0.17	0.20	0.26	0.17	0.21	0.40
unio-1000	0.16	0.13	0.13	0.16	0.18	0.21	0.16	0.19	0.30
zaca-50	0.74	0.58	0.61	0.61	0.53	0.50	0.55	0.52	0.42
zaca-250	0.43	0.31	0.28	0.38	0.55	0.58	0.43	0.48	0.39
zaca-500	0.22	0.19	0.16	0.22	0.26	0.32	0.21	0.29	0.45
zaca-750	0.18	0.15	0.13	0.17	0.23	0.28	0.20	0.22	0.44
zaca-1000	0.18	0.15	0.13	0.17	0.20	0.24	0.19	0.21	0.44
ecatc.s1-225	0.38	0.27	0.26	0.37	0.49	0.58	0.41	0.44	0.40
ecatc.s1-450	0.20	0.16	0.17	0.21	0.22	0.29	0.19	0.24	0.46
taftatc.s1-225	0.32	0.24	0.25	0.35	0.43	0.59	0.34	0.49	0.46
taftatc.s1-450	0.23	0.17	0.17	0.20	0.24	0.35	0.21	0.30	0.49

TABLE 4.8 FD Model Story Energy Dissipation Ratios

TEST	STORY ENERGY DISSIPATION RATIO AT LEVEL								
	1	2	3	4	5	6	7	8	9
ec-150	0.40	0.23	0.14	0.11	0.05	0.04	0.03	0.01	0.0
ec-200	0.37	0.21	0.13	0.12	0.08	0.05	0.03	0.01	0.0
ec-250	0.34	0.20	0.11	0.13	0.10	0.07	0.04	0.02	0.0
ec-300	0.36	0.22	0.01 †	0.14	0.11	0.09	0.04	0.02	0.0
ec-350	0.36	0.22	0.01 †	0.14	0.11	0.09	0.04	0.02	0.0
ec-400	0.30	0.19	0.15	0.12	0.10	0.08	0.04	0.02	0.0
taft-200	0.46	0.27	0.02 †	0.12	0.05	0.04	0.03	0.01	0.0
taft-250	0.44	0.25	0.01 †	0.12	0.07	0.04	0.04	0.02	0.0
taft-300	0.36	0.21	0.16	0.11	0.07	0.05	0.03	0.02	0.0
taft-400	0.32	0.20	0.16	0.11	0.08	0.06	0.04	0.02	0.0
miyagi-150	0.61	0.29	0.0 †	0.05	0.01	0.03	0.01	0.0	0.0
miyagi-200	0.52	0.30	0.0 †	0.12	0.02	0.02	0.02	0.0	0.0
miyagi-275	0.37	0.24	0.01 †	0.16	0.11	0.06	0.04	0.02	0.0
miyagi-350	0.27	0.18	0.15	0.14	0.11	0.09	0.04	0.02	0.0
miyagi-400	0.26	0.18	0.15	0.14	0.12	0.09	0.04	0.02	0.0
pac-220	0.47	0.22	0.15	0.07	0.04	0.02	0.02	0.0	0.0
pac-350	0.34	0.20	0.15	0.12	0.07	0.05	0.04	0.02	0.0
park-220	0.39	0.23	0.18	0.11	0.04	0.03	0.02	0.0	0.0
park-350	0.37	0.22	0.16	0.11	0.06	0.04	0.02	0.01	0.0
sf-200	0.28	0.16	0.12	0.10	0.09	0.10	0.07	0.05	0.02
sf-300	0.25	0.15	0.12	0.11	0.11	0.11	0.06	0.05	0.02
sf-400	0.25	0.15	0.12	0.11	0.11	0.12	0.06	0.05	0.02

† Negligible deformation in damper due to loose mounting beam bolts

No results are listed for the span-50 tests because damper deformations were too small for SDRs to be reliably calculated

TABLE 4.8 cont. FD Model Story Energy Dissipation Ratios

TEST	STORY ENERGY DISSIPATION RATIO AT LEVEL								
	1	2	3	4	5	6	7	8	9
buc-200	0.41	0.25	0.18	0.09	0.03	0.03	0.01	0.0	0.0
buc-300	0.37	0.22	0.17	0.12	0.07	0.03	0.02	0.01	0.0
sct-400	0.51	0.21	0.11	0.02	0.05	0.06	0.01	0.01	0.0
chile.u-200	0.37	0.21	0.16	0.11	0.06	0.04	0.04	0.01	0.0
chile.u-400	0.29	0.17	0.14	0.13	0.10	0.08	0.05	0.03	0.0
chile.u-500	0.27	0.16	0.13	0.13	0.11	0.10	0.05	0.03	0.01
chile.u-750	0.25	0.15	0.13	0.13	0.11	0.11	0.06	0.04	0.01
chile.s-200	0.40	0.25	0.19	0.04	0.05	0.06	0.01	0.01	0.0
chile.s-400	0.39	0.23	0.17	0.11	0.06	0.03	0.02	0.0	0.0
unio-250	0.41	0.24	0.18	0.09	0.03	0.02	0.01	0.0	0.0
unio-500	0.32	0.19	0.15	0.13	0.09	0.07	0.04	0.02	0.0
unio-750	0.29	0.17	0.14	0.13	0.10	0.08	0.05	0.02	0.0
unio-1000	0.28	0.17	0.14	0.14	0.11	0.09	0.05	0.03	0.01
zaca-250	0.41	0.23	0.19	0.09	0.04	0.02	0.01	0.0	0.0
zaca-500	0.34	0.20	0.16	0.12	0.08	0.05	0.03	0.01	0.0
zaca-750	0.31	0.18	0.14	0.13	0.10	0.08	0.04	0.02	0.0
zaca-1000	0.29	0.17	0.14	0.13	0.11	0.09	0.05	0.03	0.0
ecatc.s1-225	0.41	0.24	0.19	0.08	0.04	0.03	0.01	0.0	0.0
ecatc.s1-450	0.33	0.20	0.16	0.12	0.08	0.06	0.03	0.02	0.0
taftatc.s1-225	0.41	0.23	0.17	0.10	0.04	0.02	0.01	0.0	0.0
taftatc.s1-450	0.30	0.18	0.14	0.14	0.10	0.08	0.04	0.02	0.0

No results are listed for the span-50 tests because damper deformations were too small for SDRs to be reliably calculated

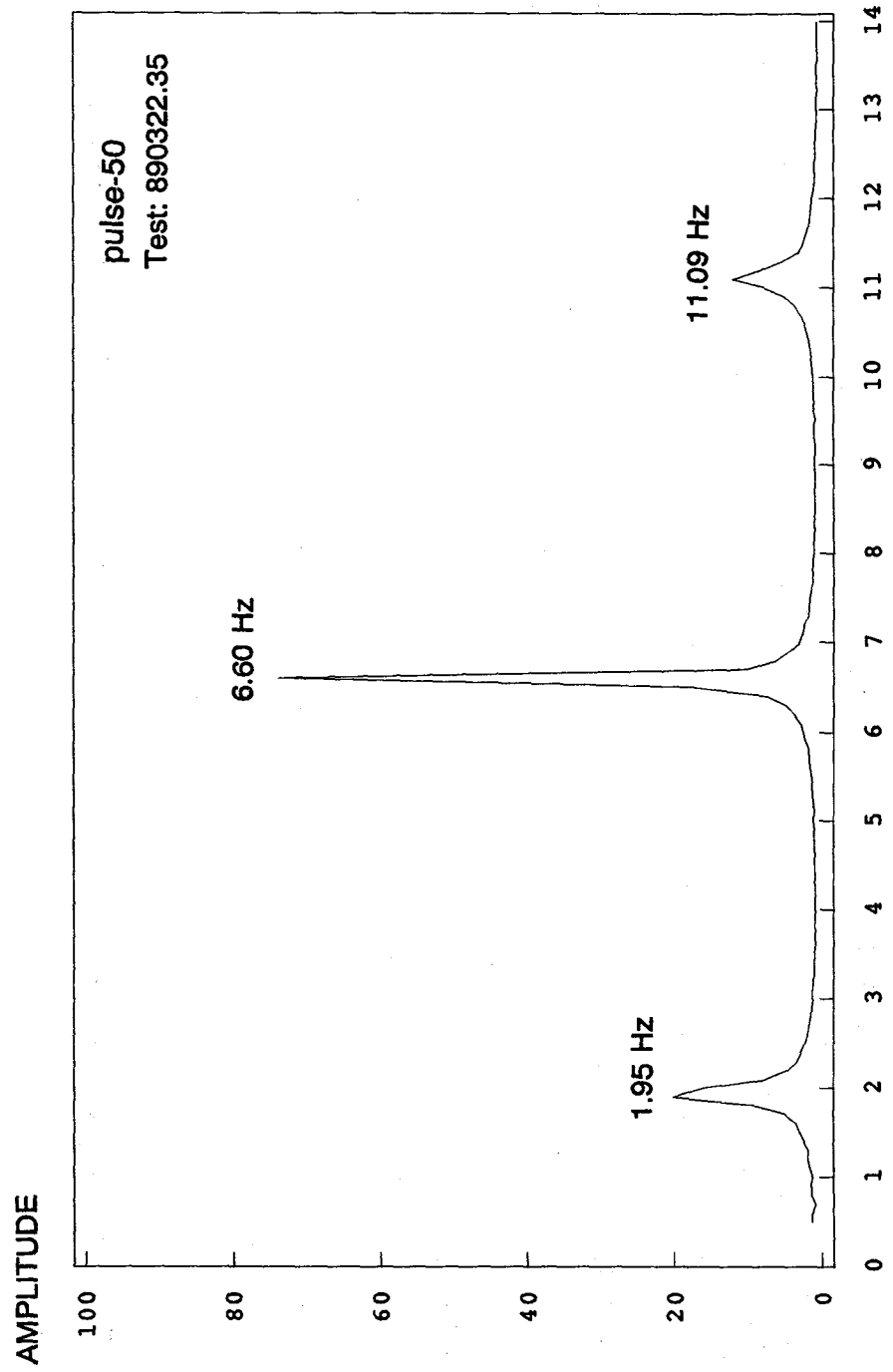

Fig. 4.1 MRF Roof Acceleration Transfer Function From Pulse Free Vibration Test

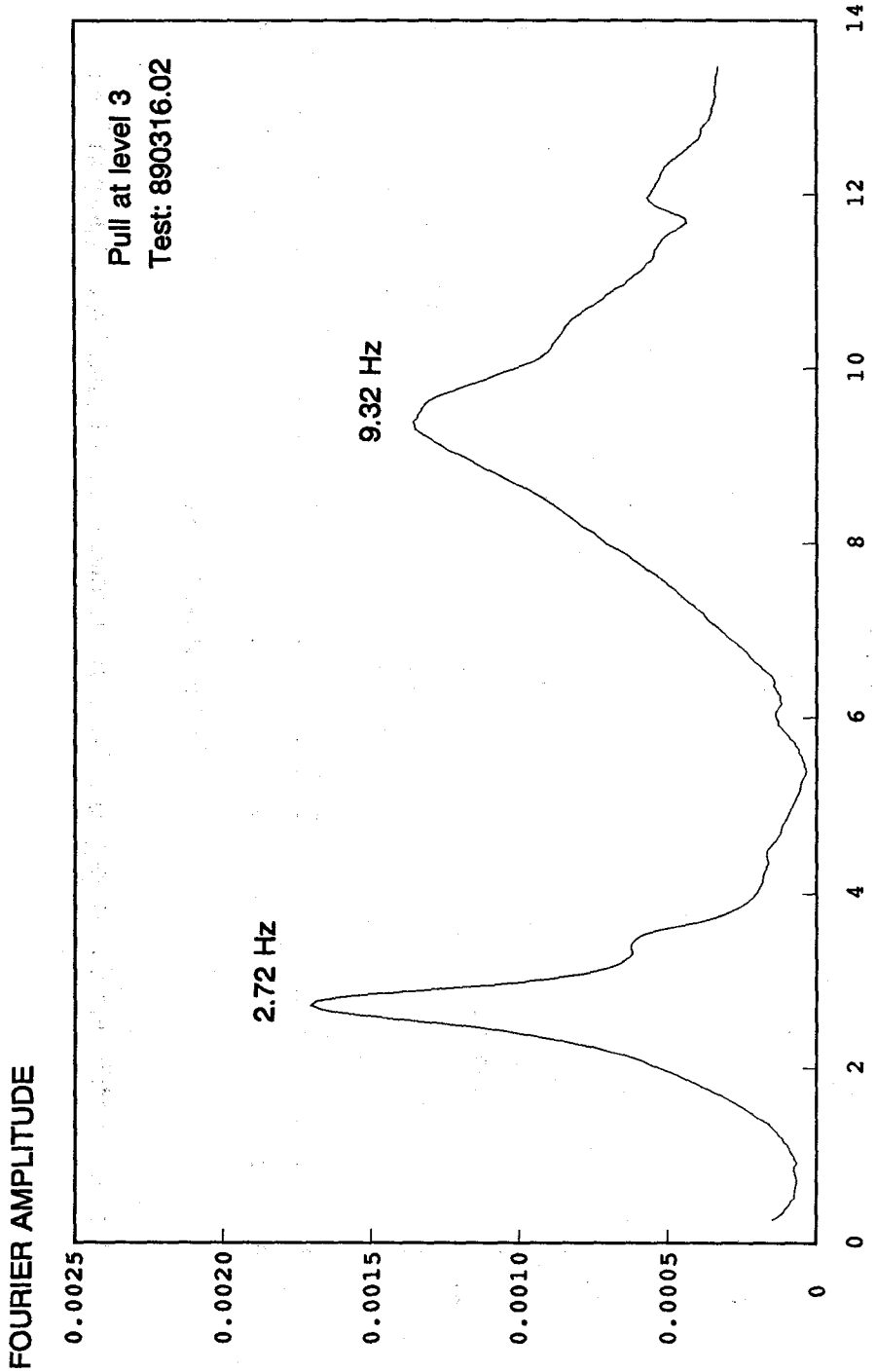

Fig. 4.2 VD Roof Acceleration Fourier Amplitude Spectrum From Pull-Back Free Vibration Test

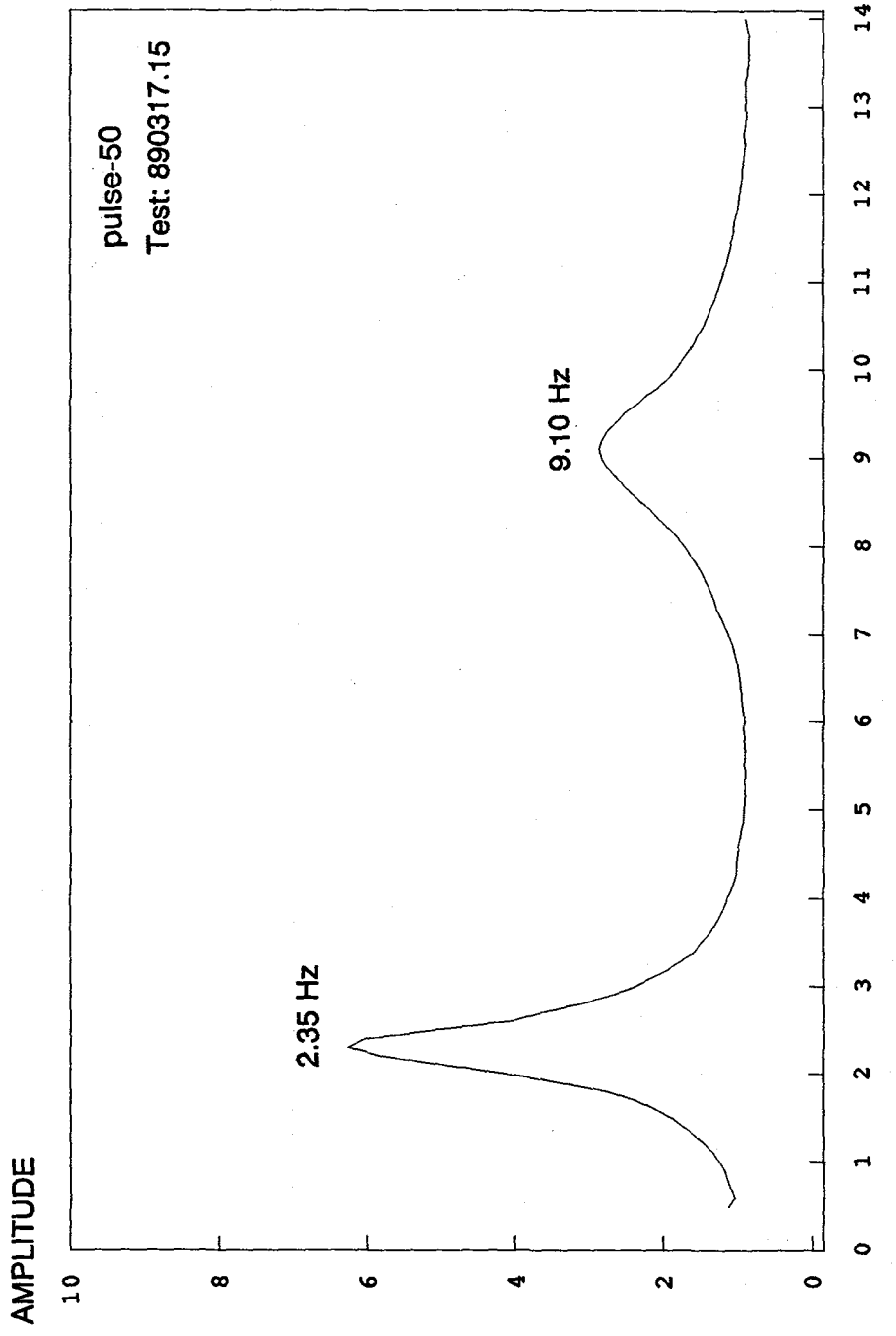

Fig. 4.3 VD Roof Acceleration Transfer Function From Pulse Free Vibration Test

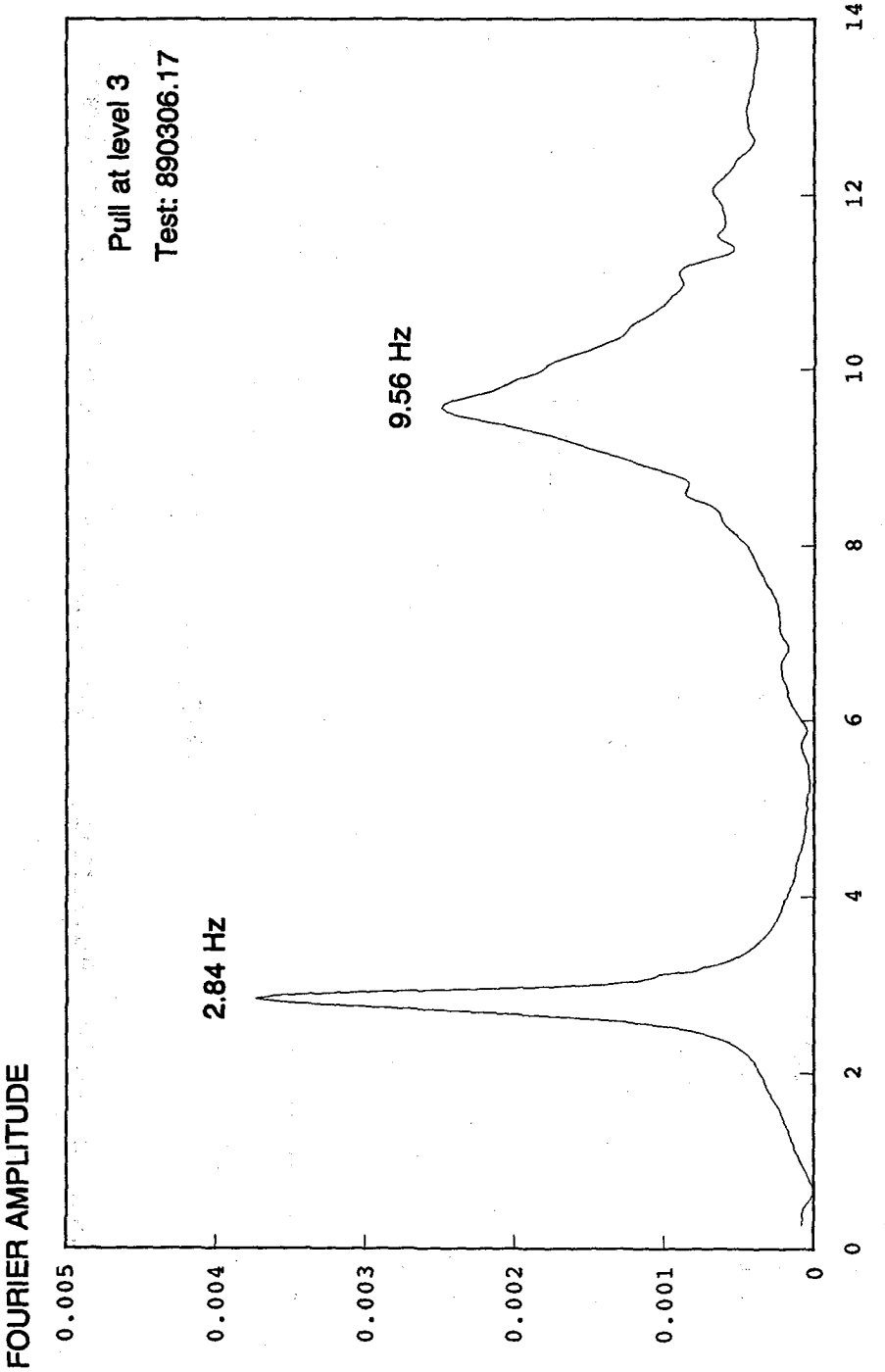

Fig. 4.4 FD Roof Acceleration Fourier Amplitude Spectrum From Pull-Back Free Vibration Test

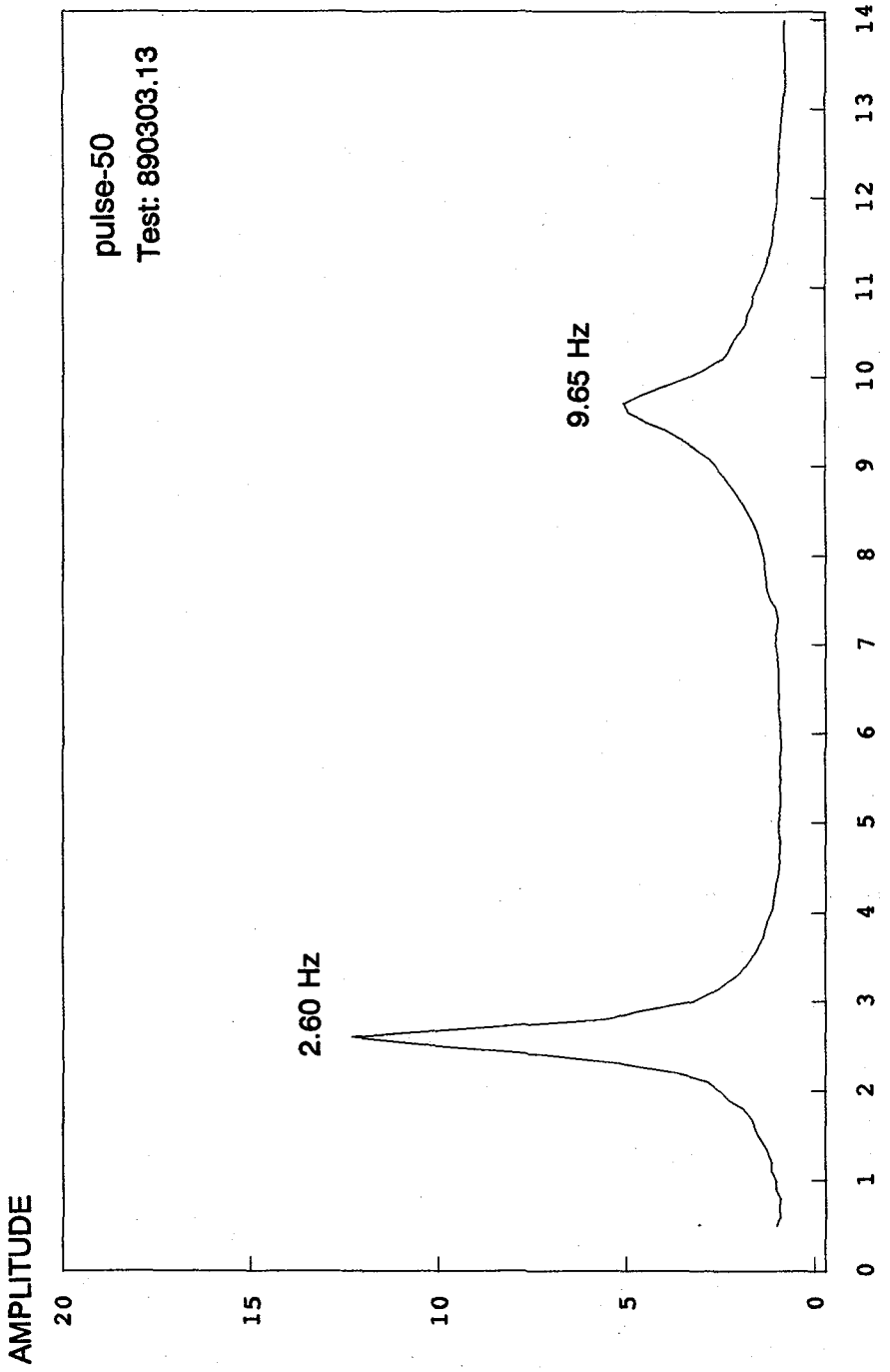

Fig. 4.5 FD Roof Acceleration Transfer Function From Pulse Free Vibration Test

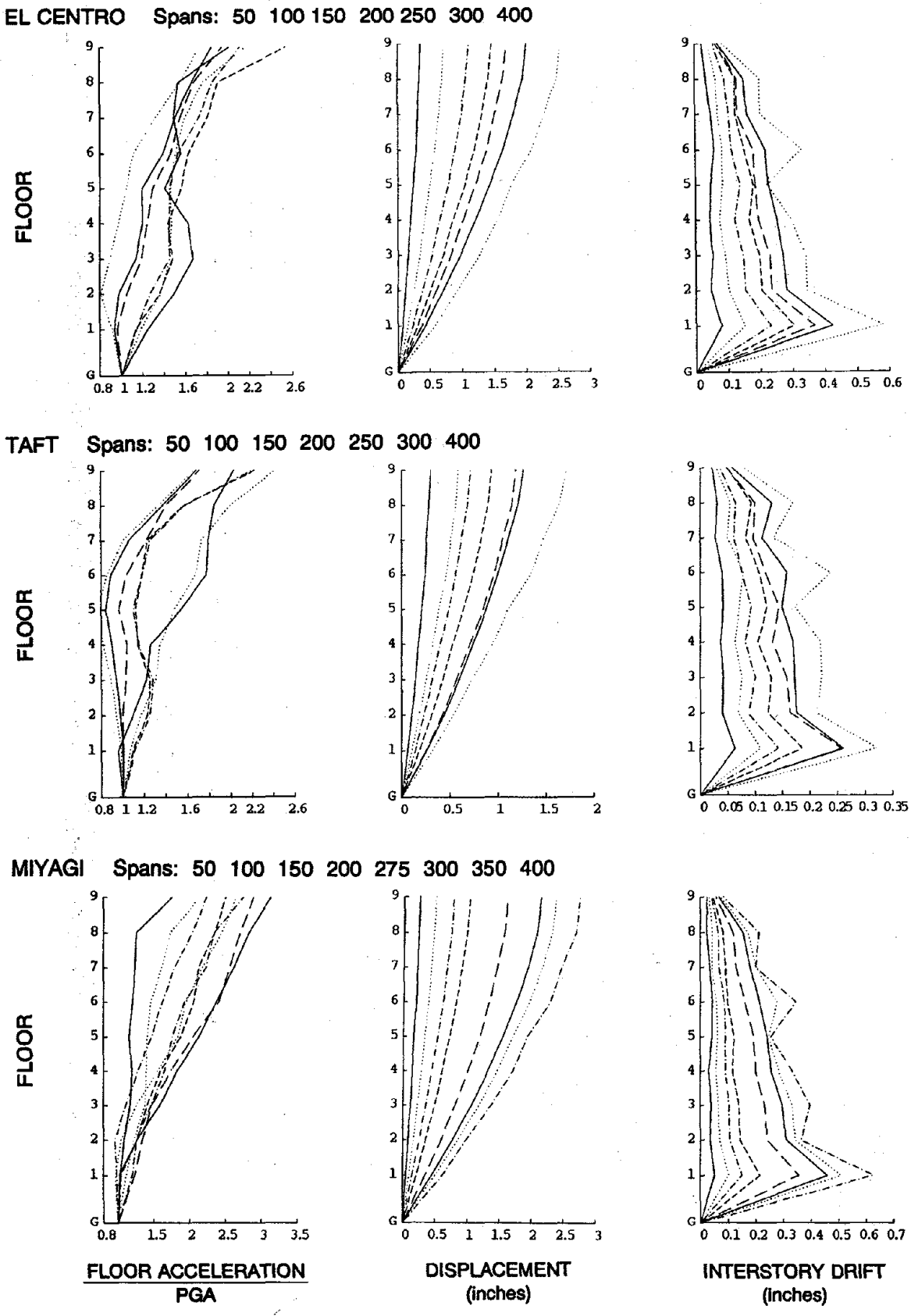

Fig. 4.6 VD Response Profiles for El Centro, Taft, and Miyagi Tests

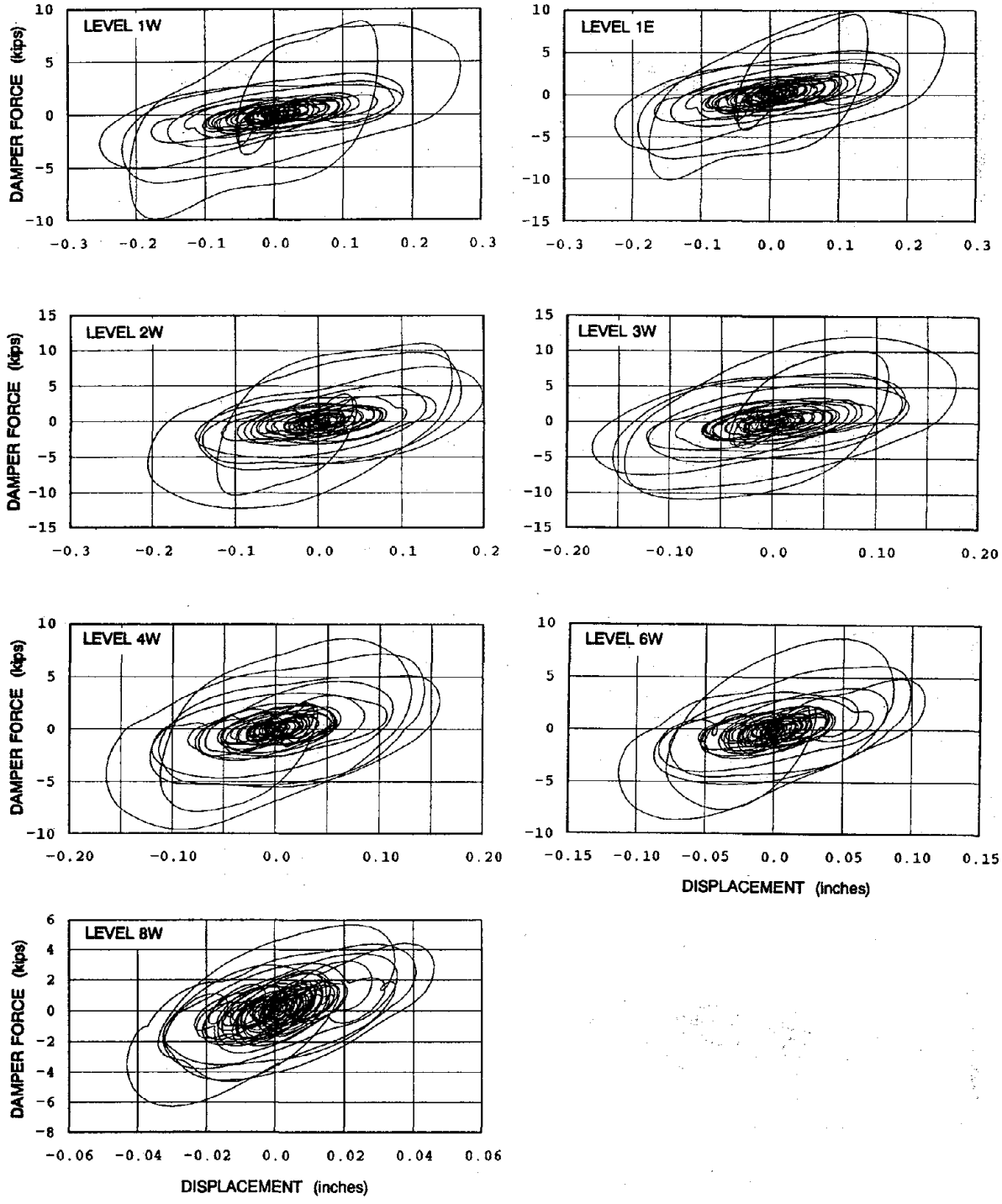

Fig. 4.7 Force-Deformation Plots for VE Dampers, ec-400 Test

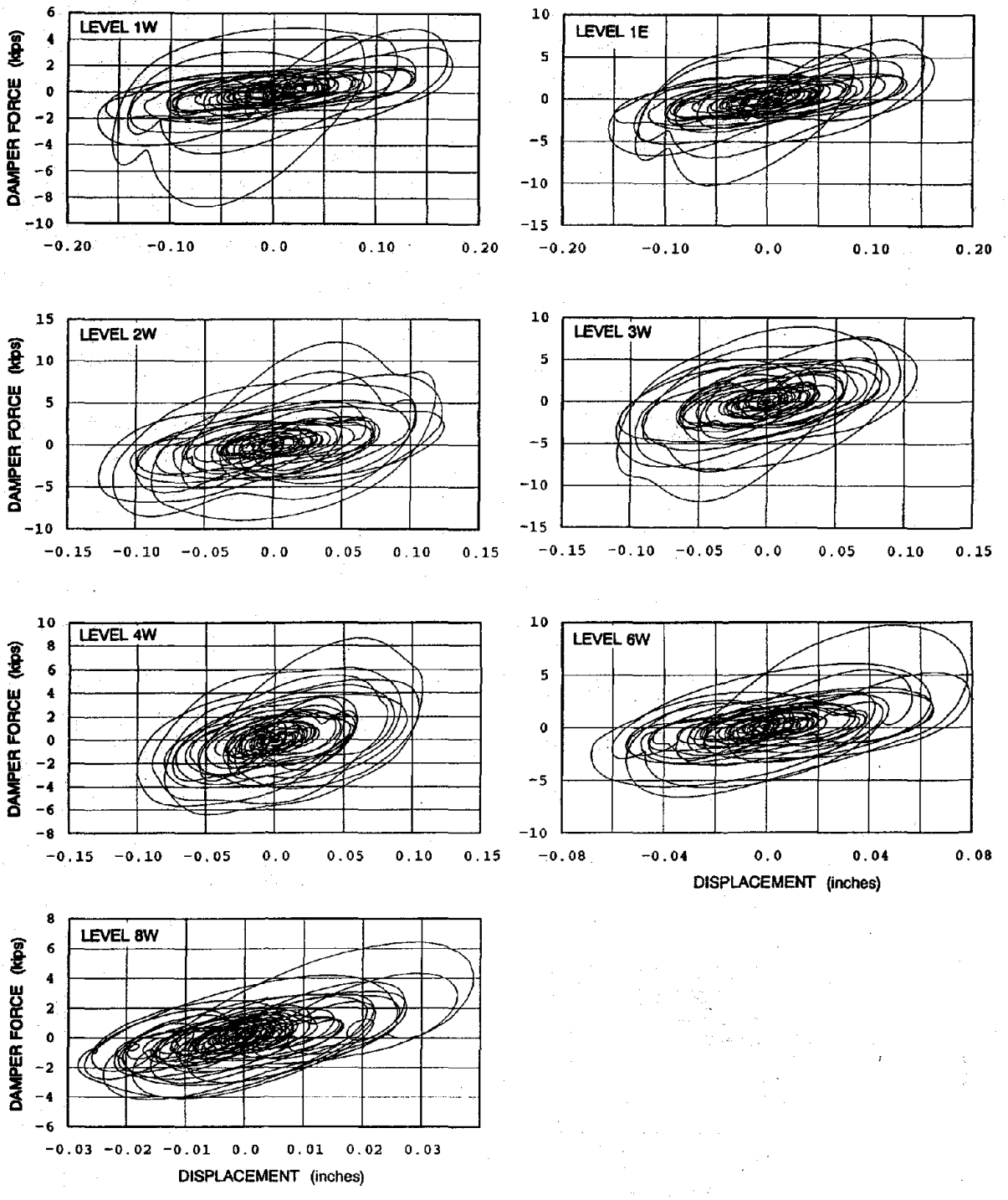

Fig. 4.8 Force-Deformation Plots for VE Dampers, taft-400 Test

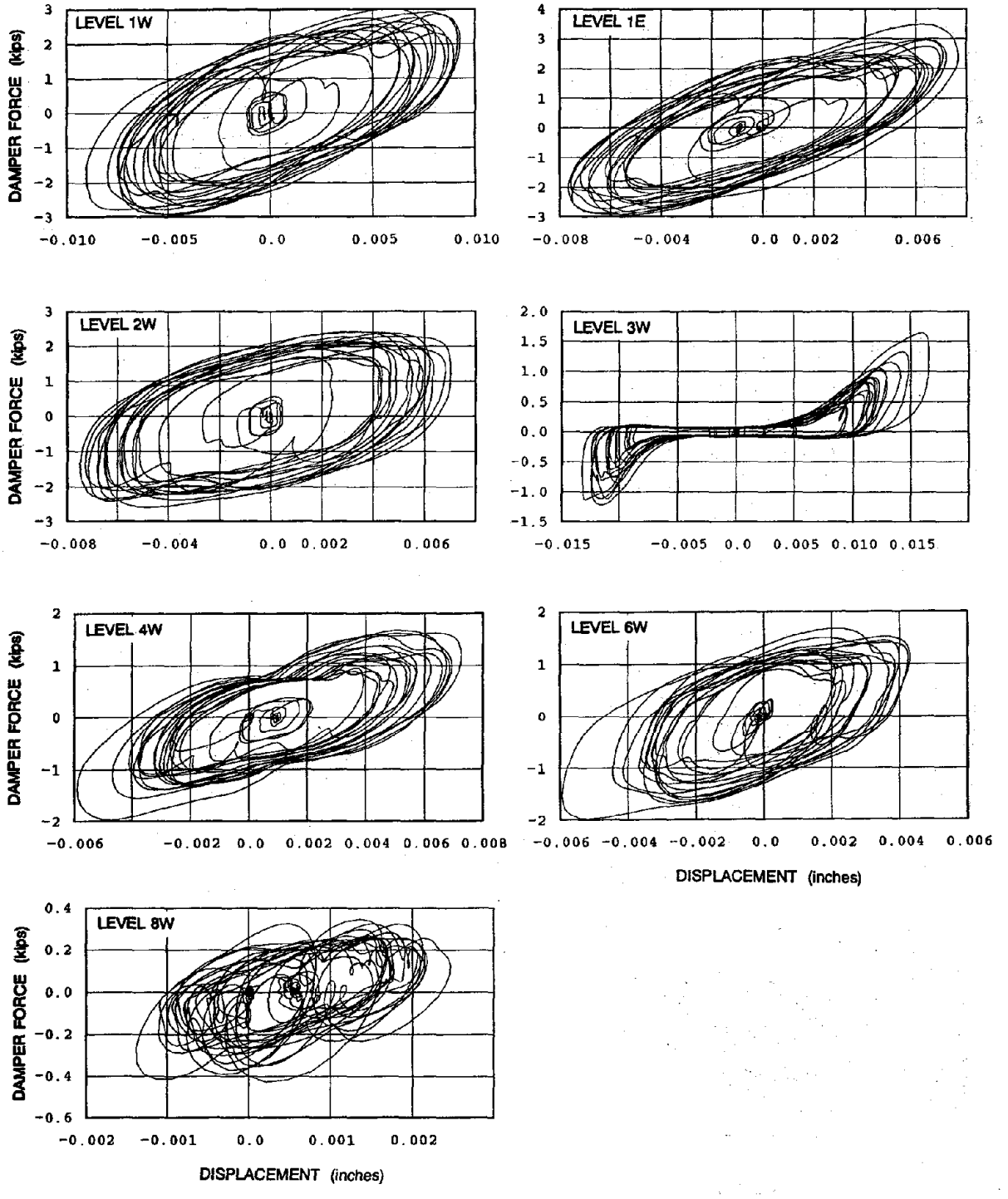

Fig. 4.9 Force-Deformation Plots for VE Dampers, miyagi-50 Test

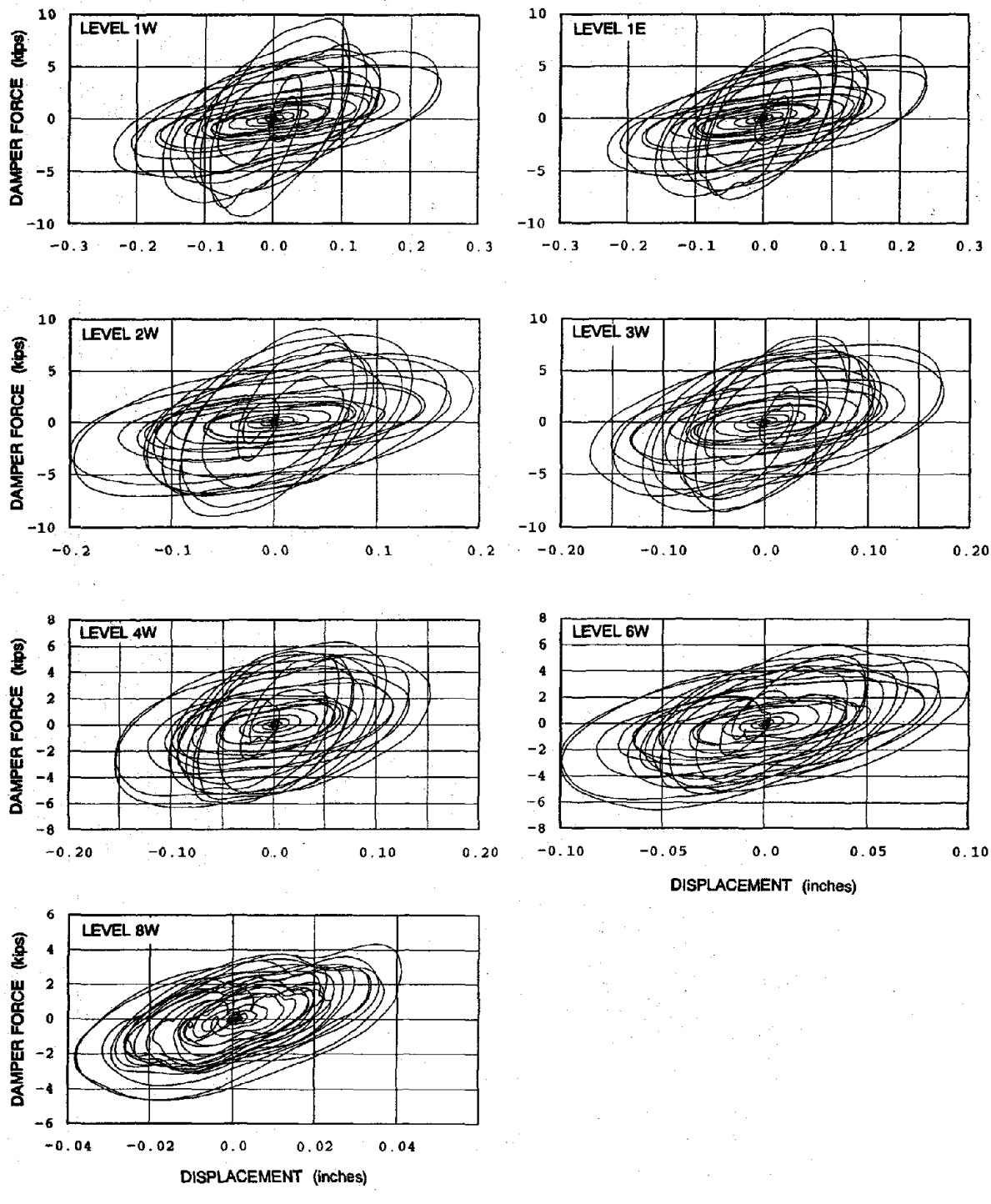

Fig. 4.10 Force-Deformation Plots for VE Dampers, miyagi-300 Test

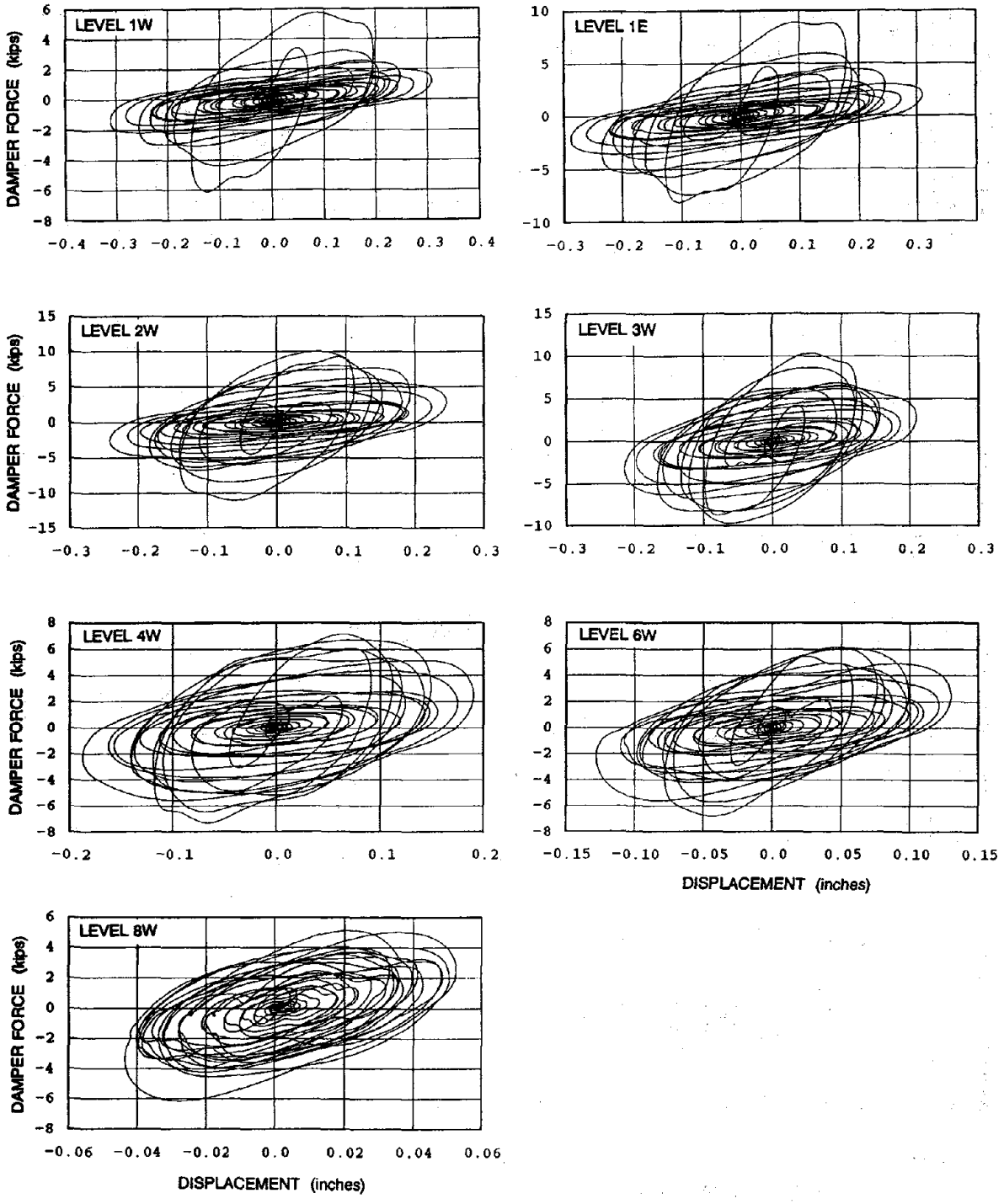

Fig. 4.11 Force-Deformation Plots for VE Dampers, miyagi-400 Test

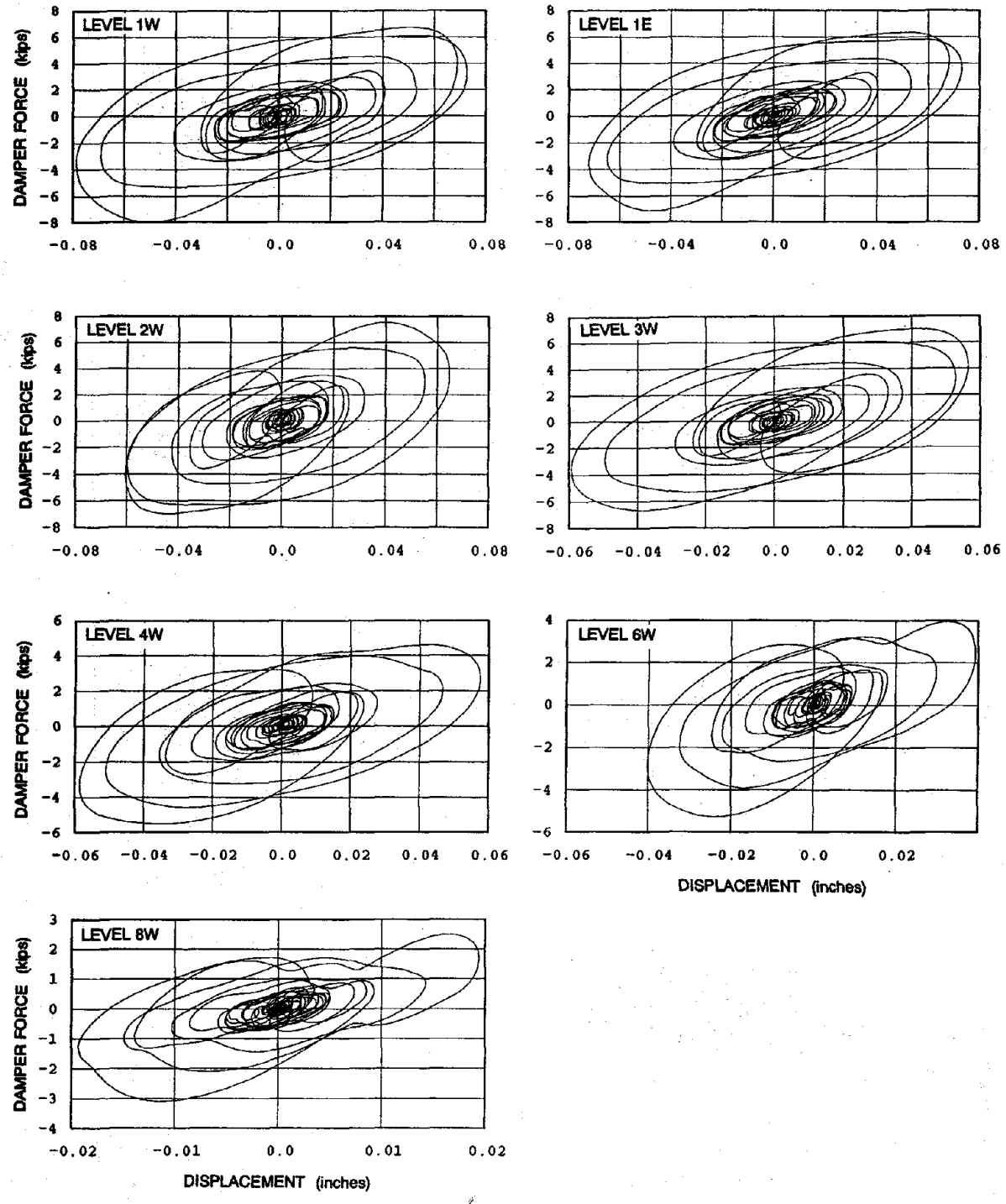

Fig. 4.12 Force-Deformation Plots for VE Dampers, park-350 Test

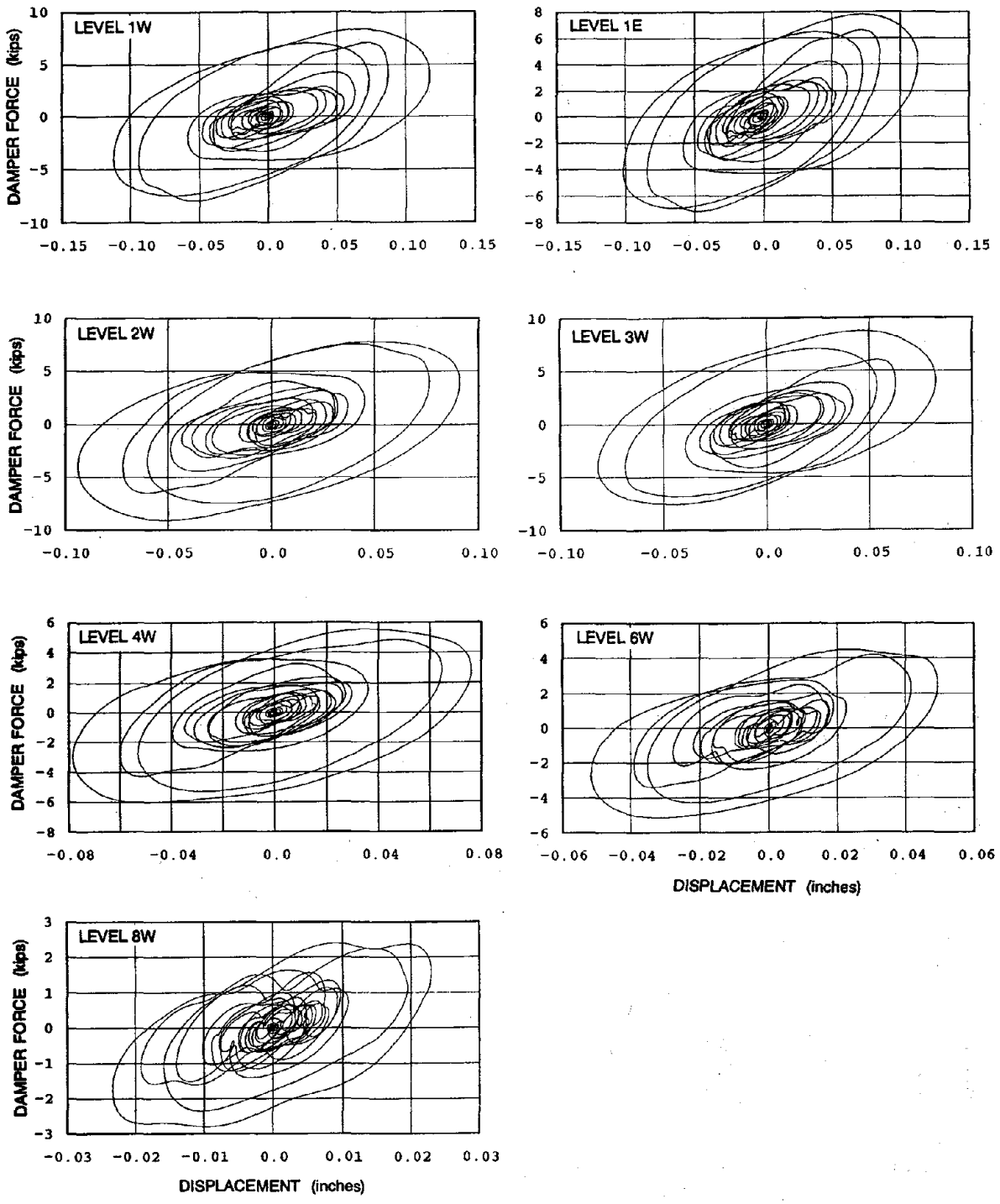

Fig. 4.13 Force-Deformation Plots for VE Dampers, buc-300 Test

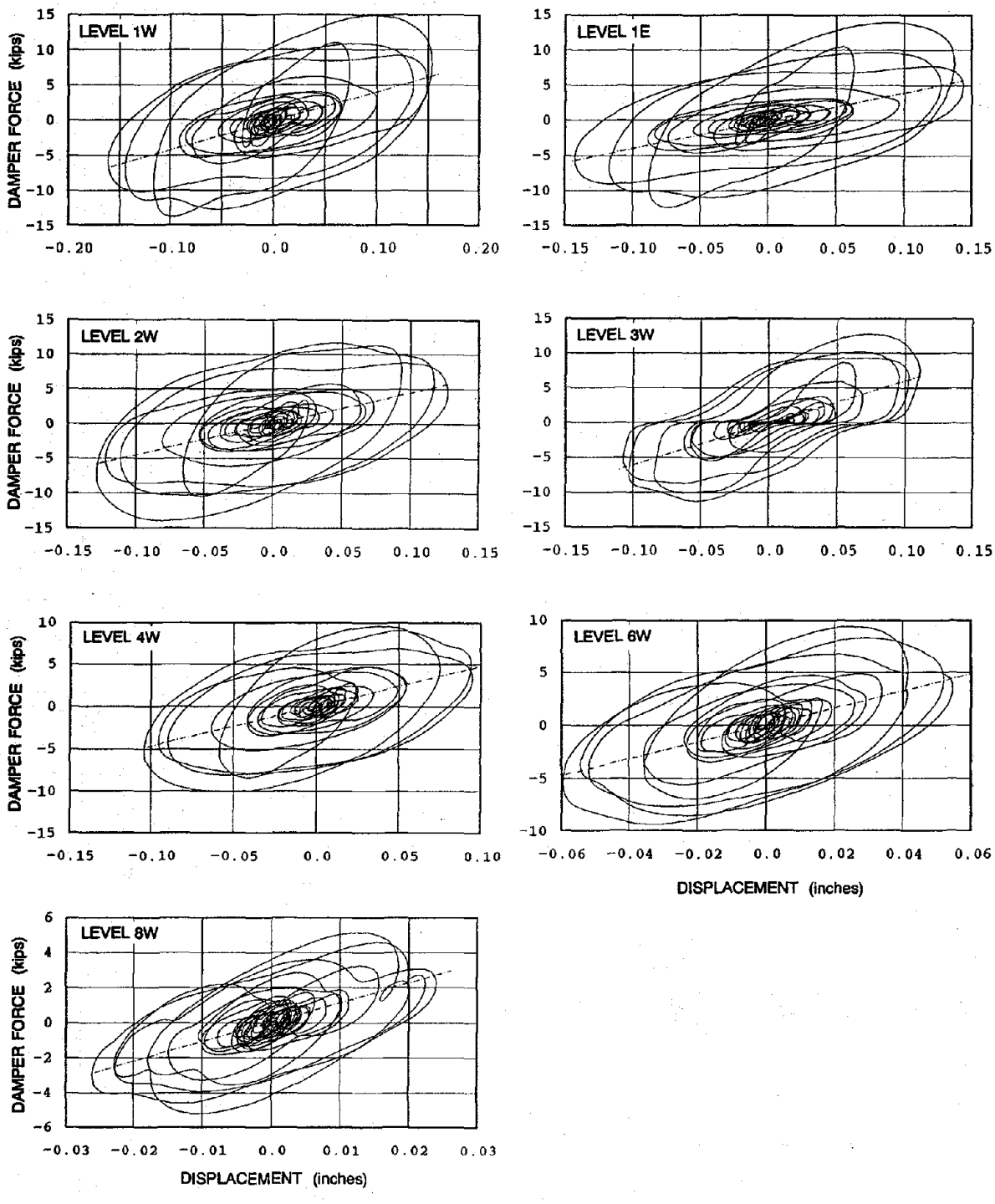

Fig. 4.14 Equivalent Linear Stiffness of VE Dampers, ec-250 Test

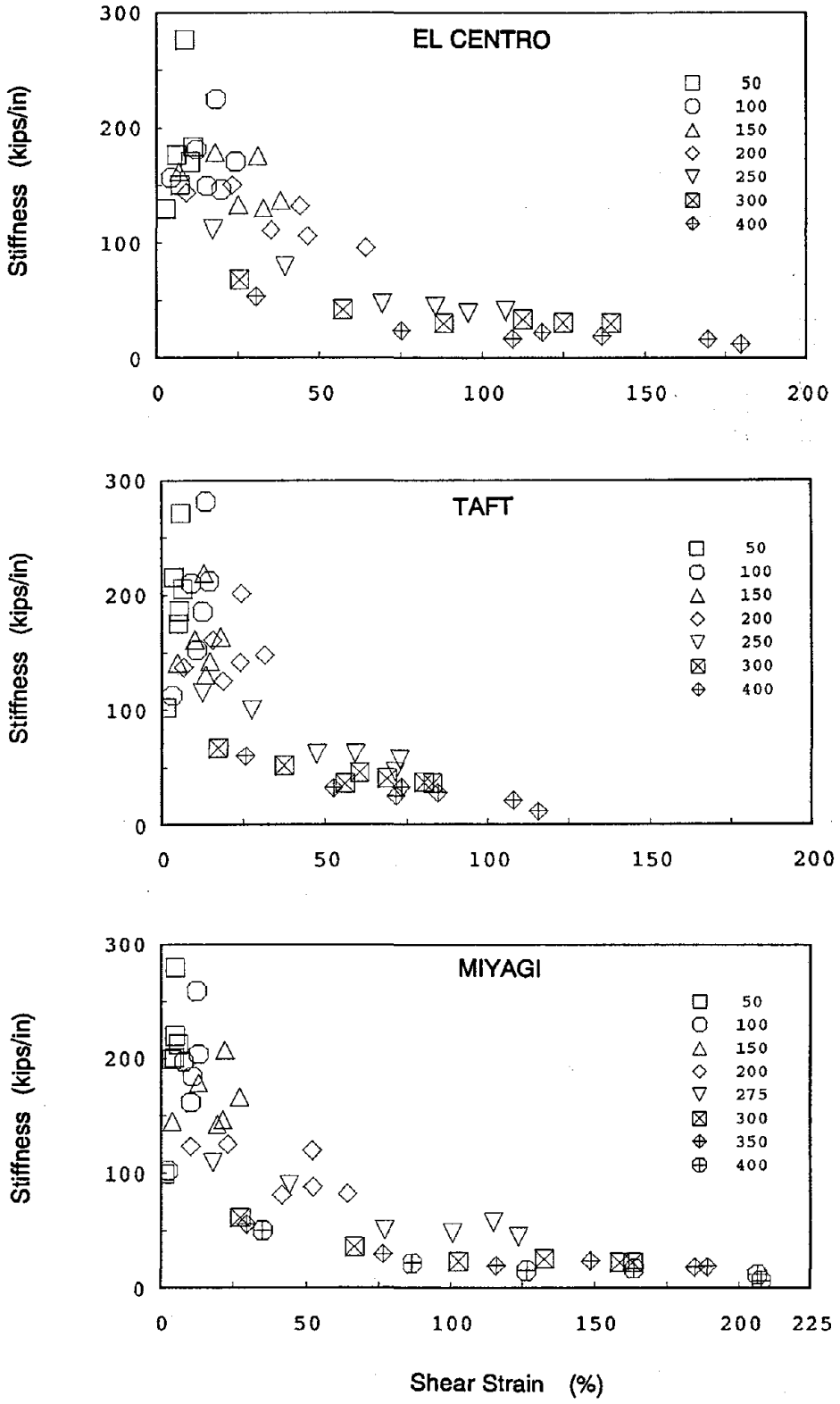

Fig. 4.15 VE Damper Stiffness vs. Shear Strain

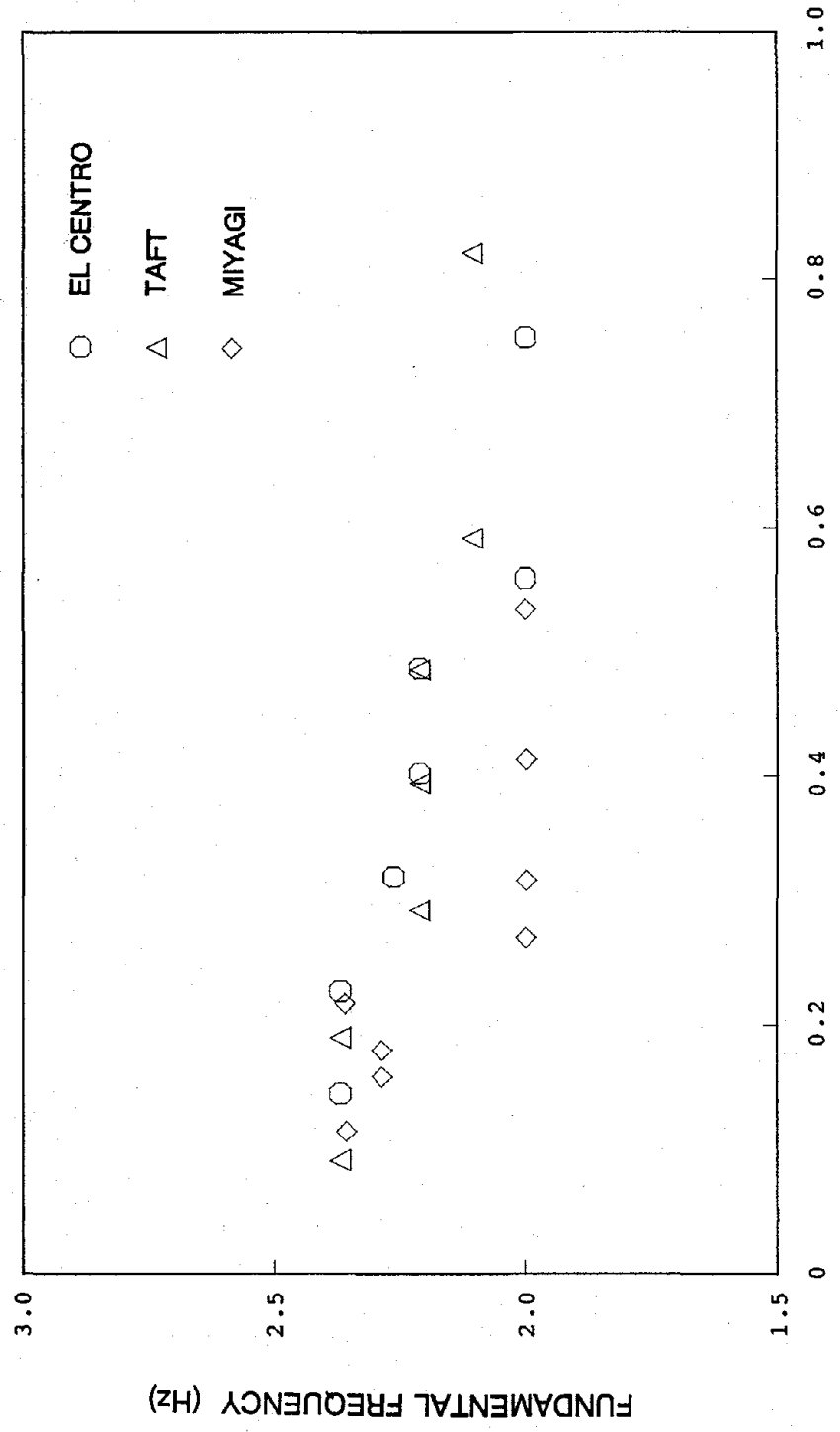

Fig. 4.16 VD Fundamental Frequency vs. PGA

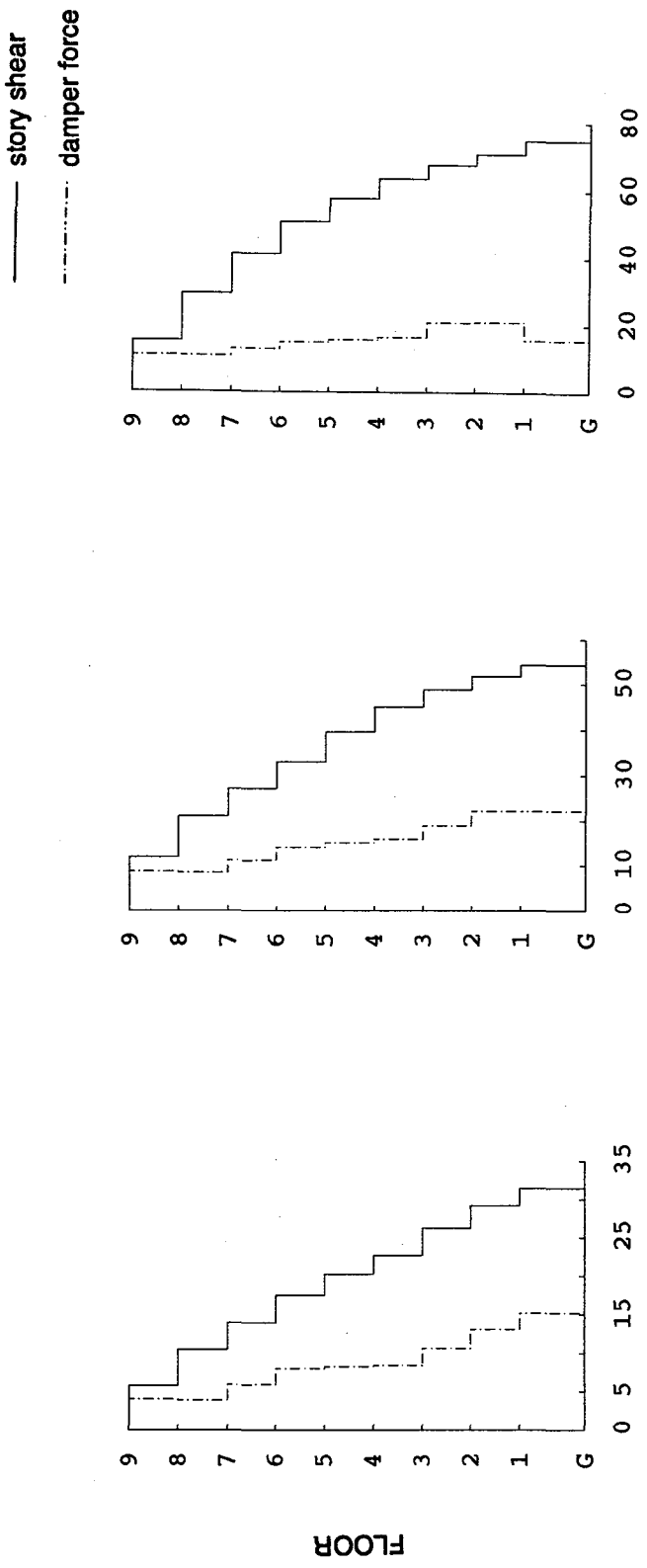

Fig. 4.17 VD Peak Story Shears and Device Forces, ec-100, ec-200, and ec-400 Tests

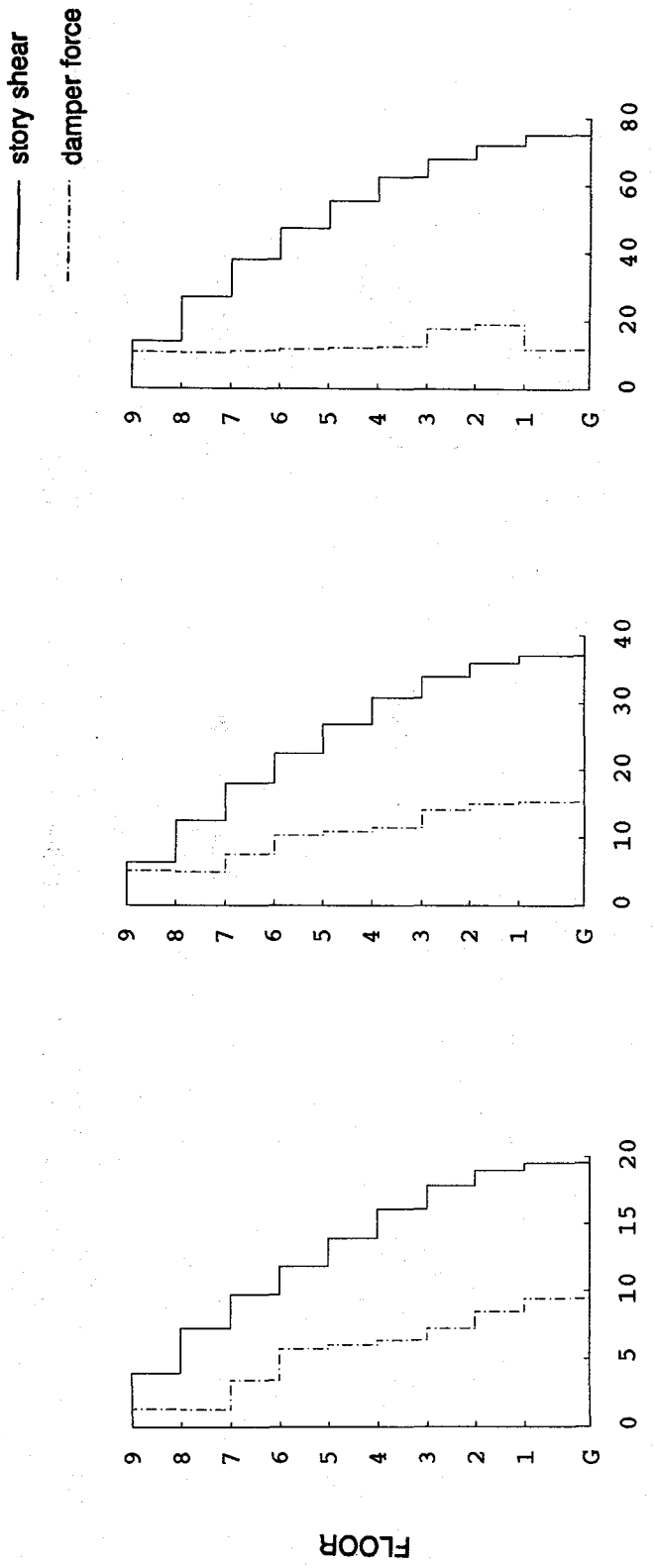

Fig. 4.18 VD Peak Story Shears and Device Forces, miyagi-100, miyagi-200, and miyagi-400 Tests

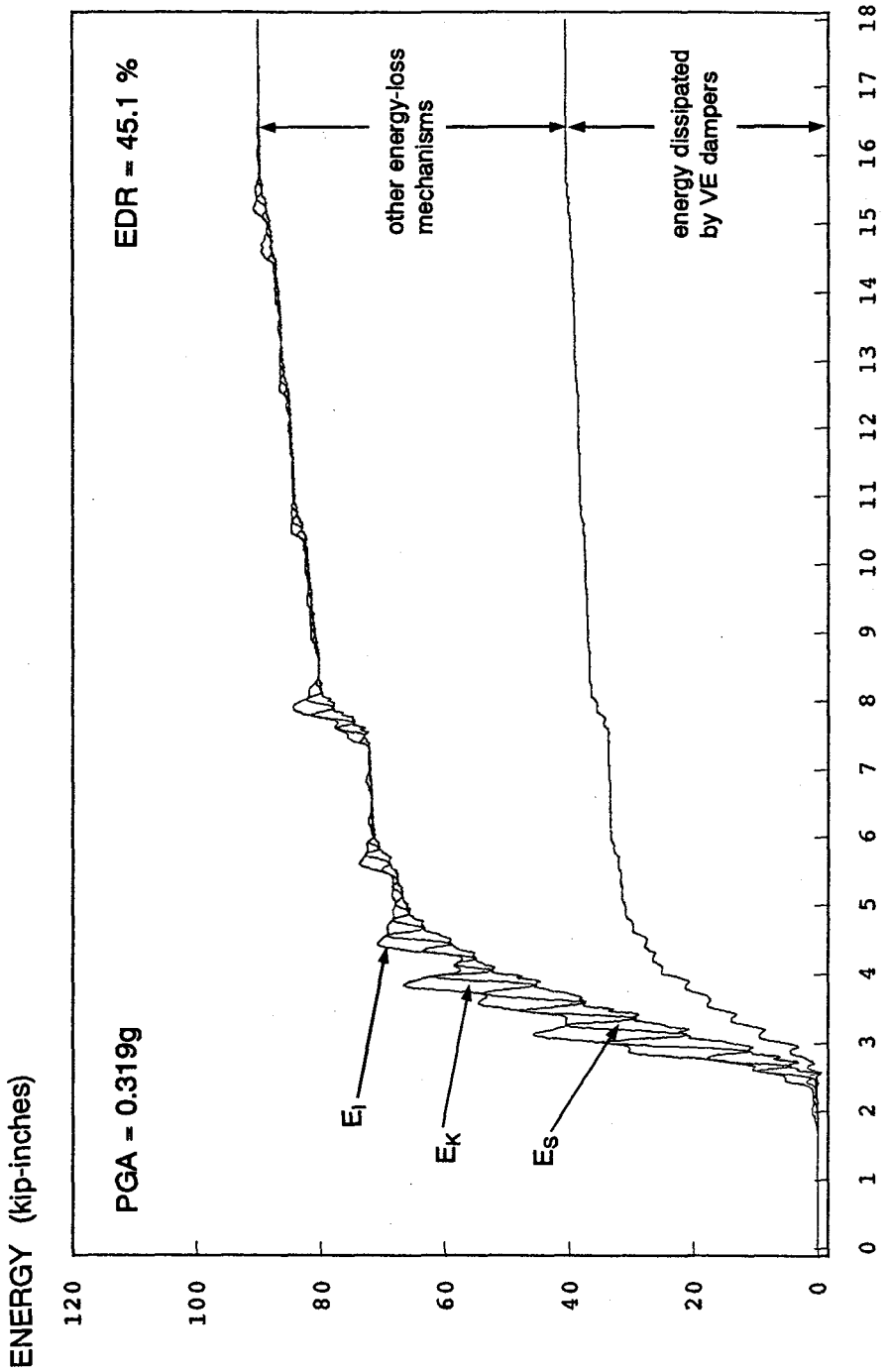

Fig. 4.19 VD Energy Time Histories, ec-150 Test

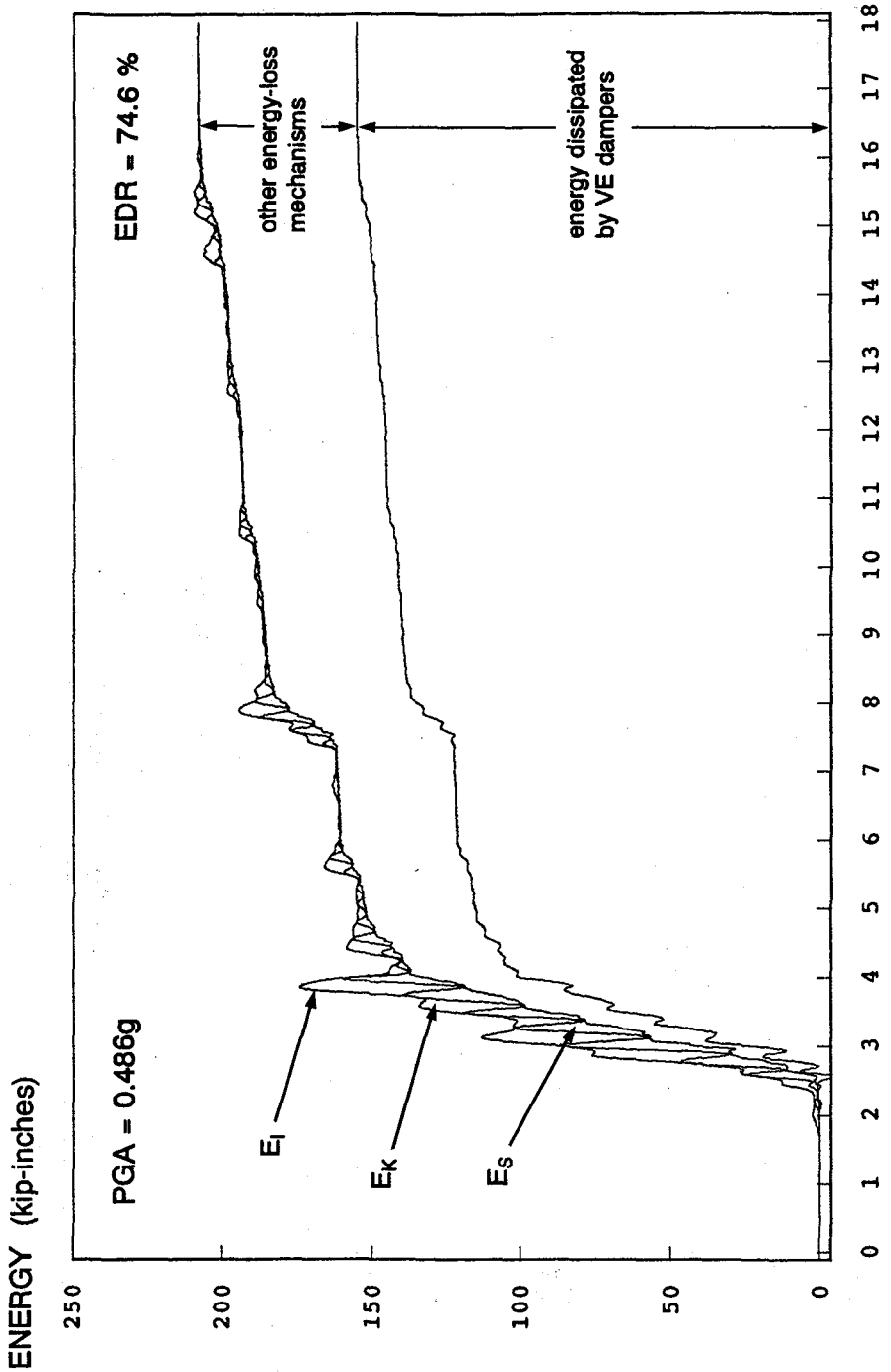

Fig. 4.20 VD Energy Time Histories, ec-250 Test

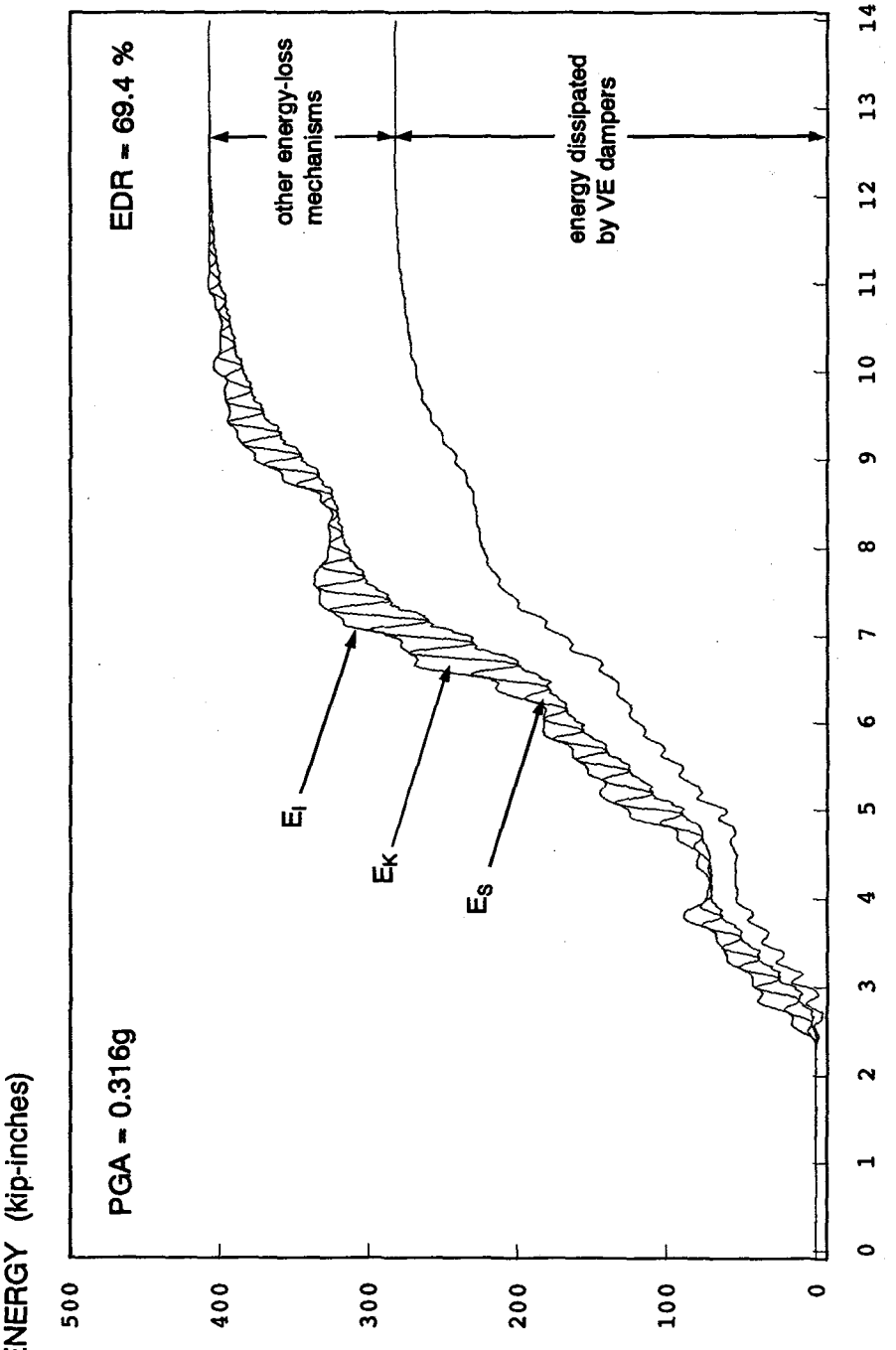

Fig. 4.21 VD Energy Time Histories, miyagi-300 Test

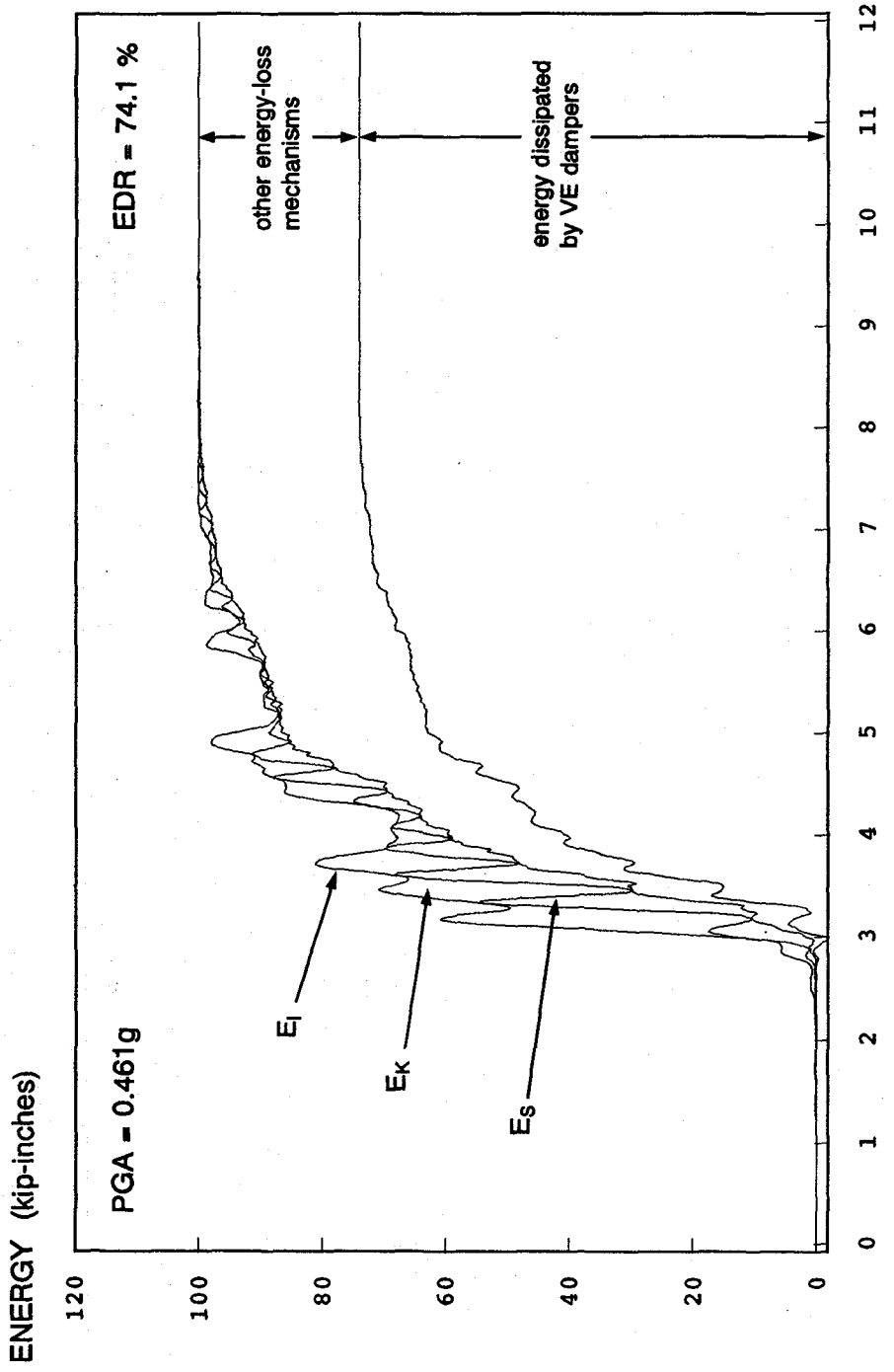

Fig. 4.22 VD Energy Time Histories, pac-350 Test

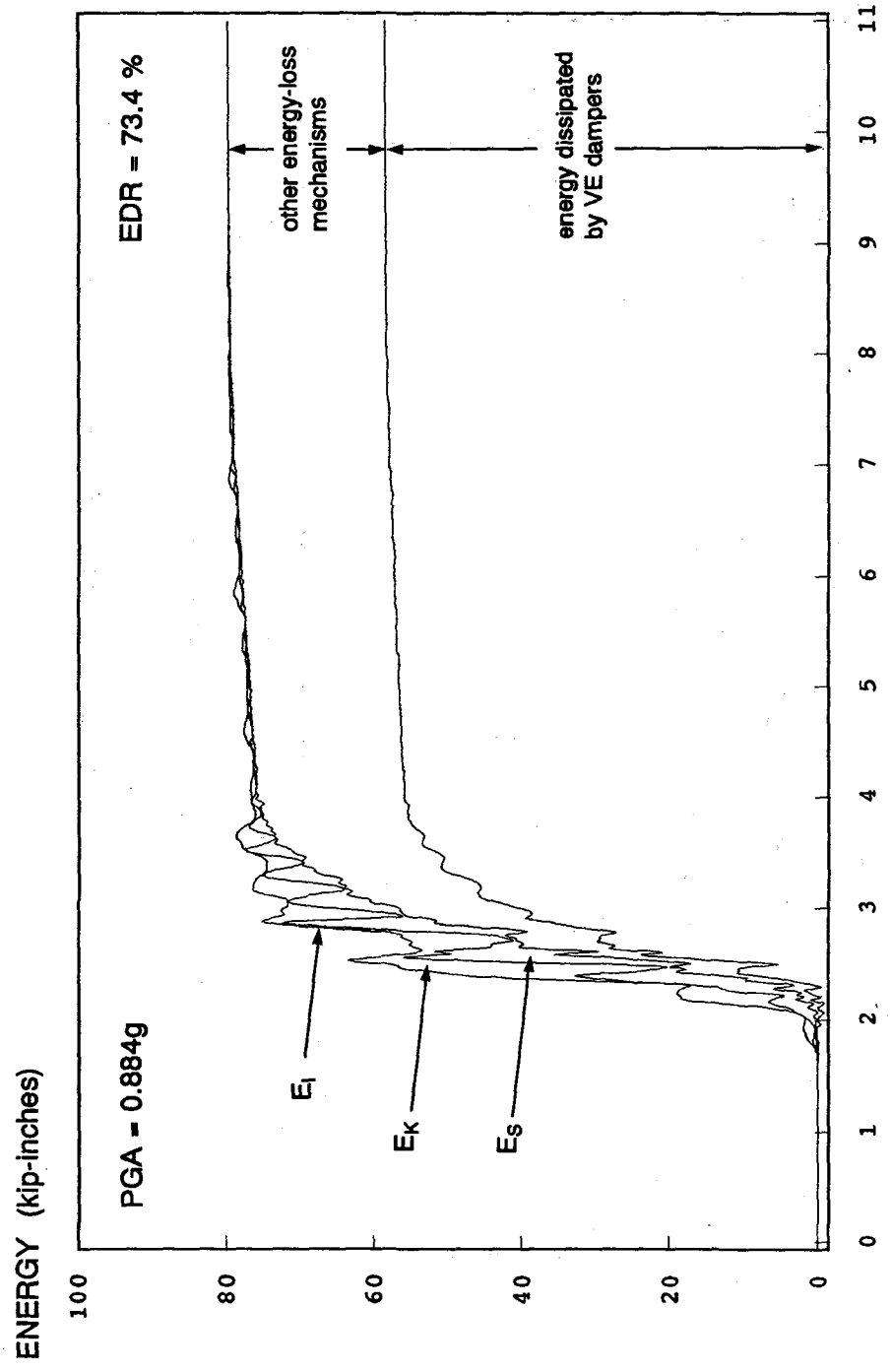

Fig. 4.23 VD Energy Time Histories, sf-200 Test

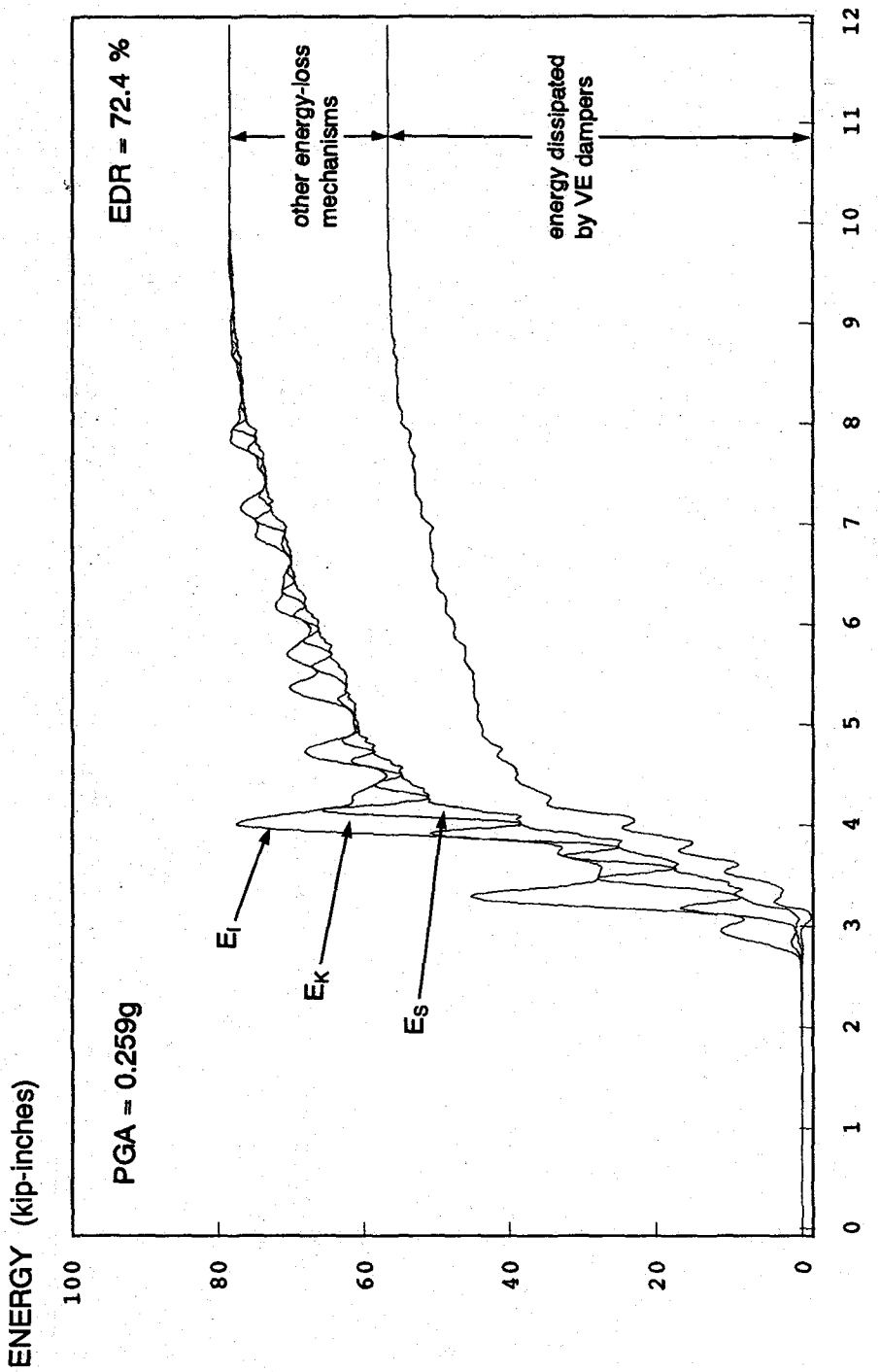

Fig. 4.24 VD Energy Time Histories, buc-300 Test

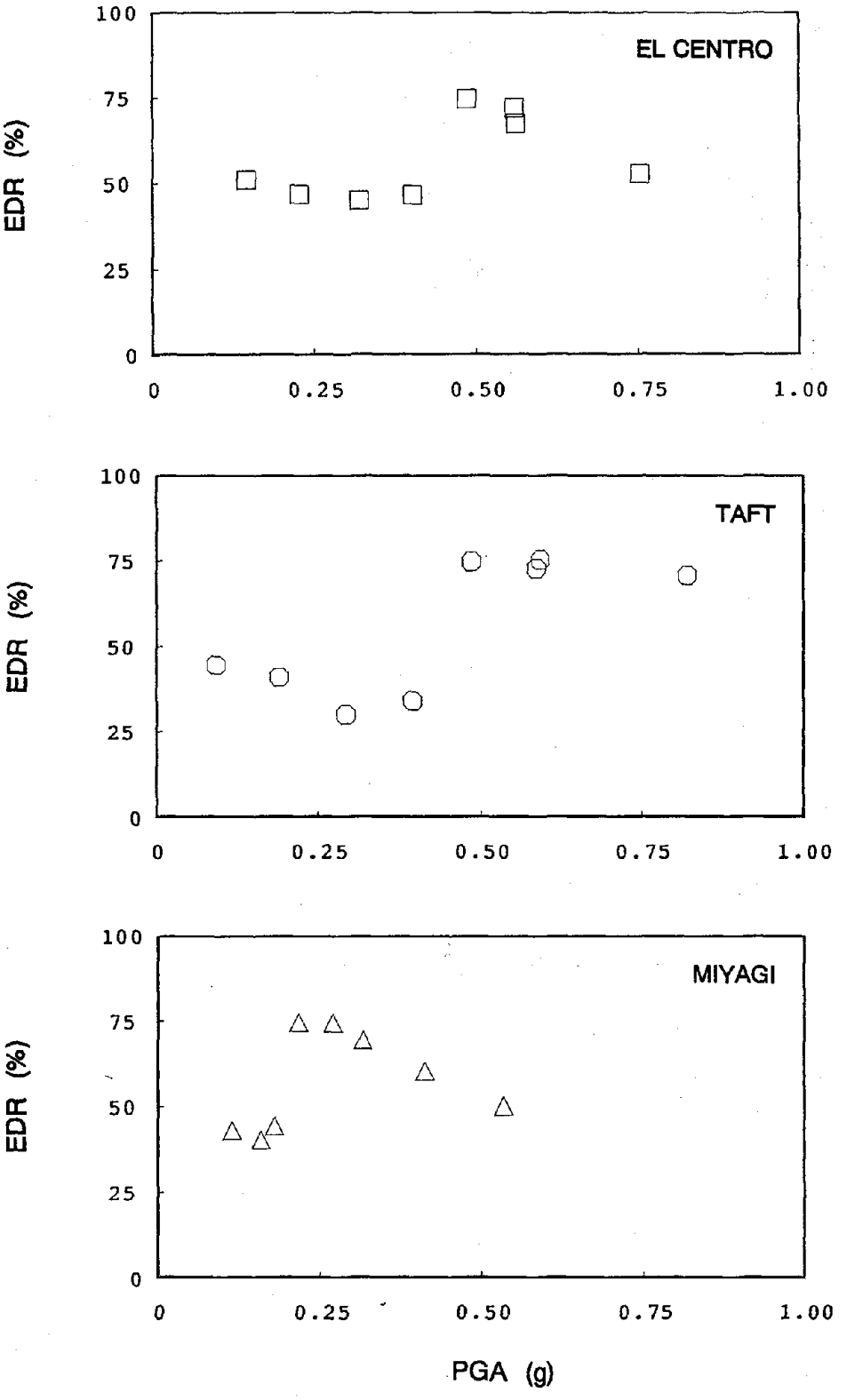

Fig. 4.25 VD Energy Dissipation Ratio vs. PGA for El Centro, Taft, and Miyagi Tests

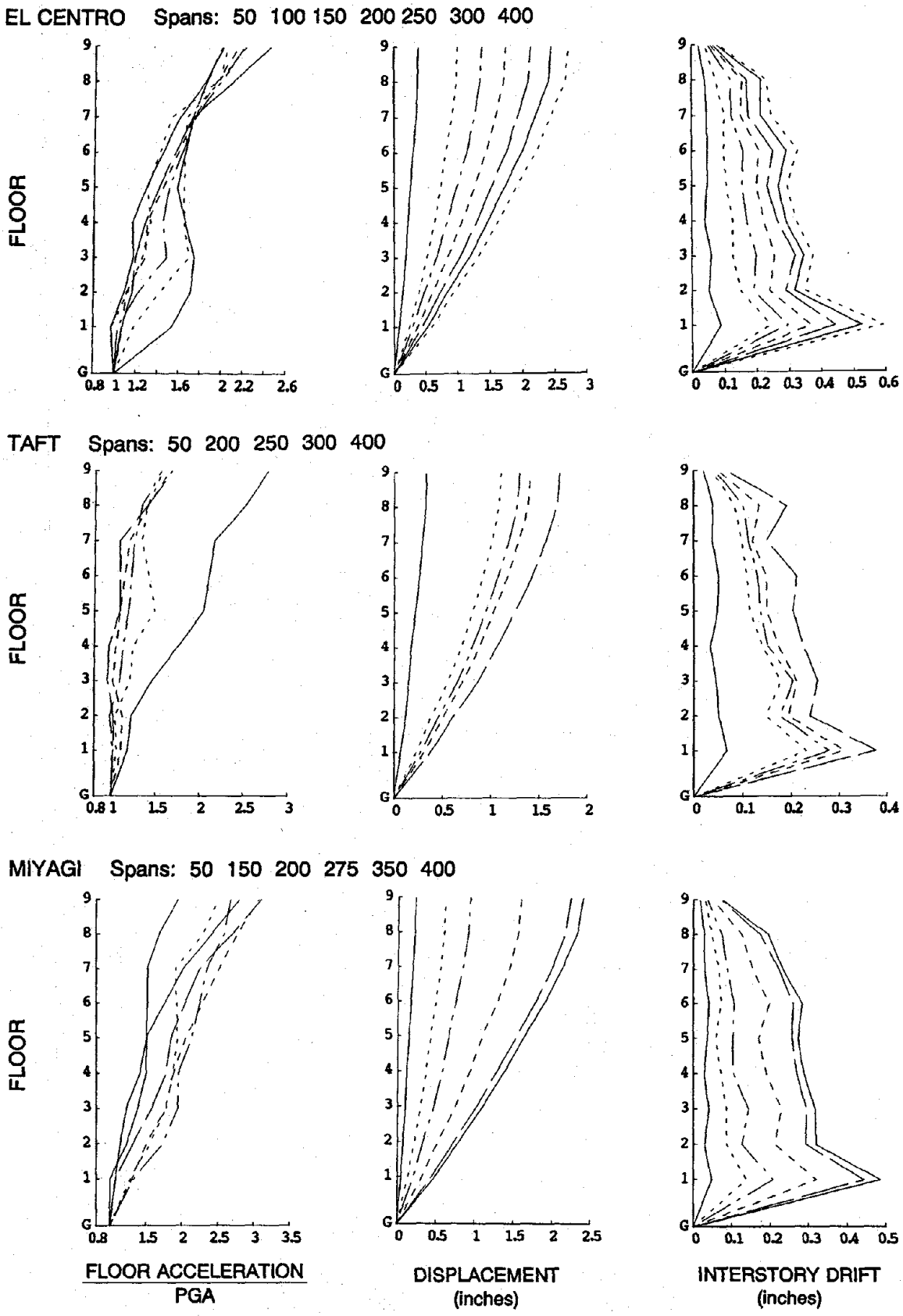

Fig. 4.26 FD Response Profiles for El Centro, Taft, Miyagi, Chile.u, La Union, and Zacatula Tests

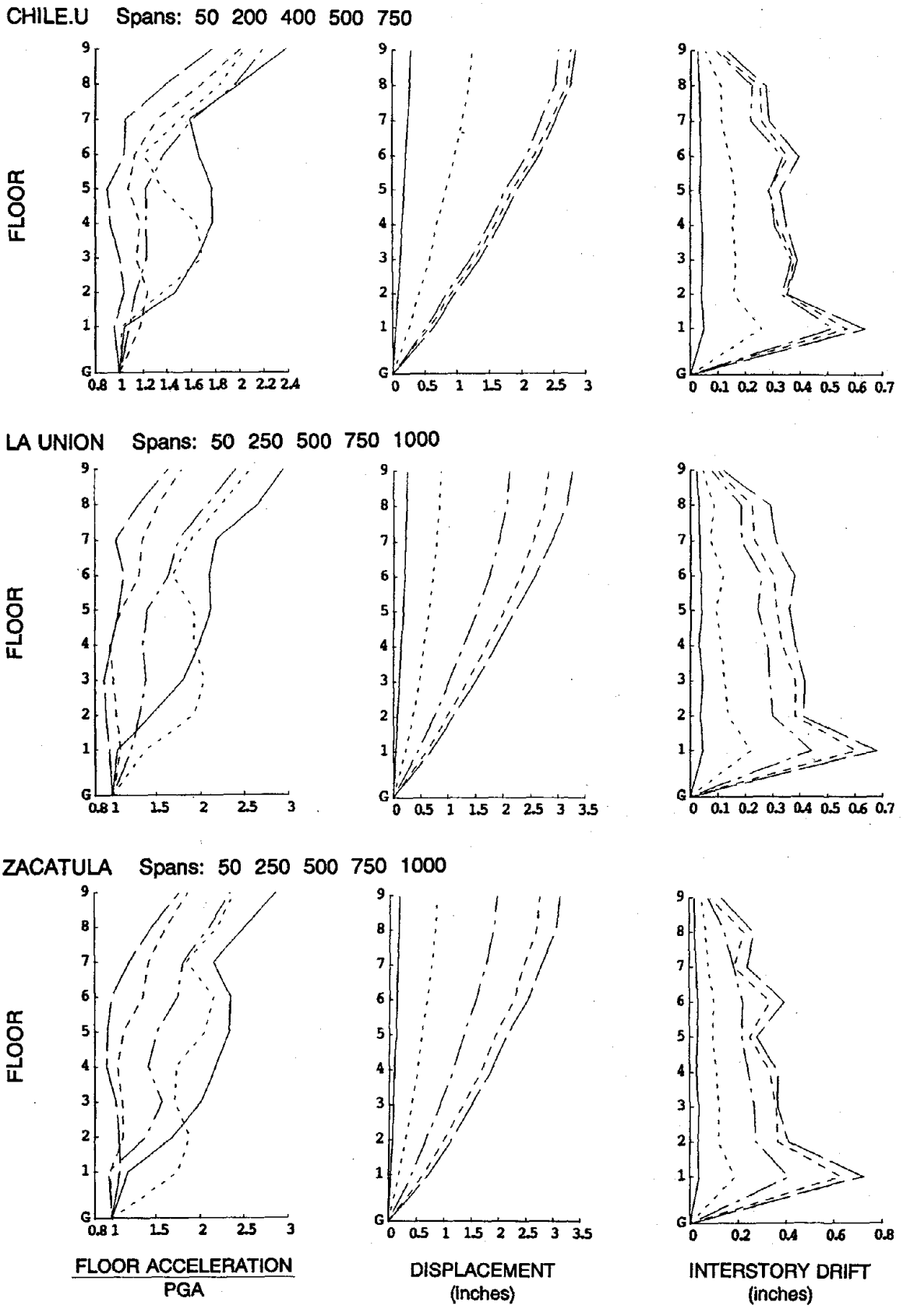
CHILE.U Spans: 50 200 400 500 750
LA UNION Spans: 50 250 500 750 1000
ZACATULA Spans: 50 250 500 750 1000
FLOOR
FLOOR ACCELERATION / PGA
DISPLACEMENT (Inches)
INTERSTORY DRIFT (inches)

Fig. 4.26 cont.

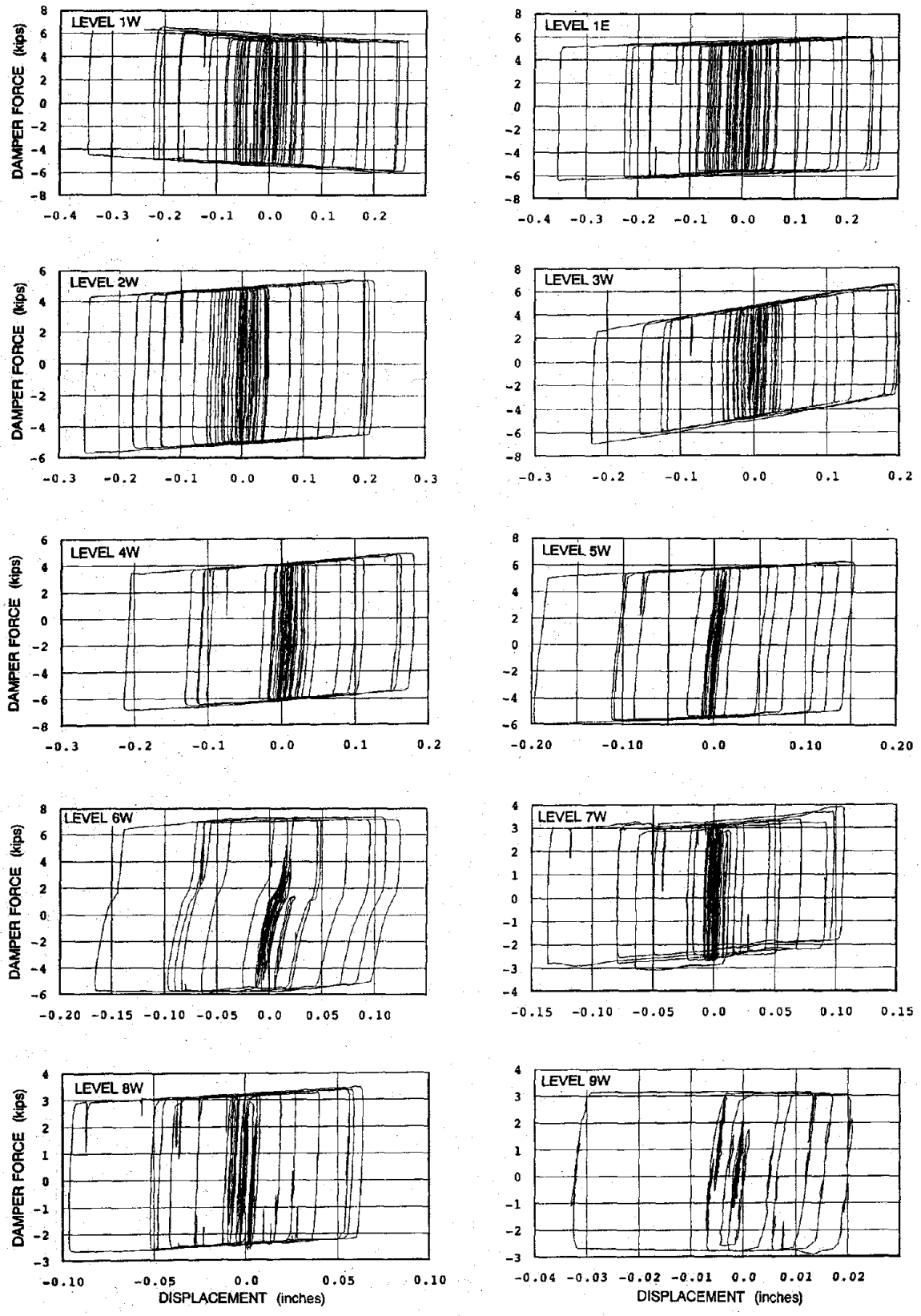

Fig. 4.27 Force-Displacement Plots for all Friction Dampers, ec-400 Test

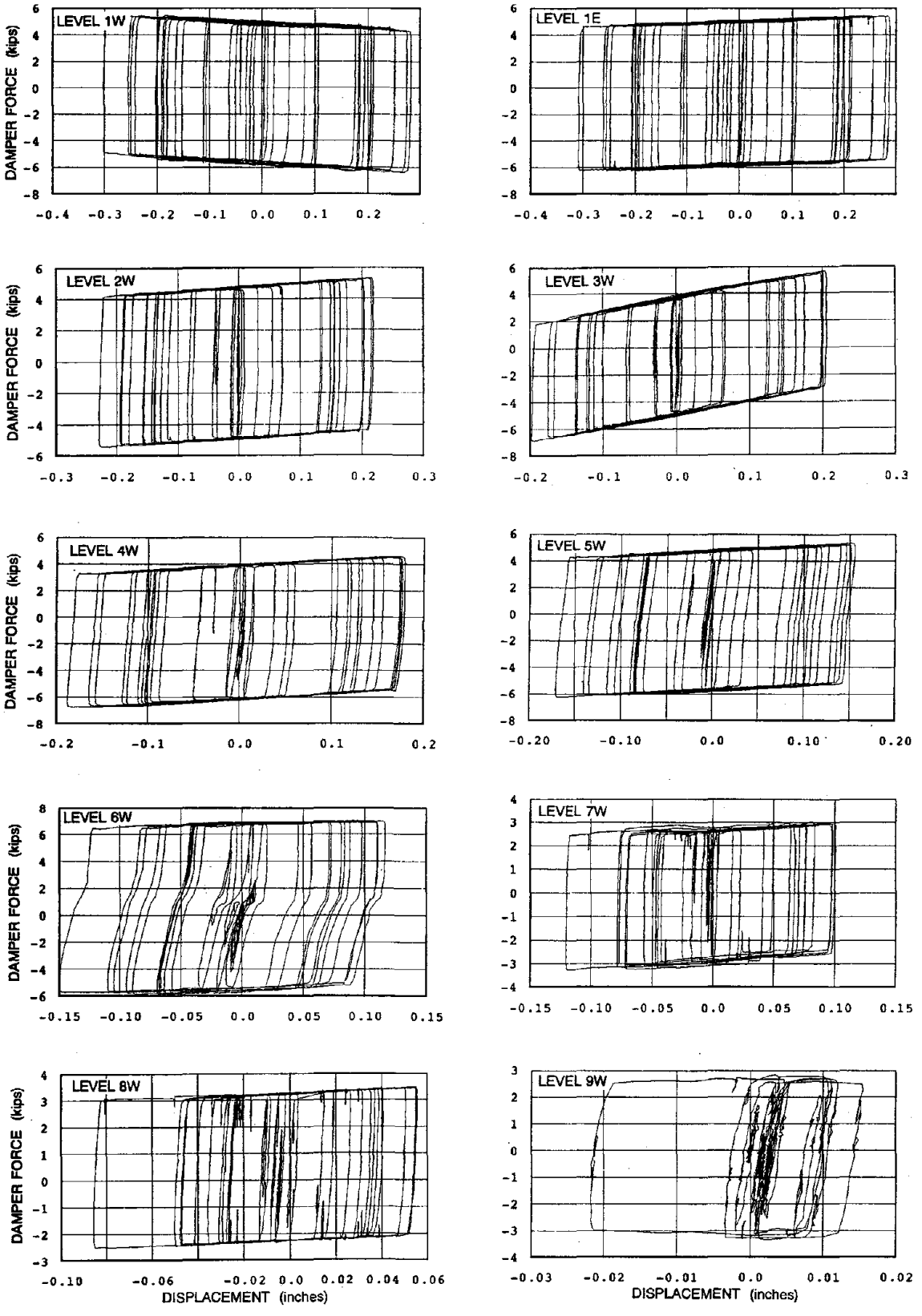

Fig. 4.28 Force-Displacement Plots for all Friction Dampers, miyagi-400 Test

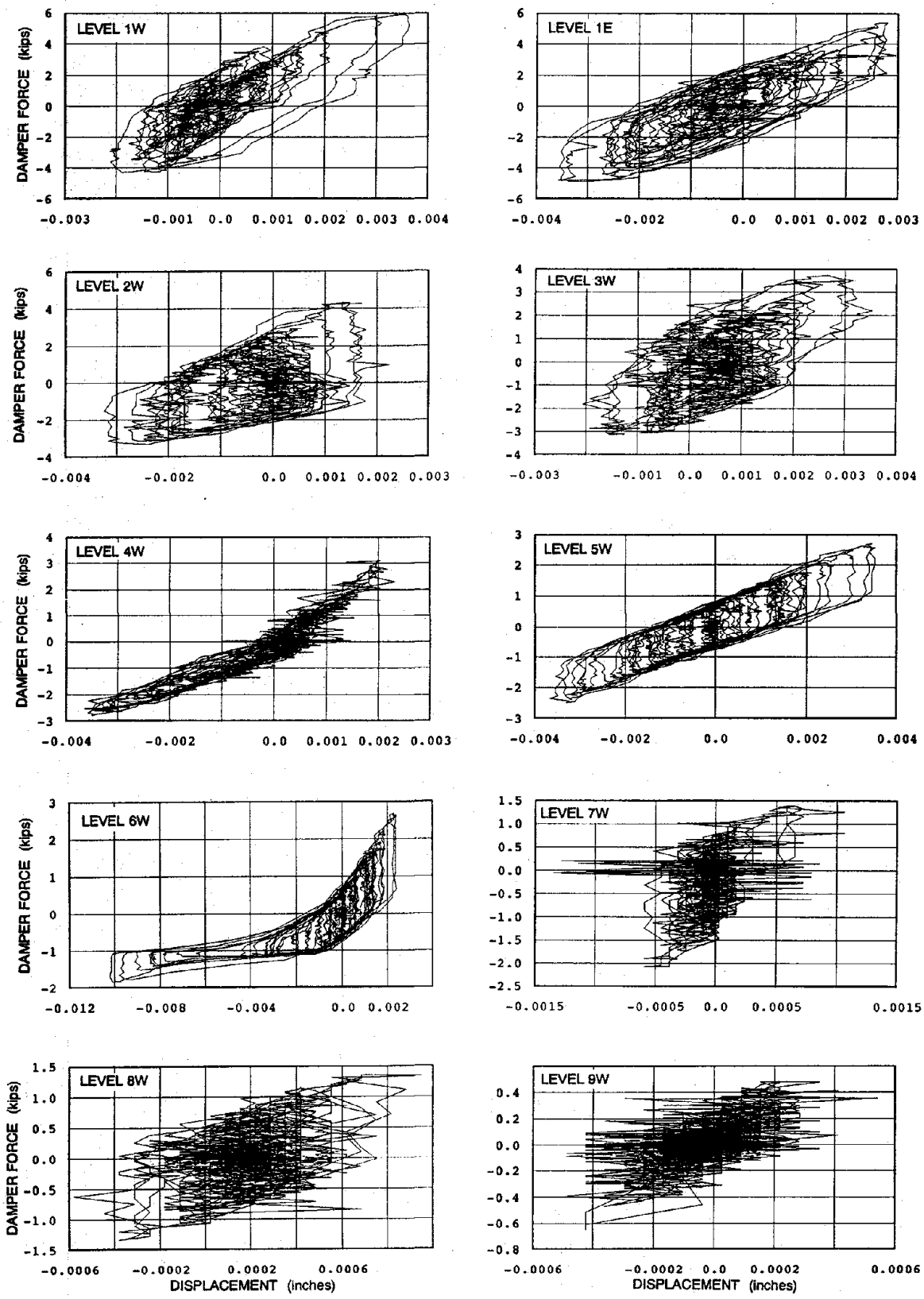

Fig. 4.29 Force-Displacement Plots for all Friction Dampers, chile.u-50 Test

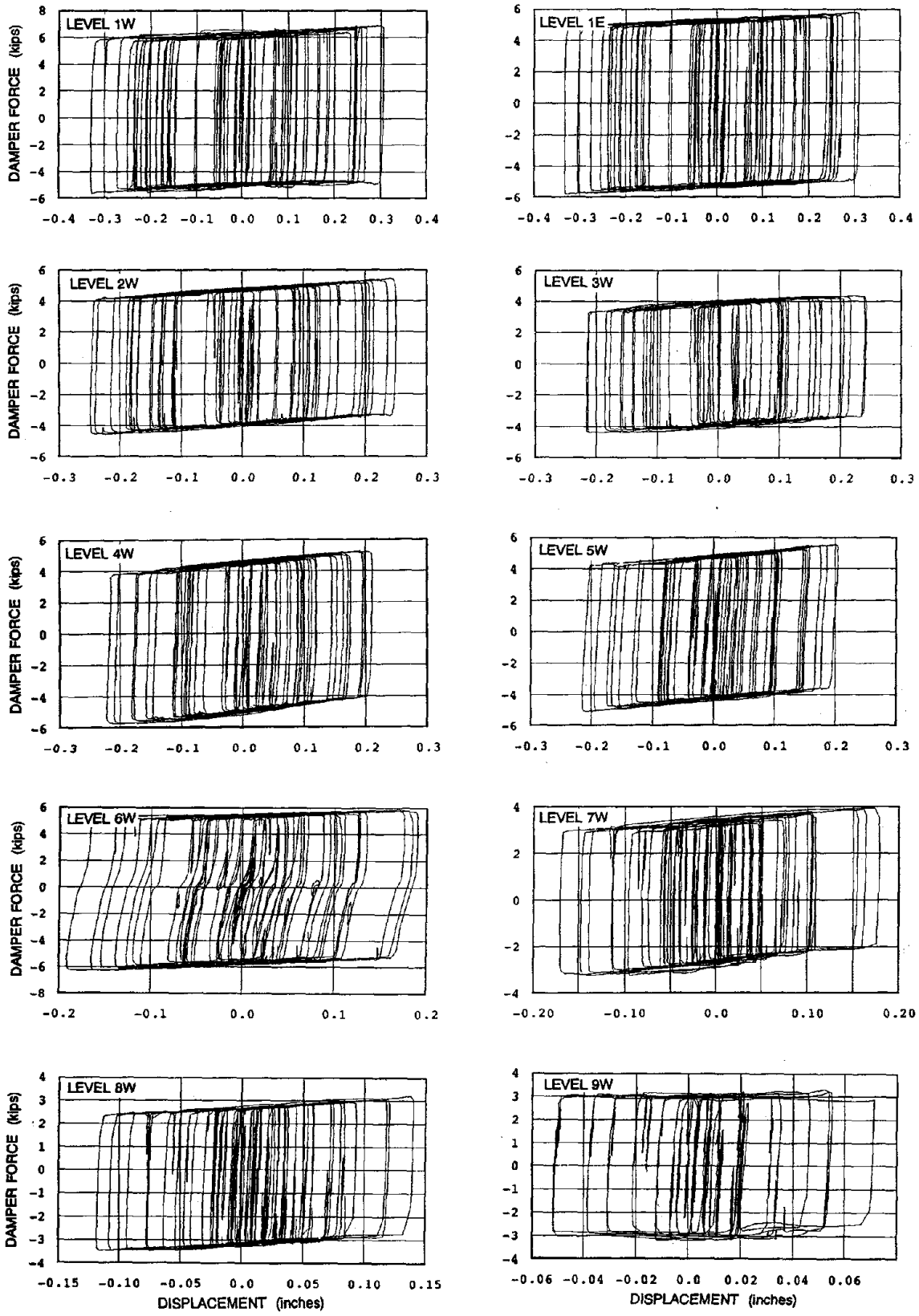

Fig. 4.30 Force-Displacement Plots for all Friction Dampers, chile.u-750 Test

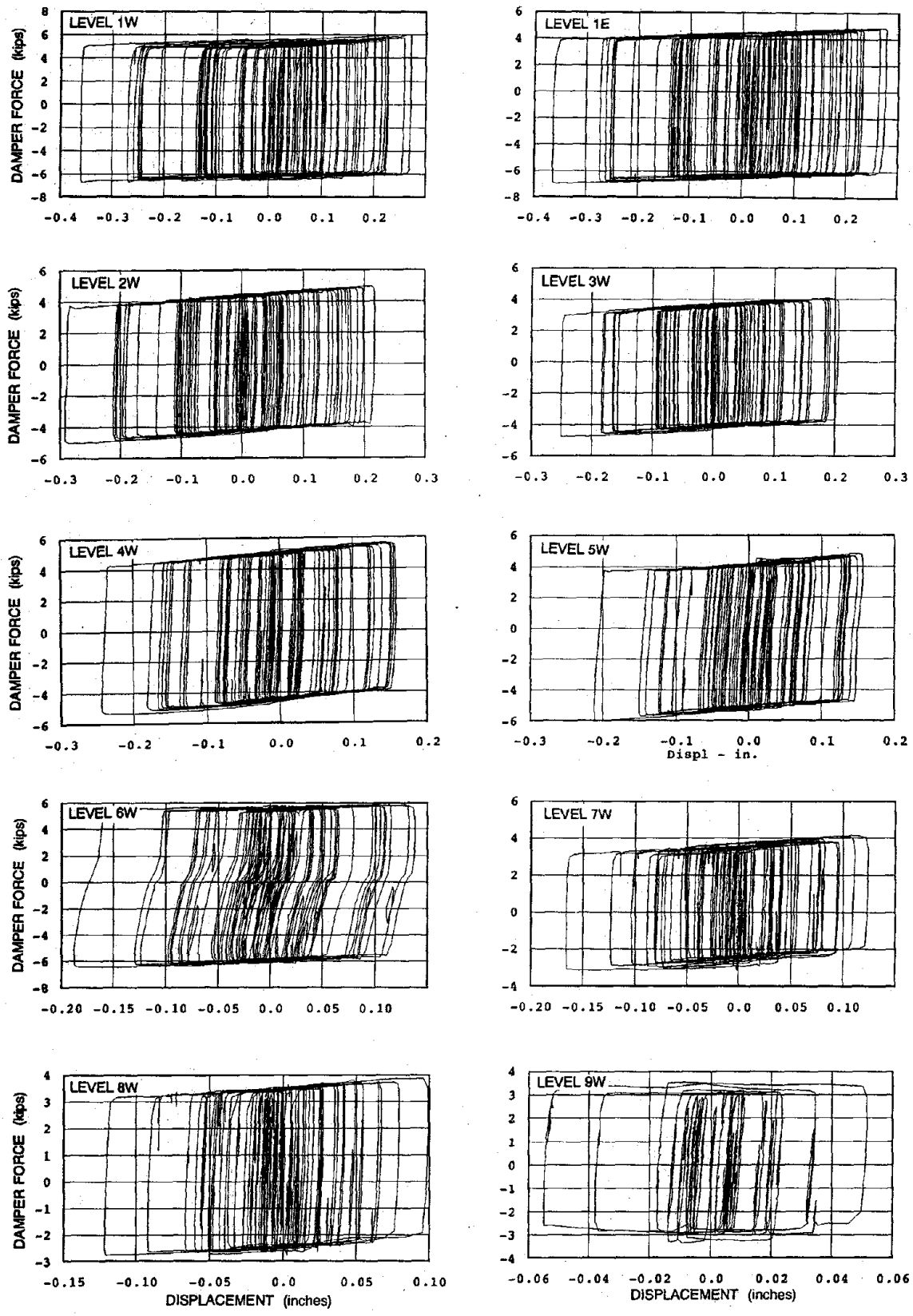

Fig. 4.31 Force-Displacement Plots for all Friction Dampers, unio-1000 Test

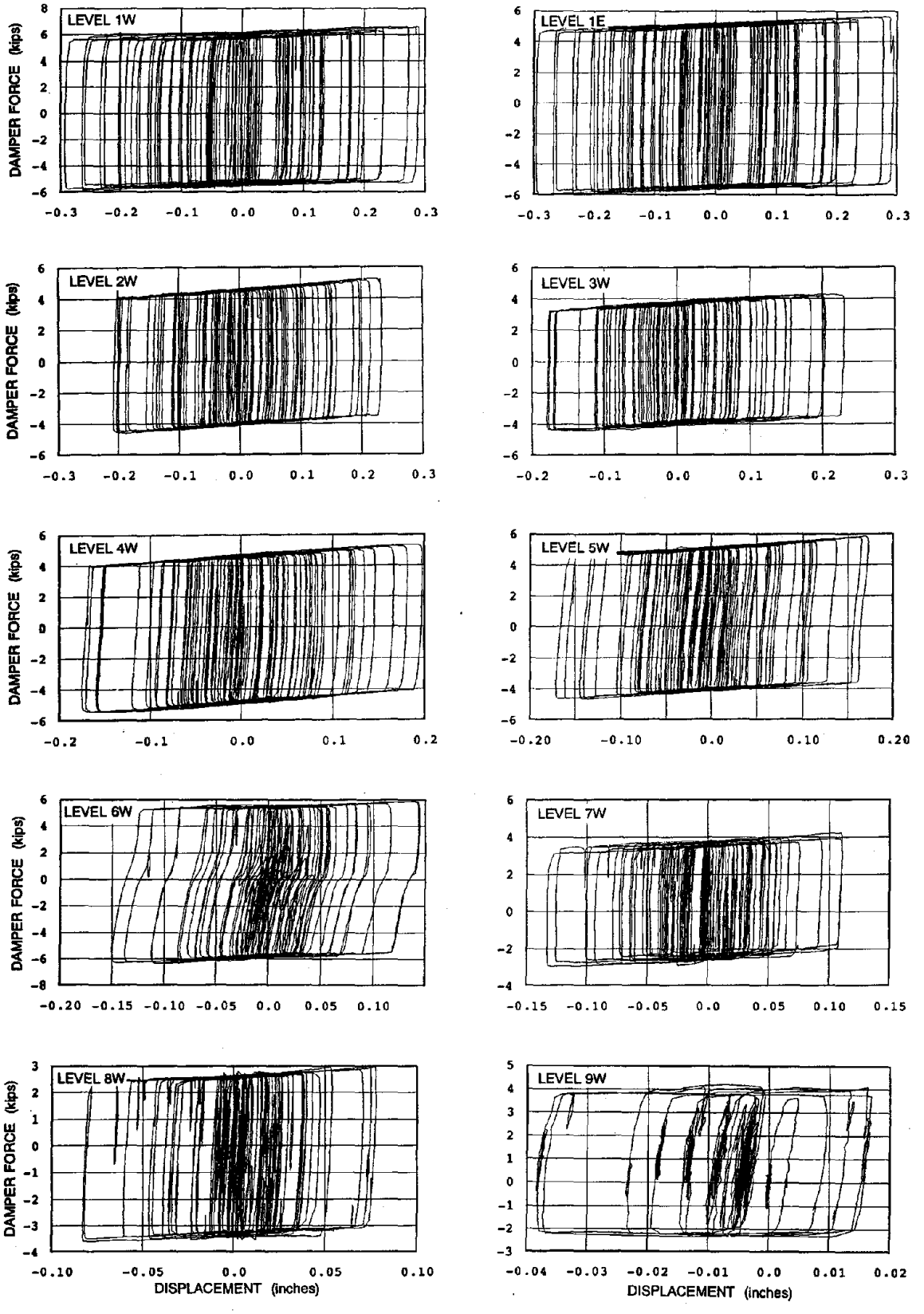

Fig. 4.32 Force-Displacement Plots for all Friction Dampers, zaca-1000 Test

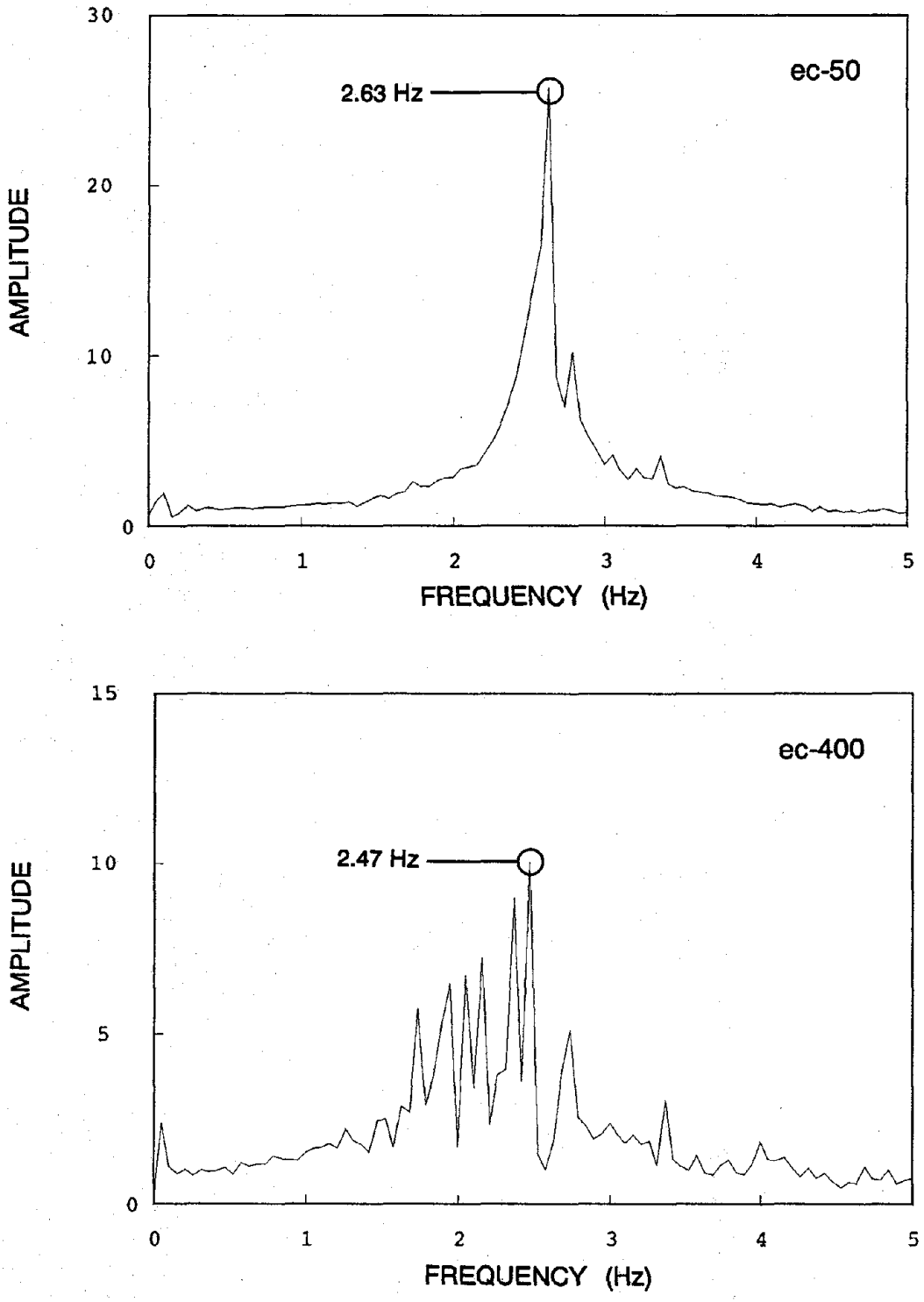

Fig. 4.33 FD Level 4 Acceleration Transfer Functions, ec-50 and ec-400 Tests

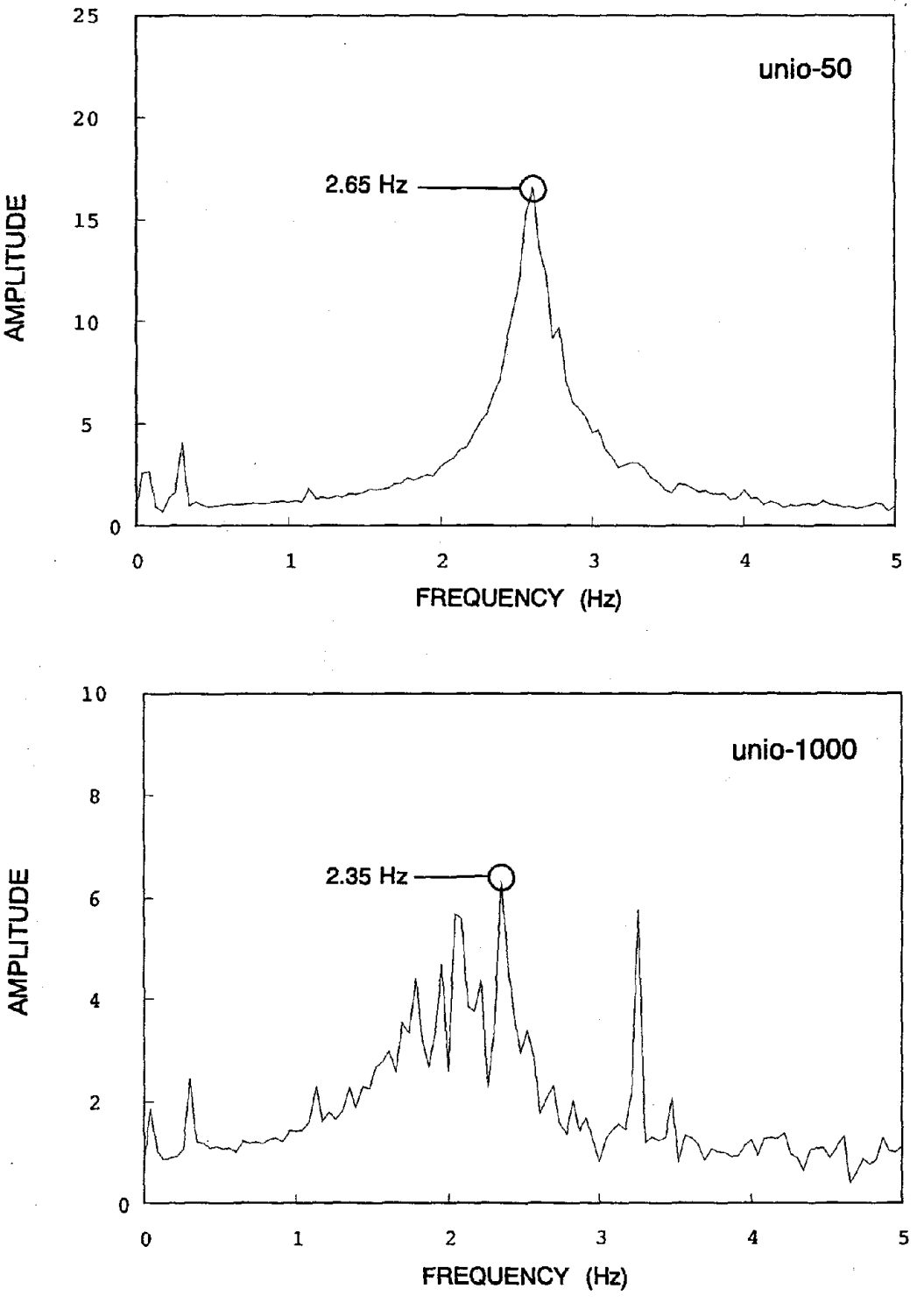

Fig. 4.34 FD Level 4 Acceleration Transfer Functions, unio-50 and unio-1000 Tests

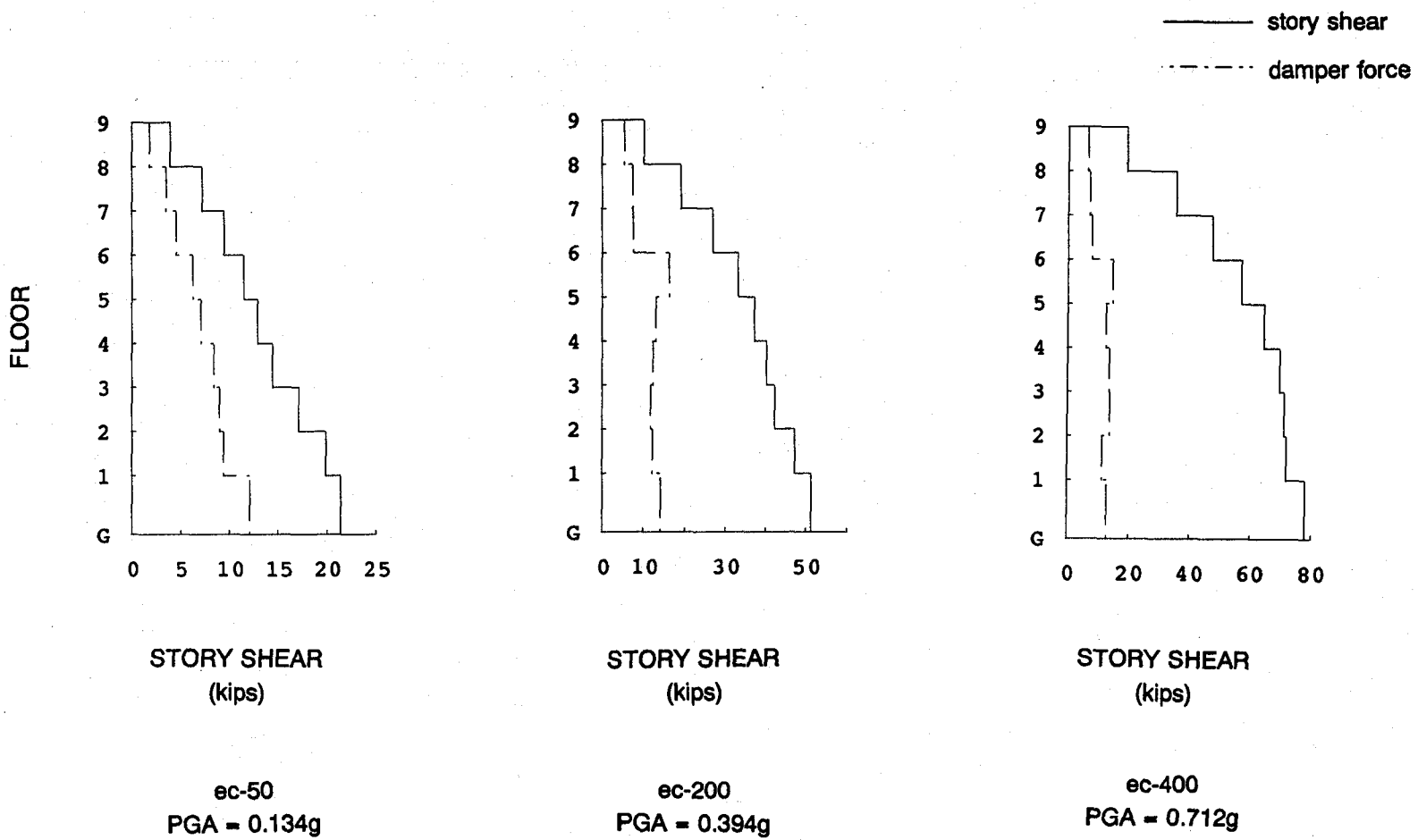

Fig. 4.35 FD Peak Story Shears and Device Forces, ec-50, ec-200, and ec-400 Tests

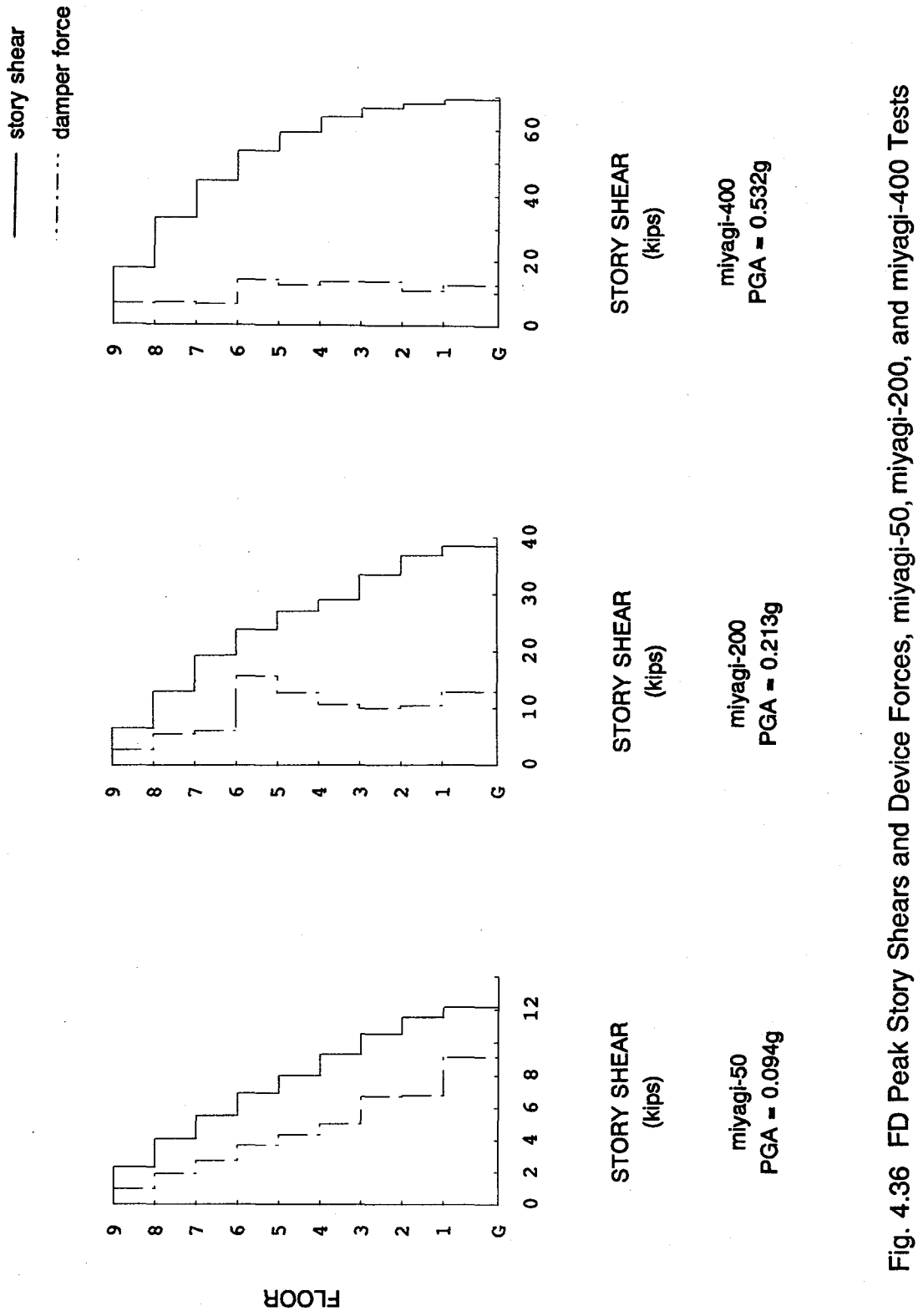

Fig. 4.36 FD Peak Story Shears and Device Forces, miyagi-50, miyagi-200, and miyagi-400 Tests

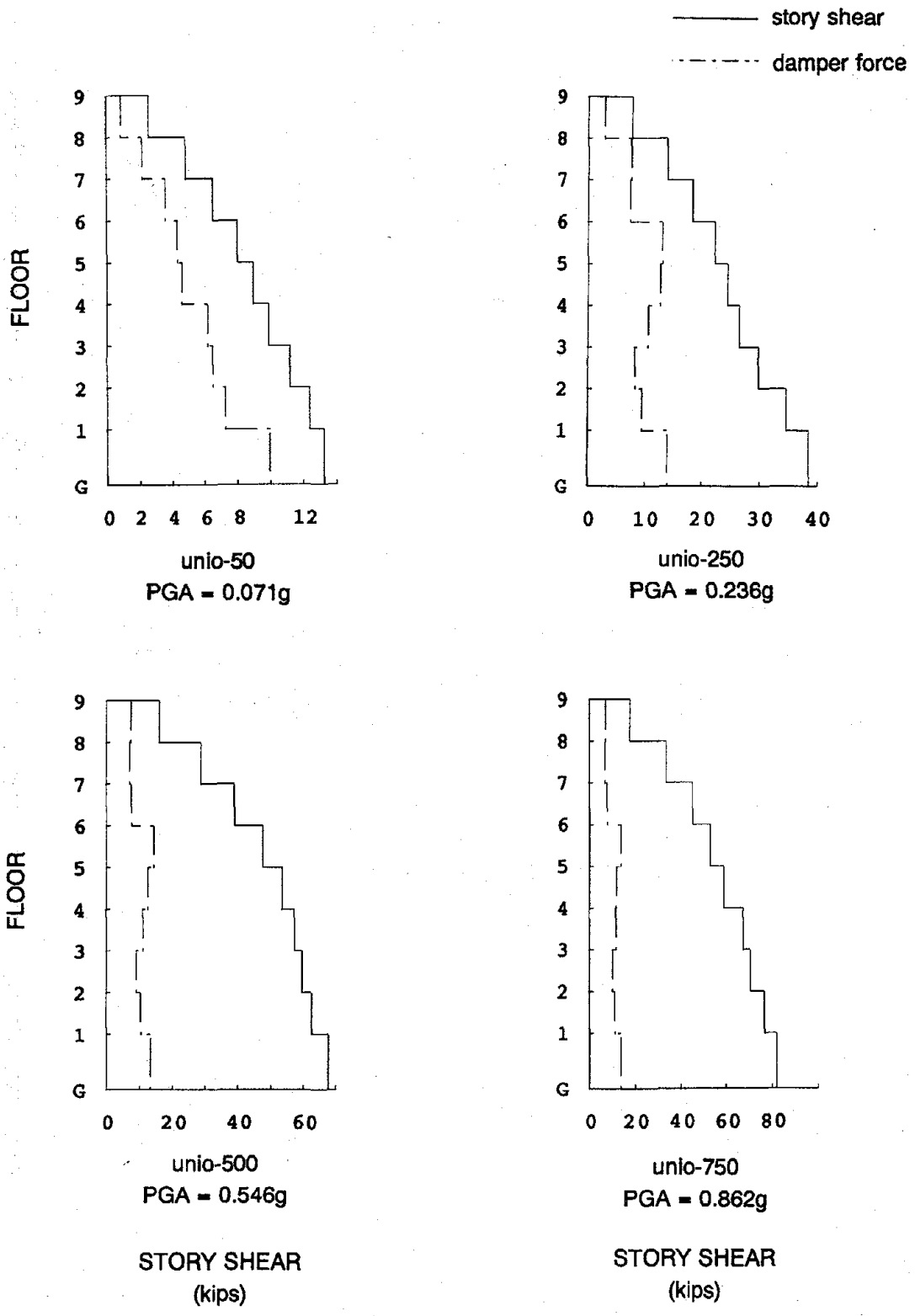

Fig. 4.37 FD Peak Story Shears and Device Forces, unio-50, unio-250, unio-500, and unio-1000 Tests

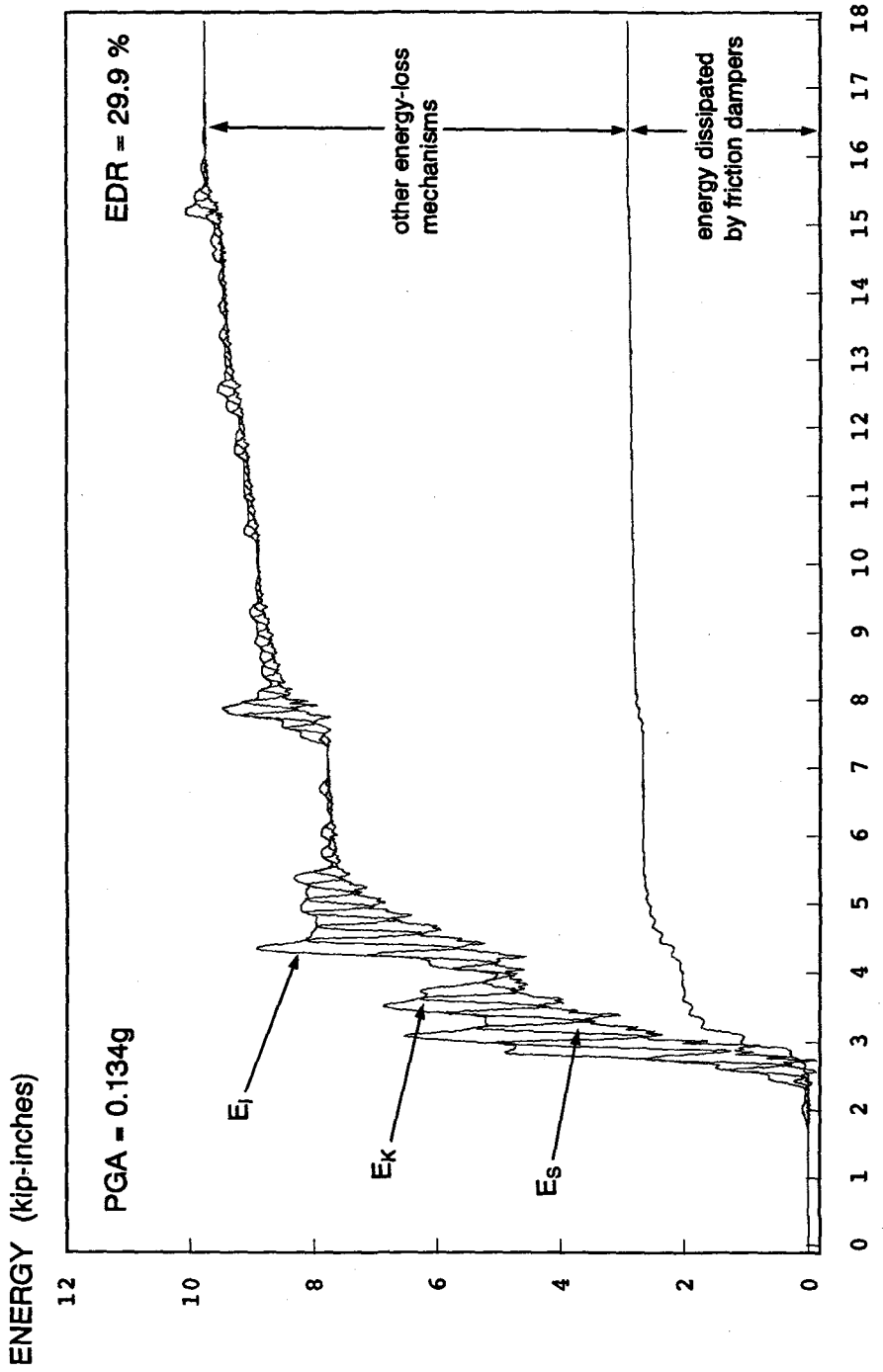

Fig. 4.38 FD Energy Time Histories, ec-50 Test

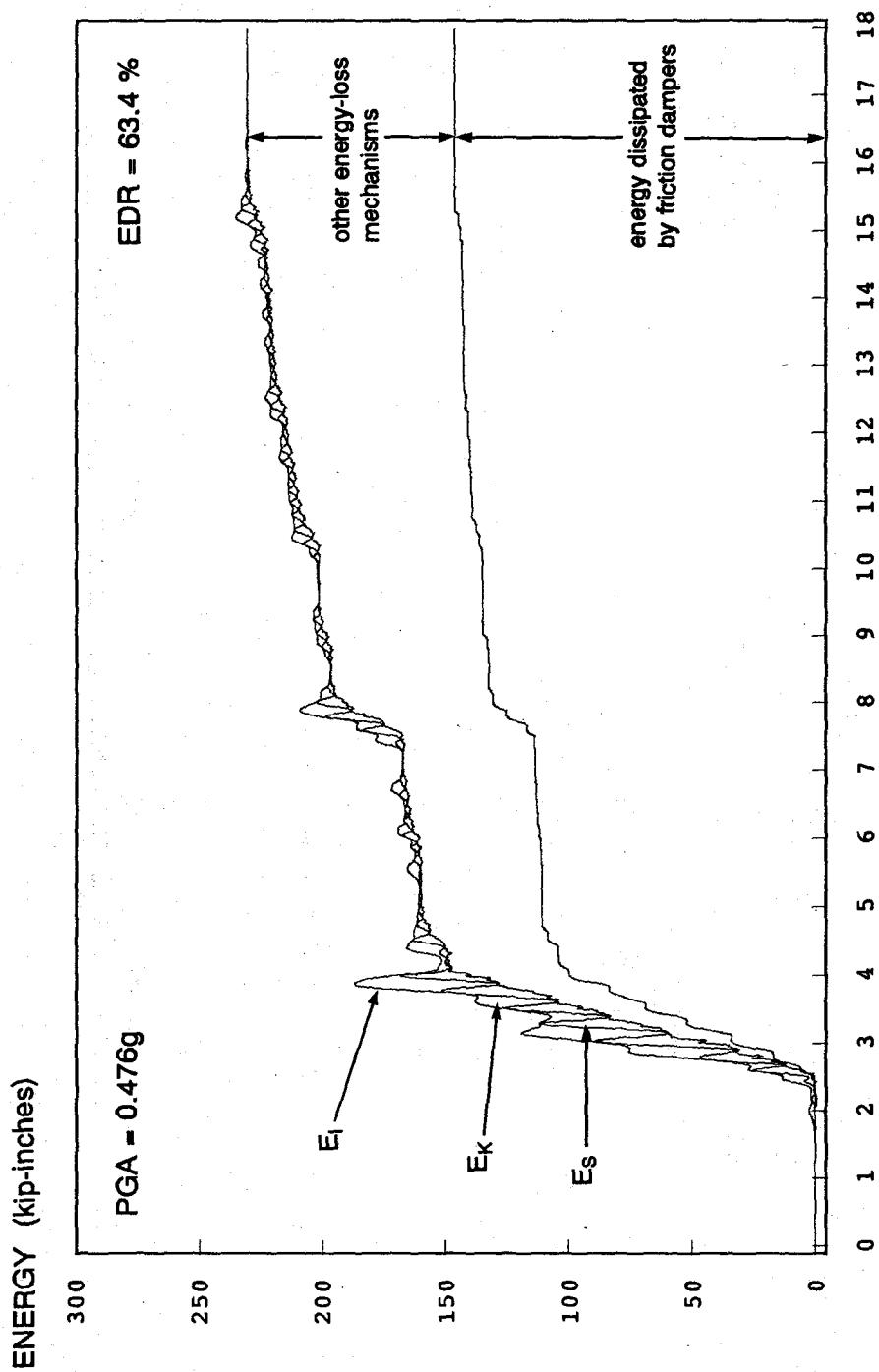

Fig. 4.39 FD Energy Time Histories, ec-250 Test

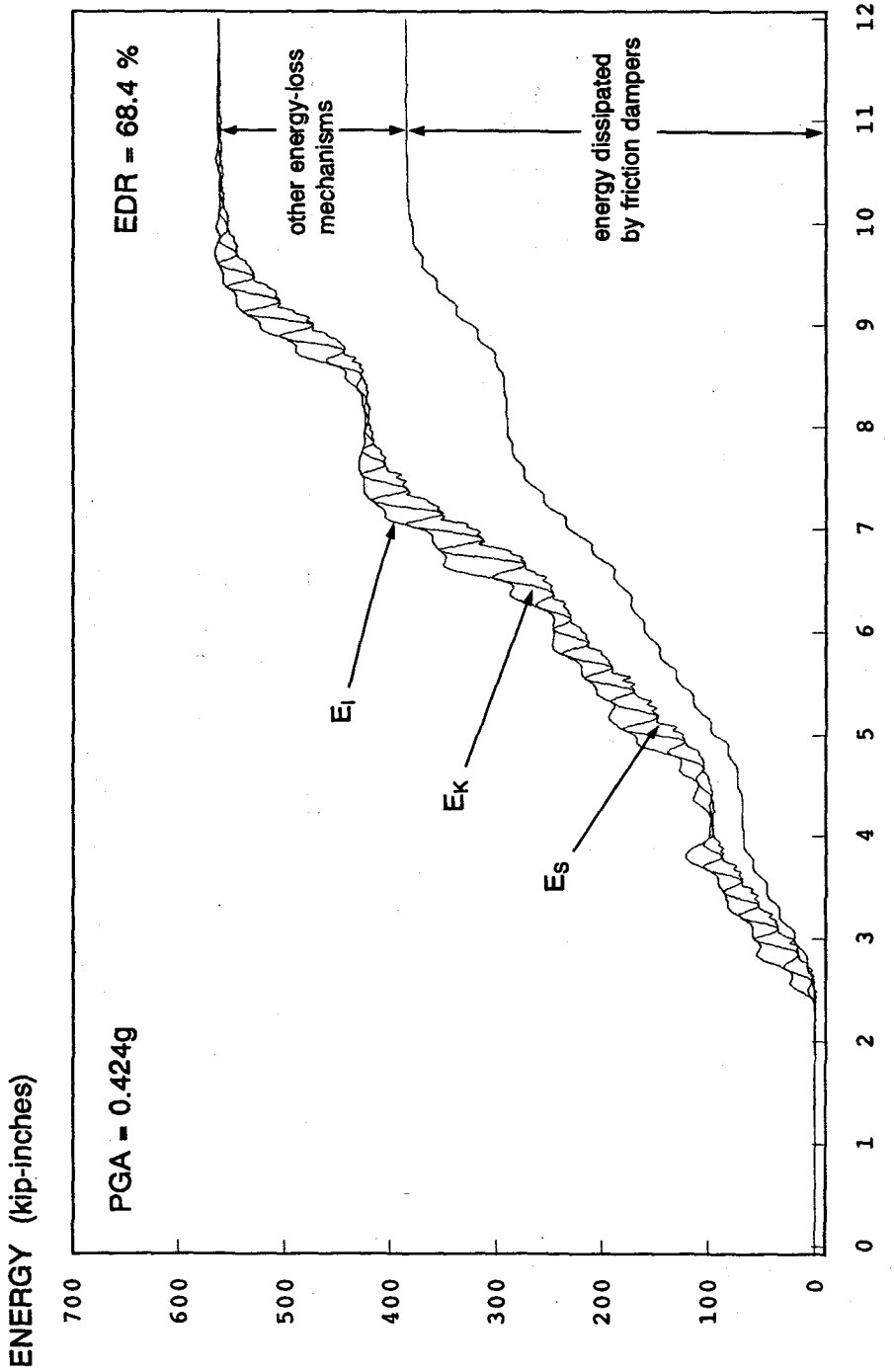

Fig. 4.40 FD Energy Time Histories, miyagi-350 Test

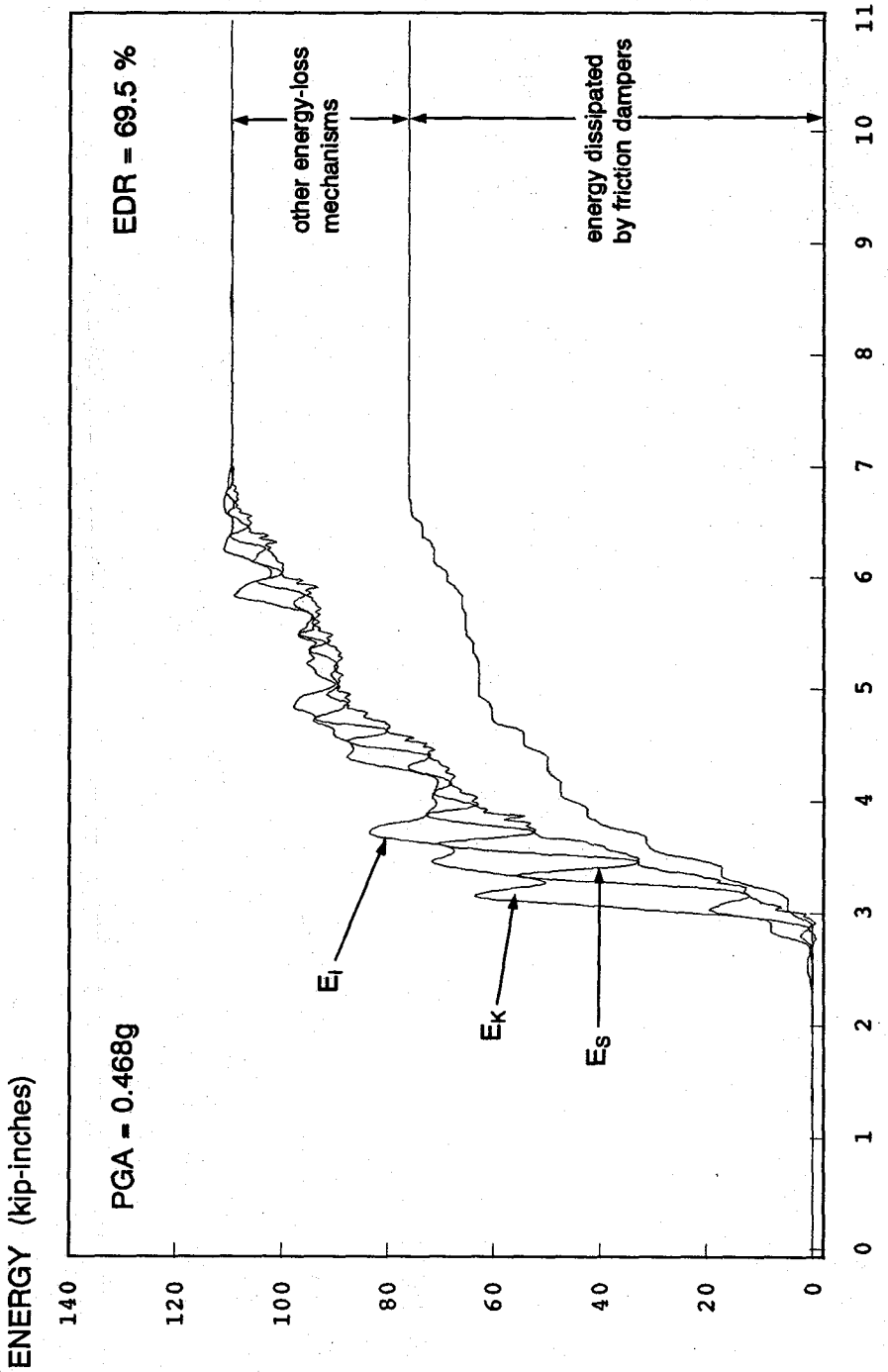

Fig. 4.41 FD Energy Time Histories, pac-350 Test

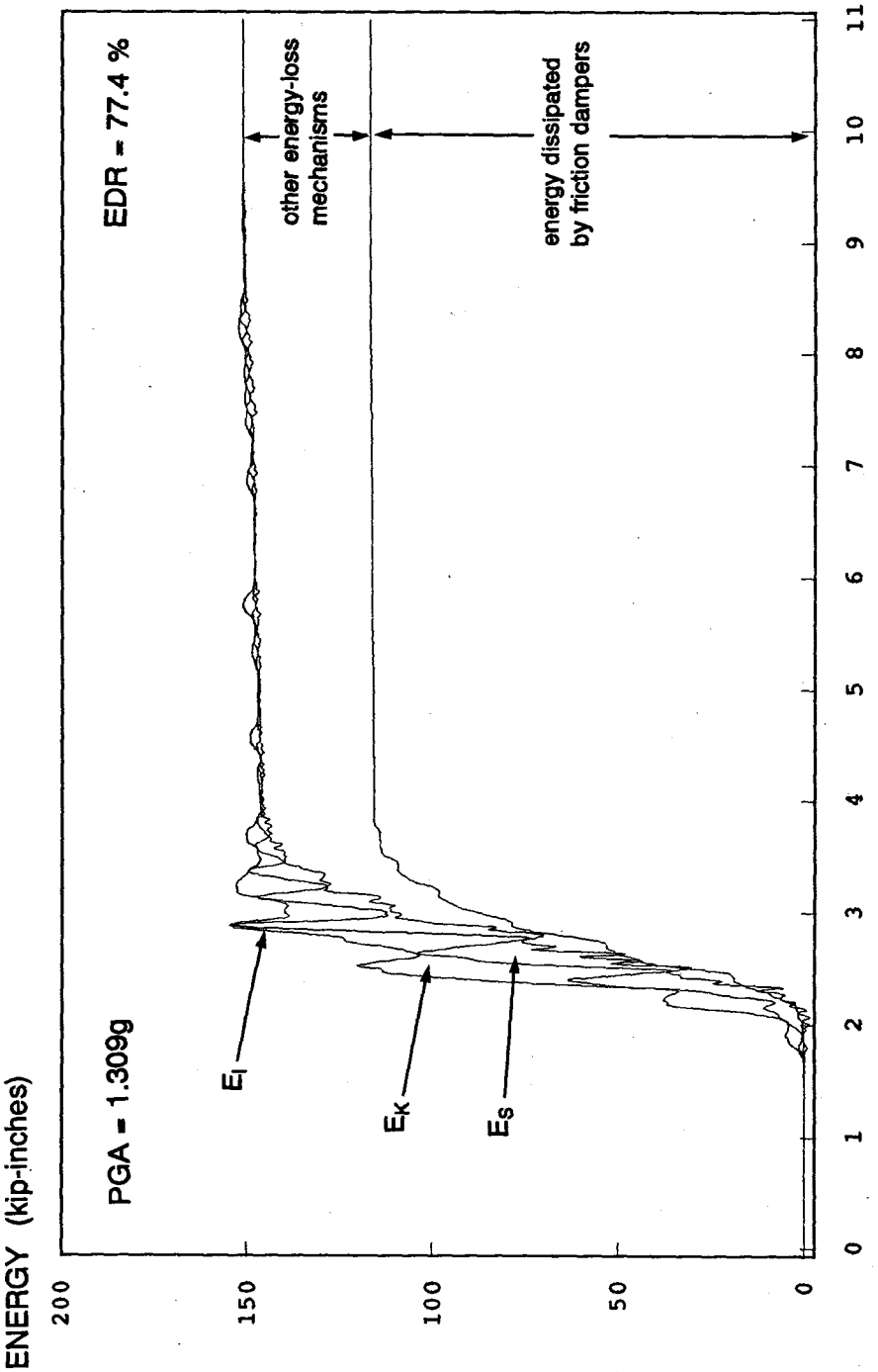

Fig. 4.42 FD Energy Time Histories, sf-300 Test

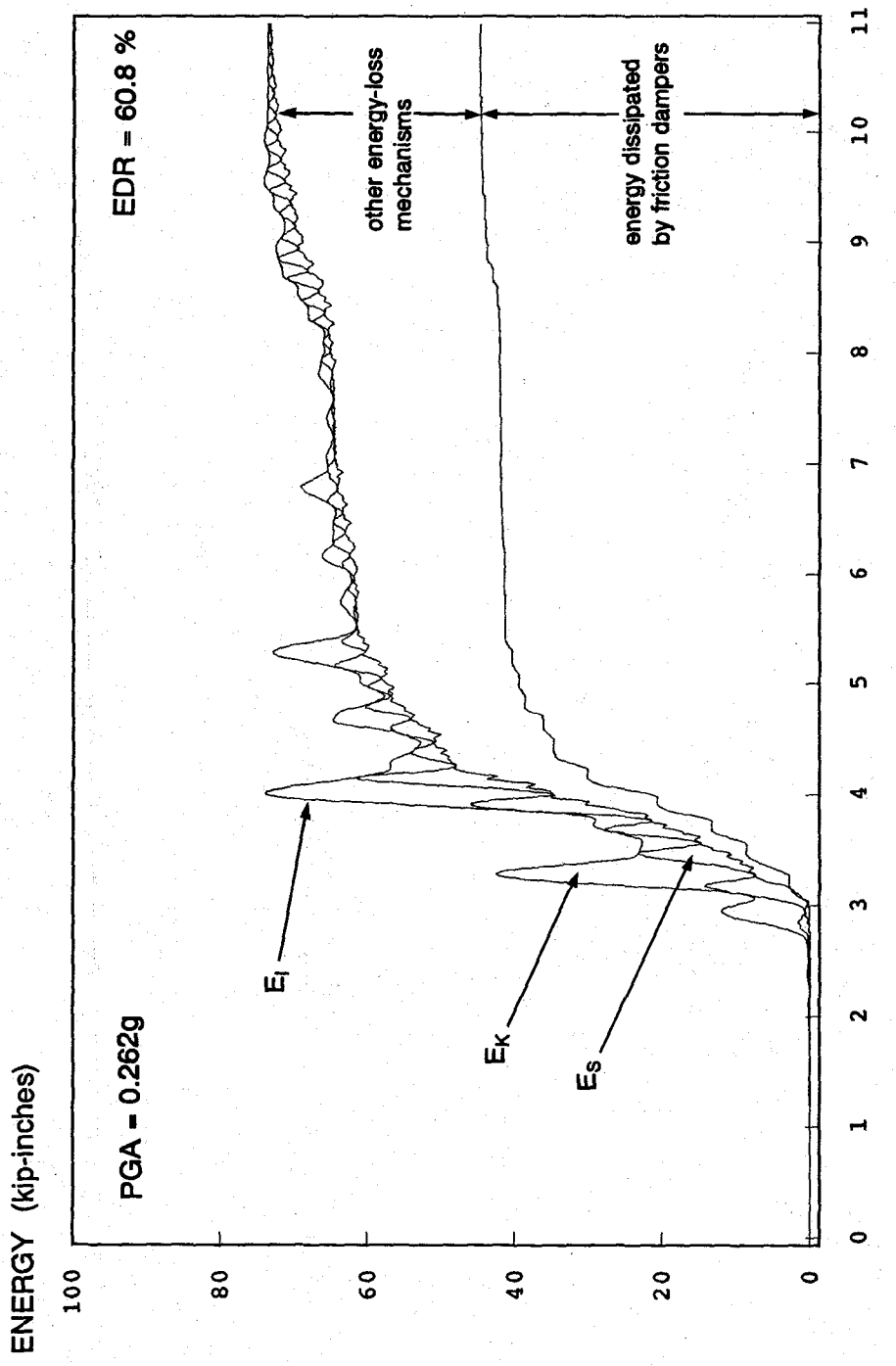

Fig. 4.43 FD Energy Time Histories, buc-300 Test

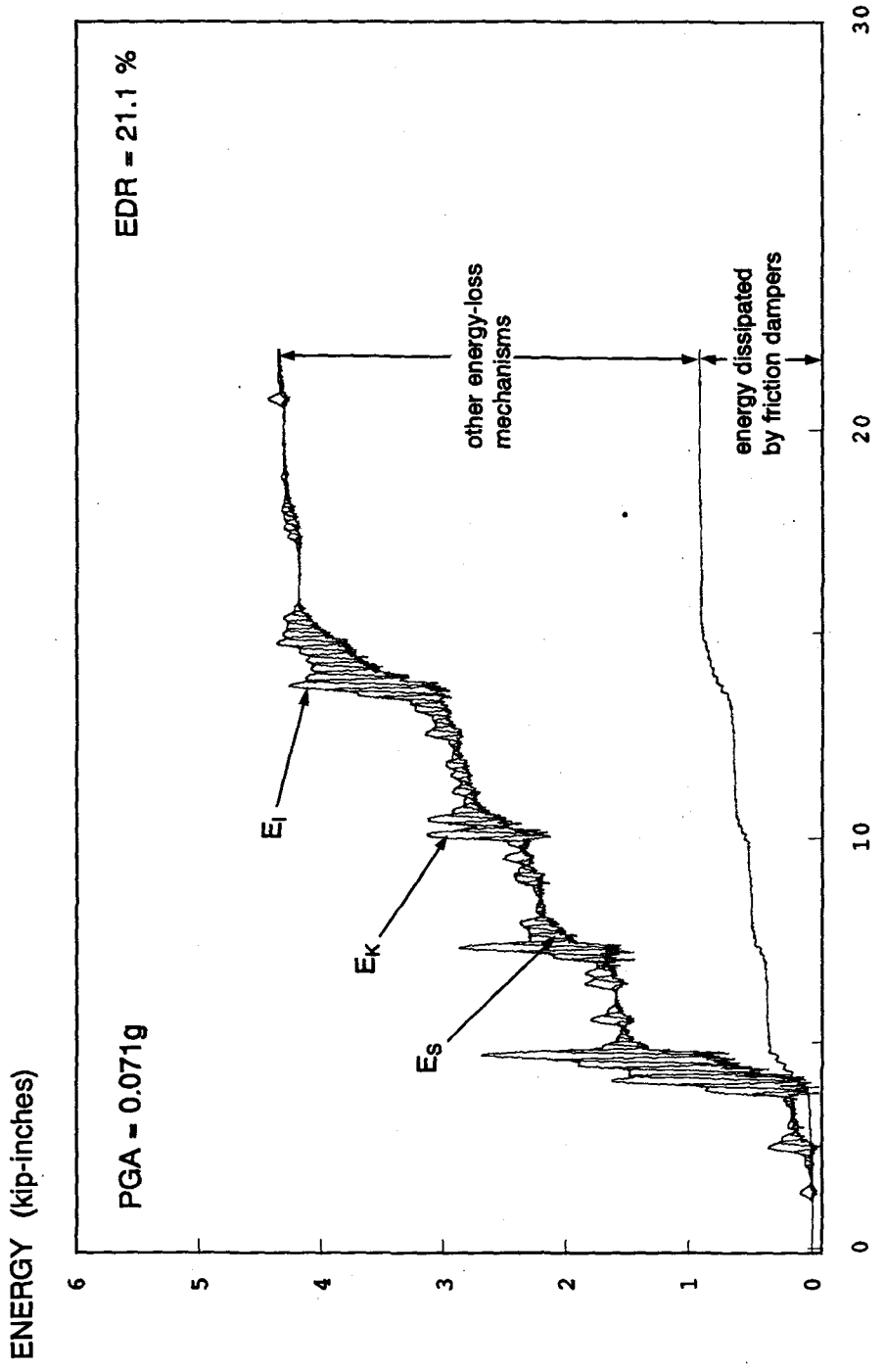

Fig. 4.44 FD Energy Time Histories, unio-50 Test

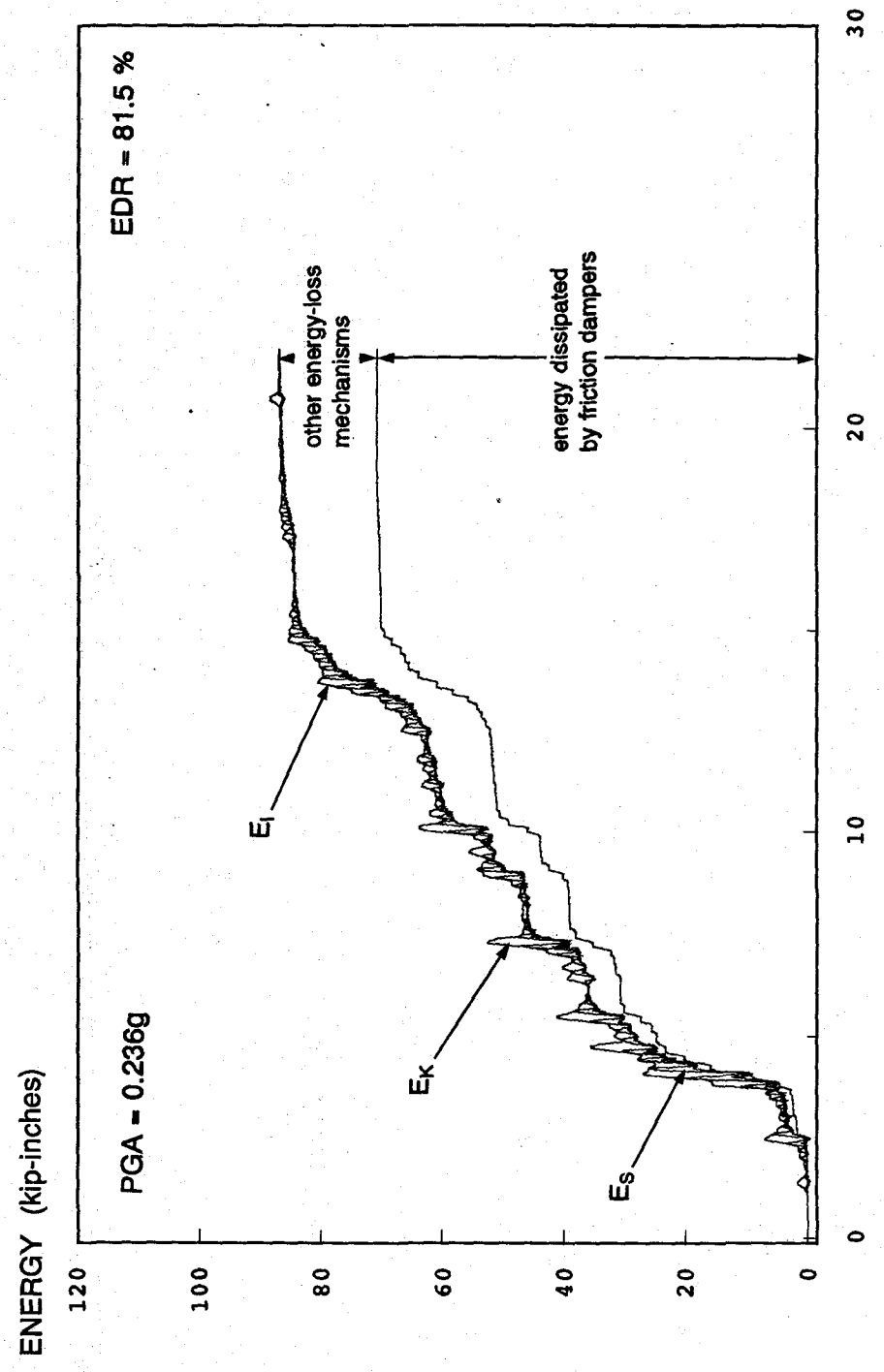

Fig. 4.45 FD Energy Time Histories, unio-250 Test

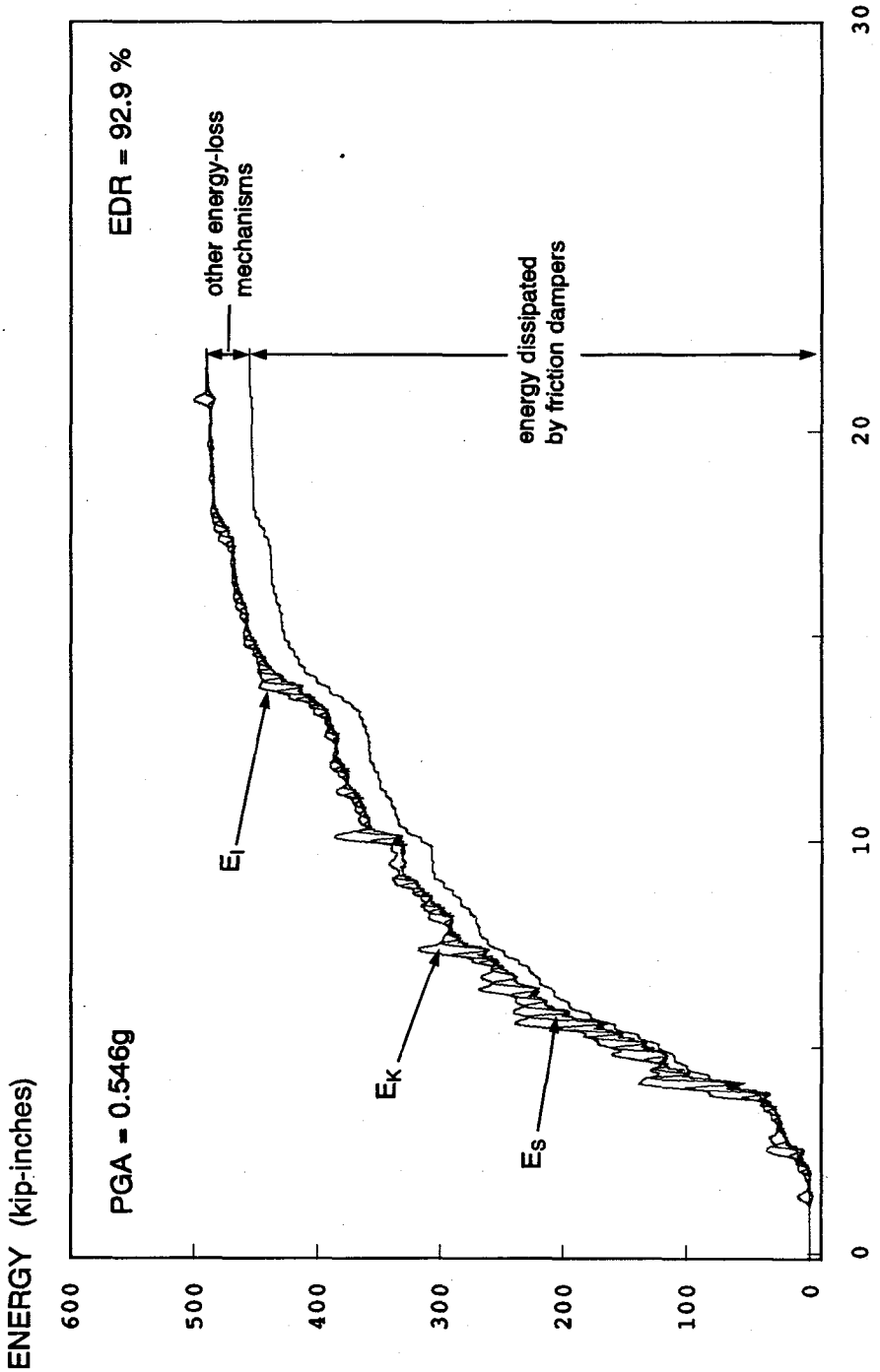

Fig. 4.46 FD Energy Time Histories, unio-500 Test

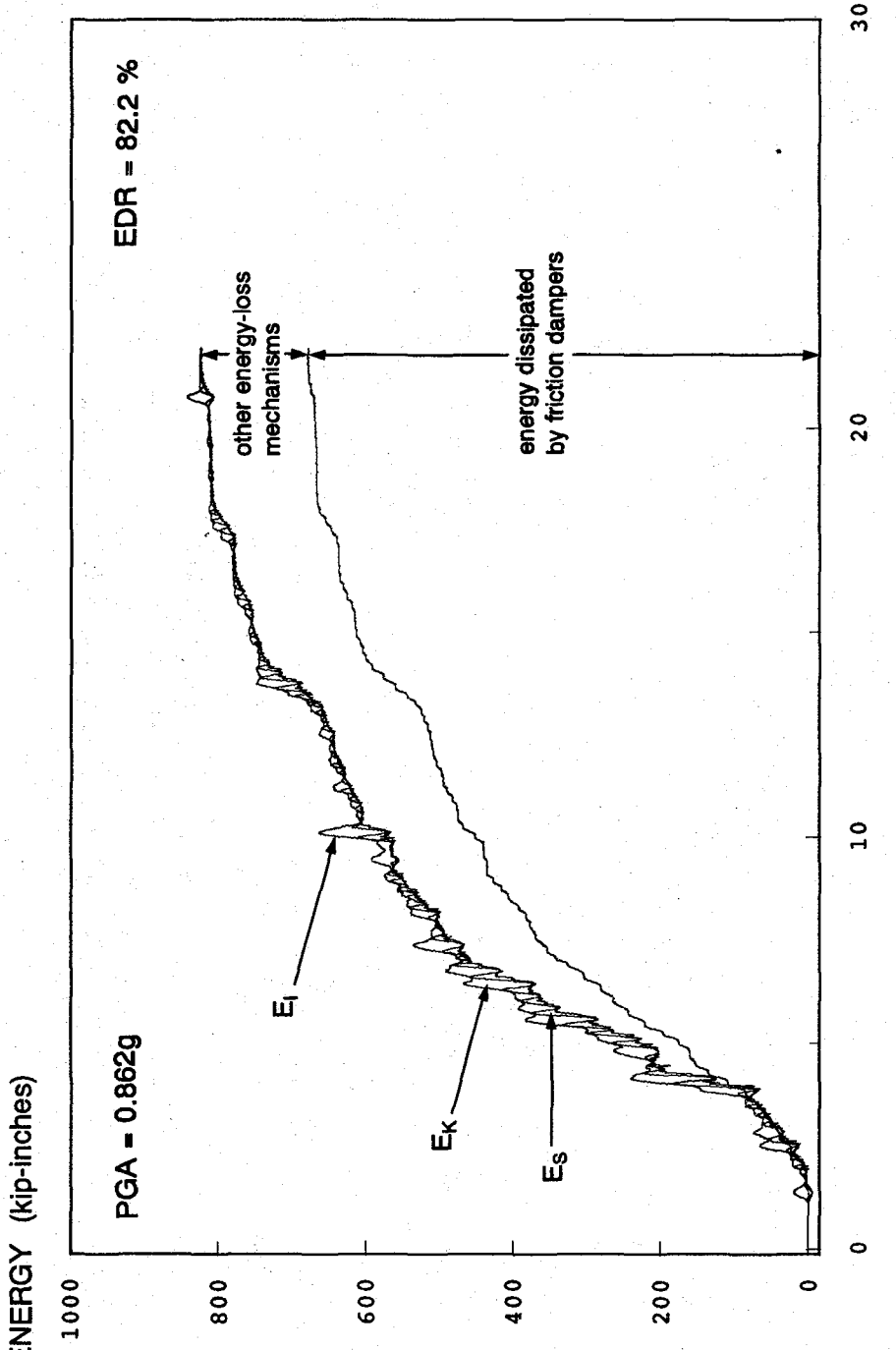

Fig. 4.47 FD Energy Time Histories, unio-750 Test

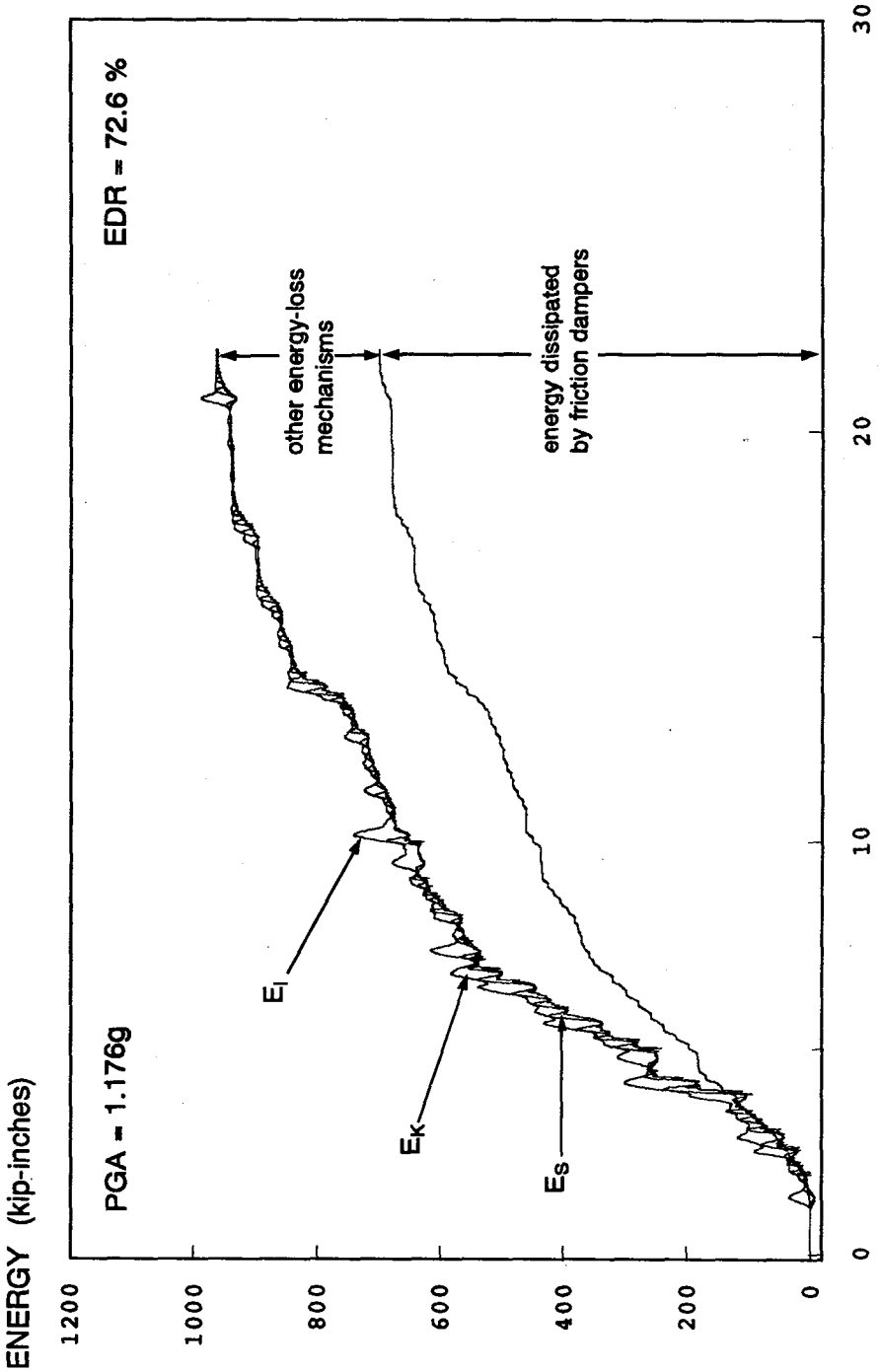

Fig. 4.48 FD Energy Time Histories, unio-1000 Test

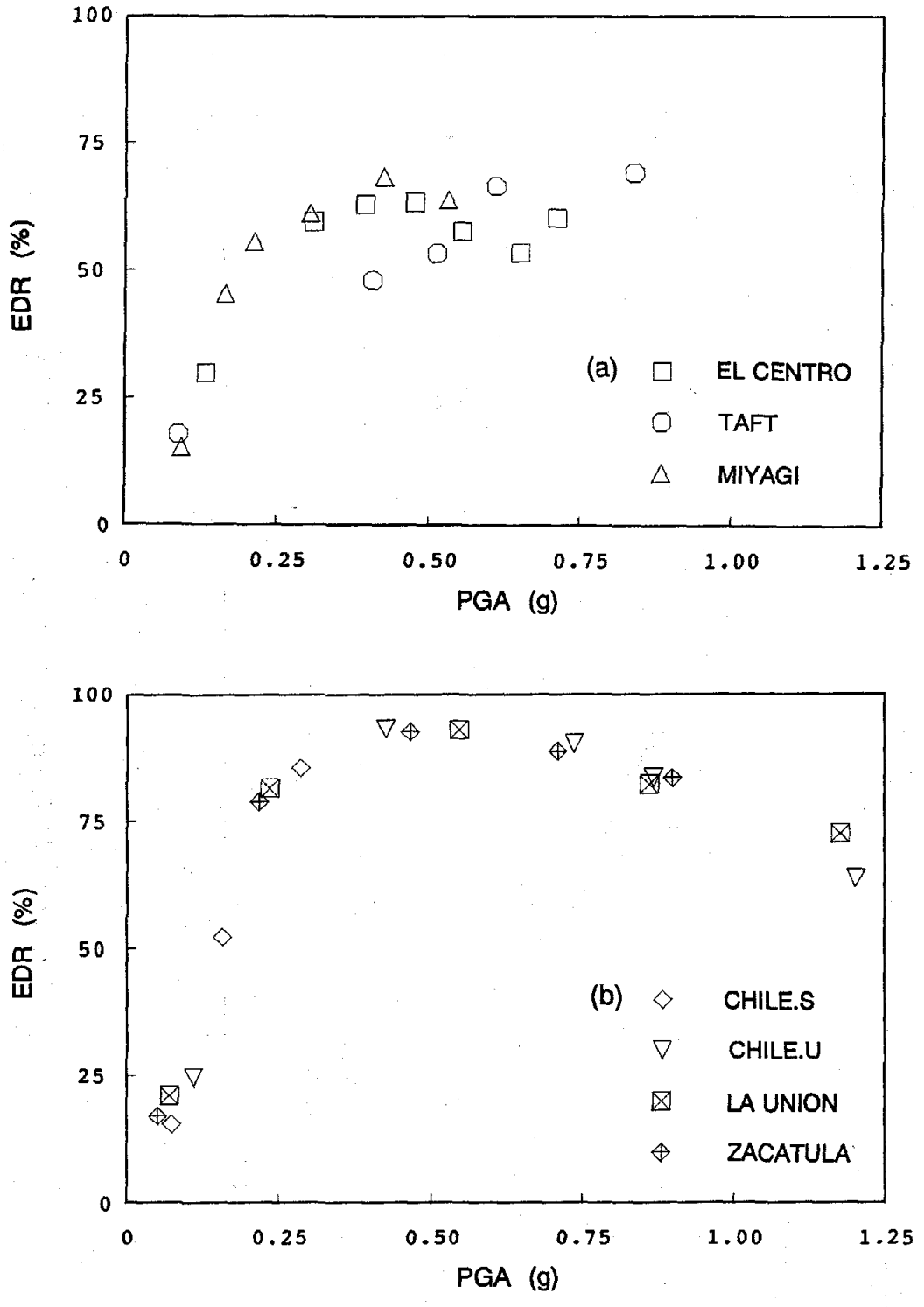

Fig. 4.49 FD Energy Dissipation Ratio vs. PGA

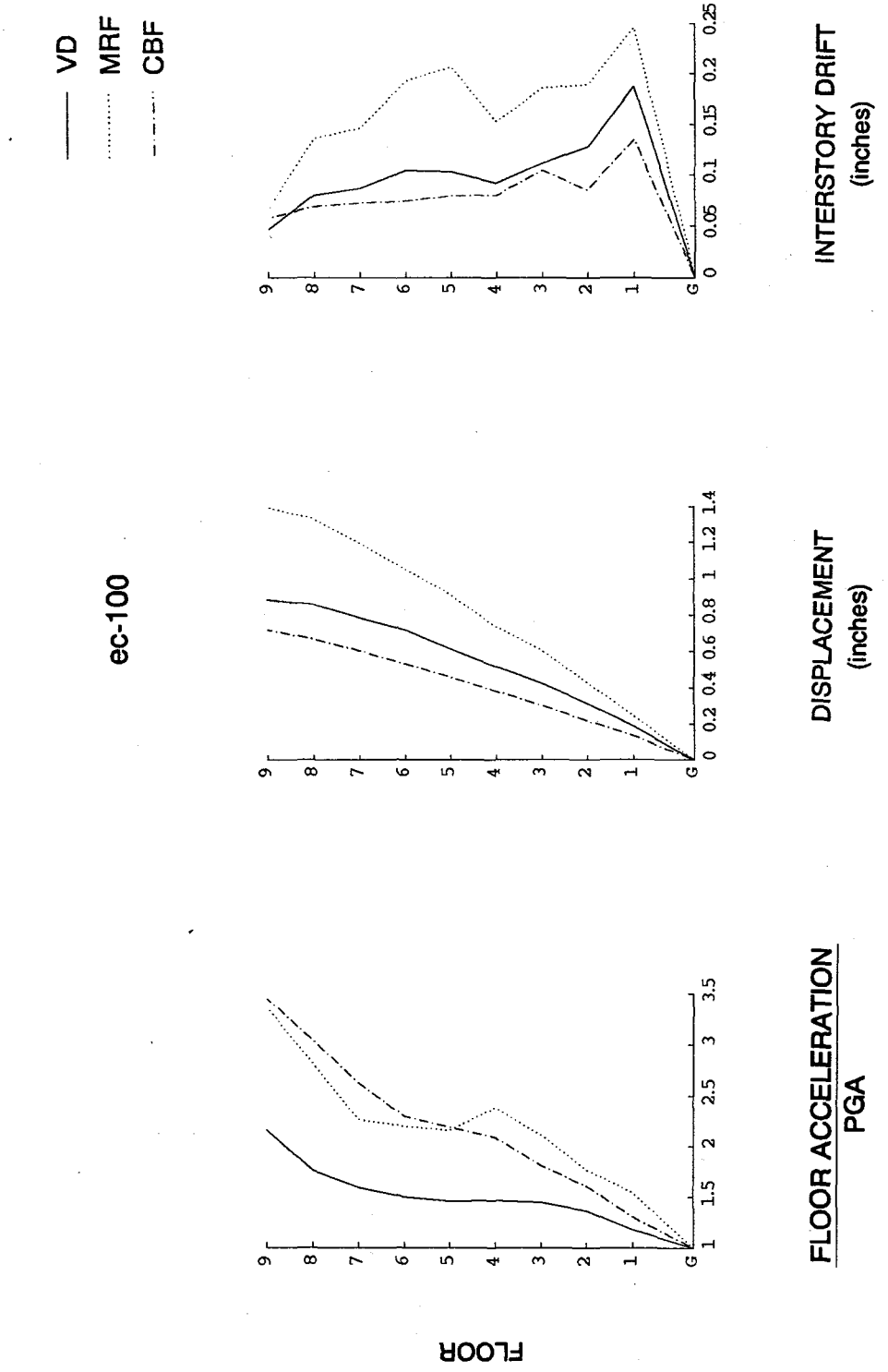

Fig. 4.50 VD, MRF, and CBF Acceleration, Displacement and Interstory Drift Response Profiles, ec-100, ec-200, ec-300, and ec-400 Tests

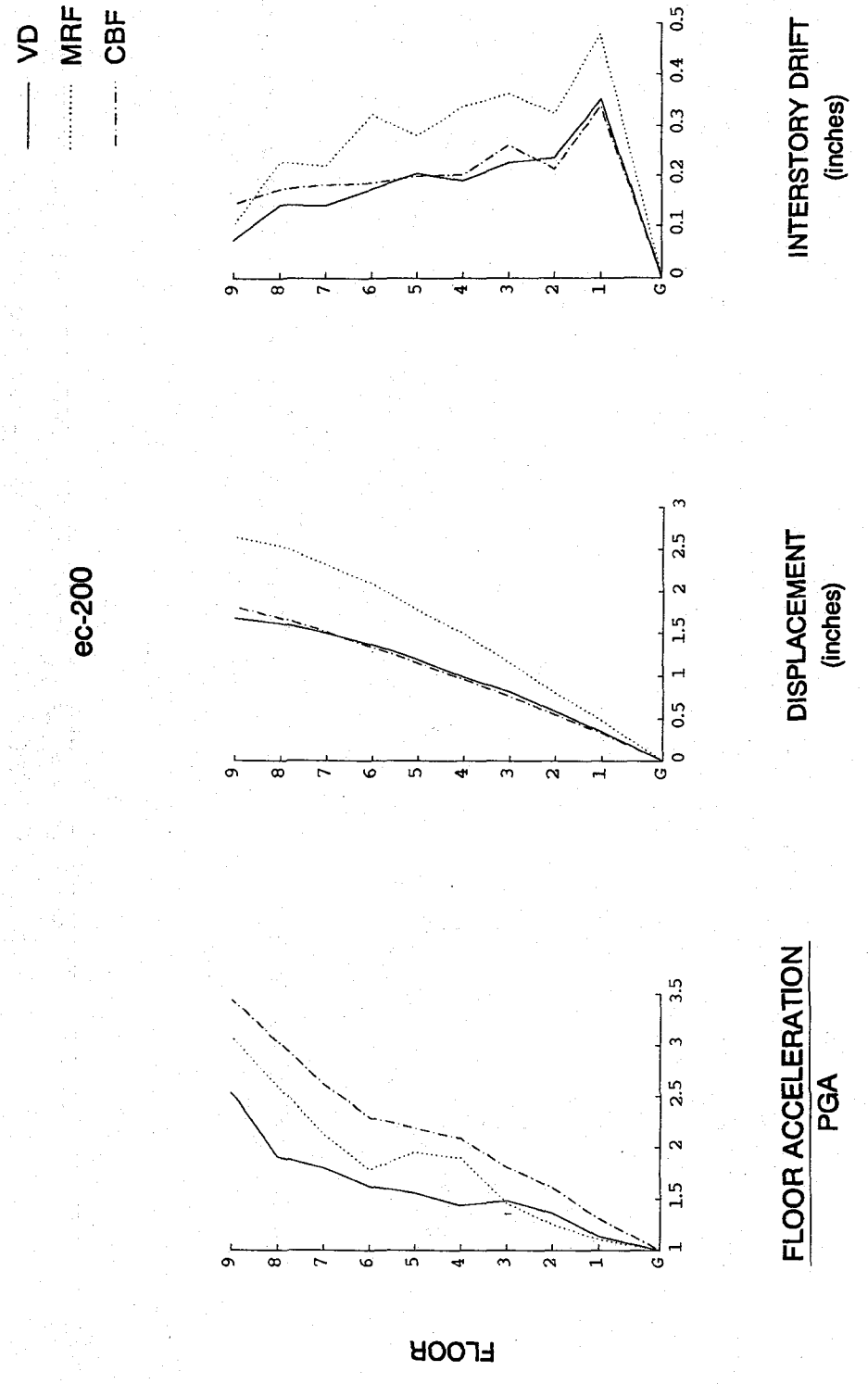
VD
MRF
CBF
ec-200
FLOOR
FLOOR ACCELERATION
PGA
DISPLACEMENT
(inches)
INTERSTORY DRIFT
(inches)

Fig. 4.50 cont.

ec-300

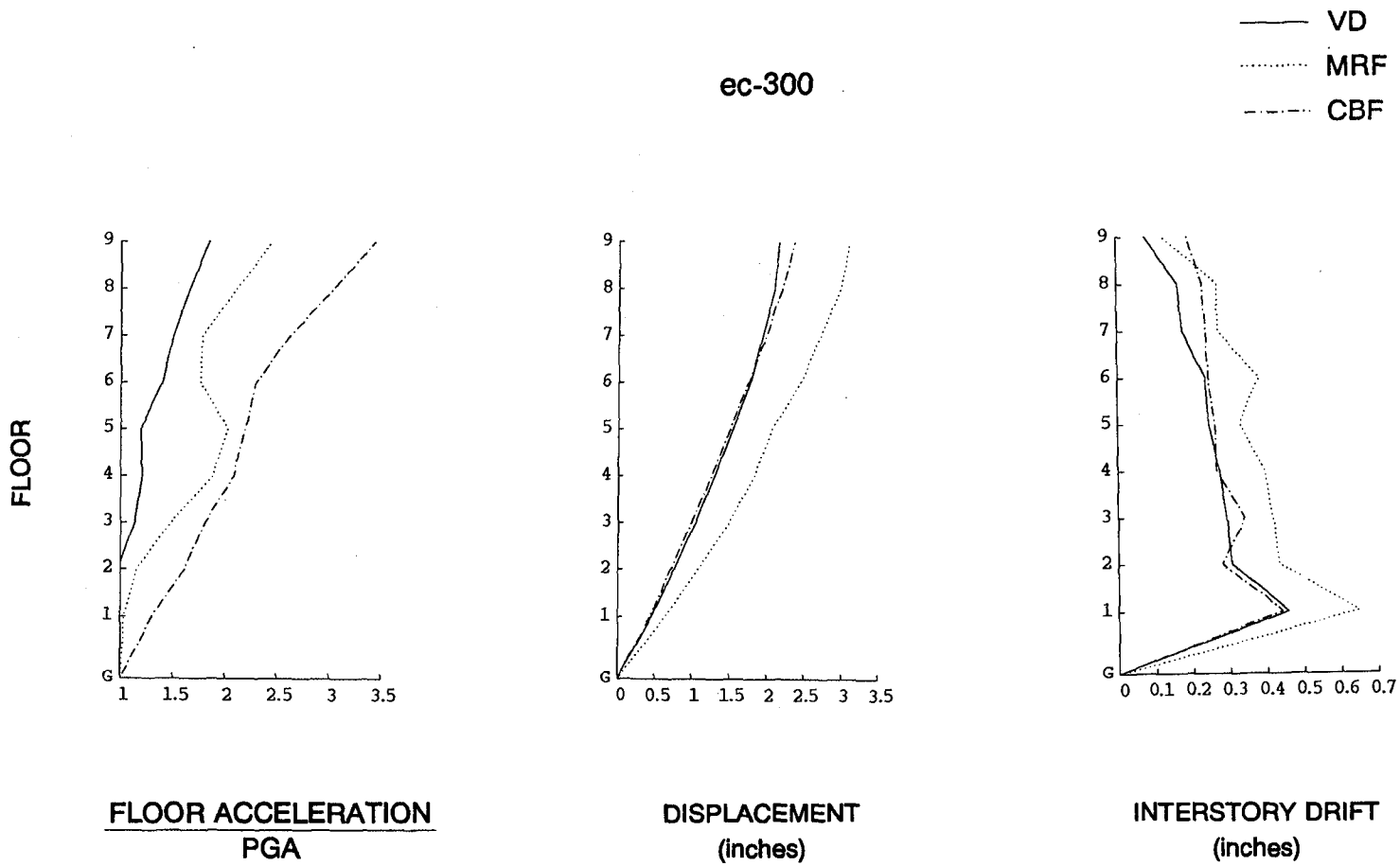

Fig. 4.50 cont.

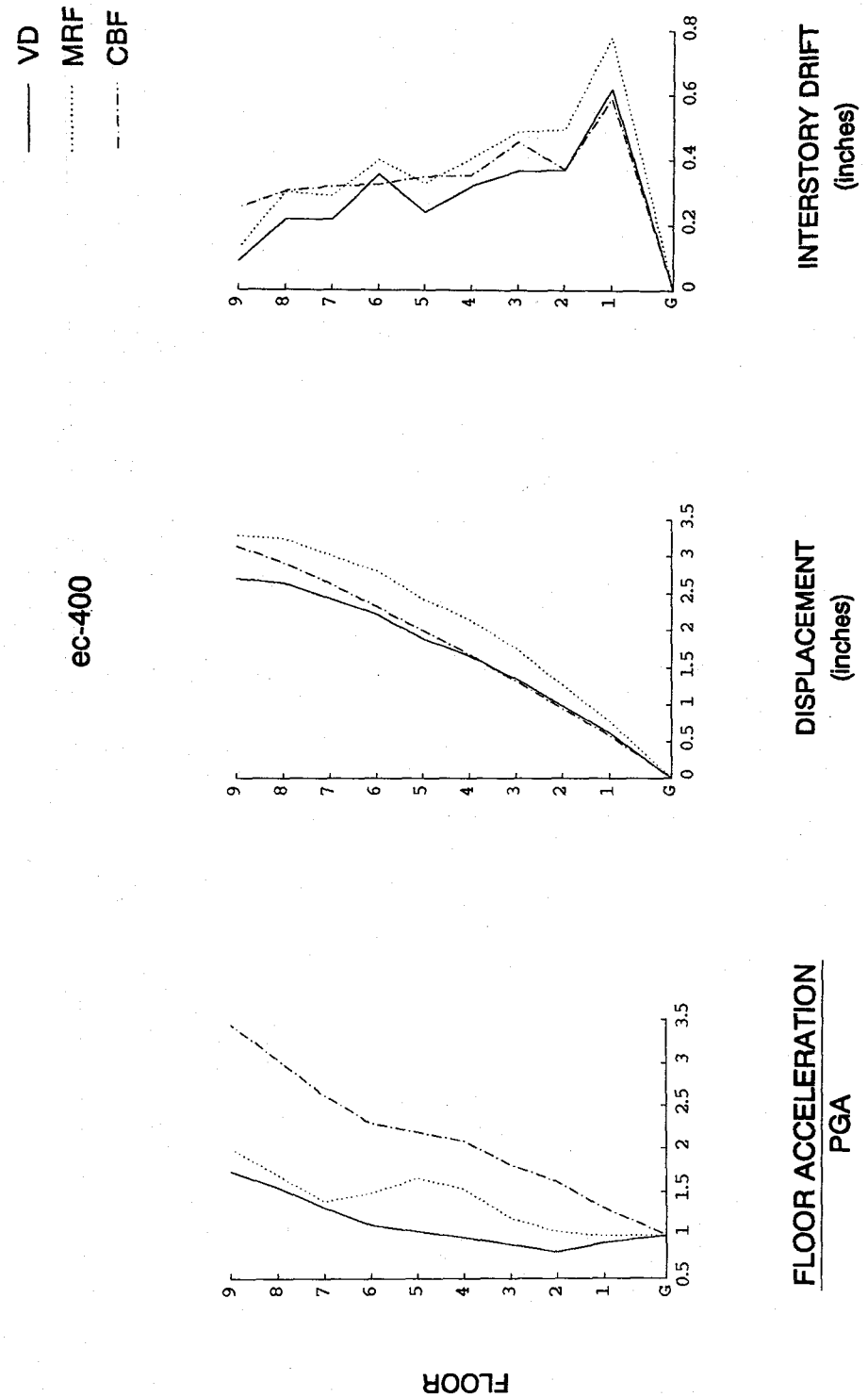
VD
MRF
CBF
ec-400
FLOOR
FLOOR ACCELERATION
PGA
DISPLACEMENT
(inches)
INTERSTORY DRIFT
(inches)

Fig. 4.50 cont.

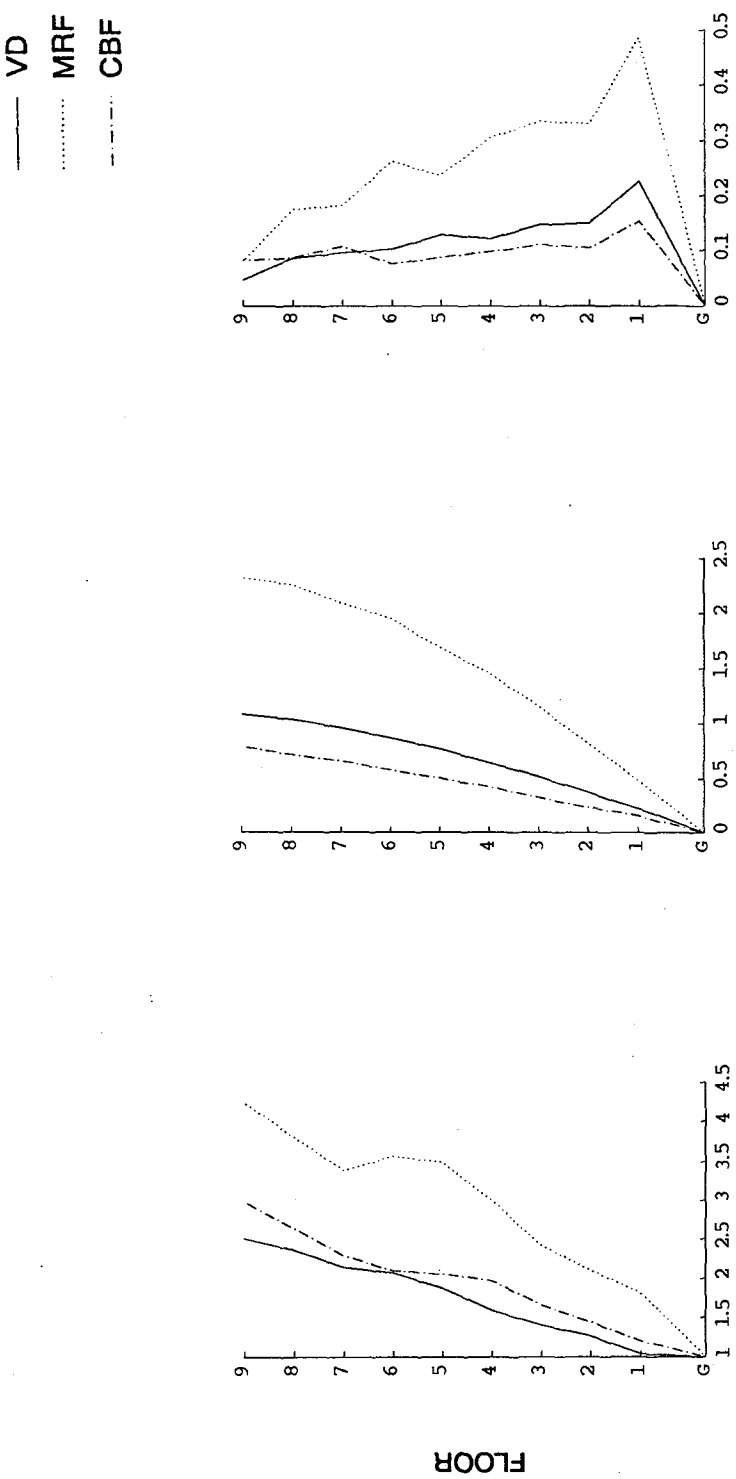

Fig. 4.51 VD, MRF, and CBF Acceleration, Displacement and Interstory Drift Response Profiles, miyagi-200 Test

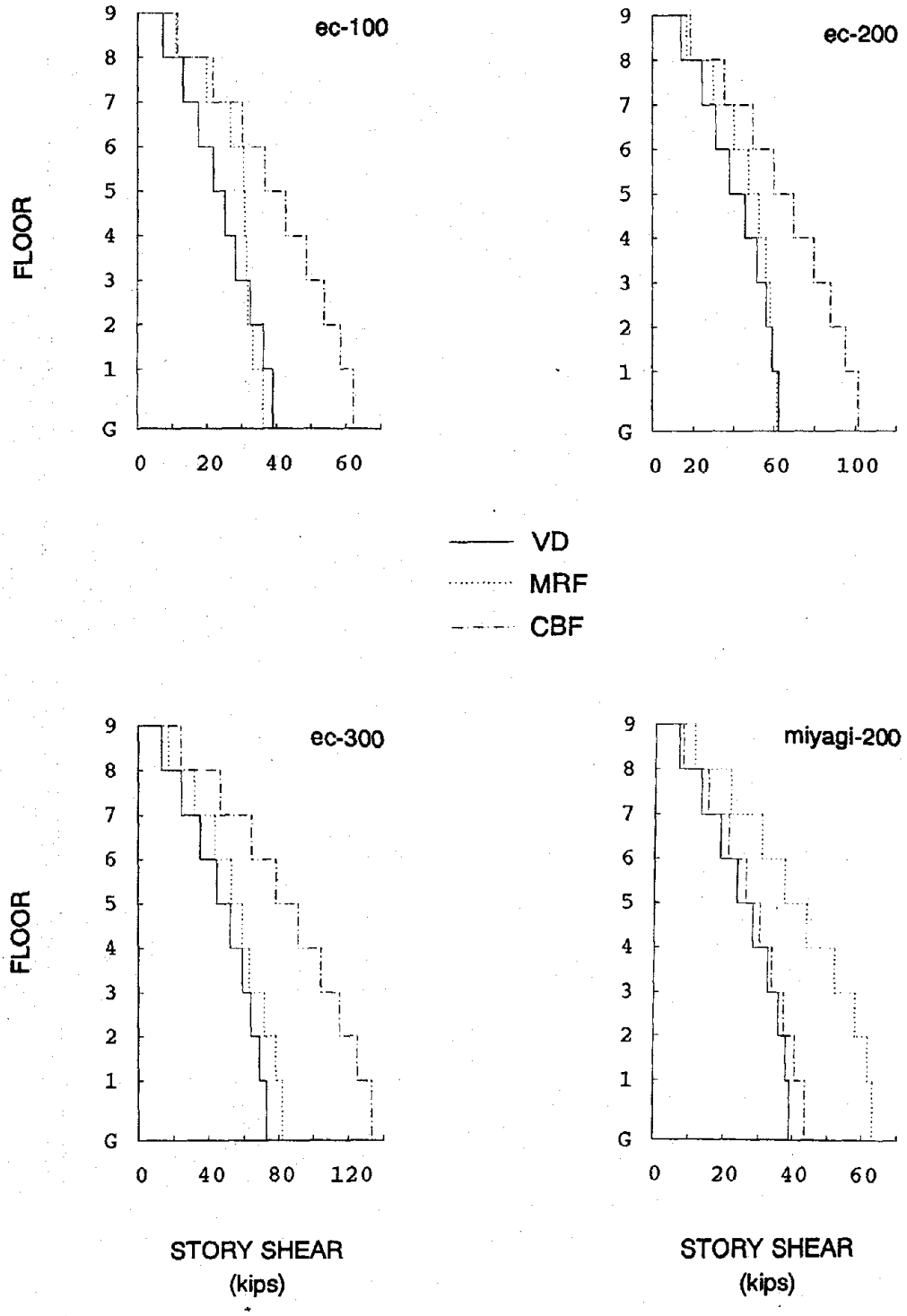

Fig. 4.52 VD, MRF, and CBF Peak Story Shear Profiles, ec-100, ec-200, ec-300, and miyagi-200 Tests

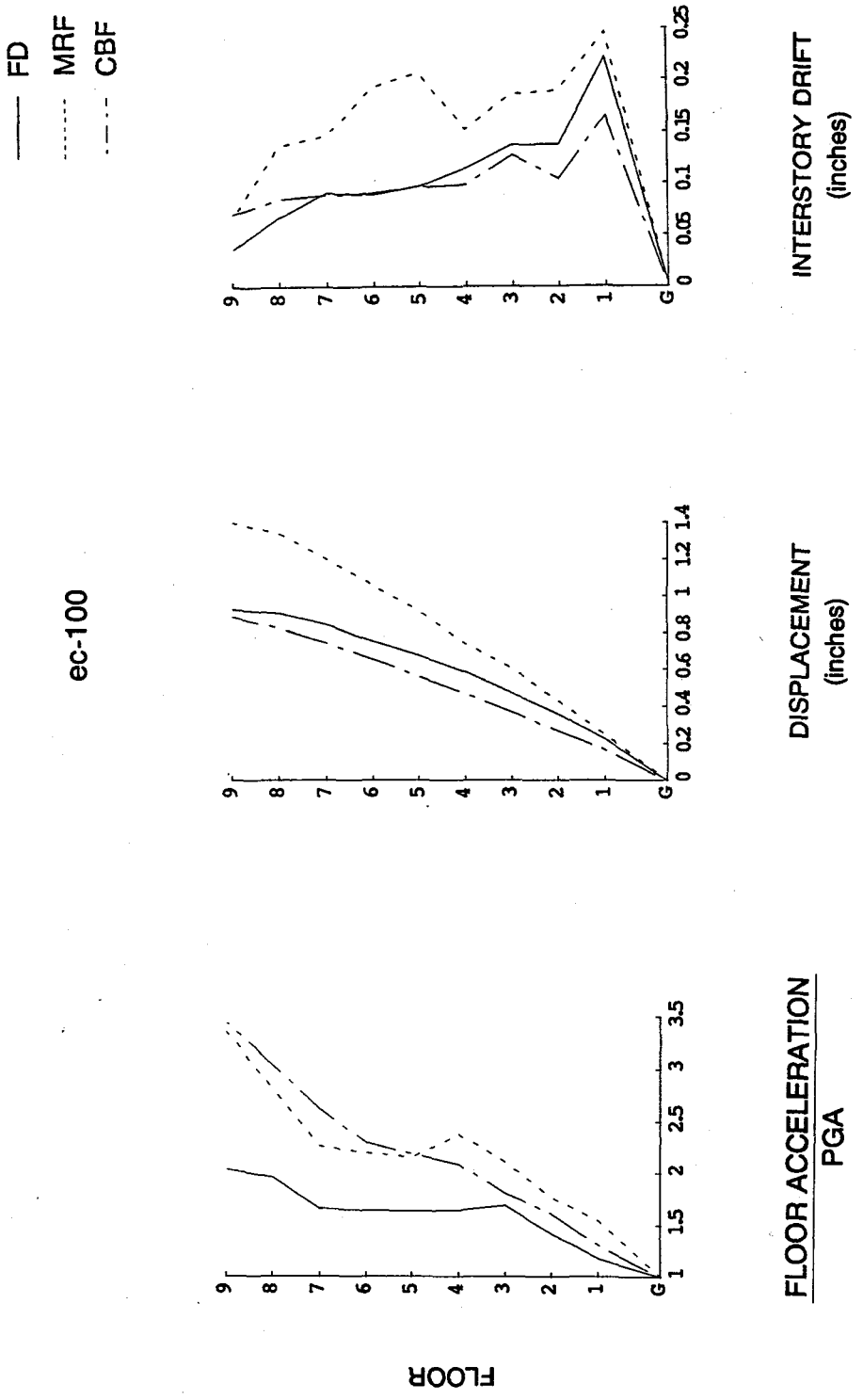

Fig. 4.53 FD, MRF, and CBF Acceleration, Displacement and Interstory Drift Response Profiles, ec-100, ec-200, ec-300, and ec-400 Tests

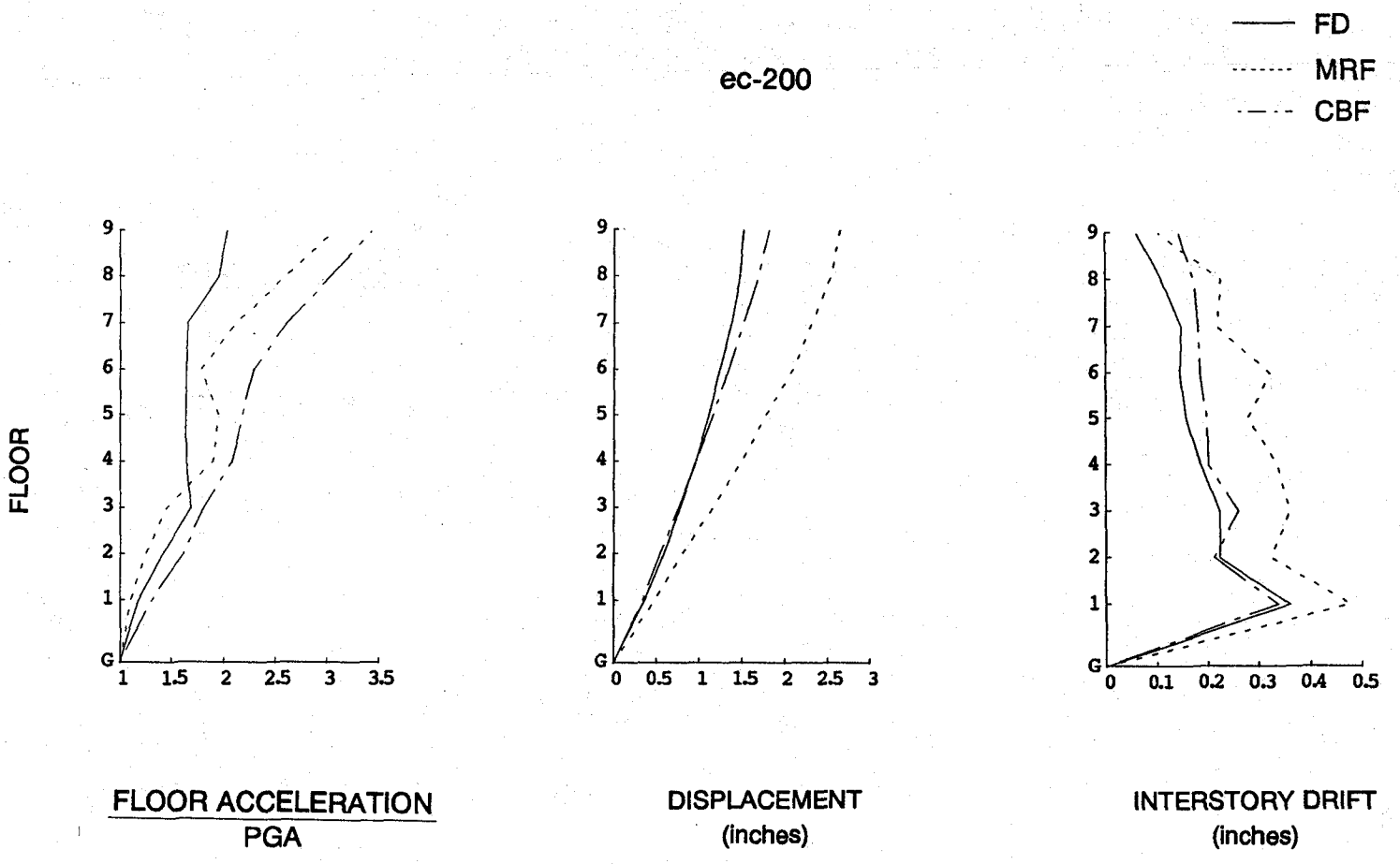
ec-200
FD
MRF
CBF
FLOOR
9
8
7
6
5
4
3
2
1
G
1
1.5
2
2.5
3
3.5
FLOOR ACCELERATION
PGA
0
0.5
1
1.5
2
2.5
3
DISPLACEMENT
(inches)
0
0.1
0.2
0.3
0.4
0.5
INTERSTORY DRIFT
(inches)

Fig. 4.53 cont.

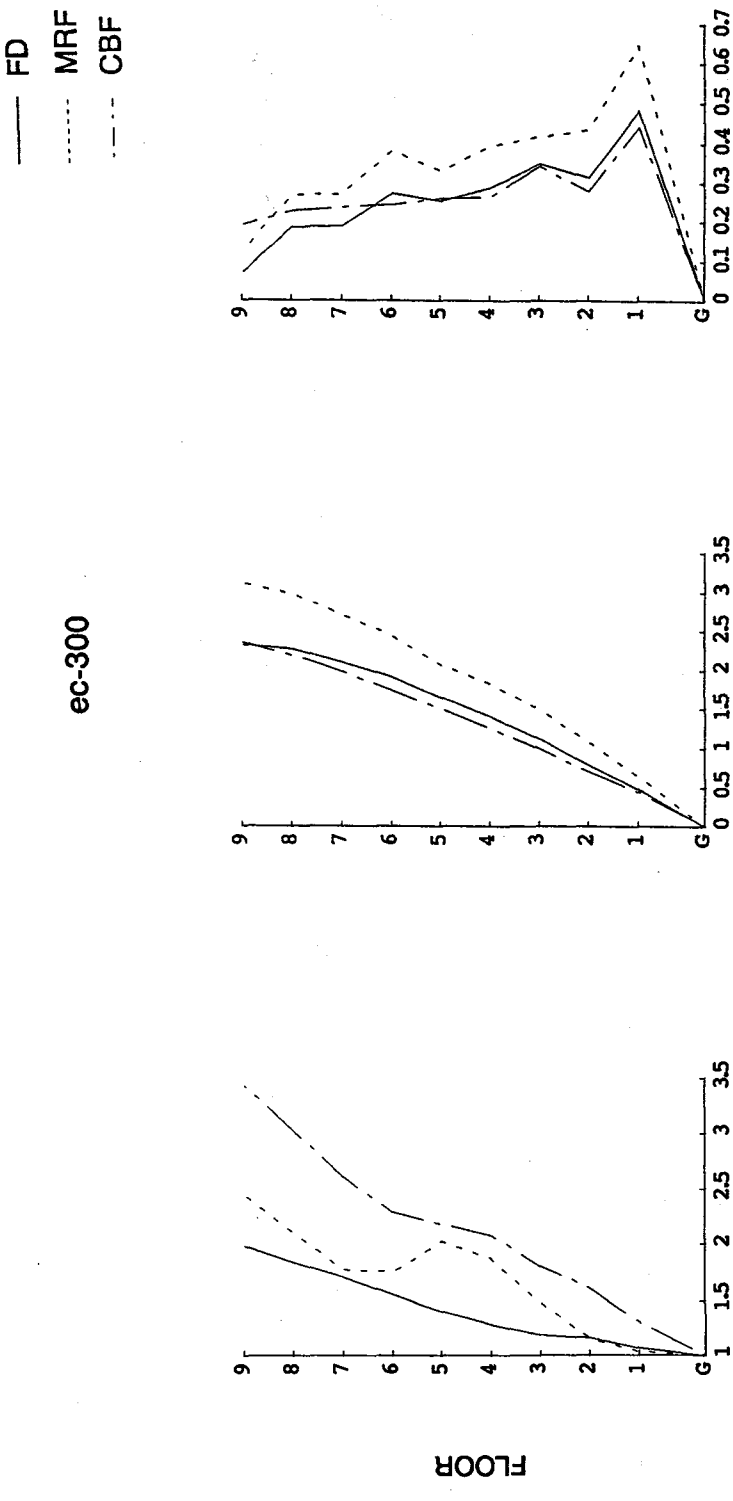
FD
MRF
CBF
ec-300
FLOOR
FLOOR ACCELERATION
PGA
DISPLACEMENT
(inches)
INTERSTORY DRIFT
(inches)

Fig. 4.53 cont.

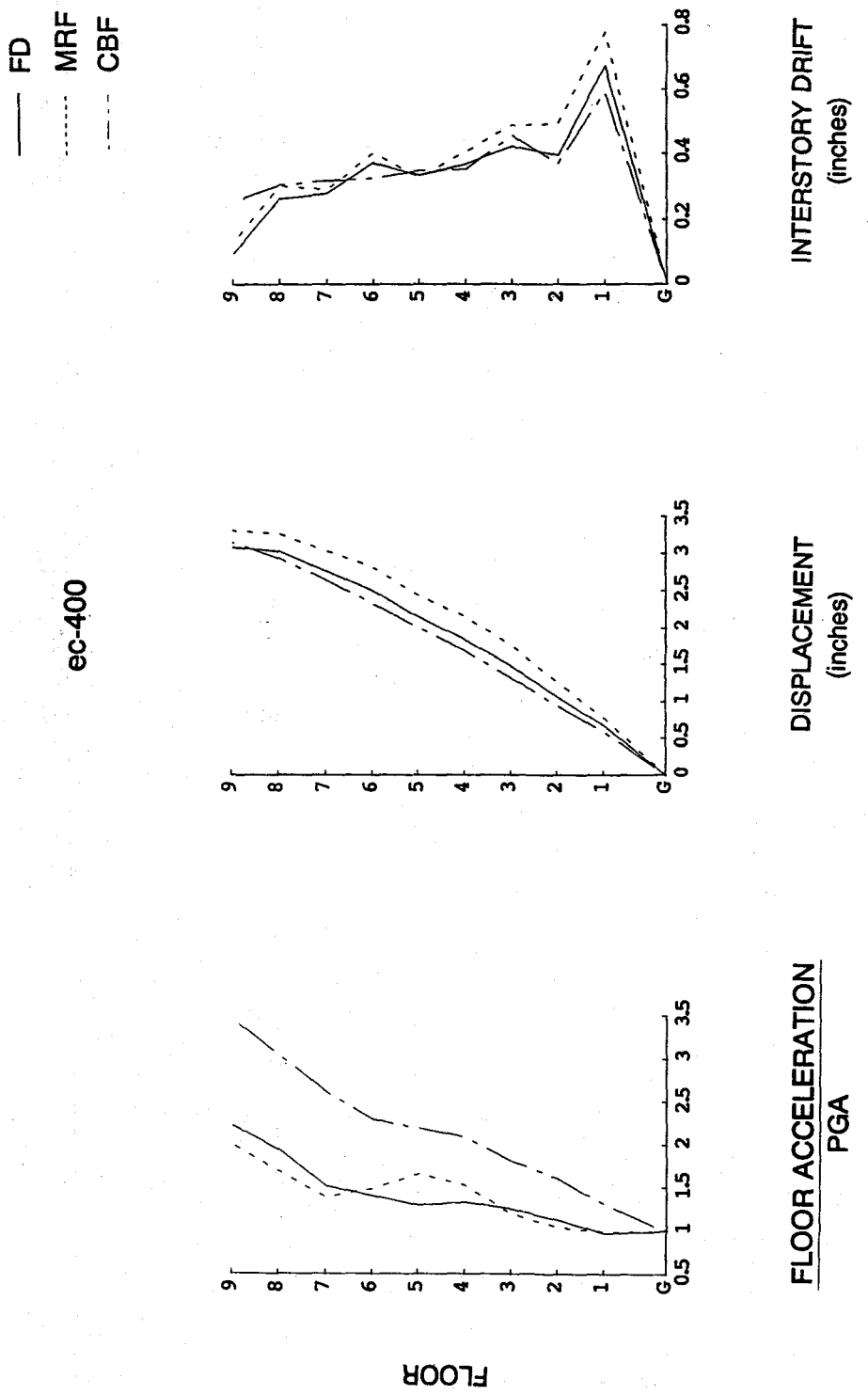
FD
MRF
CBF
ec-400
FLOOR
FLOOR ACCELERATION
PGA
DISPLACEMENT
(inches)
INTERSTORY DRIFT
(inches)

Fig. 4.53 cont.

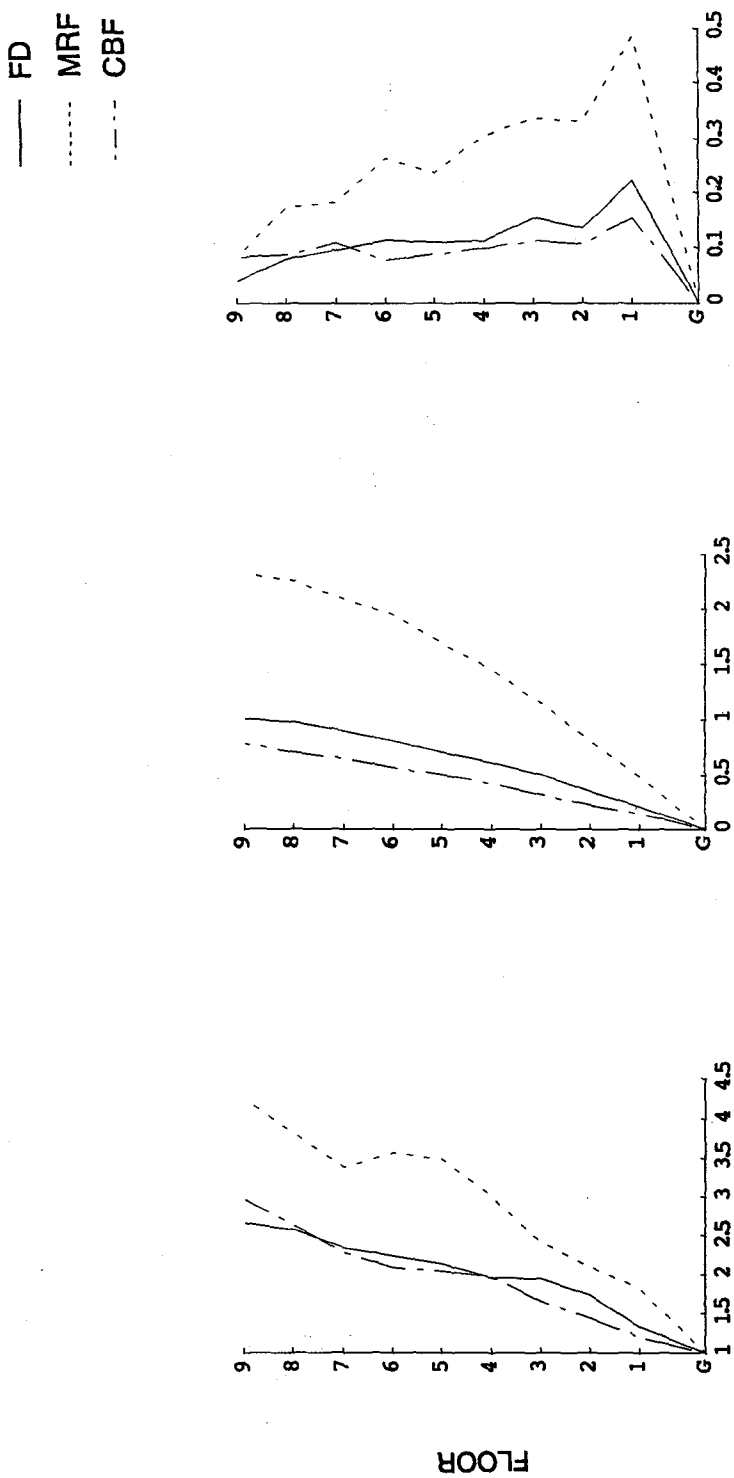

Fig. 4.54 FD, MRF, and CBF Acceleration, Displacement and Interstory Drift Response Profiles, miyagi-200 Test

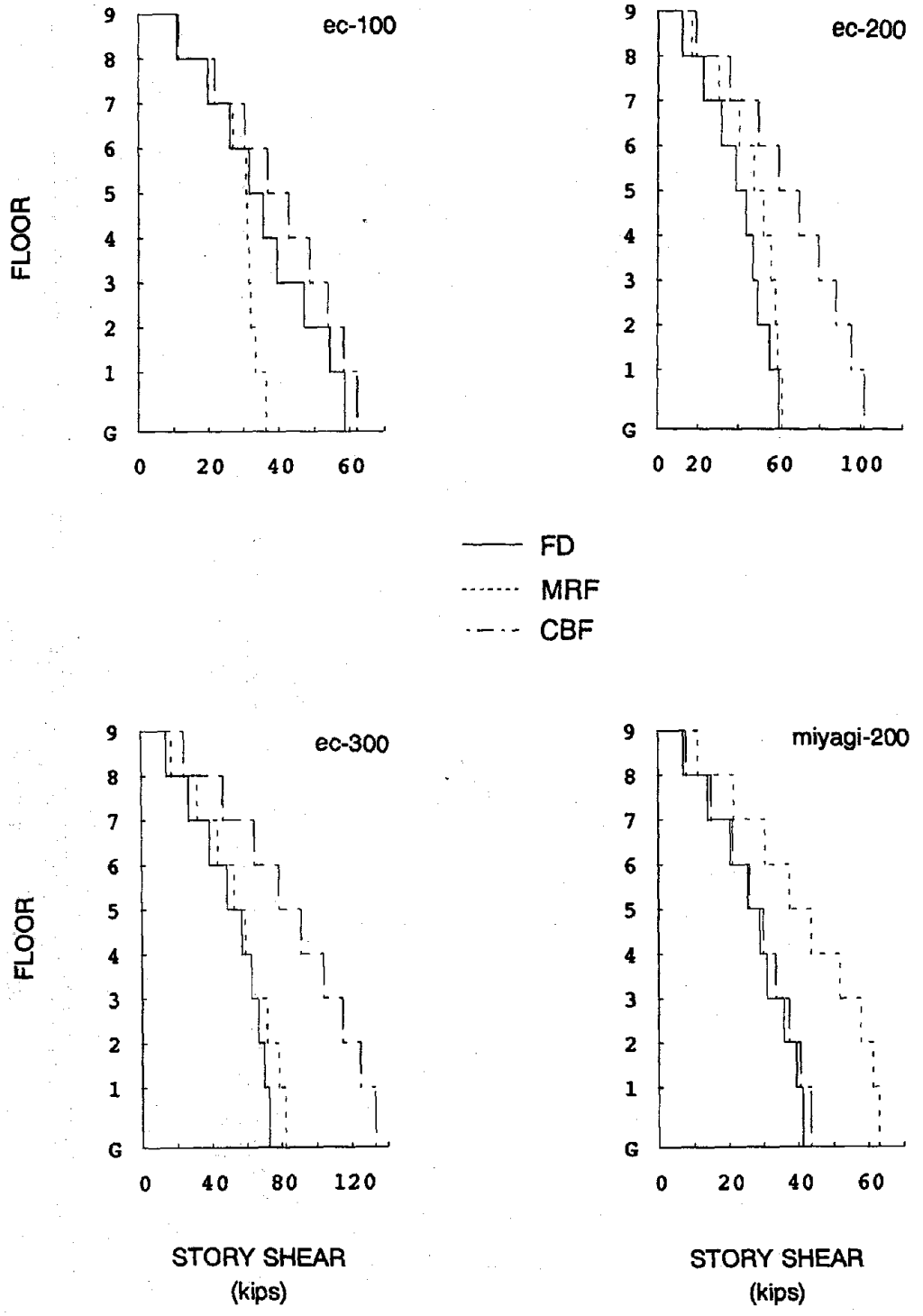

Fig. 4.55 FD, MRF, and CBF Peak Story Shear Profiles, ec-100, ec-200, ec-300, and miyagi-200 Tests

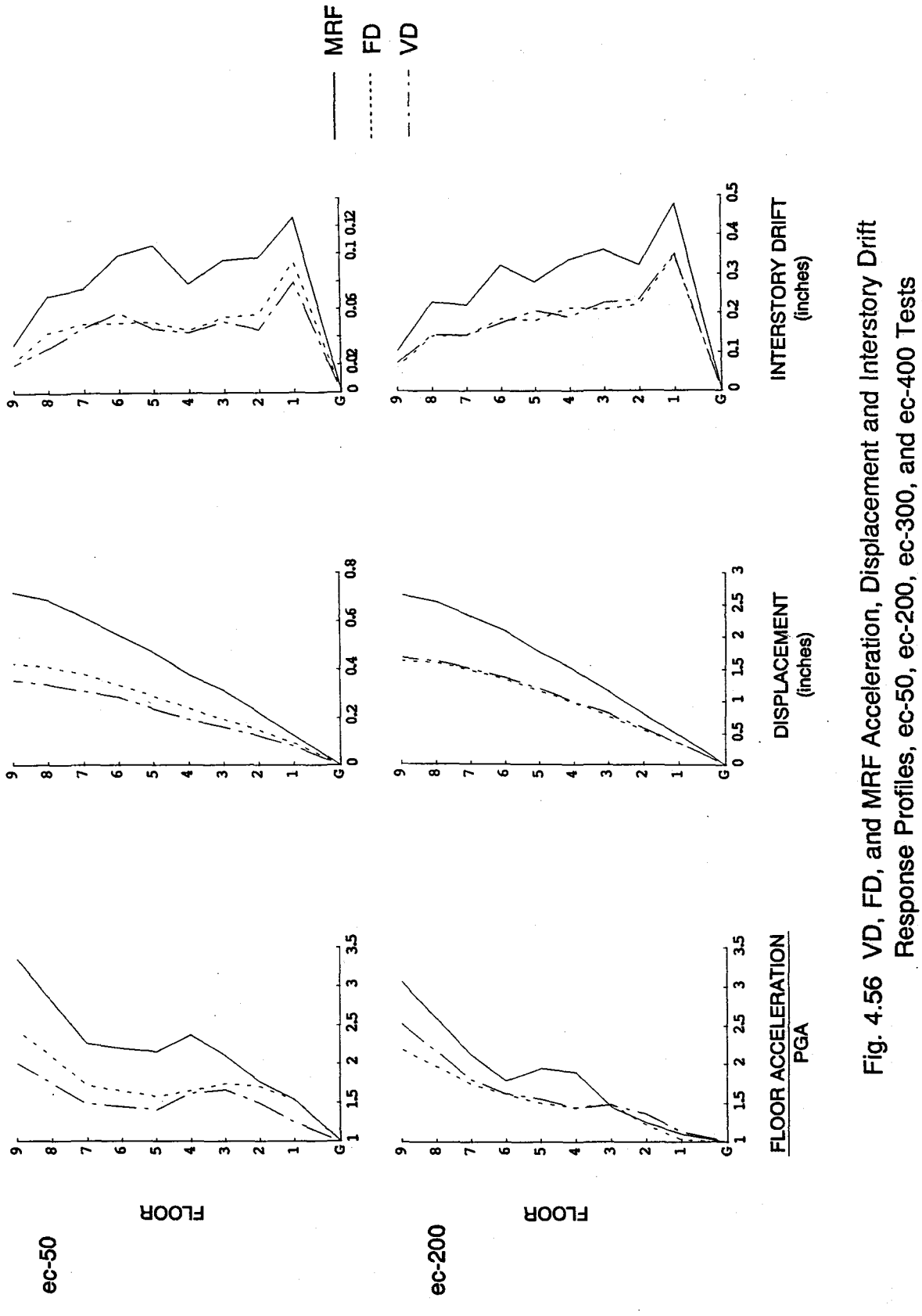

Fig. 4.56 VD, FD, and MRF Acceleration, Displacement and Interstory Drift Response Profiles, ec-50, ec-200, ec-300, and ec-400 Tests

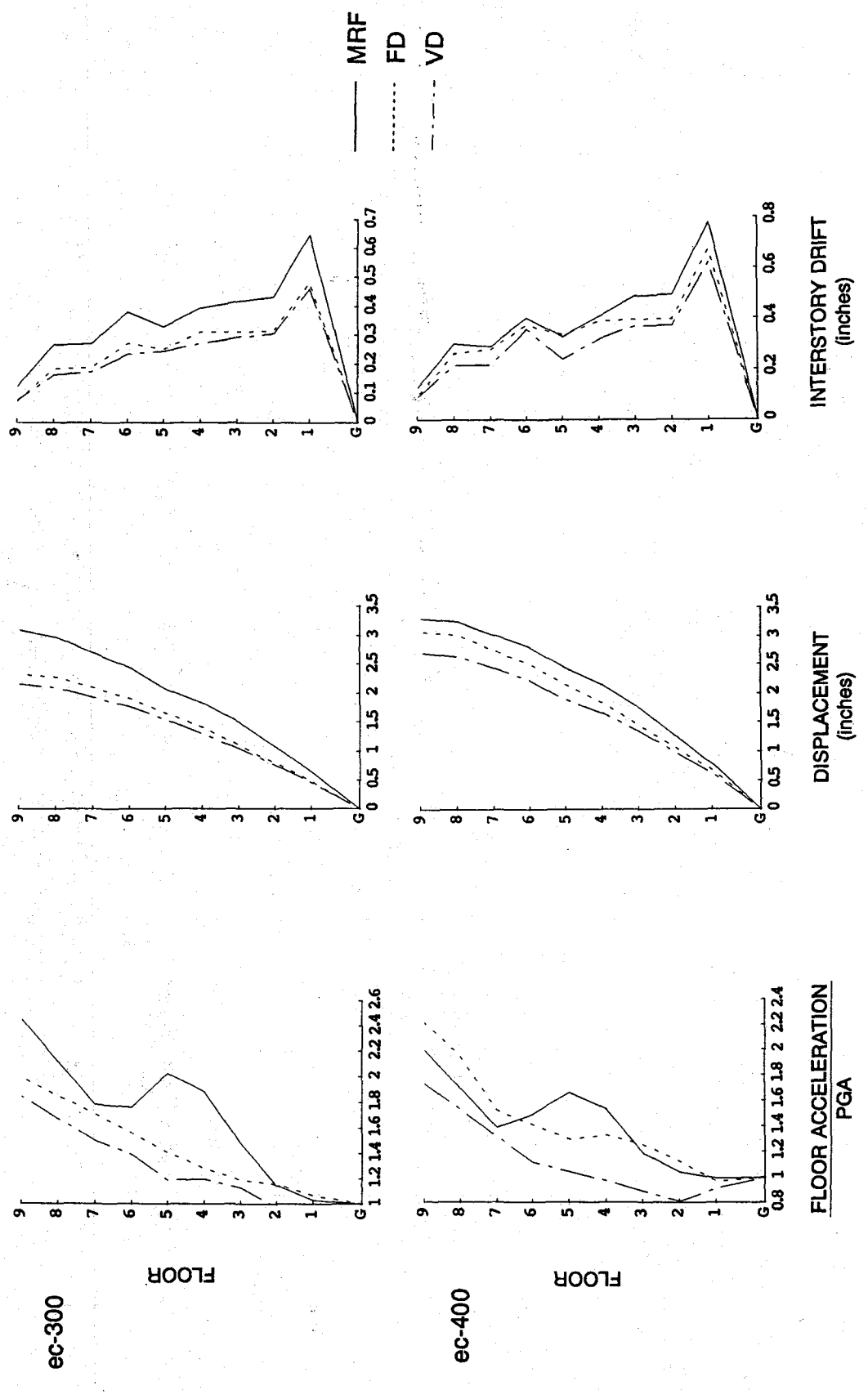
MRF
FD
VD
ec-300
ec-400
FLOOR
FLOOR
FLOOR ACCELERATION
PGA
DISPLACEMENT
(inches)
INTERSTORY DRIFT
(inches)

Fig. 4.56 cont.

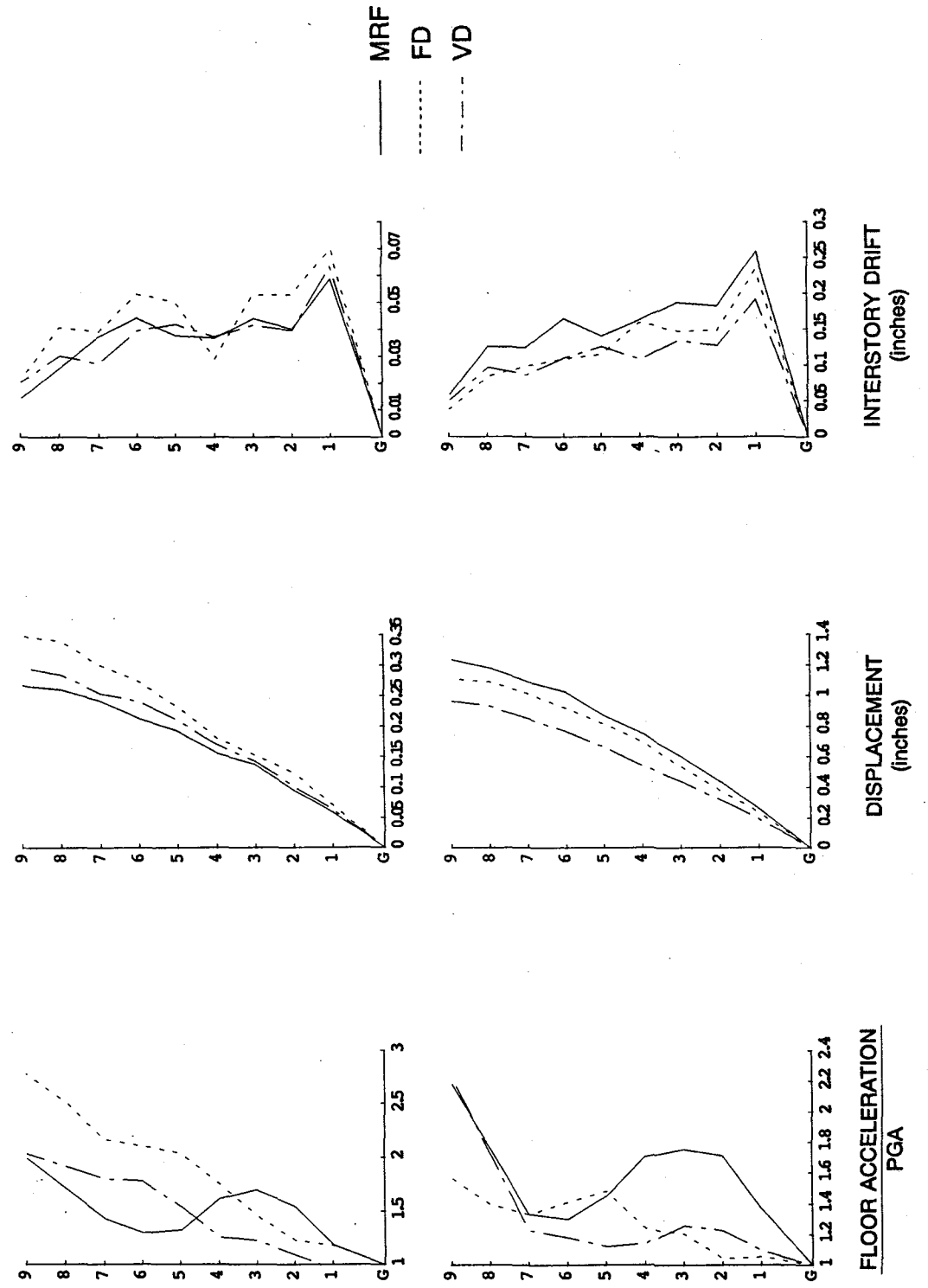

Fig. 4.57 VD, FD, and MRF Acceleration, Displacement and Interstory Drift Response Profiles, taft-50 and taft-200 Tests

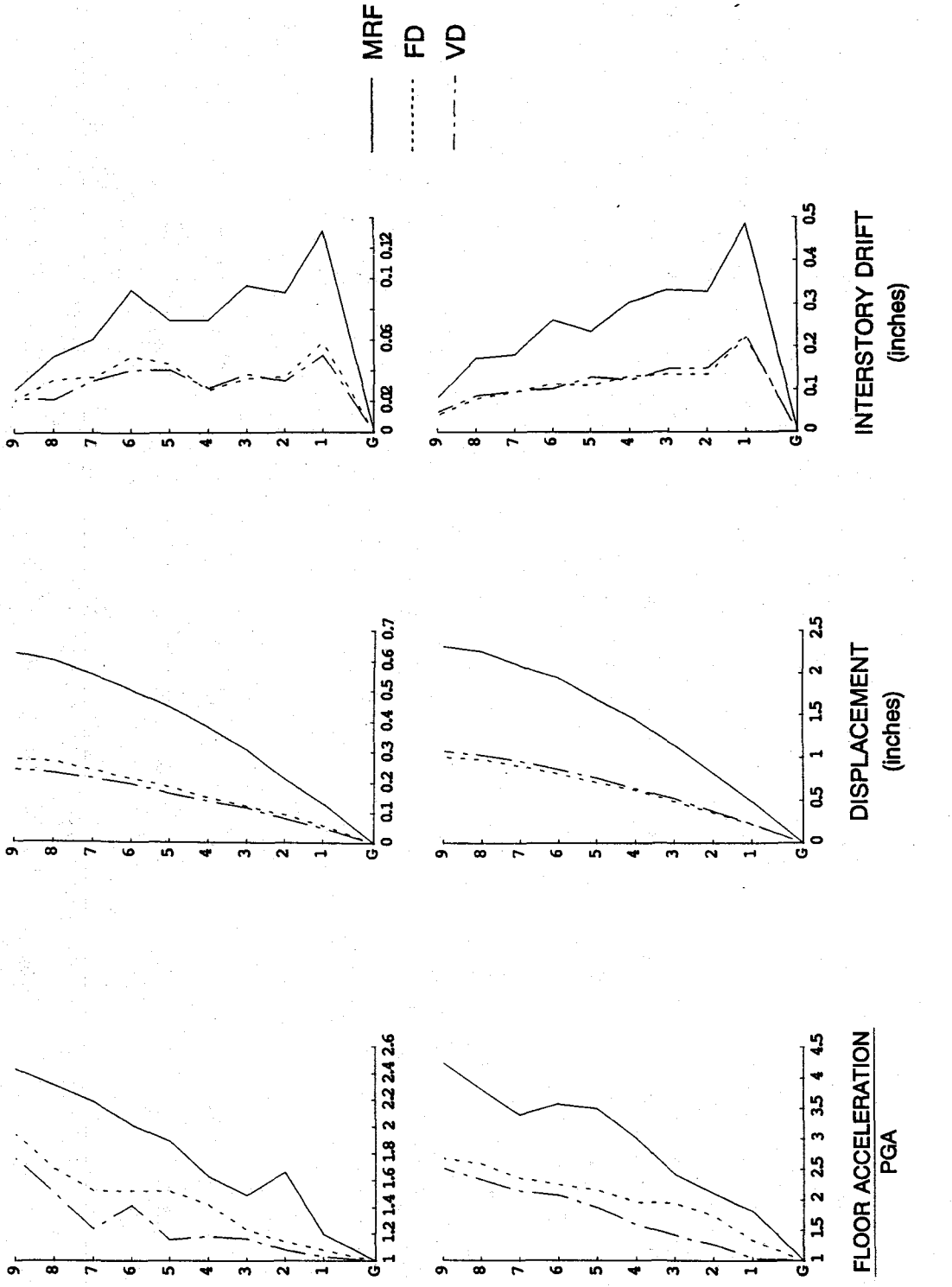

Fig. 4.58 VD, FD, and MRF Acceleration, Displacement and Interstory Drift Response Profiles, miyagi-50 and miyagi-200 Tests

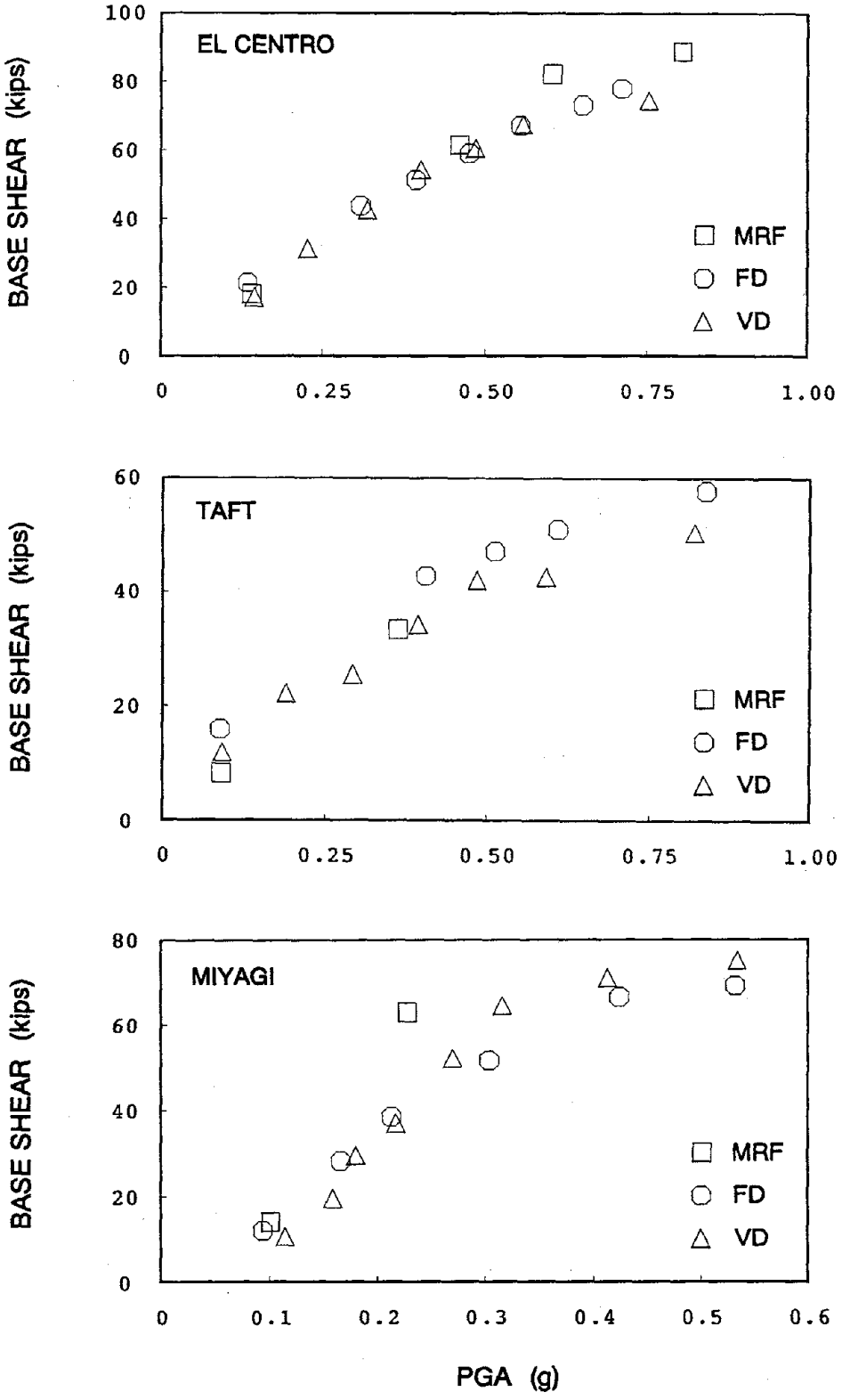

Fig. 4.59 VD, FD, and MRF Peak Base Shear vs. PGA for El Centro, Taft, and Miyagi Tests

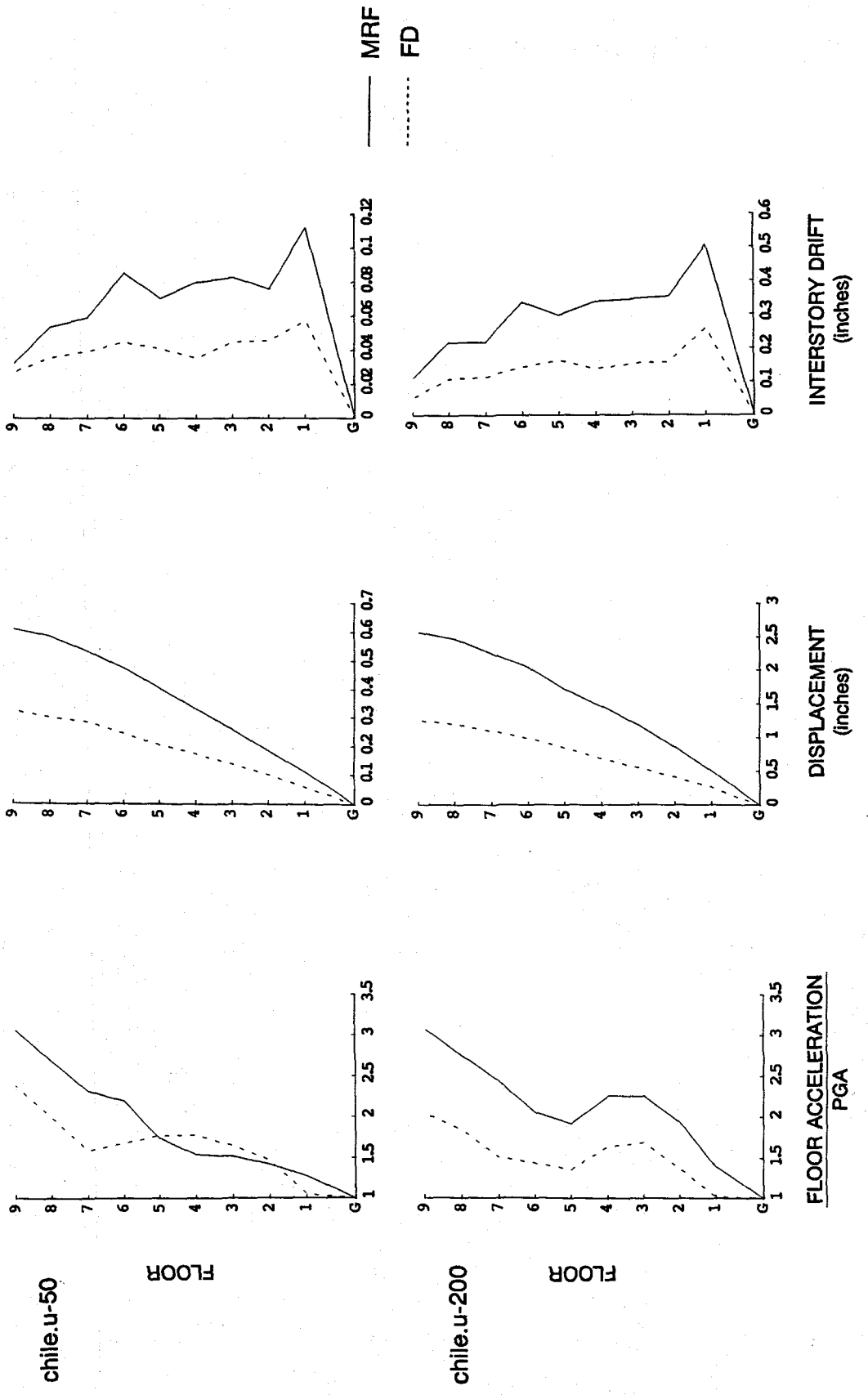

Fig. 4.60 FD and MRF Acceleration, Displacement and Interstory Drift Response Profiles, chile.u-50 and chile.u-200 Tests

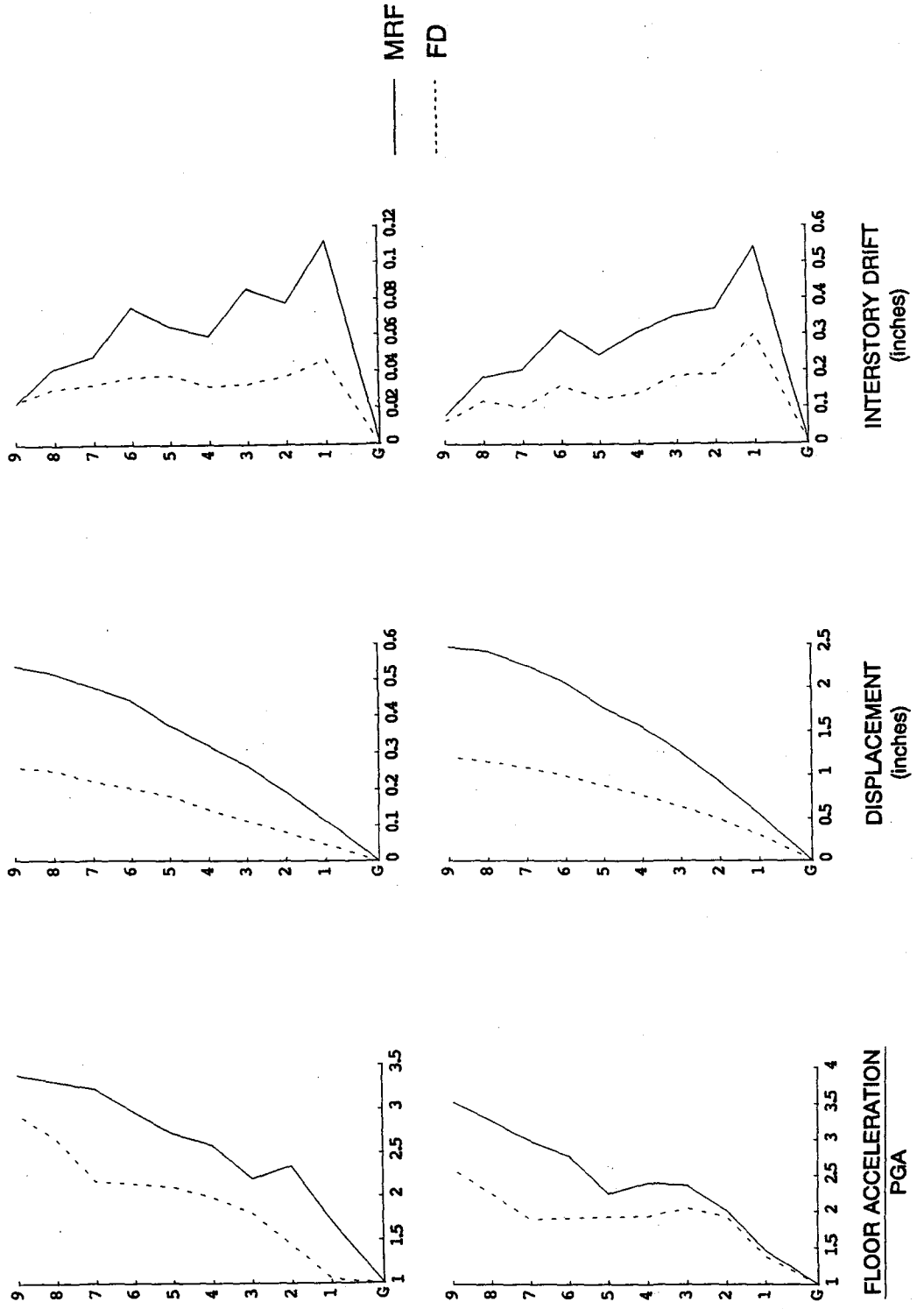

Fig. 4.61 FD and MRF Acceleration, Displacement and Interstory Drift Response Profiles, unio-50 and unio-250 Tests

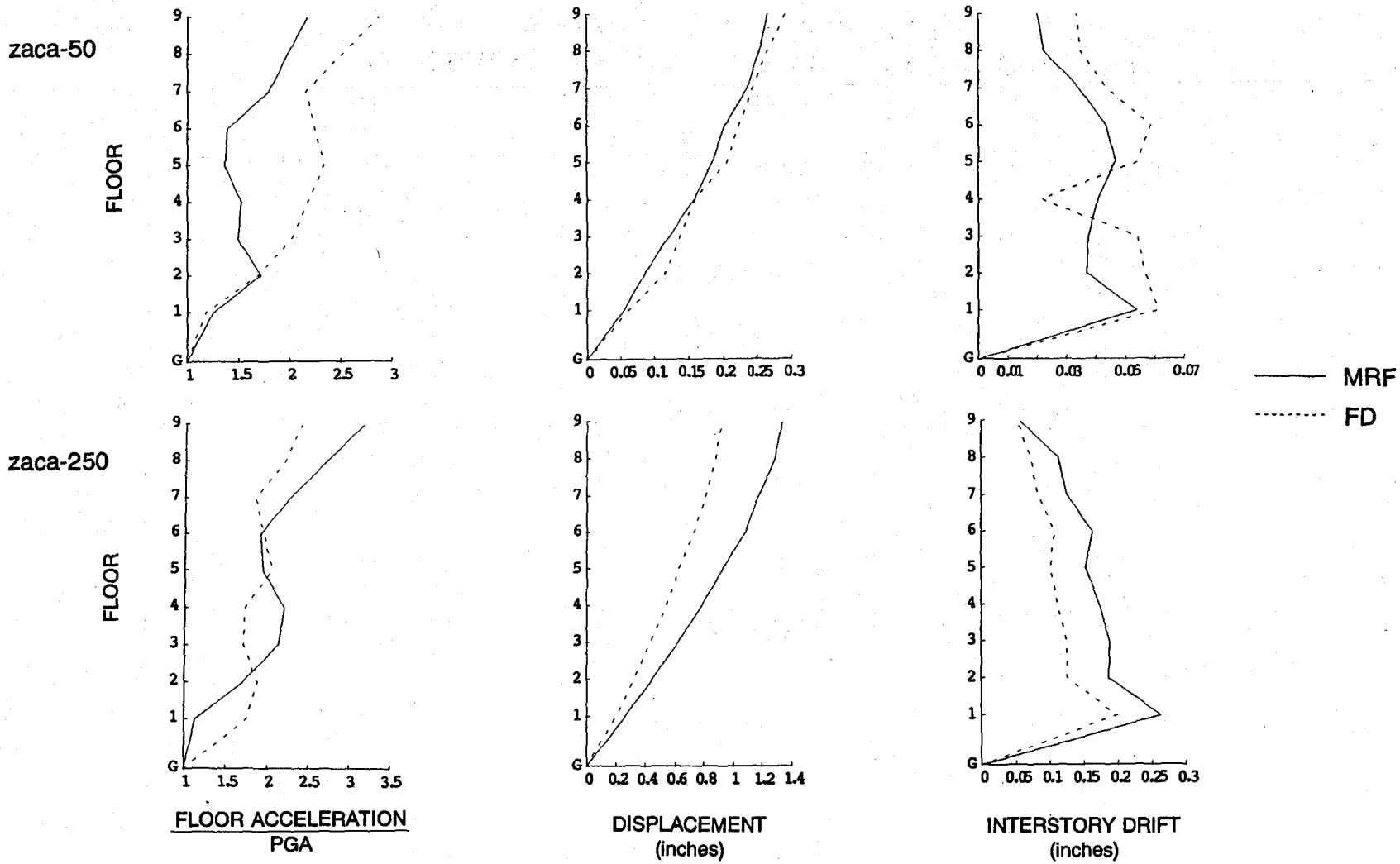

Fig. 4.62 FD and MRF Acceleration, Displacement and Interstory Drift Response Profiles, zaca-50 and zaca-250 Tests

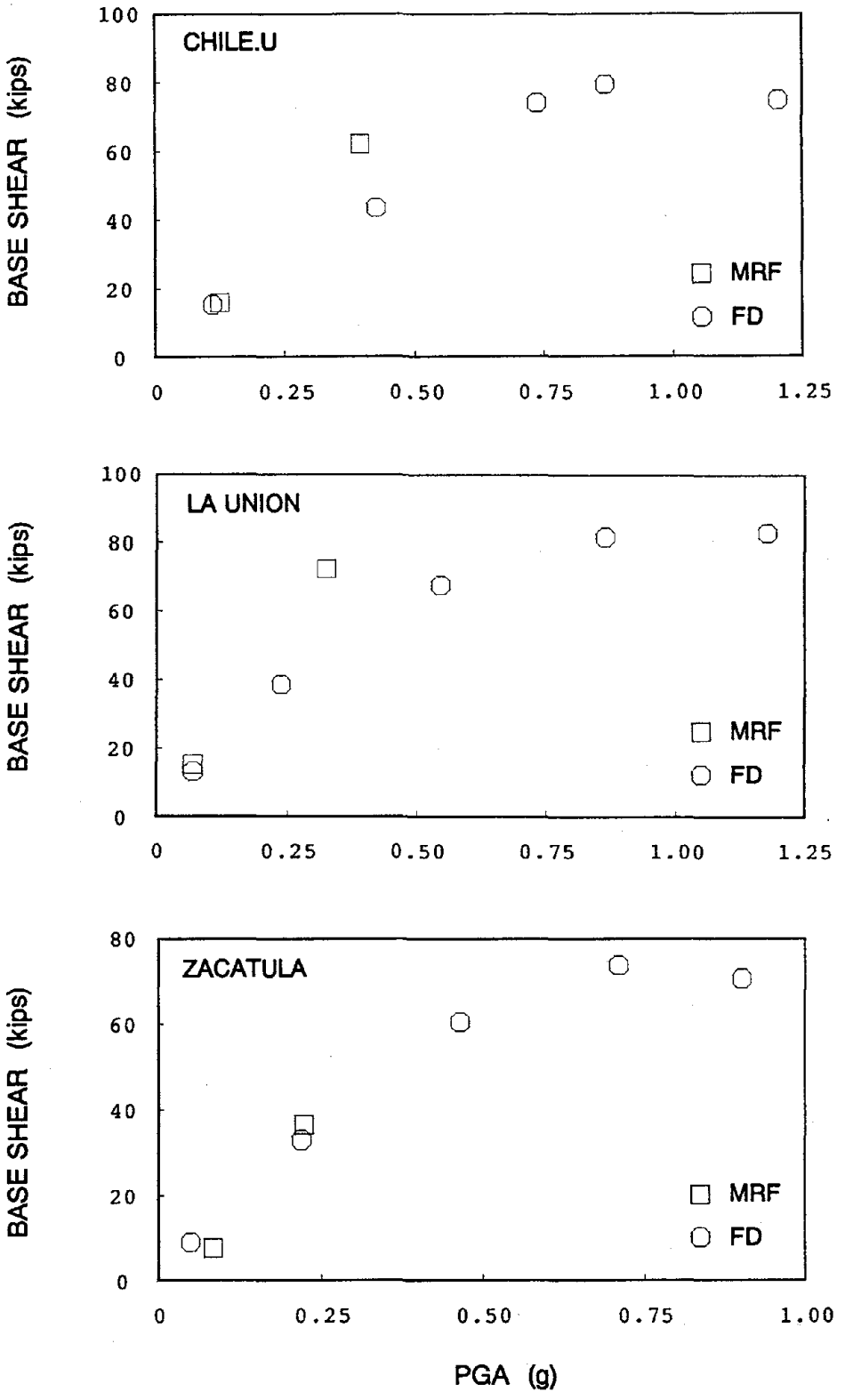

Fig. 4.63 FD and MRF Peak Base Shear vs. PGA for Chile.u, La Union, and Zacatula Tests

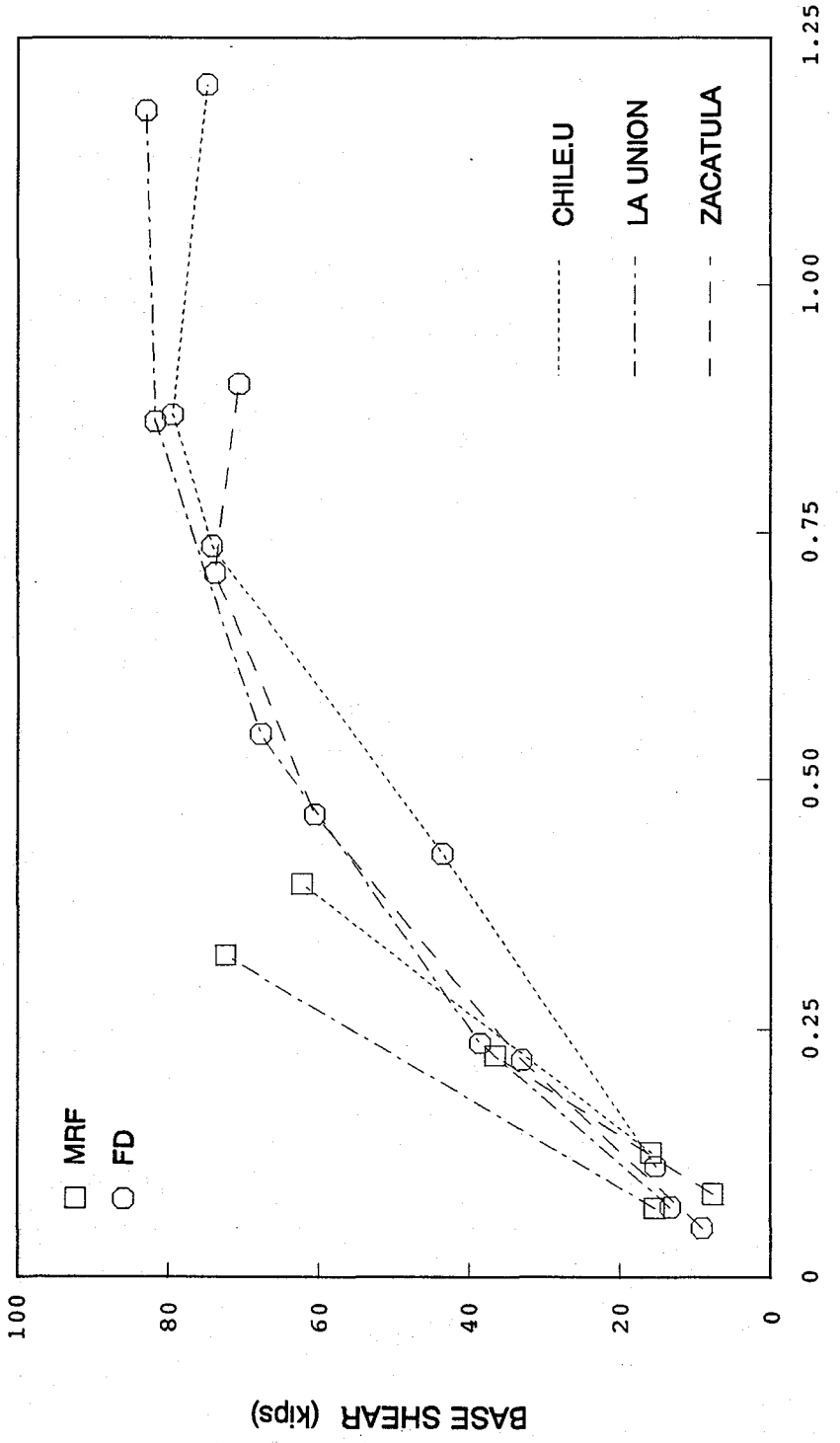

Fig. 4.64 Summary of FD and MRF Peak Base Shear vs. PGA for Chile.u, La Union, and Zacatula Tests

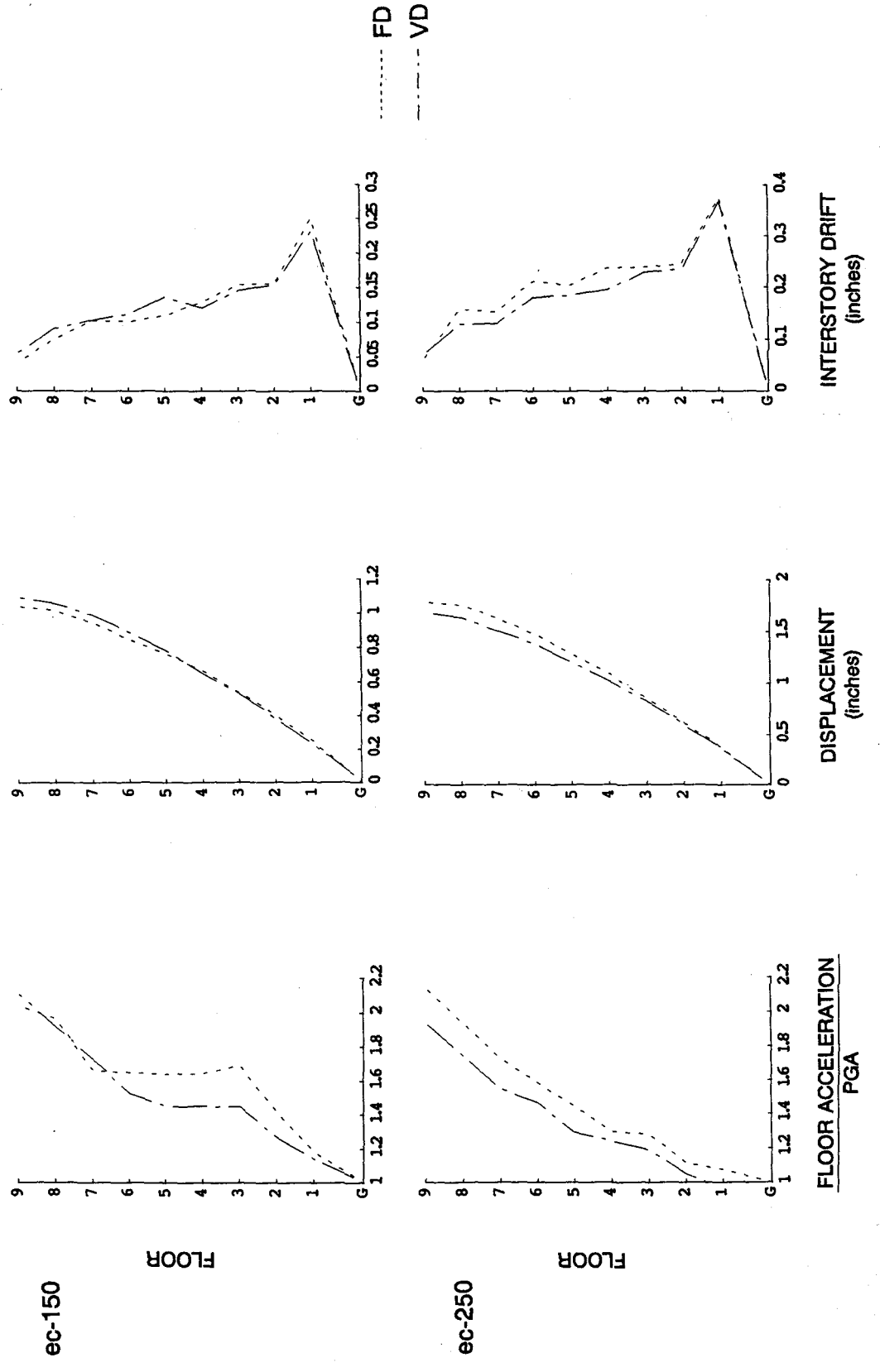

Fig. 4.65 VD and FD Acceleration, Displacement and Interstory Drift Response Profiles, ec-150 and ec-250 Tests

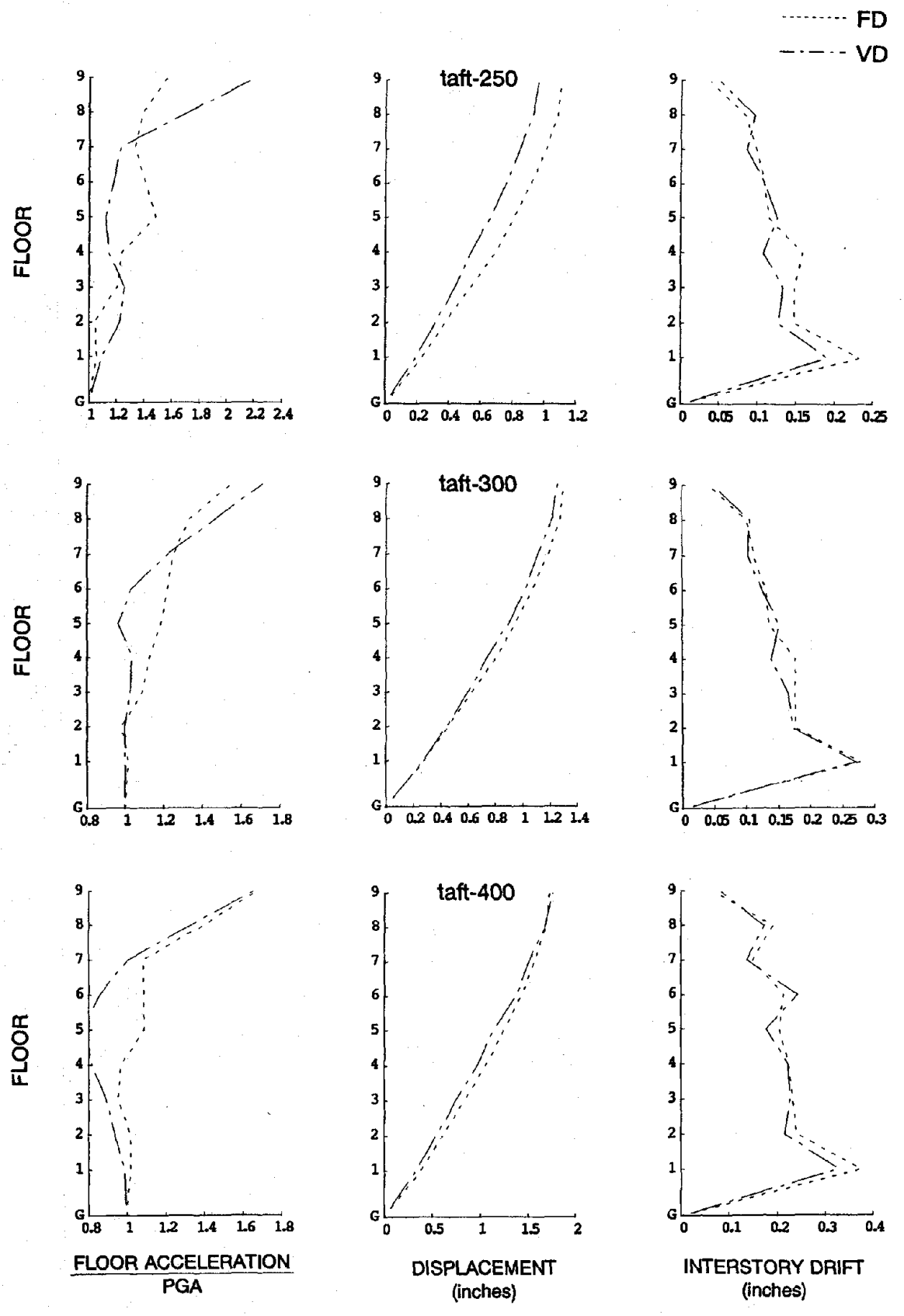

Fig. 4.66 VD and FD Acceleration, Displacement and Interstory Drift Response Profiles, taft-250, taft-300, and taft-400 Tests

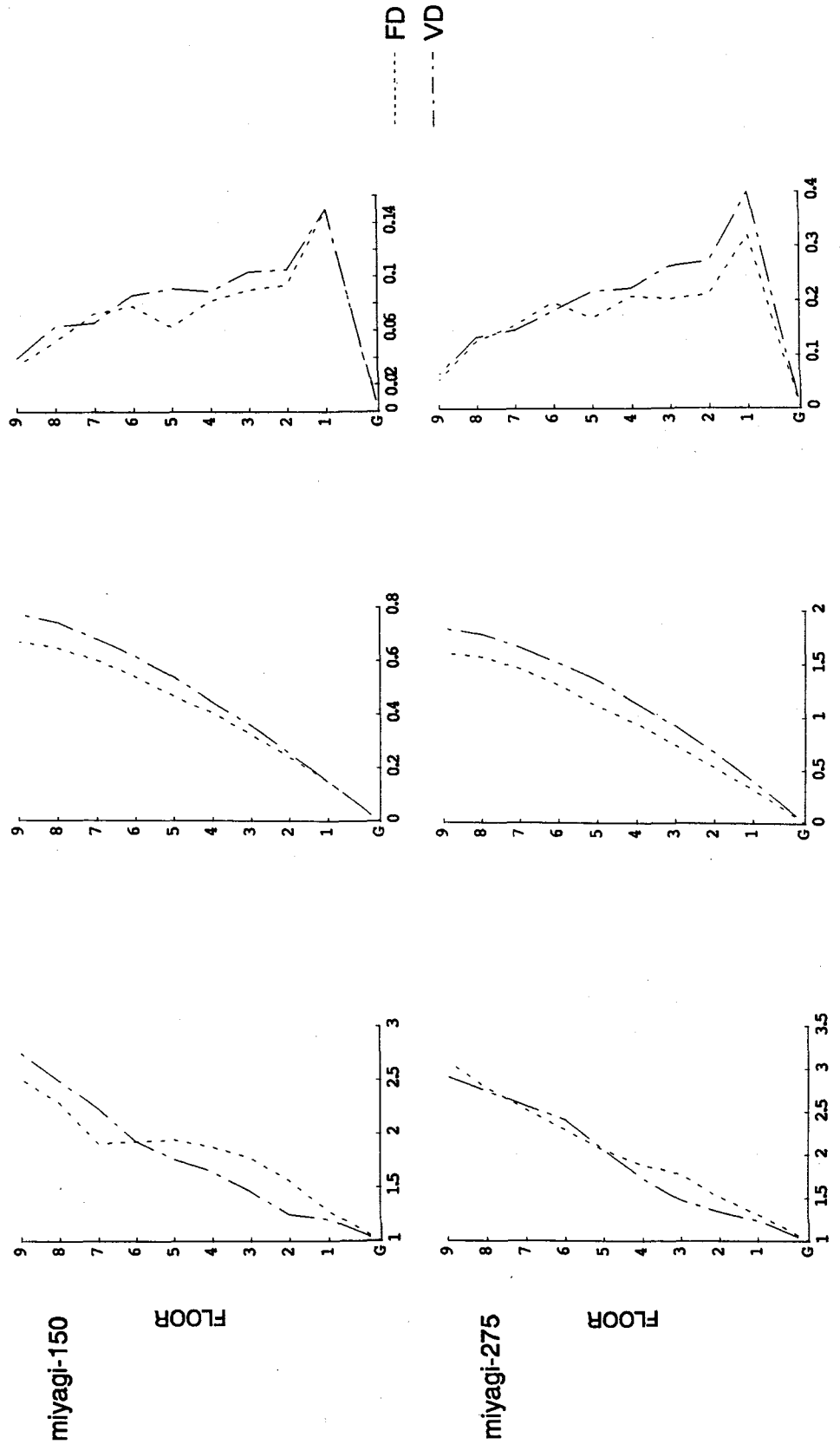

Fig. 4.67 VD and FD Acceleration, Displacement and Interstory Drift Response Profiles, miyagi-150, miyagi-275, miyagi-350, and miyagi-400 Tests

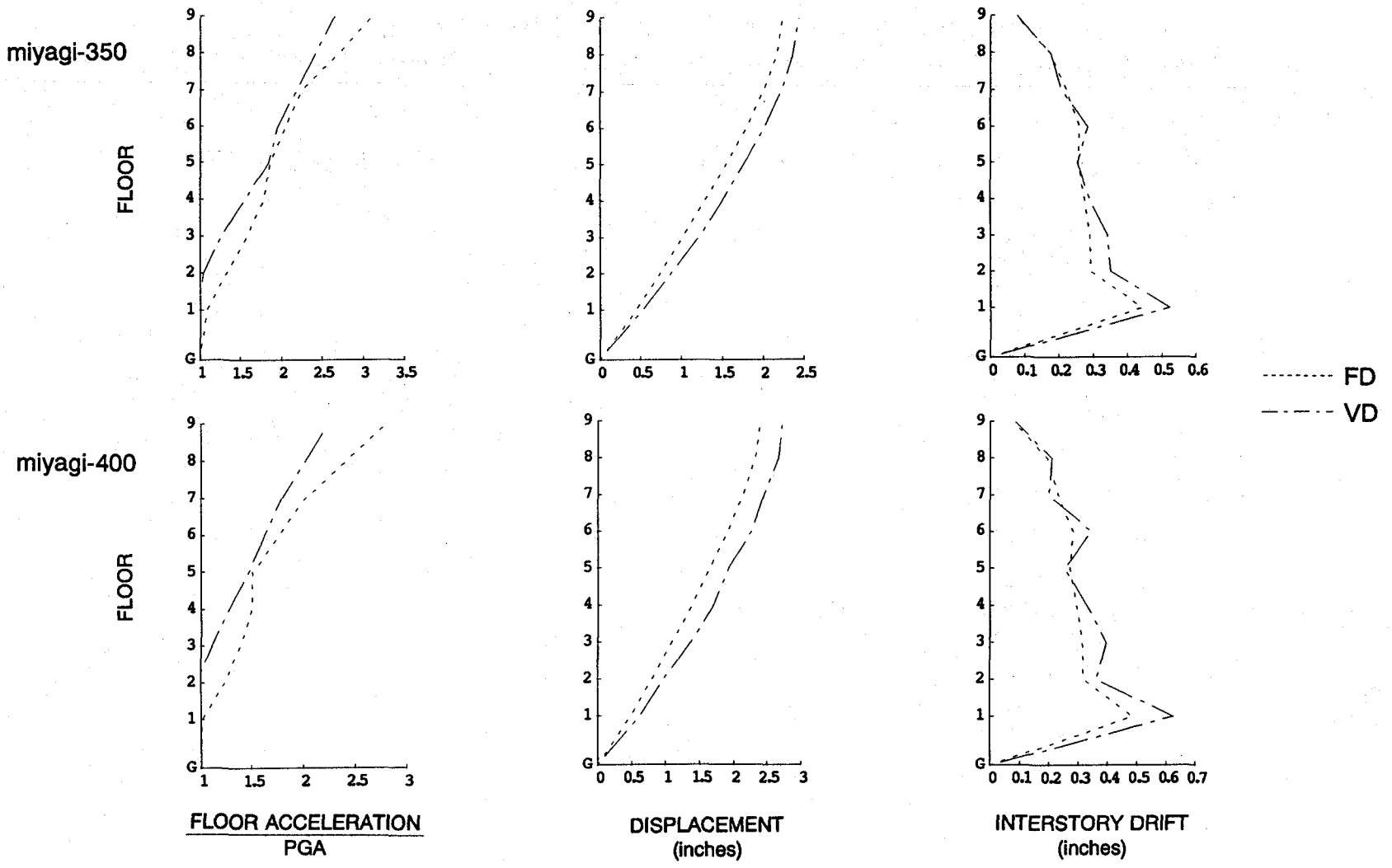
miyagi-350
miyagi-400
FLOOR
FLOOR
G 1 2 3 4 5 6 7 8 9
1 1.5 2 2.5 3 3.5
0 0.5 1 1.5 2 2.5
0 0.1 0.2 0.3 0.4 0.5 0.6
1 1.5 2 2.5 3
0 0.5 1 1.5 2 2.5 3
0 0.1 0.2 0.3 0.4 0.5 0.6 0.7
FD
VD
FLOOR ACCELERATION
PGA
DISPLACEMENT
(inches)
INTERSTORY DRIFT
(inches)

Fig. 4.67 cont.

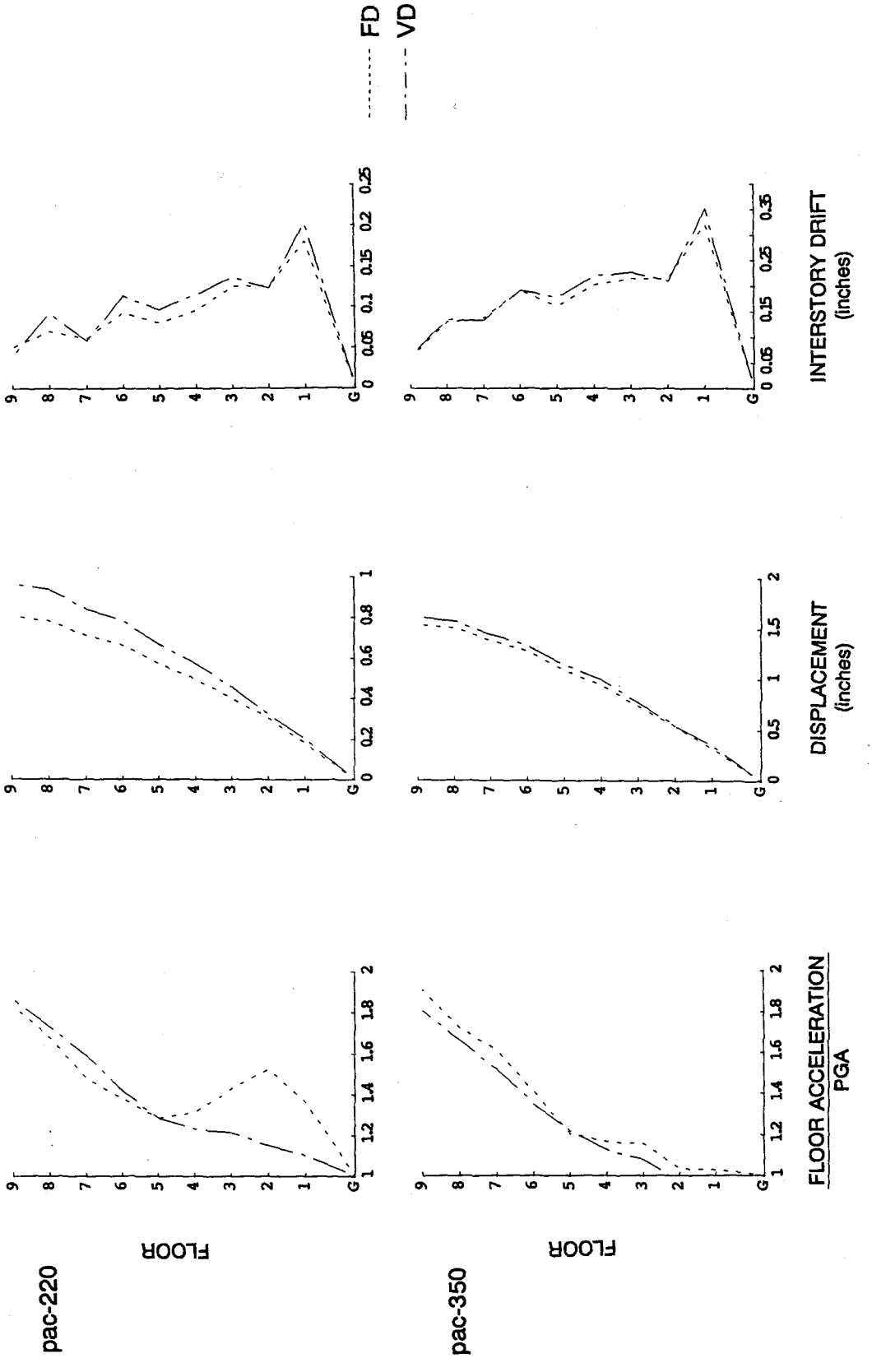

Fig. 4.68 VD and FD Acceleration, Displacement and Interstory Drift Response Profiles, pac-220 and pac-350 Tests

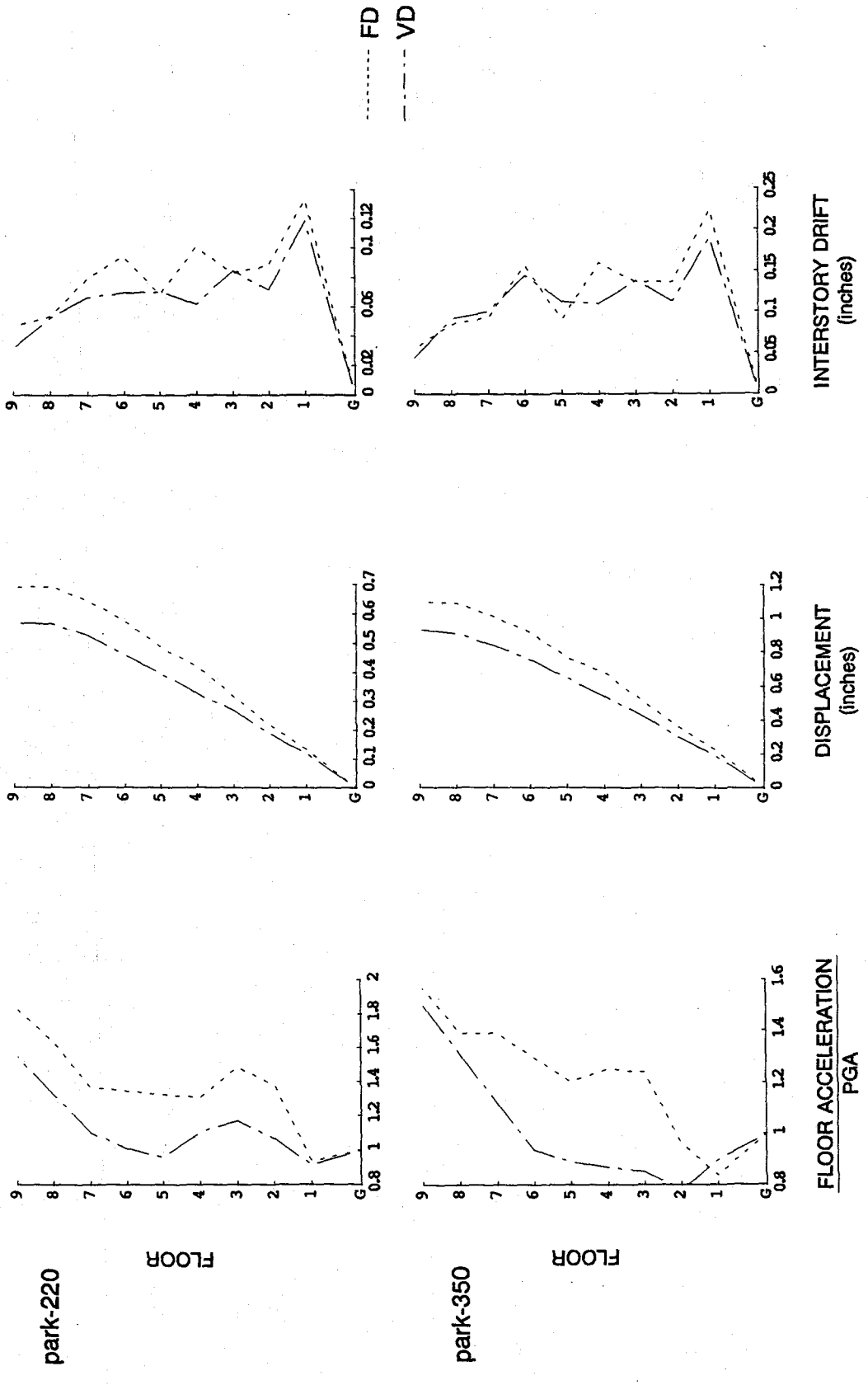

Fig. 4.69 VD and FD Acceleration, Displacement and Interstory Drift Response Profiles, park-220 and park-350 Tests

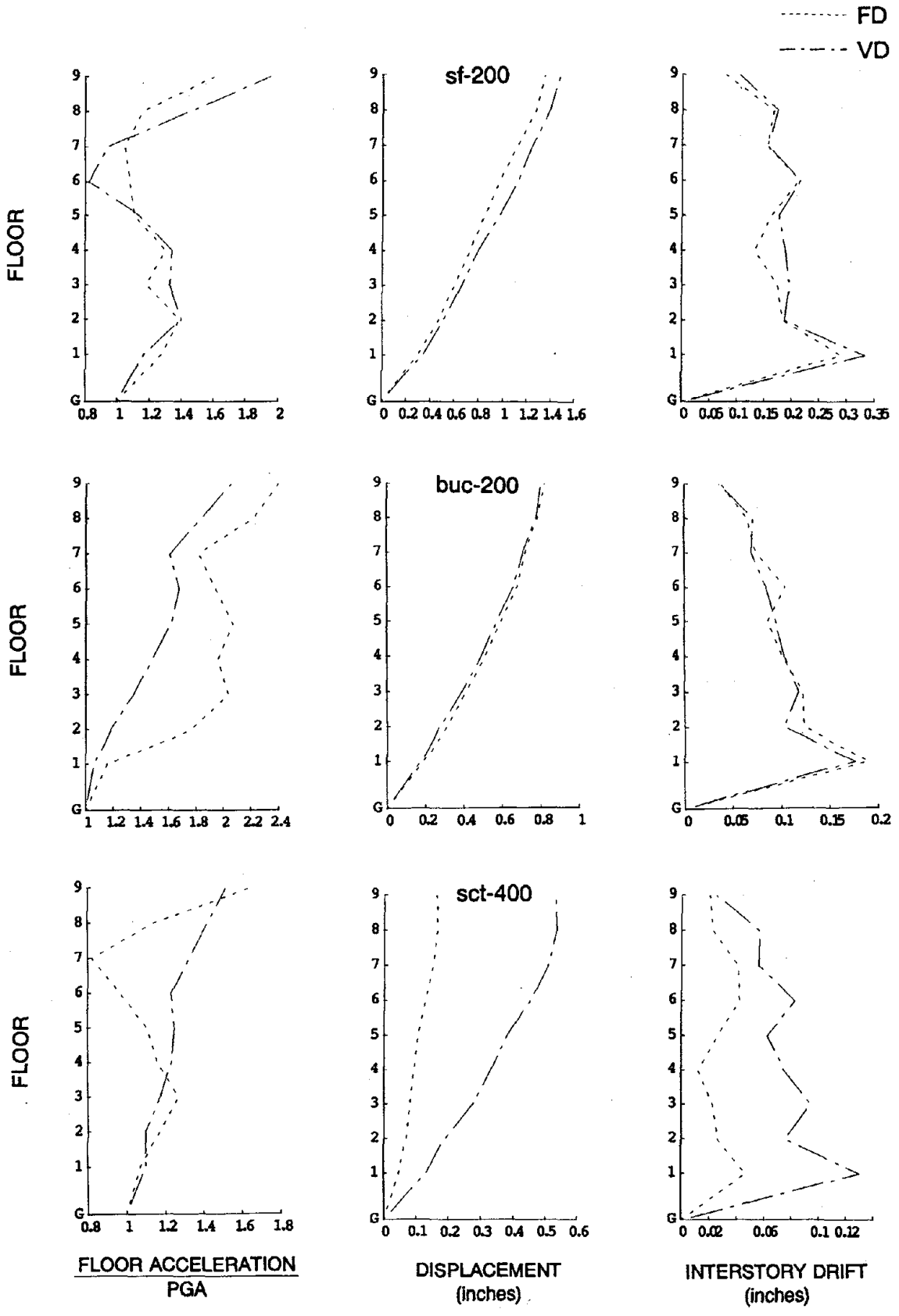

Fig. 4.70 VD and FD Acceleration, Displacement and Interstory Drift Response Profiles, sf-200, buc-200, and sct-400 Tests

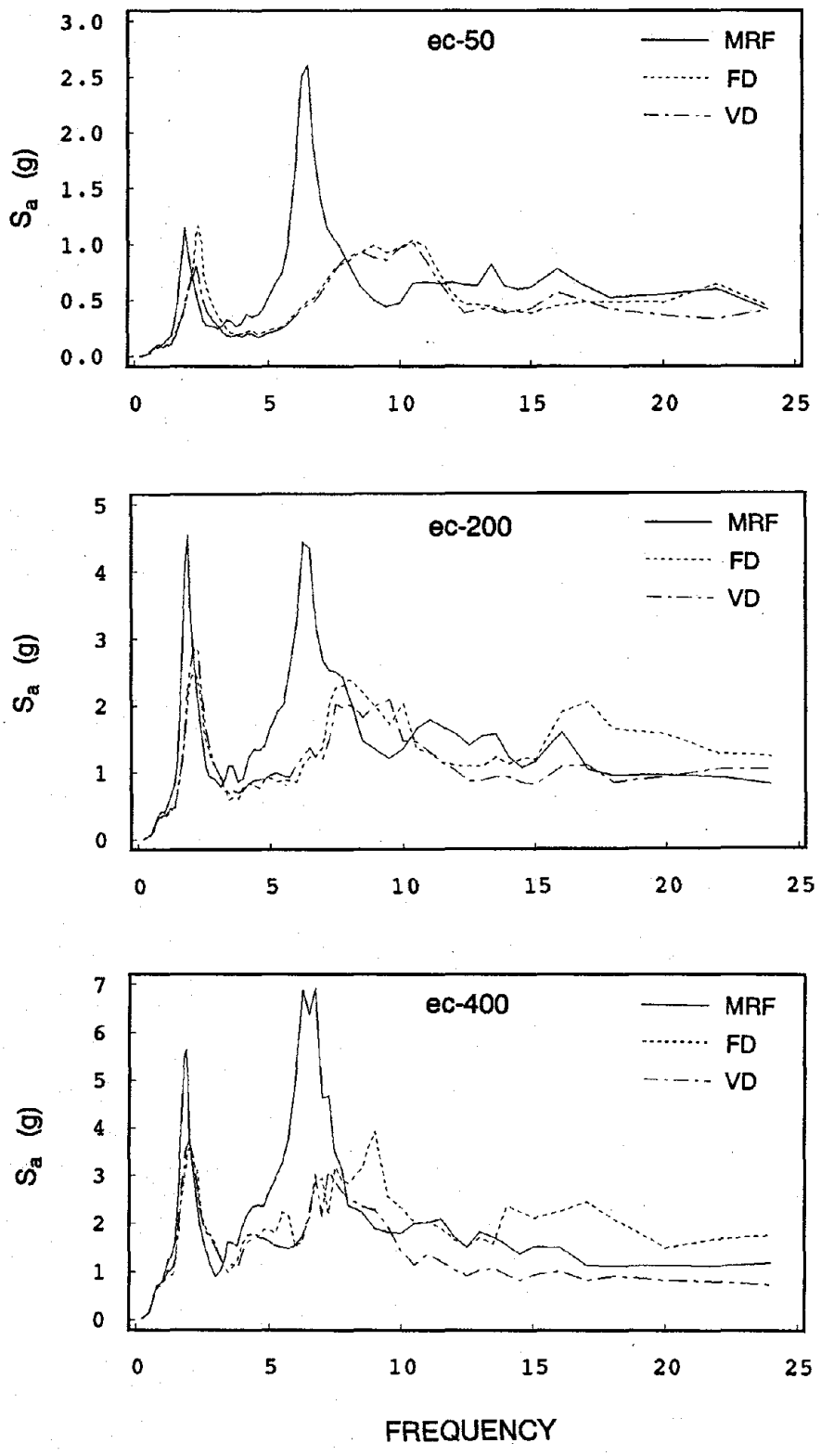

Fig. 4.71 VD, FD, and MRF Level 3 Two Percent-Damped Floor Response Spectra, ec-50, ec-200, and ec-400 Tests

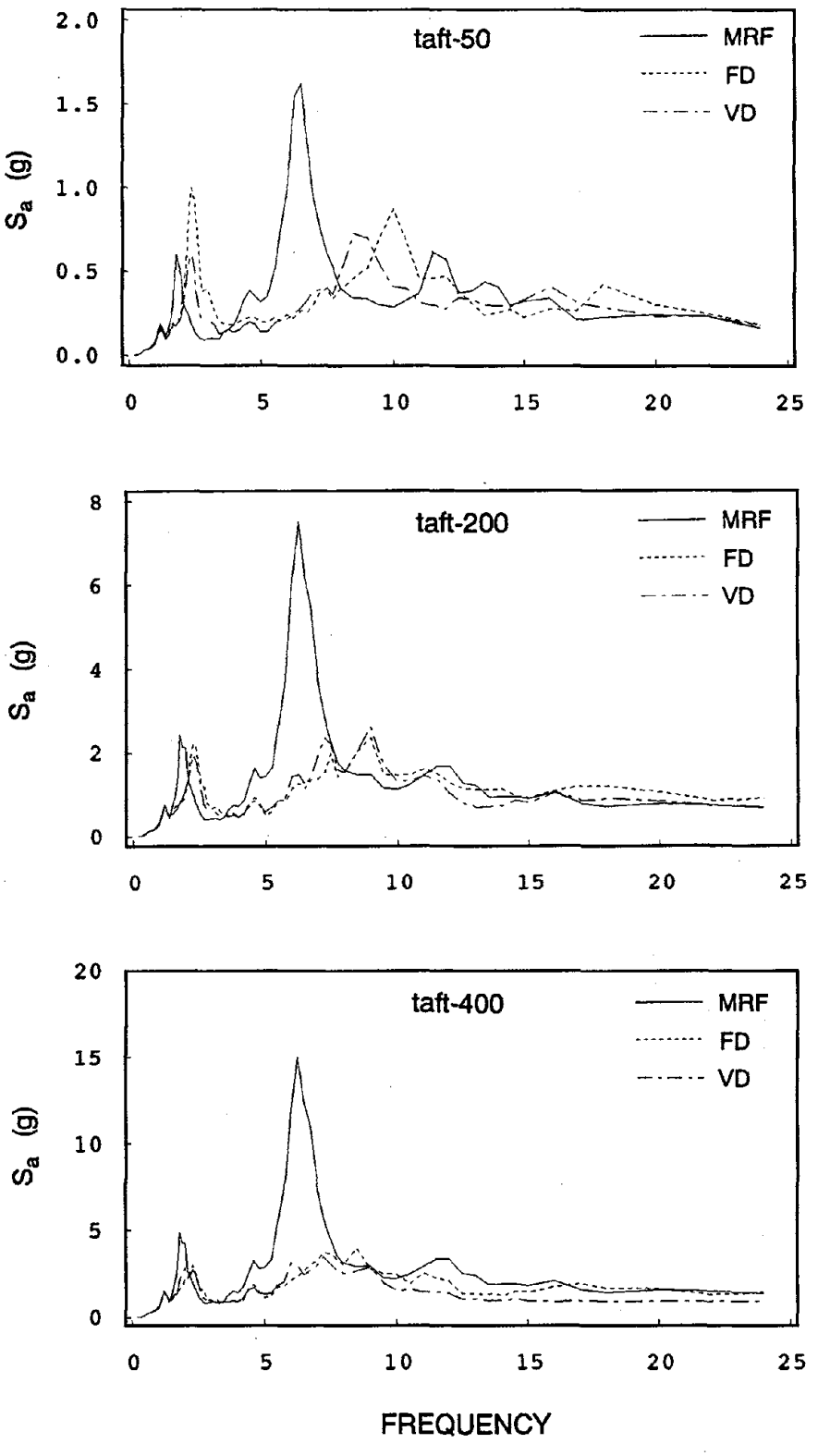

Fig. 4.72 VD, FD, and MRF Level 3 Two Percent-Damped Floor Response Spectra, taft-50, taft-200, and taft-400 Tests

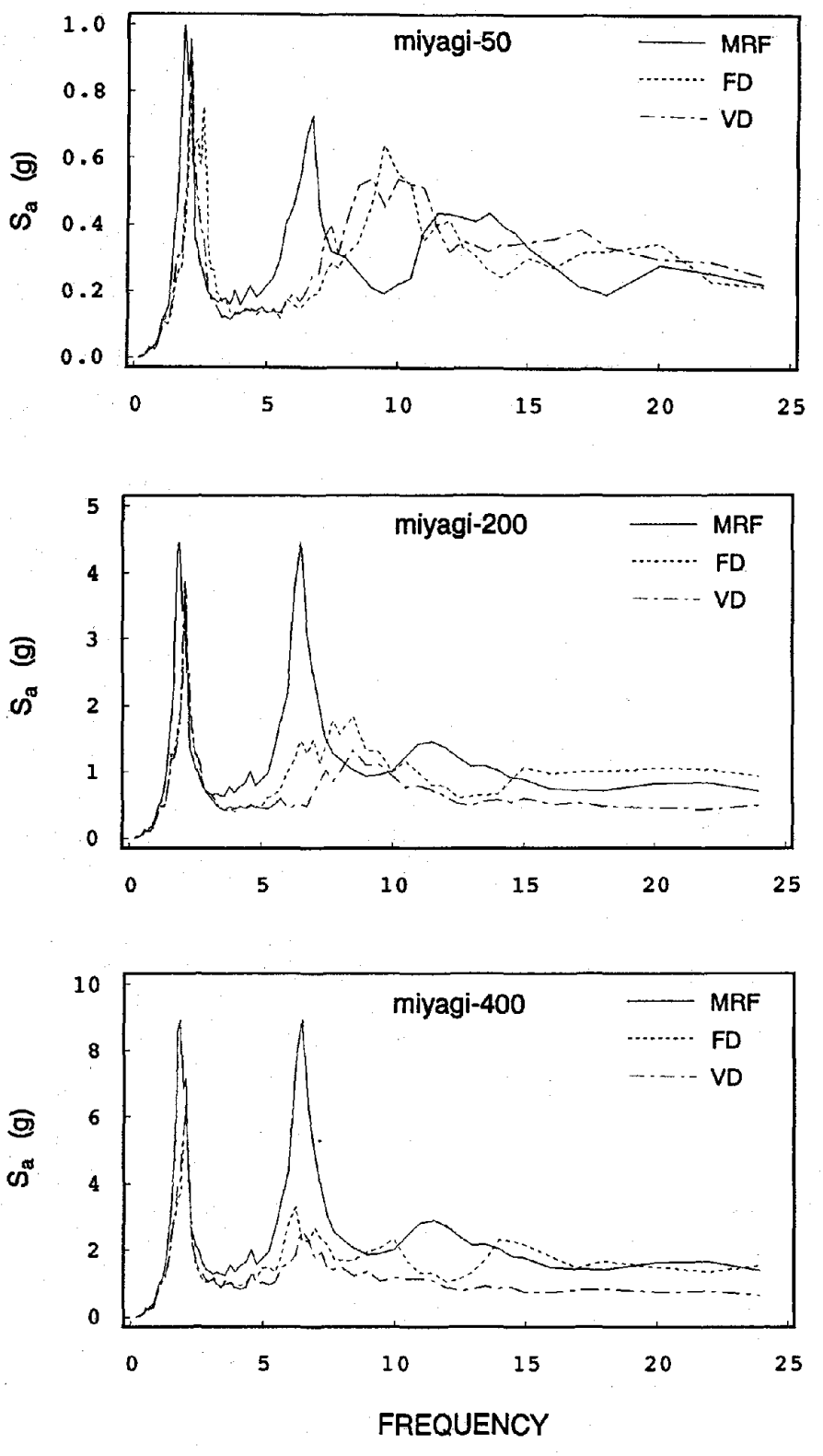

Fig. 4.73 VD, FD, and MRF Level 3 Two Percent-Damped Floor Response Spectra, miyagi-50, miyagi-200, and miyagi-400 Tests

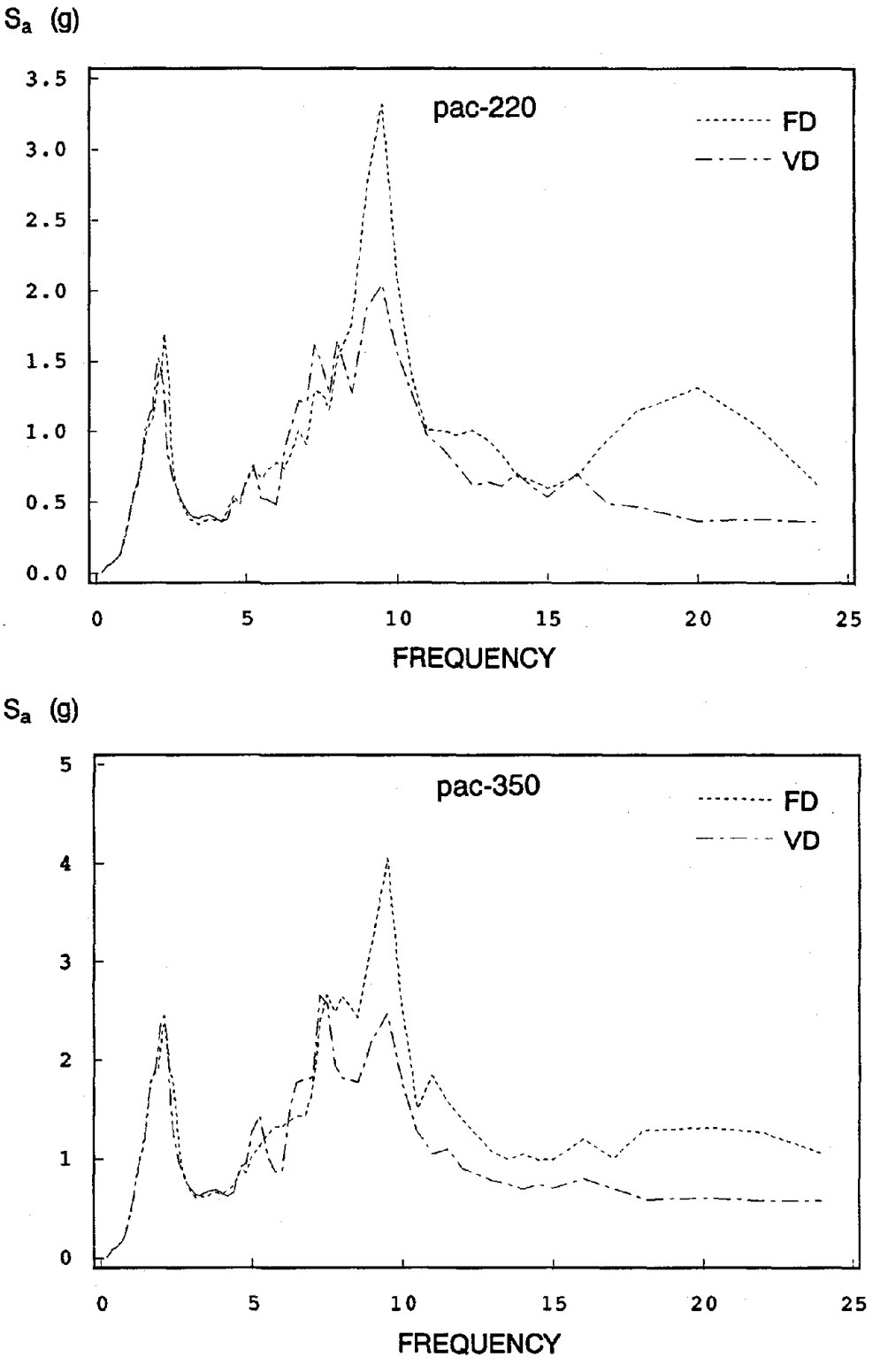

Fig. 4.74 VD and FD Level 3 Two Percent-Damped Floor Response Spectra, pac-220 and pac-350 Tests

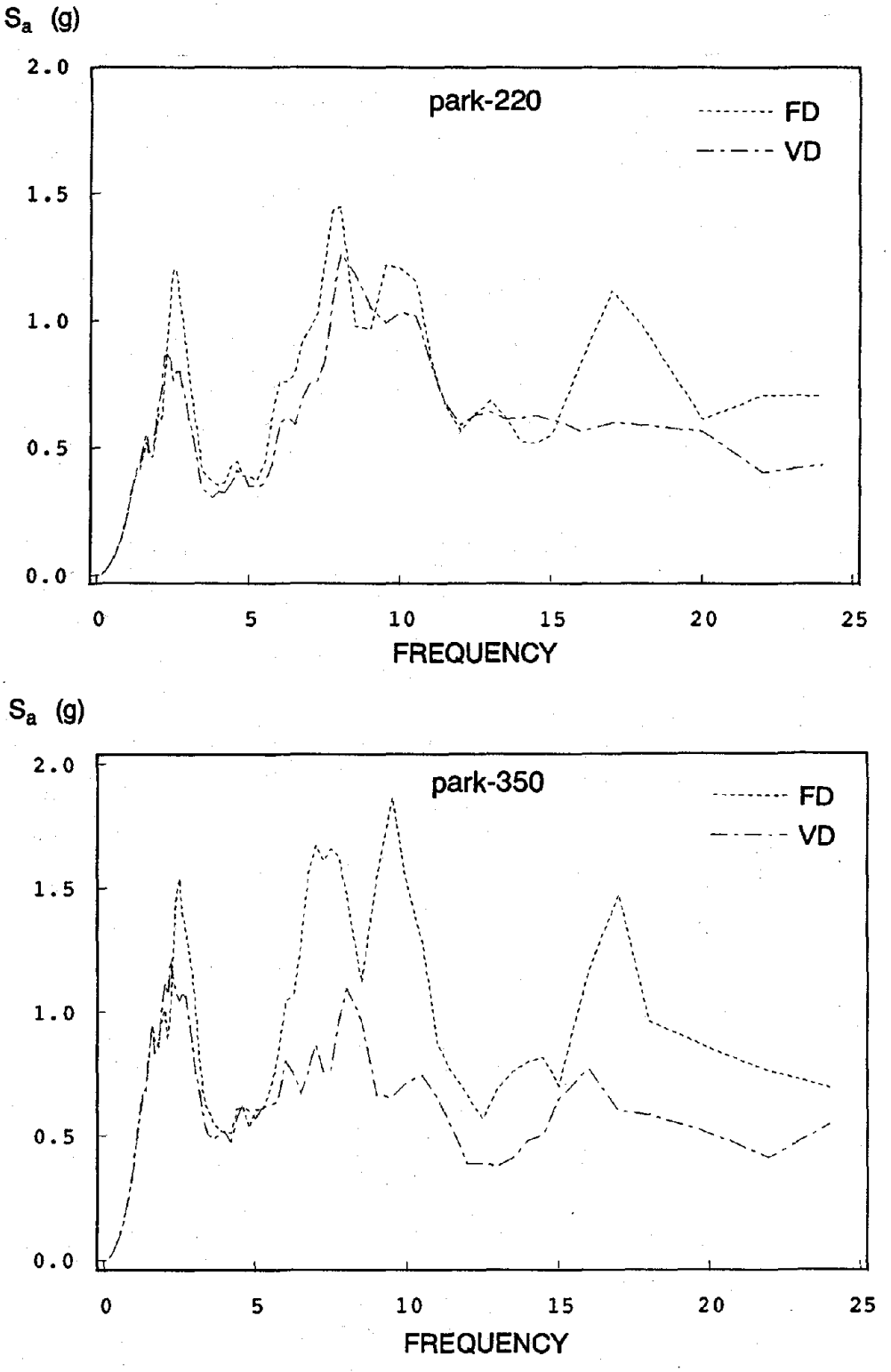

Fig. 4.75 VD and FD Level 3 Two Percent-Damped Floor Response Spectra, park-220 and park-350 Tests

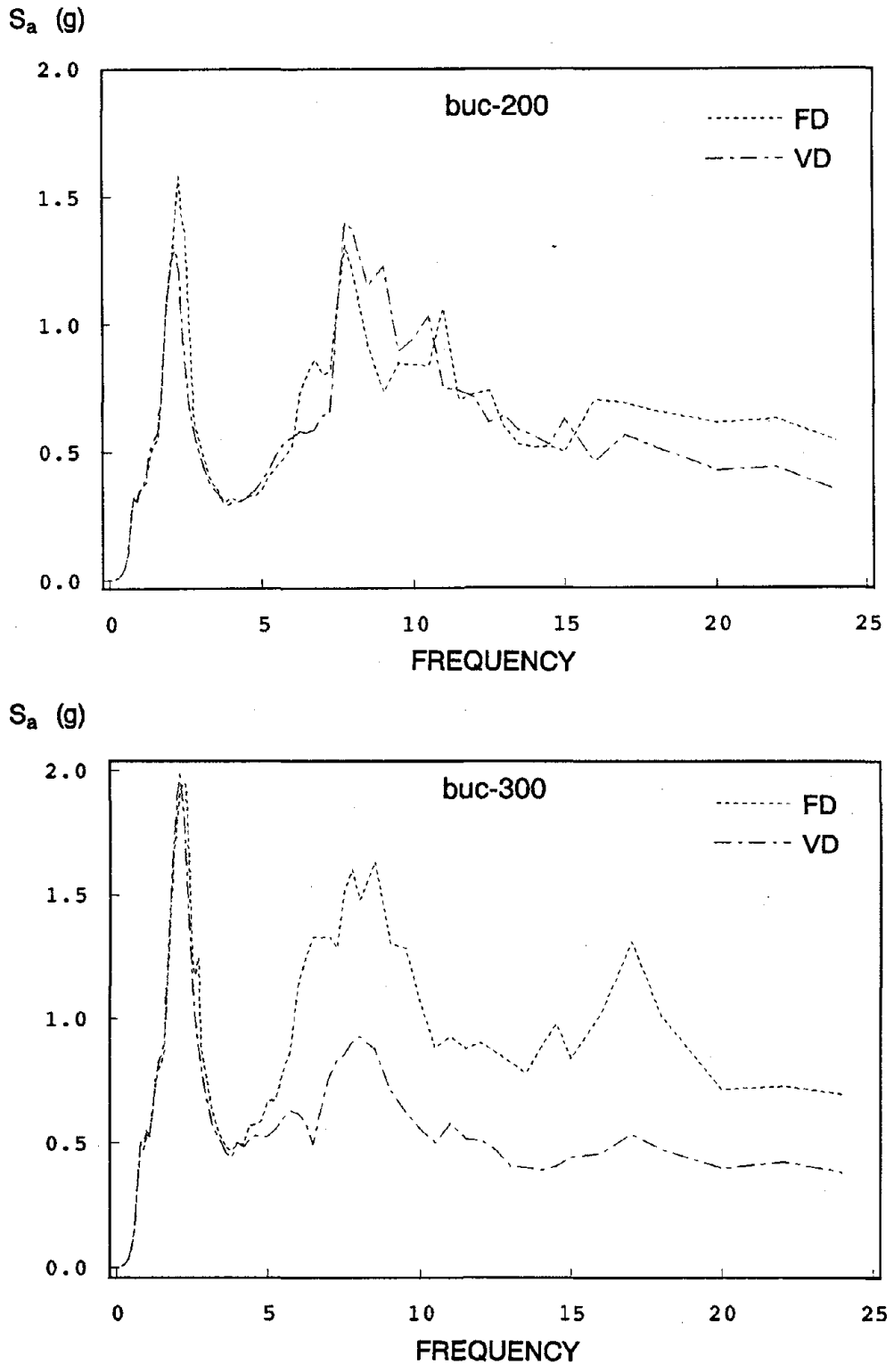

Fig. 4.76 VD and FD Level 3 Two Percent-Damped Floor Response Spectra, buc-200 and buc-300 Tests

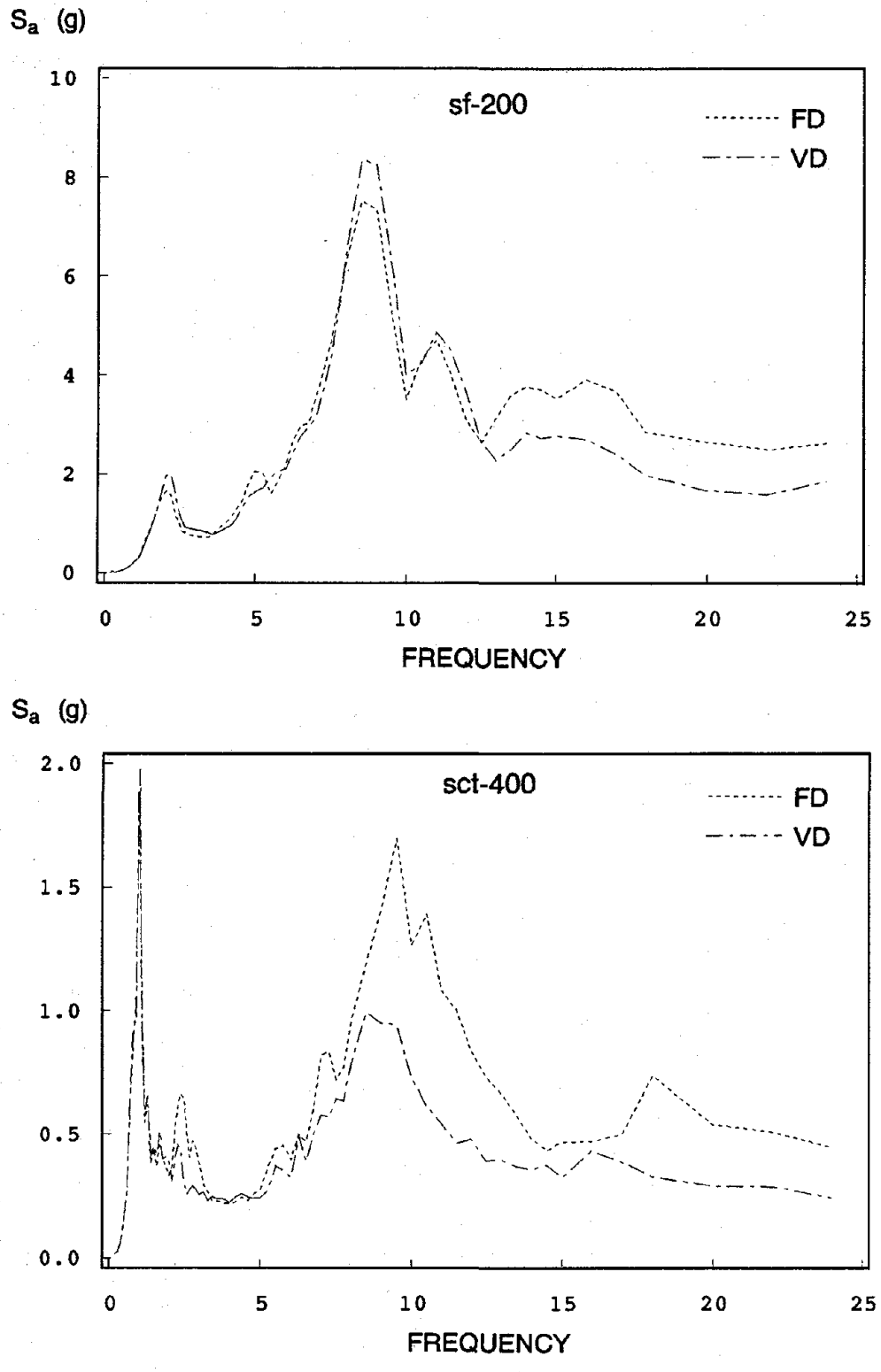

Fig. 4.77 VD and FD Level 3 Two Percent-Damped Floor Response Spectra, sf-200 and sct-400 Tests

CHAPTER 5

ANALYTICAL STUDIES OF TEST STRUCTURES

5.1 Introduction

To complement the experimental studies of the viscoelastic and friction damped test structures numerical analyses were conducted. In Section 5.2 the analytical study of the VD structure is described. The nature of the numerical model, results obtained for selected earthquakes, and correlation with the experimental results are presented. Section 5.3 contains the corresponding numerical study of the FD structure. The importance and relevance of these results to the design of structures incorporating energy-absorbing devices is discussed in Sec. 5.4. Conclusions drawn from the numerical studies are offered in Sec. 5.5.

5.2 Analyses of Viscoelastic-Damped Structure

5.2.1 Mathematical Model

A linear elastic analysis was chosen for the VD structure. There were two main reasons for this choice:

(i) The VE damper stiffness — γ relationships determined from the earthquake tests indicated that the dampers could be considered as having a constant stiffness over quite a large strain range (about 50 — 150 %, Fig. 4.15).

(ii) Other researchers have identified 3M VE materials as having velocity-proportional damping up to γ = 80 % and for frequencies to about 1 Hz [34]. This suggests that viscous damping should accurately model the damping characteristics of a VD structure. The γ_{max} and frequency conditions in the VD model tests are outside the velocity-linear range identified in [34]. It was, therefore, of particular interest to investigate the applicability of the viscous-damping assumption to the shake table test conditions.

A well-established, finite element structural analysis program, SAP90, was used for the numerical studies of the VD structure [49]. The program offers three dimensional, linear elastic, finite element analysis capabilities for static and dynamic loading conditions. A satisfactory numerical model of the VD structure must adequately represent the stiffness and damping characteristics of the VE dampers. Since both of these properties are functions of nonlinear material properties, any linear analysis is inherently an approximation to the actual response.

The test structure was modeled as a 2D planar frame, with all out-of-plane degrees of freedom constrained to zero. The structural frame was modeled using frame (beam-column) elements. The damped braces were modeled as discrete members using spring (truss) elements capable of carrying only axial load. A schematic diagram of the mathematical model of the VD structure is shown in Fig. 5.1. The spring elements were provided with an "effective" axial stiffness that corresponded to the shear stiffness of the VE dampers. This stiffness was determined from the hysteresis loops of the dampers for the ec-250 test and represented a best-fit linear value. The hysteresis loops for the ec-250 test are shown in Fig. 4.14, with the effective linear stiffness superimposed on each loop. In this fashion, the stiffness contribution of the VE dampers to the dynamic behavior of the test structure was accounted for. The damping provided by the dampers to the structure was included in the analysis by increasing the modal damping of the structure over that of the MRF. This increase was determined from the shake table test results. Discussion on the suitability of this way of including the energy dissipation provided by the devices to the structure in the analysis is presented in Secs. 5.2.3 and 5.4.1.

5.2.2 Correlation with Experimental Results

Time history analyses were performed for three earthquake motions: El Centro at seven different intensities, and Taft and Miyagi each at one intensity. All of the analyses were performed using shake table response signals as the input for the analysis. The earthquakes for which the analyses were performed are listed in Table 5.1, together with the PGA of each signal, the peak roof displacement measured during the test (D_{expt}), the peak roof displacement

obtained from the analysis (D_{sap}), and the difference between D_{sap} and D_{expt} expressed as a percentage of D_{expt}.

Figures 5.2 — 5.4 present comparisons of the experimental and analytical roof displacement time histories for the ec-250, taft-200, and miyagi-200 signals, respectively. Figure 5.5 shows the experimental and analytical profiles of peak story displacements for these tests. In general, it can be seen that the analysis closely predicts the actual response. The good phase agreement indicates that the stiffness characteristics of the test structure have been captured by the analytical model. For the ec-250 and taft-200 inputs, in particular, the magnitude of the response is very closely predicted, with the exception of the one or two cycles associated with the peak displacement. The ec-250 analysis predicts a peak roof displacement of 1.68 inches, which compares well with the experimental value of 1.69 inches. The taft-200 analysis predicts a peak roof displacement of 0.94 inch, compared with the experimental value of 0.85 inch. Figure 5.4 indicates that while the frequency characteristics of the response to the miyagi-200 input have been well-captured by the analytical model the displacement peaks are slightly higher than the experimental results. The peak displacements are 1.03 inches and 1.12 inches from experiment and analysis, respectively.

The differences between the analyses and experiment are attributed to two factors: (i) the decrease in stiffness of the VE dampers at the larger strains associated with the peak displacement cycles, and (ii) the effect of shake table-structure interaction. The first factor points to the approximation involved in assuming an equivalent linear stiffness for the VE dampers, which in itself is bound to introduce some error into the analysis. As described in Sec. 5.2.1, the stiffness used for the brace elements representing the dampers was obtained by identifying an effective linear stiffness for the elliptical hysteresis loops of the dampers. This is clearly an approximation, but nonetheless has produced good results in this study. Shake table-structure interaction was not considered in the analyses of the VD structure, the reason being that for the small to moderate intensity inputs studied, interaction was not expected to be important. Although ignored without severe consequences, interaction effects are present to some degree,

and if accounted for and combined with nonlinear modeling of the VE dampers would improve the accuracy of the analytical results from those obtained. The effect of interaction on the FD structure, and a suitable method of modeling this effect are discussed in Sec. 5.3.

5.2.3 Other Results

The good results obtained in the analyses showed that the salient aspects of the behavior of the VD structure were well predicted by the "equivalent-linear" analytical model. After the suitability of the analytical model was demonstrated, a number of additional studies were undertaken to investigate some aspects related to adding viscous damping to the test structure.

Damping vs. Stiffness Contribution of VE Dampers

While the primary purpose of adding the VE dampers to the structure was to increase its damping, they also served to add stiffness to the moment frame and to change its frequency characteristics. This dual contribution to the structural behavior is a characteristic of all energy-absorbing systems, and raises the significant issue of the relative merits of adding damping versus adding stiffness to a structure. The accuracy of the analytical model provided a means by which these two properties could be effectively decomposed and separately identified.

The numerical model for the ec-250 analysis was modified to reduce the structure damping from 10 % (in all modes) to 2 %, while at the same time making no change to the stiffness characteristics of the model. Thus, the computer model represented a 2 %-damped structure with the same frequency as the VD structure. Any difference between the response of this model and that of the test structure is therefore due to the difference between the amount of damping possessed by the two structures. The analytical roof displacement time history for the ec-250 input is compared with the experimental result for the VD structure in Fig. 5.6. It can be seen that the frequency has been well-matched, indicating that the stiffness properties of the two structures are very close. Of note, therefore, are the differences in displacement between the experimental and analytical structures. The difference between the analytical and

experimental displacements clearly illustrates the reduction in response due to the increase in damping from 2 % to 10 %. The experimental peak displacement was 1.69 inches, and the 2 %-damped analysis gave a peak roof displacement of 3.44 inches, approximately twice the experimental value.

Using the same computer model, a series of analyses were performed for the ec-250 input with different structure damping ratios. The damping was varied from 1 % to 20 % of critical. Figure 5.7 presents profiles of peak story displacements obtained from the analyses. It can be seen that the increase of damping from 1 % to 10 % has the biggest impact on reducing the response of the structure. The additional benefit of a further 10 % increase in damping to 20 % is not nearly as great as the improvement attained by increasing the damping from 1 to 10 %.

Higher Mode Damping

One question that arises in the development of a suitable computer model of the VD structure is the appropriate value for the damping ratio in the higher modes, that is, ξ_i for $i > 1$. Transfer function and half-power bandwidth analyses of the experimental results consistently indicated that the second mode damping ratio (ξ_2) was approximately 8 %. In the analyses of the VD structure, four modes were assumed to contribute to the response, and 8 % damping was assumed for each of the higher modes. As already stated, 10 % was used for the damping in the first mode.

Recently, Zhang et al. [50] presented a procedure for the analysis of VD structures in which additional damping is included in the analysis on a modal basis. Their example [50] considers six modes contributing to the response of a ten-story structure. The damping in the first mode is taken as 12 %, and in the 2nd, 3rd, and 4th modes, 36 %, 33 %, and 26 %, respectively. These values are considerably higher than the 8 % observed in the current experiments.

To evaluate the importance of the values assumed for ξ_i, $i > 1$, a series of analyses were performed in which the ξ_i were varied over a wide range. In Fig. 5.8, roof displacement time

histories for the ec-250 input are overlaid for two cases: (i) ξ_1 = 10 % and ξ_{2-4} = 8 %, as assumed for all of the experimental-analytical comparisons, and (ii) ξ_1 = 10 % and ξ_{2-4} = 25 %. The dotted and solid lines in the figure are almost indistinguishable, with a difference of 0.67 % at maximum displacement. Three profiles of peak story displacements are plotted in Fig. 5.9 for the ec-250 test, corresponding to (i) the experimental result, (ii) the analytical result for ξ_1 = 10 % and ξ_{2-4} = 8 %, and (iii) the analytical result for ξ_1 = 10 % and ξ_{2-4} = 25 %. These results indicate that, at least for this structure in which the response occurred predominantly in the first mode, the actual values of damping assumed for the higher modes have a negligible effect on its overall response.

Response Spectrum Analyses

Response spectrum analyses of the VD structure were performed for each of the input signals used in the shake table tests. Only the first mode of the structure was considered and ξ = 10 % was assumed for all analyses. The first mode shape as determined from the free vibration tests was used, and the fundamental frequency was that identified by transfer function evaluation for each input earthquake. This varied from 2.43 Hz to 2.00 Hz, depending on the intensity of the input. A linear elastic response spectrum (LERS) was calculated for each input, then peak spectral displacement and base shear were determined.

Table 5.2 presents the experimental and response spectrum values of peak roof displacement and peak base shear for all of the earthquake inputs. Experimental and response spectrum peak story displacements and story shears are compared for the ec-250, taft-200, and buc-300 tests in Fig. 5.10. With only a few exceptions, there is very good agreement between the experimental observations and the response spectrum calculations. In most cases the peak displacement is estimated within 10 % of the actual value, and invariably the response spectrum overestimates the experimental displacement. The single-mode analysis tends to underestimate the experimental base shear by about 10 %, although in a few cases the difference is about 20 — 25 %. Given that only one mode has been considered in the analyses, and that the 10 % value assumed for damping is an approximation (in some cases) the results obtained are very

good.

5.3 Analyses of Friction-Damped Structure

5.3.1 Mathematical Model

The highly nonlinear performance characteristics of the friction devices required a non-linear analysis to predict the response of the FD structure suitably. The inelastic time history analysis program Drain-2D was used for the numerical studies [51]. The program possesses a variety of nonlinear elements and offers two dimensional analysis capabilities for static and dynamic loads.

The structural frame was modeled using bilinear beam-column elements. The nodes at each floor level were constrained to a single horizontal degree of freedom at that level. The friction devices were modeled explicitly by yielding truss elements having equal tension and compression yield forces. A very high elastic stiffness and a very low post-elastic stiffness (0.1% strain hardening) were specified to model the rectangular force-displacement behavior of the friction devices. One end of the truss element was connected to the top of the chevron bracing and the other to a short rigid link extending down from the beam-column joint above. This detail is shown in Fig. 5.11. The rigid link was necessary to ensure that the length, and thus the stiffness, of the chevron bracing was correctly modeled. A more simplistic model in which the bracing extended to the level of the floor above and the truss element was connected from the apex of the bracing directly to the beam-column joint (in the plane of the floor) would have been conceptually incorrect.

A number of researchers have studied the interaction between the shake table and test structures [42,47]. This interaction becomes particularly important for tall, heavy test structures such as the 9-story steel frame, which are capable of generating large overturning moments during high intensity excitations. The shake table control system is designed to resist the pitching motion caused by overturning of the test structure by a system of passive stabilizing actuators, but when the excitation (and thus the induced overturning moments) is large the

stabilizing system cannot satisfactorily control the pitching motion in the table. Shake table-structure interaction was taken into account in the analyses of the FD structure.

The equivalent viscous damping of the FD structure was 2.1 % as found from free vibration tests (locked table condition). Damping increases considerably when the table is active during earthquake tests, making it appropriate to use an "active" damping value for the analyses. Damping of 4 % (as determined from the pulse tests) was used, and inspection of analytical free vibration decay at the end of several signals (for example, the last 3 seconds of El Centro) showed that this value was reasonable. The damping was defined to be stiffness dependent, based on the initial tangent stiffness.

5.3.2 Correlation with Experimental Results

Preliminary analyses of the FD structure were performed without considering foundation flexibility introduced by shake table-structure interaction (Fig. 5.11(a)). The results indicated that for good agreement with the experimental results, interaction should be considered, particularly for large intensity inputs. The nine-story model is about the largest (both tallest and heaviest) structure that can be reasonably tested on the shake table, and under large inputs it can readily generate overturning moments that exceed the pitching resistance of the shake table. In the case of a large input with this structure a significant amount of interaction can be expected.

The model shown in Fig. 5.11(b) was developed to account for table-structure interaction in the analyses. The shake table was modeled as a rigid beam with a rotational mass of 625 kip-inches, and with a rotational degree of freedom about its midpoint constrained by two spring (truss) elements each with spring constant, k_p. This was one of two modeling schemes investigated in a previous shake table test program [47] and was found to give good results. It was decided to limit the interaction model to one employing linear elastic springs, primarily because correlating the numerical model (identifying a reasonable value for k_p) is an iterative procedure, and if the interaction springs are considered to be linear then there exists only one

unknown, namely k_p, whereas if they are considered nonlinear then there are three unknowns, $k_{p_{elastic}}$, $k_{p_{yield}}$, and the yield force or deformation level. The additional unknowns of the nonlinear problem unnecessarily complicate the modeling task and detract from the primary objective of investigating the suitability of an existing analysis program and current techniques for predicting the response of a FD structure. Factors affecting the (nonlinearity of the) interaction are the size, weight, stiffness, and strength of the test structure, the frequency and displacement characteristics of the input motion, the performance characteristics of the hydraulic actuators, and the temperature of the oil in the hydraulic system. Of particular importance are the type and size of the test model and the intensity of the input signal. The development of either a linear or a nonlinear model which captures the major aspects of the interaction effect becomes a trial-and-error iterative task.

The suitability of the interaction model shown in Fig. 5.11(b) was first investigated by a series of analyses of the MRF subjected to the ec-300 input. The first two frequencies of the fixed-base analytical model closely matched those of the test structure ($f_{1_{expt}}$ = 1.89 Hz and $f_{1_{anal}}$ = 1.92 Hz, $f_{2_{expt}}$ = 6.6 Hz and $f_{2_{anal}}$ = 6.1 Hz). Interaction was included and k_p varied on a trial-and-error basis until the roof displacement time histories showed good agreement in both phase and amplitude. At that point, correlation of other response quantities was checked. A value of k_p = 400 kips/inch was selected for the MRF model.

The introduction of the interaction springs had almost no influence on the frequency of the table-structure system but its effect was dramatic on the time history response correlation. For the sequence of interaction analyses of the MRF it was found that the peak roof displacement increased by 9.7 % with the introduction of interaction. Inspection of various experimental results revealed that the contribution of rotational flexibility (due to table pitching) to structure horizontal displacement could be of the order of 10 — 25 % of the total displacement of the nine-story structure. Comparisons of experimental and analytical roof displacement time histories for the MRF subject to the ec-300 input are shown in Fig. 5.12. Figure 5.12(a) shows the roof displacements for the rigid foundation condition and Fig. 5.12(b) for the

interaction model with k_p = 400 kips/inch. The influence of interaction on the response is clearly seen from the two figures. The MRF analyses indicated that it was appropriate to include the effects of interaction, particularly for large inputs. A similar series of analyses of the FD structure gave k_p = 250 kips/inch as the most suitable spring constant. This value was used for all of the analyses of the FD structure.

The analyses of the FD structure are listed in Table 5.3. Roof displacement time histories obtained from the analyses are compared with experimental results in Fig. 5.13 for the ec-400, taft-400, miyagi-350, chile.u-500, unio-750, and zaca-750 inputs. Analytical and experimental profiles of peak floor displacement and story shear for these same inputs are compared in Fig. 5.14. The time histories show that the analytical model provides results in very good agreement with experiment, particularly with respect to phase. Significant differences, where they are evident, are restricted mainly to the large amplitude excursions. It is believed that this is primarily due to the fact that the actual table-structure interaction effect is nonlinear, and thus not fully captured by the use of a constant k_p. A more detailed, nonlinear interaction model would better predict the peak displacements. As seen by the very good agreement of the time histories, the variance of the peak displacements in Table 5.3 is not indicative of poor experimental-analytical correlation. The displacement profiles show that the peak values are generally underpredicted, for the reason already discussed above. As for the displacements, the analyses tended to also underpredict the peak story shears. The analytically predicted hysteretic behavior of the friction devices at levels 1, 2, 3, and 4 for the chile.u-750 and unio-750 inputs is shown in Fig. 5.15. The devices at the other levels responded similarly.

For all of the analyses performed, there was no yielding of the primary structural elements, namely the beams or the columns, of the FD structure.

5.3.3 Other Results

Large inputs, comparable to those to which the FD structure was subjected, were not applied to the MRF and CBF models because of the need to preserve the test structure for

future earthquake simulator studies. The analytical study was thus extended to provide information on the behavior of the test structure in the MRF and CBF configurations and allow performance comparisons to be made between these three structural systems.

The computer model of the MRF used to study the interaction effect was used, with the addition of buckling truss elements for the bracing in the CBF configuration. The MRF model gave excellent agreement with the experimental results for the large-intensity ec-300 and ec-400 inputs to which the MRF structure had been subjected (Fig. 5.12(b)) and this provided the confidence to extend it to other large input signals. The analyses performed of the MRF and CBF structures are listed in Table 5.4.

The results of the MRF analyses are summarized in Fig. 5.16, which shows the extent and location of plastic hinge development in the structure for each of the six inputs. It can be seen that significant yielding occurs for all inputs with the exception of taft-400, and in particular there is widespread yielding for the unio-750 and chile.u-750 inputs. Similar results for the CBF analyses are presented in Fig. 5.17, which shows the plastic hinge and brace buckling locations for each of the six inputs. The improvement obtained by the addition of bracing to the MRF is readily apparent, in the case of the taft-400 and miyagi-350 inputs the inelastic response has been eliminated, and for the ec-400 and zaca-750 inputs it has been reduced to only a few instances of brace buckling. The CBF response to the unio-750 and chile.u-750 inputs is not improved, however, and in fact shows even more widespread yielding than occurred in the MRF for these inputs.

The experimental response of the FD structure is compared with the analytical results for the MRF and CBF structures in Table 5.4. Experimental observations of both the base column strains and analytical results indicated that the FD structure did not develop yielding in any of the beams or columns of the primary structural system at any stage throughout the course of the shake table test program. The braces also remained elastic, and the only nonlinear action that occurred in the structure was confined to the friction devices. This represents a marked improvement over the response of both the MRF and CBF systems.

5.4 Implications of Analytical Studies on the Design of Structures Incorporating Energy-Absorbing Devices

5.4.1 Viscoelastically-Damped Structures

The analyses of the VD structure produced results in good agreement with the experimentally observed behavior. The commercially available and widely-used finite element structural analysis program, SAP90, was used for the numerical studies. The VE dampers were modeled by truss elements having an "equivalent-linear" axial stiffness, and their damping effect included by increasing the modal damping of the structure over that of the MRF.

The analytical study indicates that it is certainly possible to model and analyze structures incorporating VE dampers using an existing analysis program. The good agreement between analysis and experiment provides the confidence necessary to use such an (analytical) approach for the design of VD structures. Zhang et al. [50] have presented a method which extends the single-mode method used for the design of the VE damping system of the current study to include higher modes in the analysis of VD structures.

It should be recognized that in none of the shake table tests did yielding occur in the beams or columns of the primary structure, and thus the analyses have demonstrated the suitability of using SAP90 to predict the response of an elastic structure incorporating VE dampers. However, should it be necessary to perform analyses of a structure in which inelastic behavior is anticipated in the primary structural elements (namely, the beams or columns) there is no reason why a nonlinear analysis program such as Drain-2D (Sec. 5.3, [51]) could not be employed and modal damping increased in just the same fashion to include the damping contribution of the VE dampers. Recently, additions have been made to a new version of SAP, known as SAP2000, to provide several types of nonlinear elements [52] and it is expected that even better results would be obtained using these elements to model the VE dampers discretely.

A complete selection of manufacturer's datasheets should be developed providing material

loss factor and shear modulus values for the VE materials over strain ranges relevant to seismic applications, namely, 50 — 200 %.

5.4.2 Friction-Damped Structures

The nonlinear analyses of the FD structure produced results in good agreement with the experimentally observed behavior. An existing and widely known nonlinear analysis program, Drain-2D, was used for the numerical studies. The computer model of the structure used yielding truss elements with an approximately rigid-perfectly-plastic axial force deformation behavior to model the Sumitomo friction dampers. The results of the analytical study show that an existing nonlinear analysis program can be used with confidence for analytical studies and design of structures incorporating the Sumitomo type of friction-damping device.

The differences between the analytical and experimental results are attributed, at least in part, to the method used to model the table-structure interaction phenomenon. A properly correlated nonlinear interaction model would have provided better prediction of the peak responses. However, the nature of the interaction effect, and its influence on the peak response are issues not directly related to either the presence of the friction dampers in the structure or the method used to model them for analysis purposes, being rather a characteristic of the earthquake simulator and the size of the test model. The effort involved and difficulty associated with developing a nonlinear model of the interaction effect was not directly relevant to the primary aim of the analytical study, which was to investigate the suitability of existing analysis programs for modeling the behavior of a FD structure for the purposes of design. Development of a nonlinear interaction model was not undertaken.

5.5 Conclusions

The good results obtained in the analyses of the VD structure provided an opportunity to use the analytical model for further studies of the effects of adding viscous damping to the test structure. The results of these studies are summarized below:

(a) The separate effects of adding damping and adding stiffness to the structure were decomposed and evaluated. The VE dampers and bracing increased the frequency of the MRF from 1.95 Hz to 2.2 — 2.4 Hz, an increase in stiffness of approximately 25 — 50 %. The additional stiffness did not in itself significantly reduce the response of the structure. Analyses of structures of the same stiffness but with 2 % and 10 % damping revealed a significant response reduction (about 50 %) due to the added damping.

(b) The general trend of reduced response with increasing damping was identified. The damping was varied over the range of 1 — 20 %, and the peak roof displacement was reduced by 55 % in going from ξ = 1 % to 10 %, and by 70 % for an increase from ξ = 1 % to 20 %.

(c) For the VD structure studied, the actual values used for higher mode damping in the analyses proved to be insignificant to the overall response. The test structure responded primarily in the first mode, and the four modes used in the time history analyses were more than sufficient to capture the response accurately.

A 10 %-damped LERS is about the most highly-damped spectrum that could reasonably be used for analysis, before having to consider additional modifications to the spectrum to account for high damping. The use of conventional LERS for high damping values, say 10, 15, 20, and 20$^+$ %, should be investigated. Recently developed response spectra for structures with high damping [53,54,55] should also be studied with regard to their particular suitability to structures incorporating VE energy absorbers.

Nonlinear time-history analyses were performed of the MRF and CBF structures subjected to a series of large earthquakes which (for practical reasons) had not been simulated on the shake table. The results obtained and the comparisons that they permitted revealed the significant improvement in behavior attained for the FD structure, over both the MRF and CBF configurations. The MRF was found to suffer significant yielding during all but one of the earthquakes analyzed, and while the CBF response was overall improved, in two cases it was not and yielding was as extensive throughout the structure as seen in the MRF. In contrast,

the FD structure suffered no inelastic demands in any of the analyses performed or the earthquake simulator tests conducted.

TABLE 5.1 Analyses of VD Model

SIGNAL	SPAN	PGA [g]	D_{expt} [inches]	D_{sap} [inches]	DIFFERENCE [%]
ec2	50	0.145	0.36	0.33	-7.3
ec2	100	0.227	0.71	0.66	-9.8
ec2	150	0.319	1.10	0.97	-15.3
ec2	200	0.402	1.45	1.28	-11.7
ec2	250	0.486	1.69	1.68	0.2
ec2	300	0.559	2.00	1.98	-1.1
ec2	400	0.753	2.53	2.57	2.0
taft2	200	0.394	0.94	0.85	-8.0
miyagi	200	0.217	1.03	1.12	9.5

D_{expt} = experimental peak roof displacement

D_{sap} = analytical peak roof displacement

DIFFERENCE = percentage difference between D_{expt} and D_{sap}

TABLE 5.2 Response Spectrum Analyses of VD Model

SIGNAL	SPAN	PGA [g]	*ROOF DISPL. [in.]		*BASE SHEAR [kips]	
			EXPT	R.S.	EXPT	R.S.
El Centro	50	0.145	0.33	0.36	17.2	13.3
	100	0.227	0.65	0.71	31.4	26.1
	150	0.319	1.00	1.10	42.7	37.4
	200	0.402	1.30	1.45	54.4	46.7
	250	0.486	1.64	1.69	60.6	59.3
	300	0.559	2.13	2.00	67.6	65.0
	400	0.753	2.58	2.53	74.6	80.4
Taft	50	0.092	0.26	0.30	12.0	10.7
	100	0.190	0.55	0.59	22.4	22.2
	150	0.292	0.67	0.71	25.6	18.3
	200	0.394	0.89	0.94	34.4	31.5
	250	0.485	1.17	1.18	42.2	41.9
	300	0.592	1.27	1.27	42.8	41.5
	400	0.821	1.66	1.72	50.6	53.4
Miyagi	50	0.115	0.24	0.24	10.8	9.8
	100	0.159	0.44	0.49	19.6	17.3
	150	0.180	0.65	0.77	29.5	25.2
	200	0.217	0.90	1.03	37.1	33.3
	275	0.270	1.31	1.62	52.2	50.6
	300	0.316	1.93	2.14	64.7	58.0
	350	0.413	2.17	2.37	71.1	64.6
	400	0.534	2.41	2.74	75.1	66.6

TABLE 5.2 cont.

SIGNAL	SPAN	PGA [g]	*ROOF DISPL. [in.]		*BASE SHEAR [kips]	
			EXPT	R.S.	EXPT	R.S.
Pacoima	220 350	0.272 0.461	0.80 0.70	0.90 1.59	34.4 54.6	31.5 40.8
Parkfield	220 350	0.284 0.410	0.57 0.88	0.57 0.91	24.8 32.3	22.4 34.1
San Francisco	200	0.884	1.22	1.30	58.1	45.2
Bucharest	200 300	0.200 0.259	0.80 1.23	0.81 1.21	31.7 40.8	29.9 43.4
Mexico (SCT)	400	0.187	0.35	0.54	22.3	18.6

* = peak values

EXPT = experimental

R.S. = response spectrum analysis

TABLE 5.3 Analyses of FD Model

SIGNAL	SPAN	PGA [g]	*ROOF DISPL. [in.]		*BASE SHEAR [kips]	
			EXPT	ANAL	EXPT	ANAL
El Centro	200	0.394	1.38	1.10	51.4	37.5
	300	0.555	2.14	1.55	67.2	47.4
	400	0.712	2.73	1.95	78.1	59.7
Taft	300	0.610	2.24	1.30	66.6	41.6
	400	0.839	1.41	1.41	51.0	41.8
Miyagi	350	0.424	1.72	1.75	57.7	50.2
Chile.u	400	0.737	2.60	1.72	57.3	52.4
	500	0.869	2.79	2.08	61.7	61.1
	750	1.202	2.86	2.55	61.1	73.1
La Union	750	0.862	2.83	2.53	67.2	74.5
Zacatula	750	0.710	2.73	1.68	55.4	54.7

* = peak values
EXPT = experimental
ANAL = analytical

TABLE 5.4 Analyses of MRF and CBF Models

SIGNAL	SPAN	PGA [g]	PEAK ROOF DISPL. [in.]		
			MRF	CBF	FD*
El Centro	400	0.712	3.56	2.42	2.73
Taft	400	0.839	2.50	1.48	1.41
Miyagi	350	0.424	3.45	1.75	1.72
Chile.u	750	1.202	4.49	4.18	2.86
La Union	750	0.862	4.11	3.86	2.83
Zacatula	750	0.710	3.18	2.64	2.73

* = experimental results

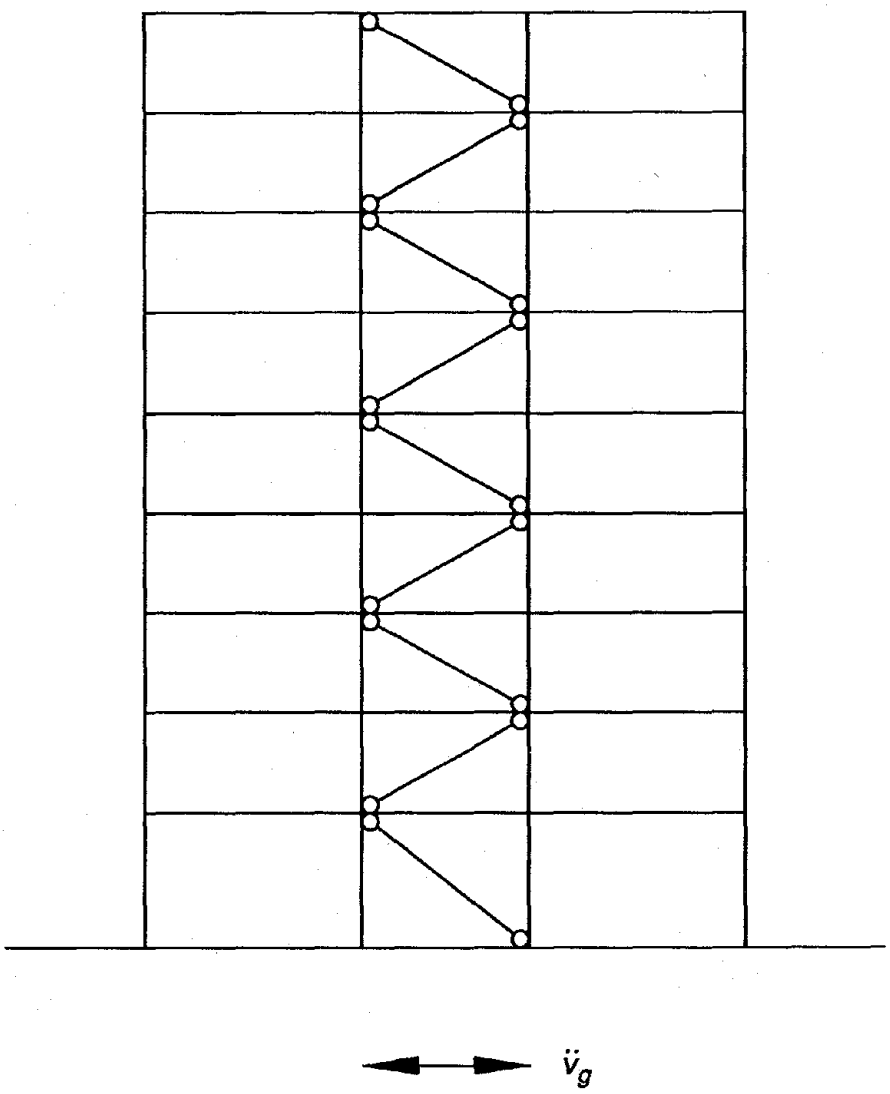

Fig. 5.1 Computer Model for Analyses of VD Structure

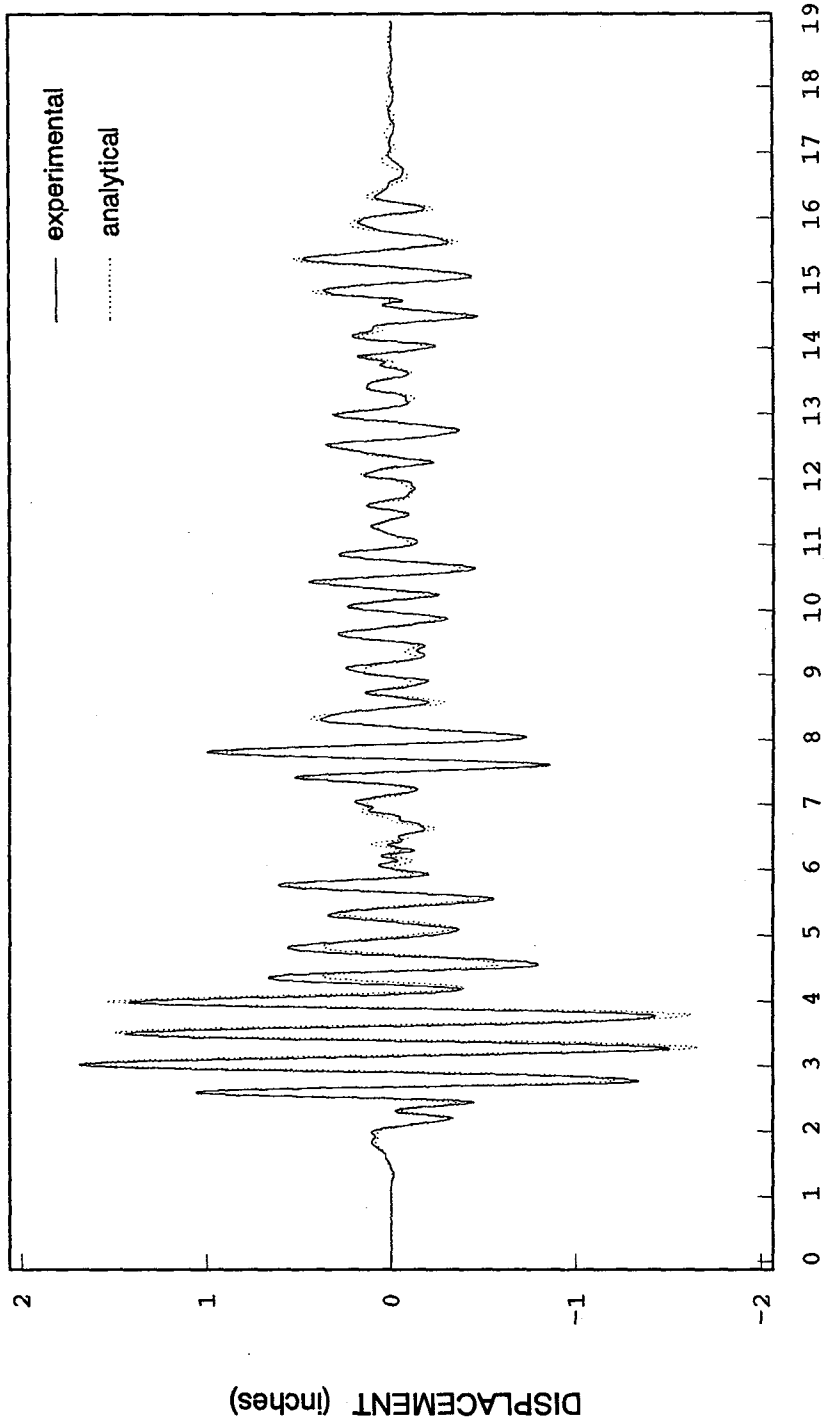

Fig. 5.2 VD Experimental and Analytical Roof Time Histories, ec-250 Input

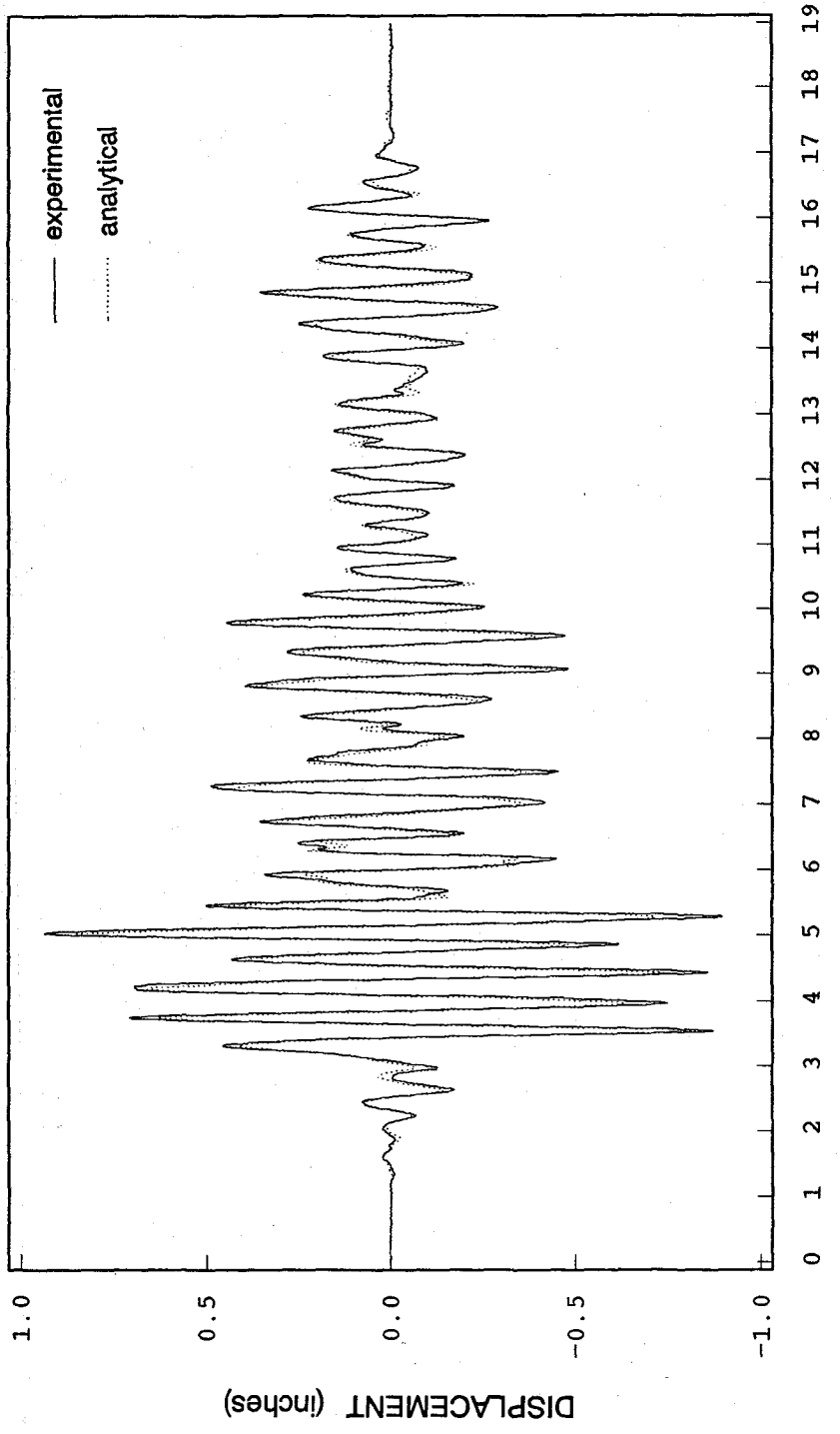

Fig. 5.3 VD Experimental and Analytical Roof Time Histories, taft-200 Input

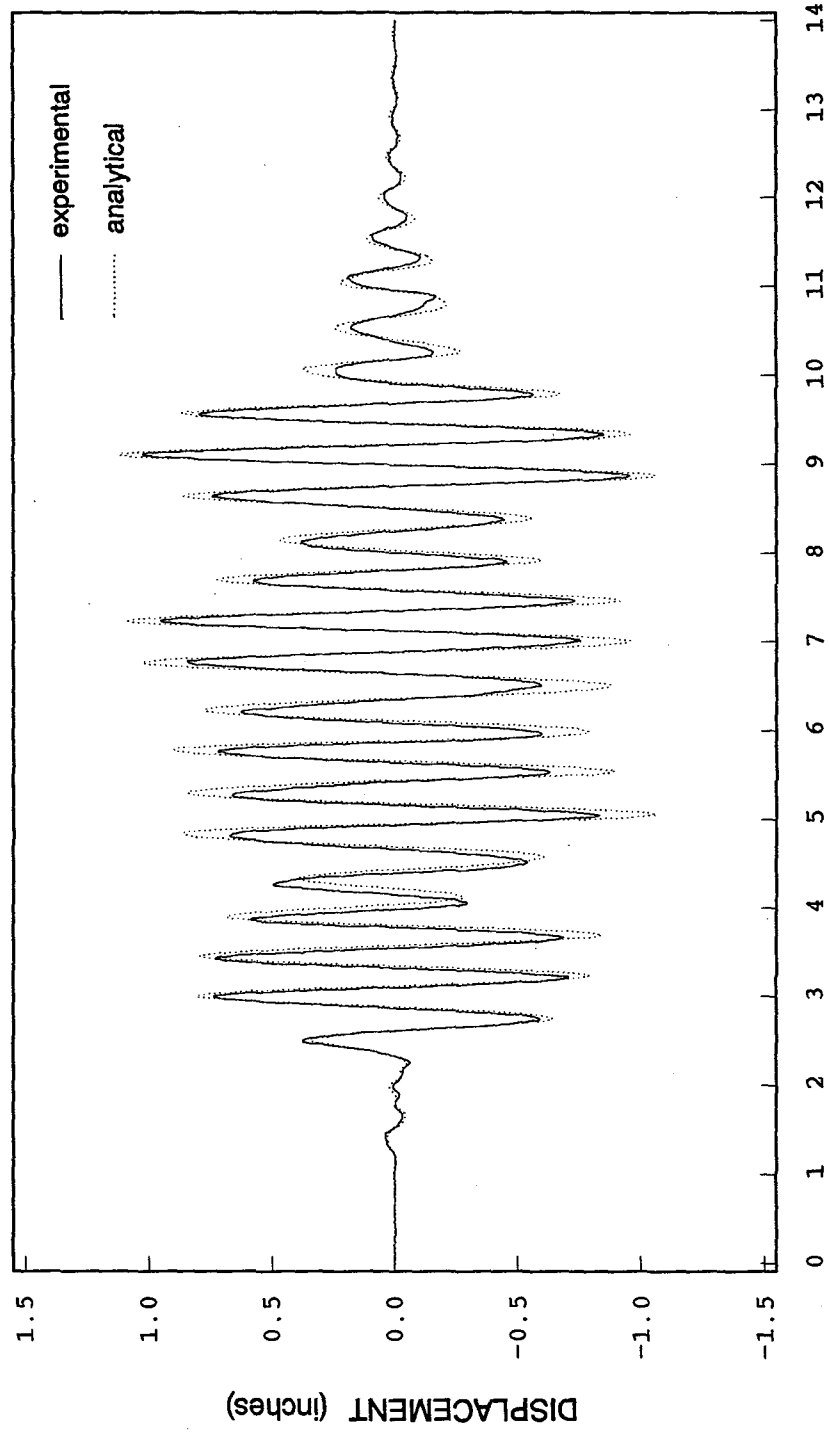

Fig. 5.4 VD Experimental and Analytical Roof Time Histories, miyagi-200 Input

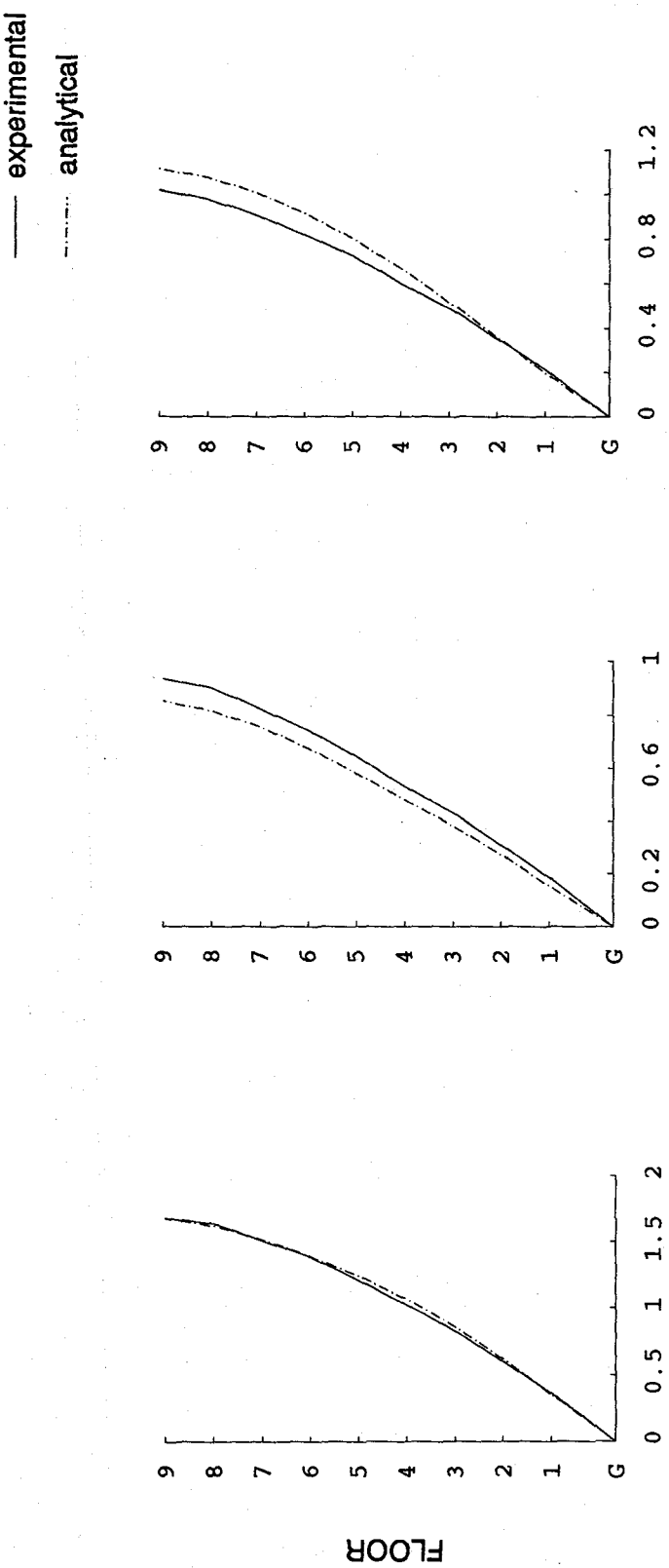

Fig. 5.5 VD Experimental and Analytical Peak Displacement Profiles

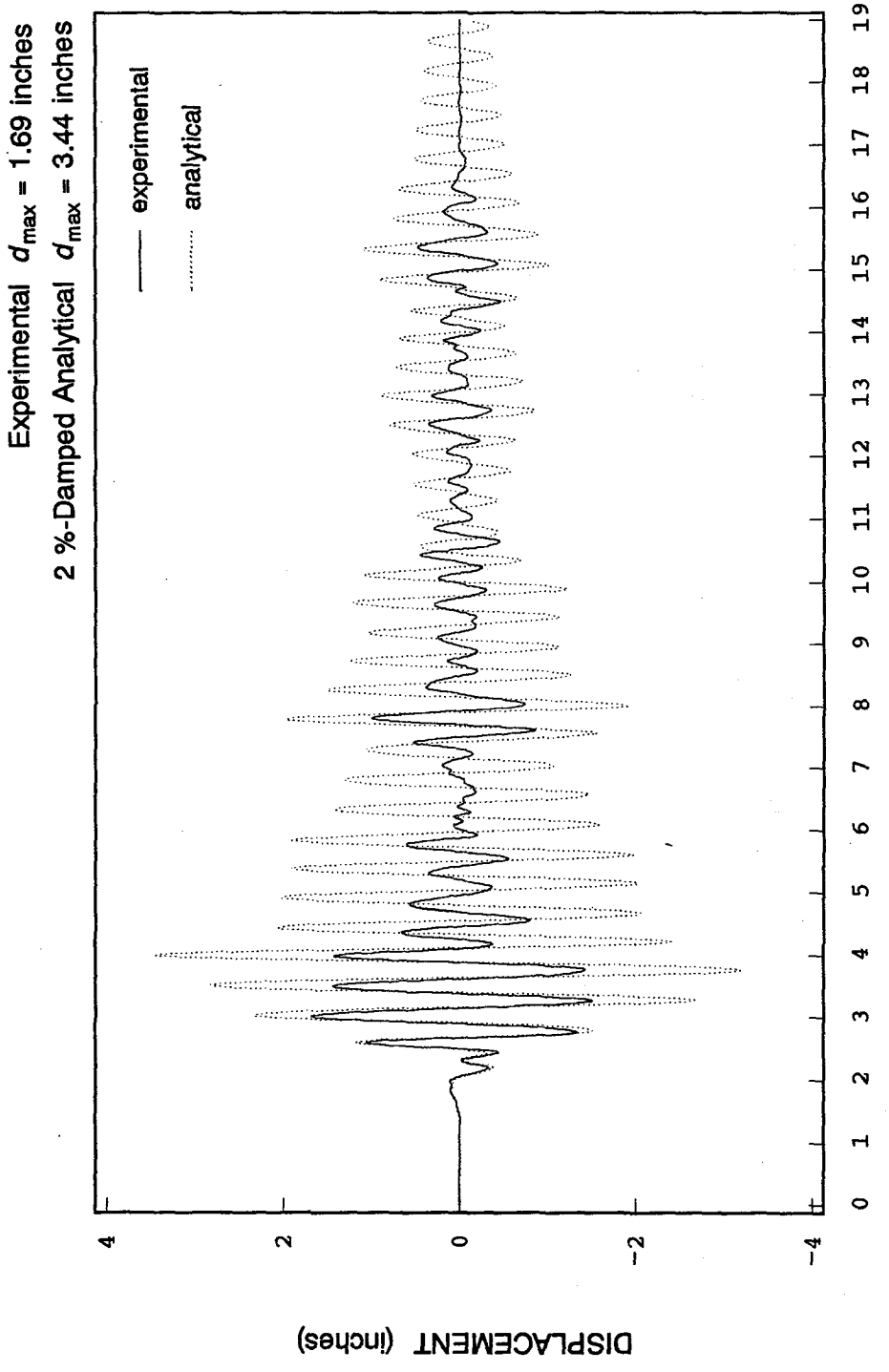

Fig. 5.6 VD Experimental and Two Percent Damped Analytical Roof Time Histories, ec-250 Input

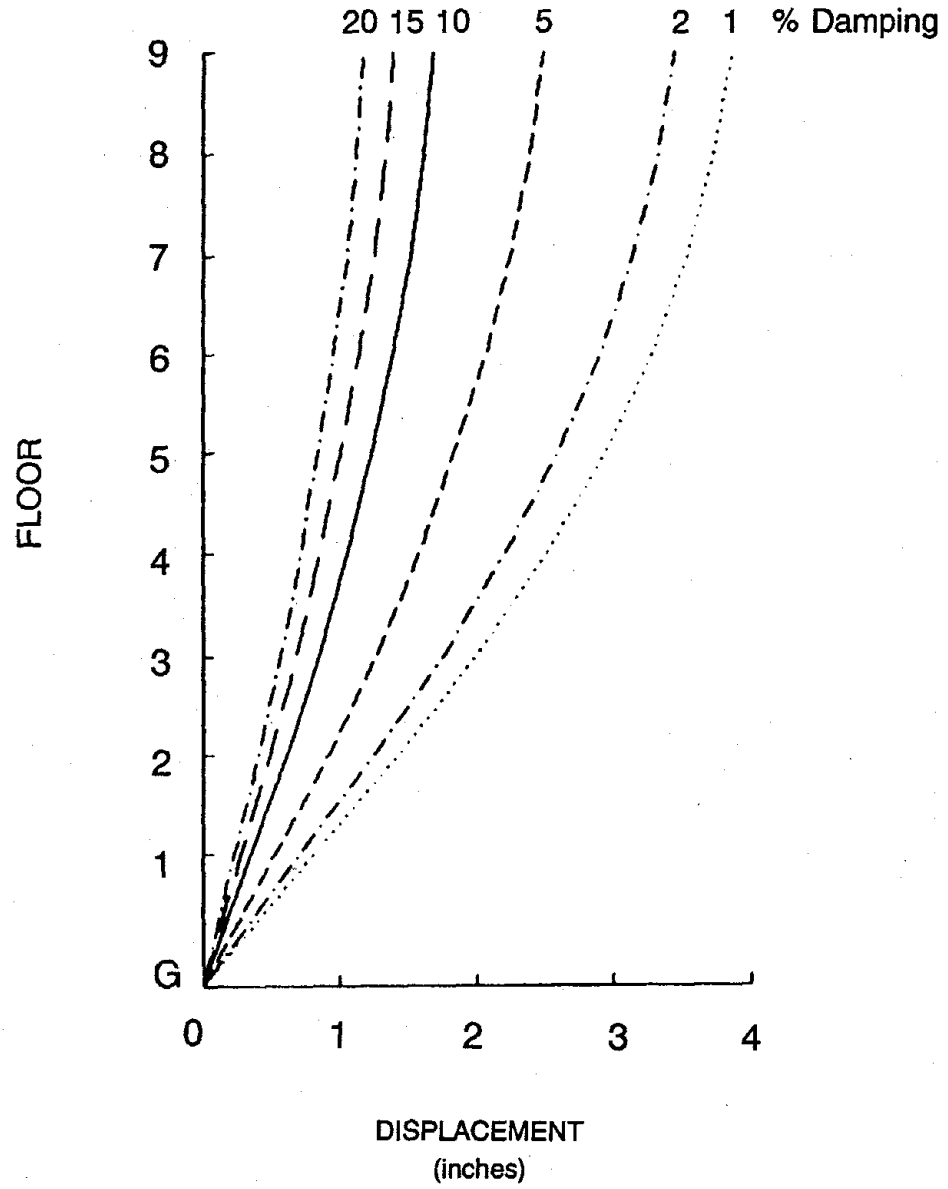

INPUT: ec-250
PGA = 0.486g

Fig. 5.7 Analytical Displacement Profiles for 1 — 20 Percent Damping

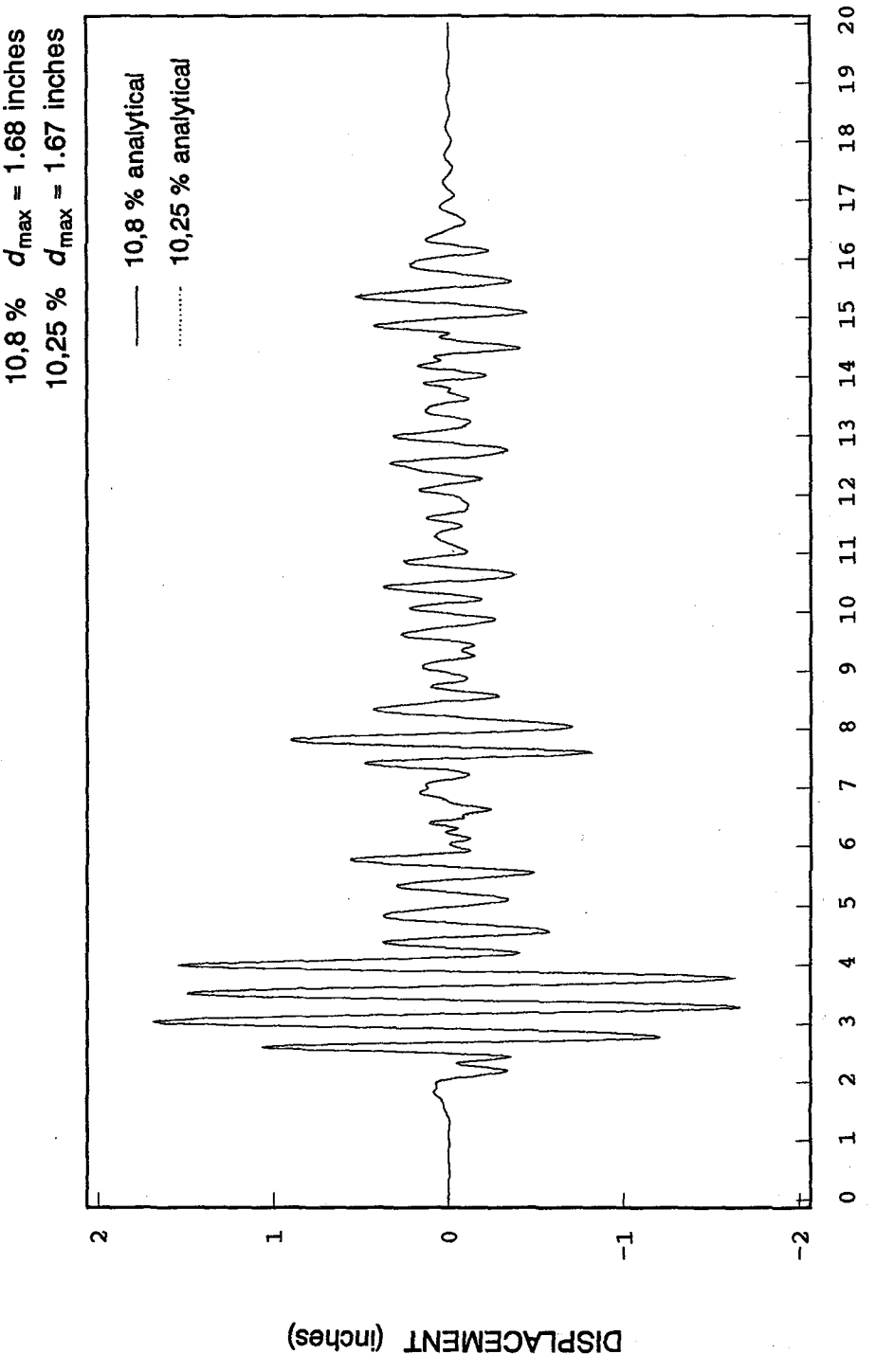

Fig. 5.8 VD Experimental and Analytical Roof Time Histories, Higher Mode Damping Varied, ec-250 Input

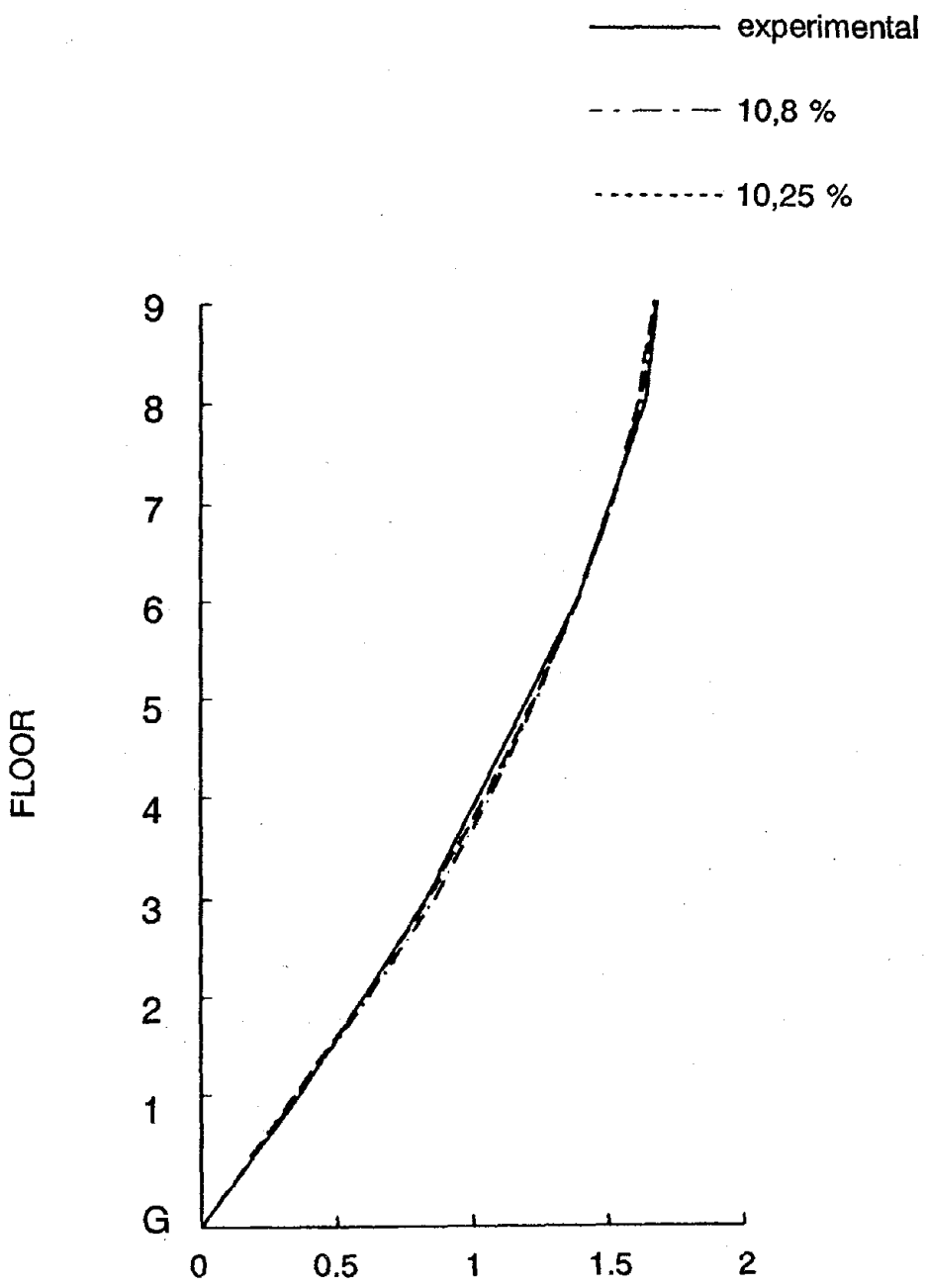

INPUT: ec-250
PGA = 0.486g

Fig. 5.9 VD Peak Displacement Profiles, Higher Mode Damping Varied

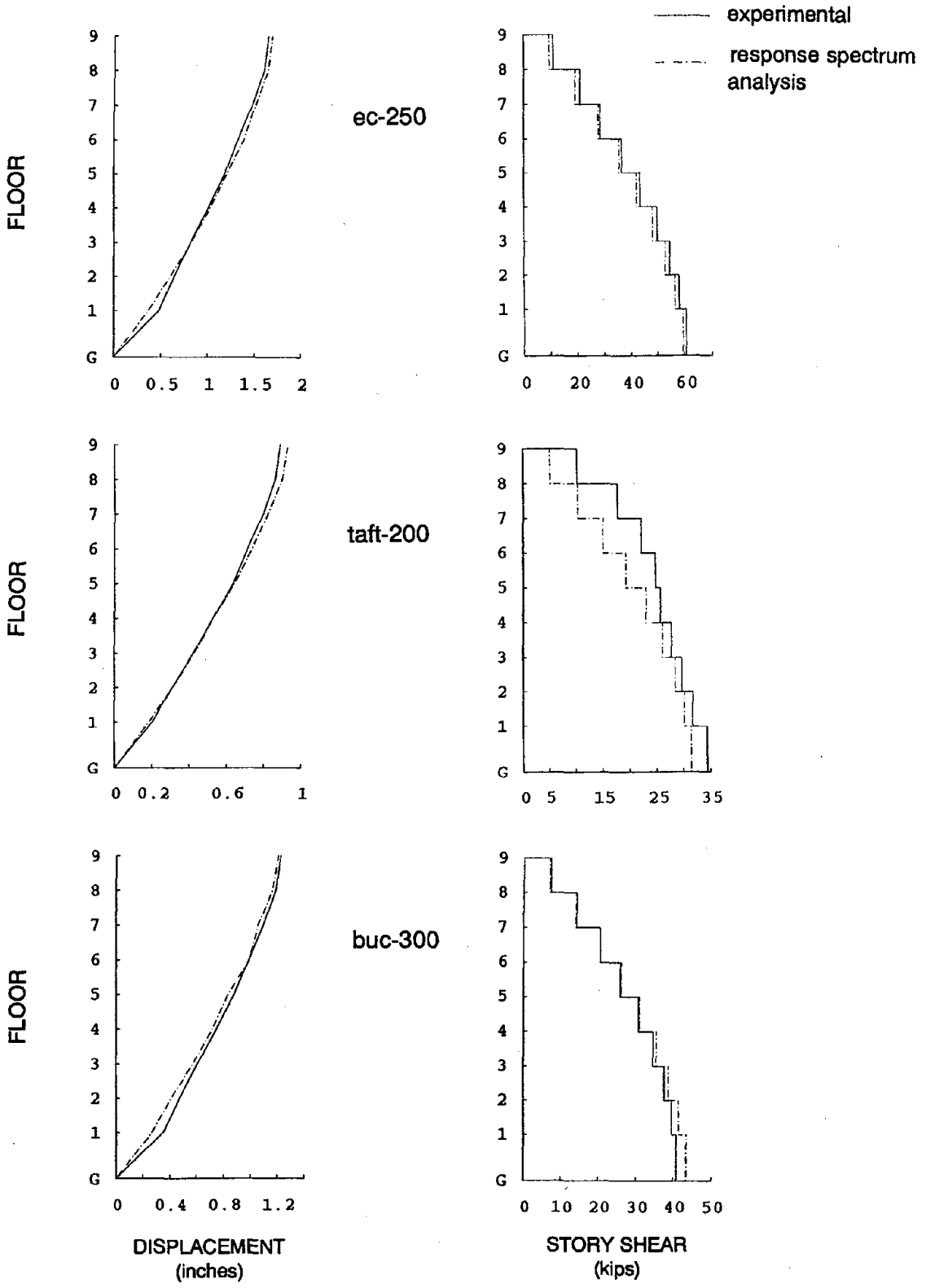

Fig. 5.10 VD Peak Displacements and Story Shears, Experimental and Response Spectrum Analyses, ec-250, taft-200, and buc-300 Inputs

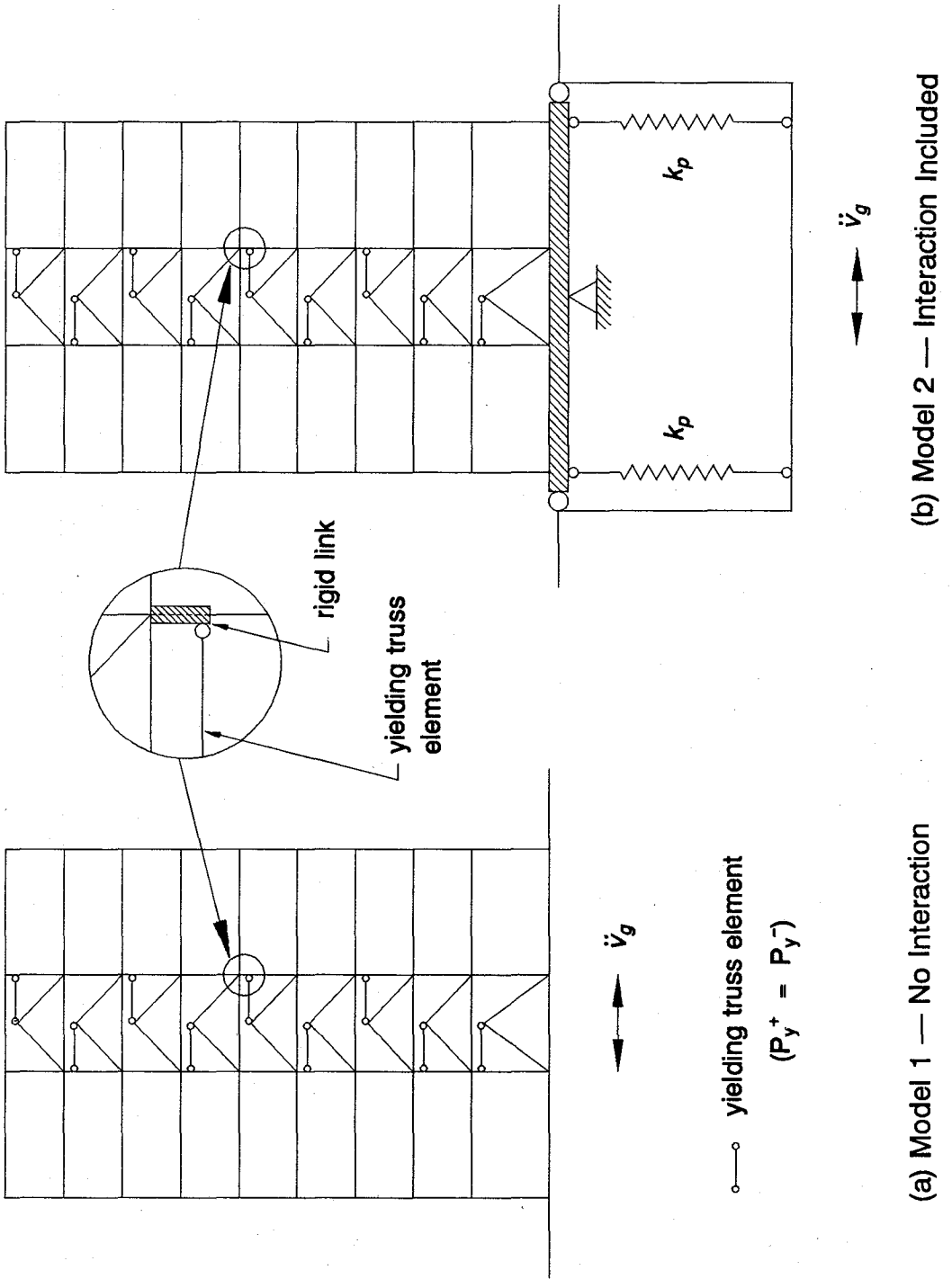

(a) Model 1 — No Interaction (b) Model 2 — Interaction Included

Fig. 5.11 Computer Models for Analyses of FD Structure

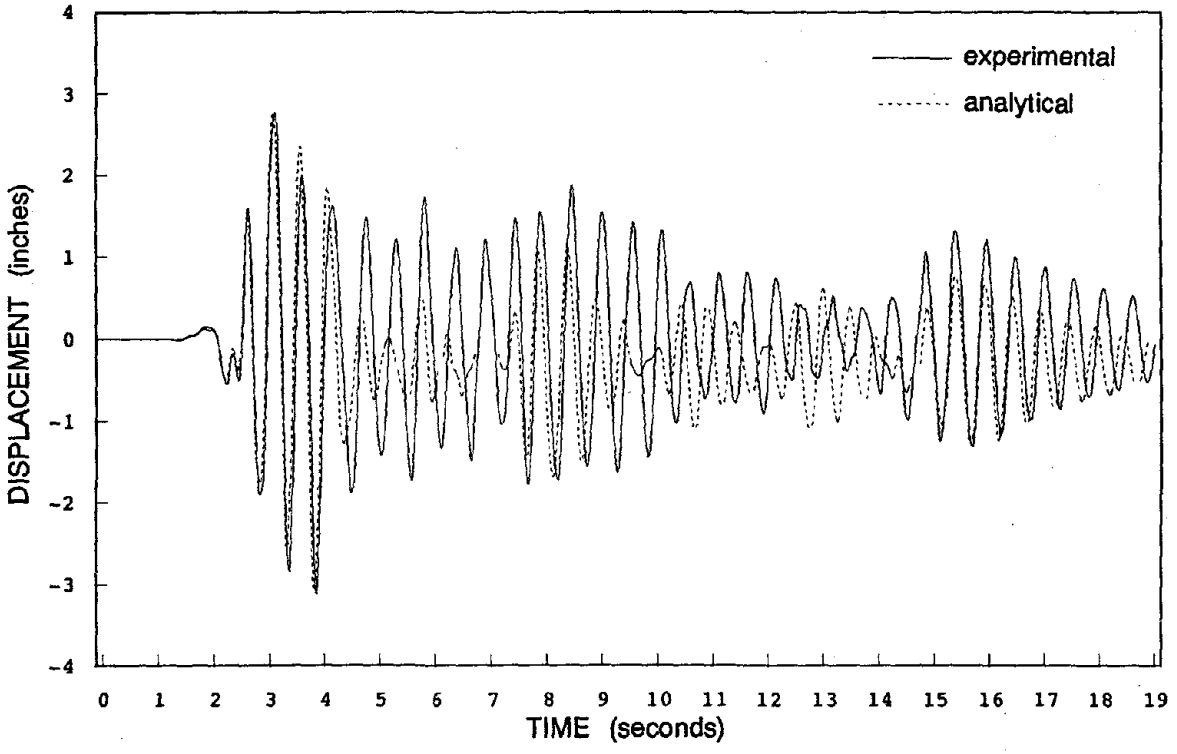

(a) No Table-Structure Interaction

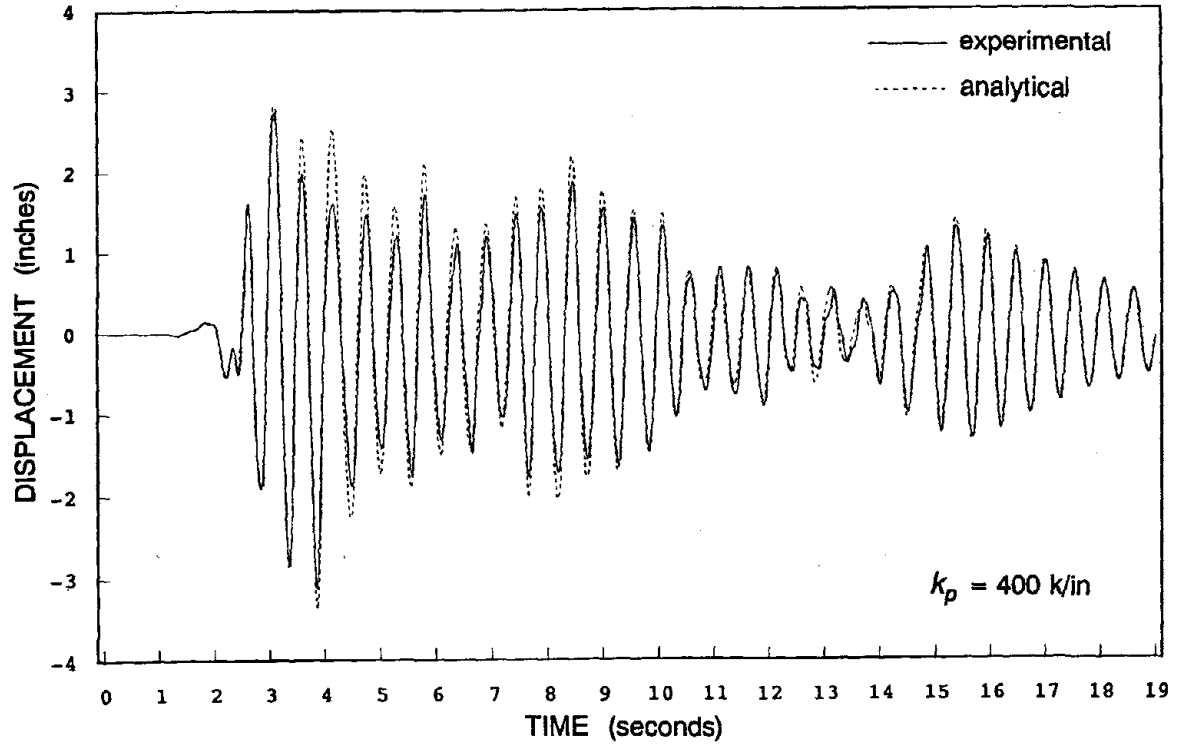

(b) Table-Structure Interaction Included

Fig. 5.12 MRF Experimental and Analytical Roof Time Histories, Without and With Table Interaction, ec-300 Input

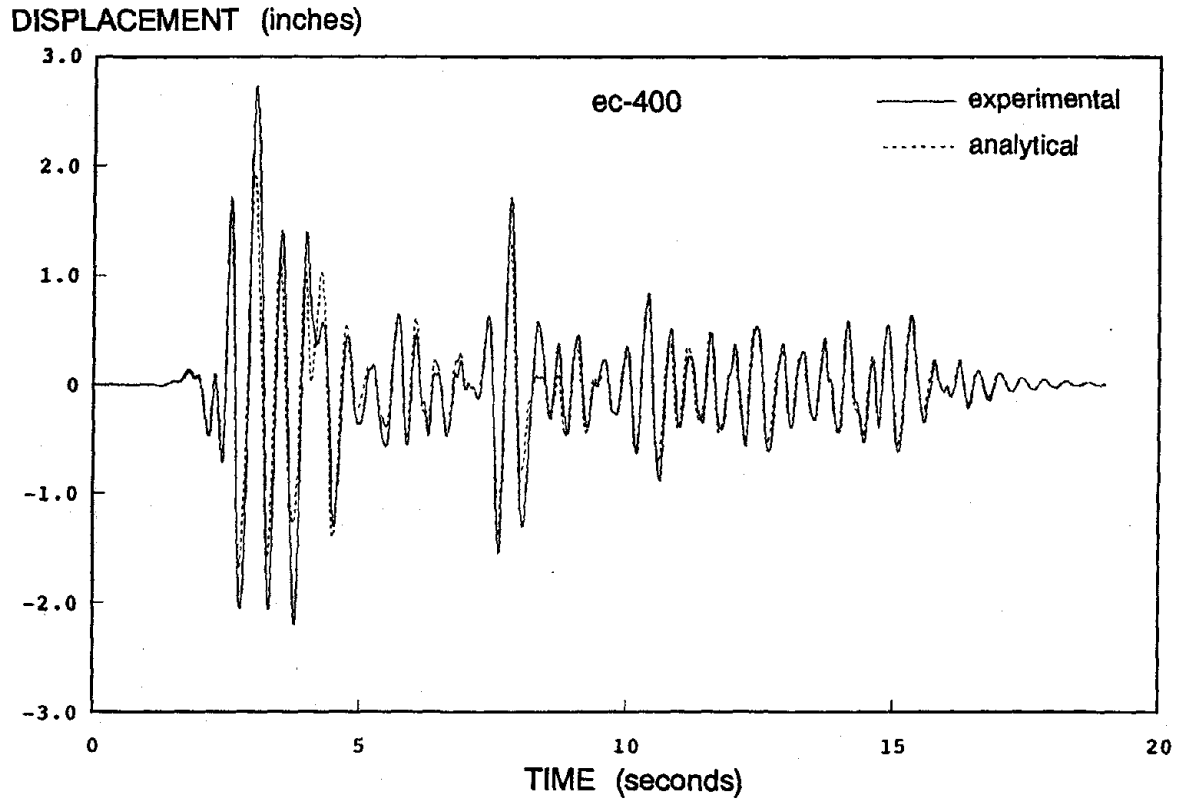

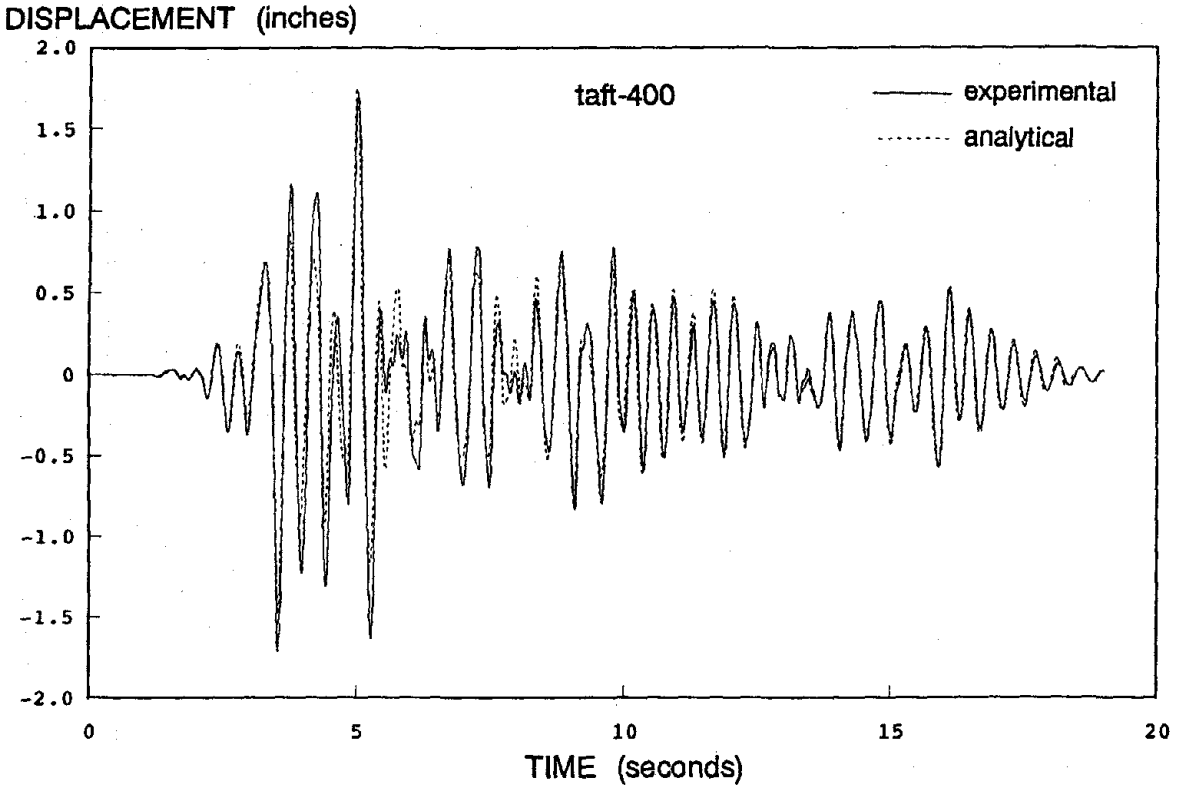

Fig. 5.13 FD Experimental and Analytical Roof Time Histories, Various Inputs

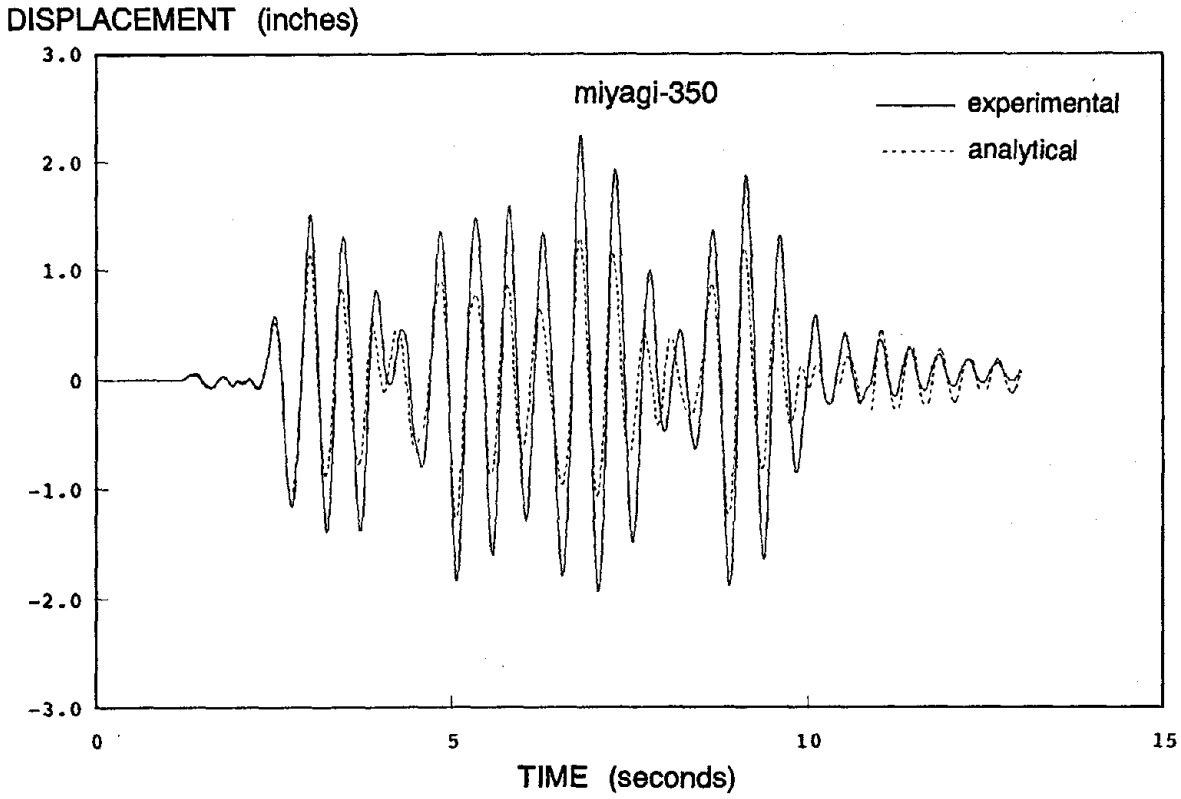
DISPLACEMENT (inches)
miyagi-350
experimental
analytical
3.0
2.0
1.0
0
-1.0
-2.0
-3.0
0
5
10
15
TIME (seconds)

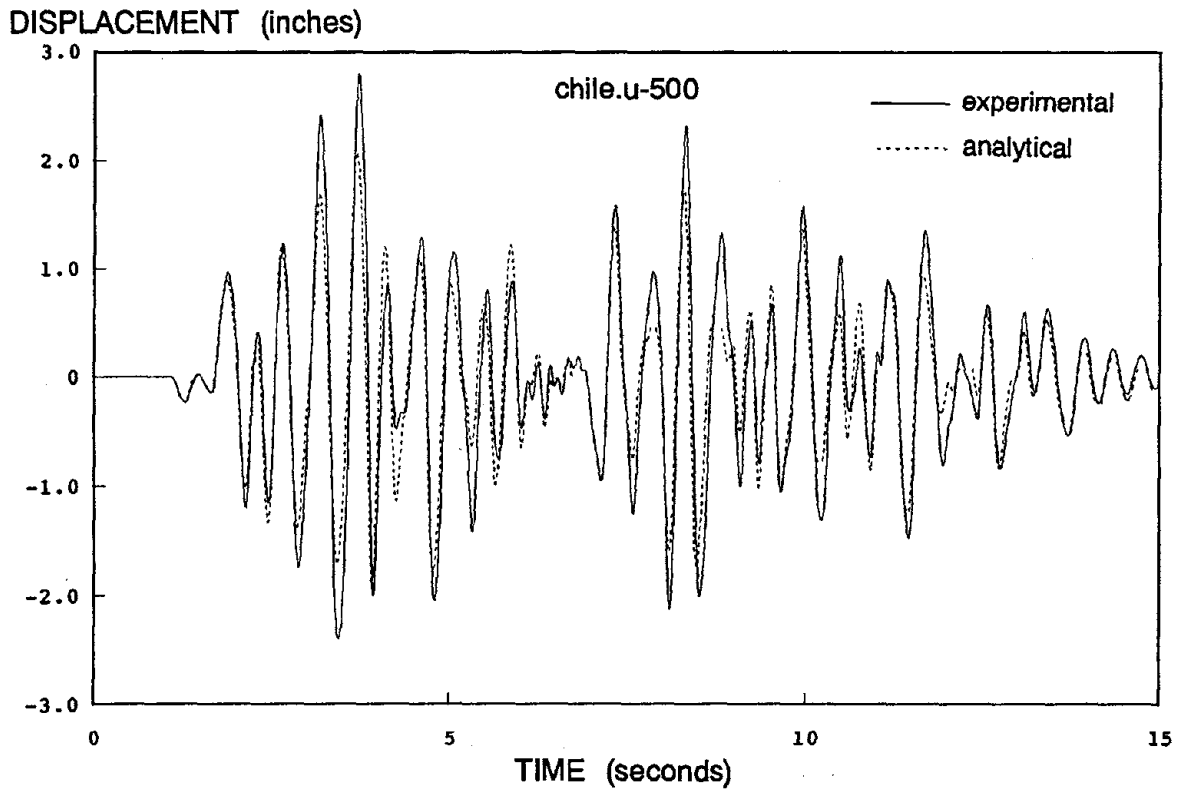
DISPLACEMENT (inches)
chile.u-500
experimental
analytical
3.0
2.0
1.0
0
-1.0
-2.0
-3.0
0
5
10
15
TIME (seconds)

Fig. 5.13 cont.

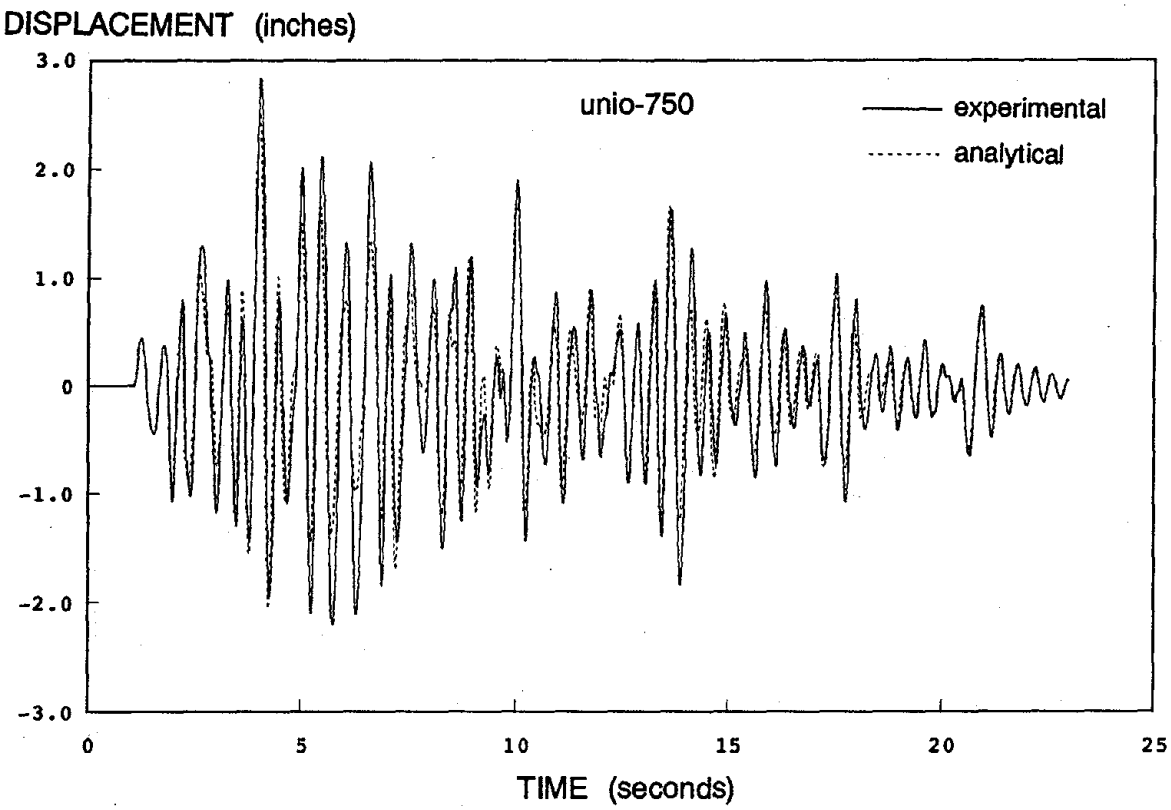
DISPLACEMENT (inches)
unio-750
experimental
analytical
3.0
2.0
1.0
0
-1.0
-2.0
-3.0
0
5
10
15
20
25
TIME (seconds)

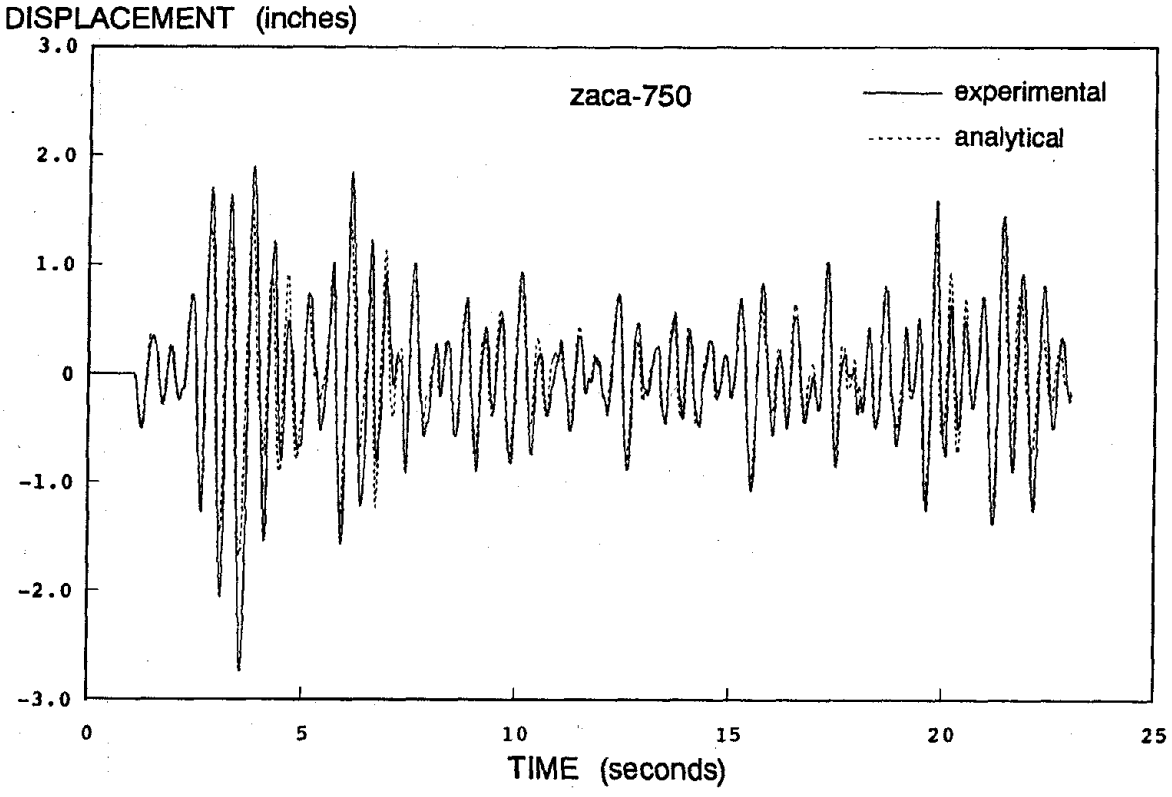
DISPLACEMENT (inches)
zaca-750
experimental
analytical
3.0
2.0
1.0
0
-1.0
-2.0
-3.0
0
5
10
15
20
25
TIME (seconds)

Fig. 5.13 cont.

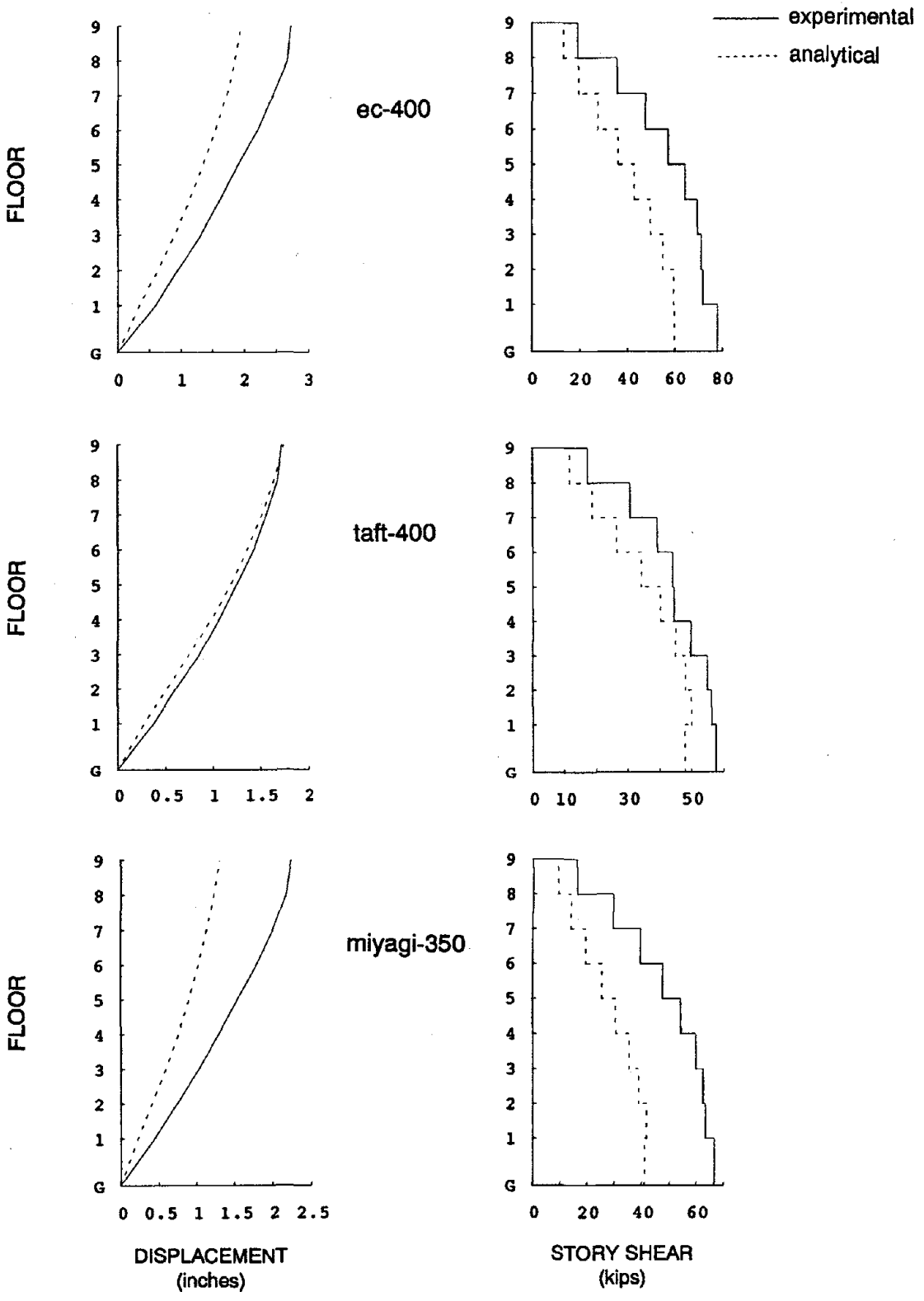

Fig. 5.14 FD Experimental and Analytical Peak Displacements and Story Shears, Various Inputs

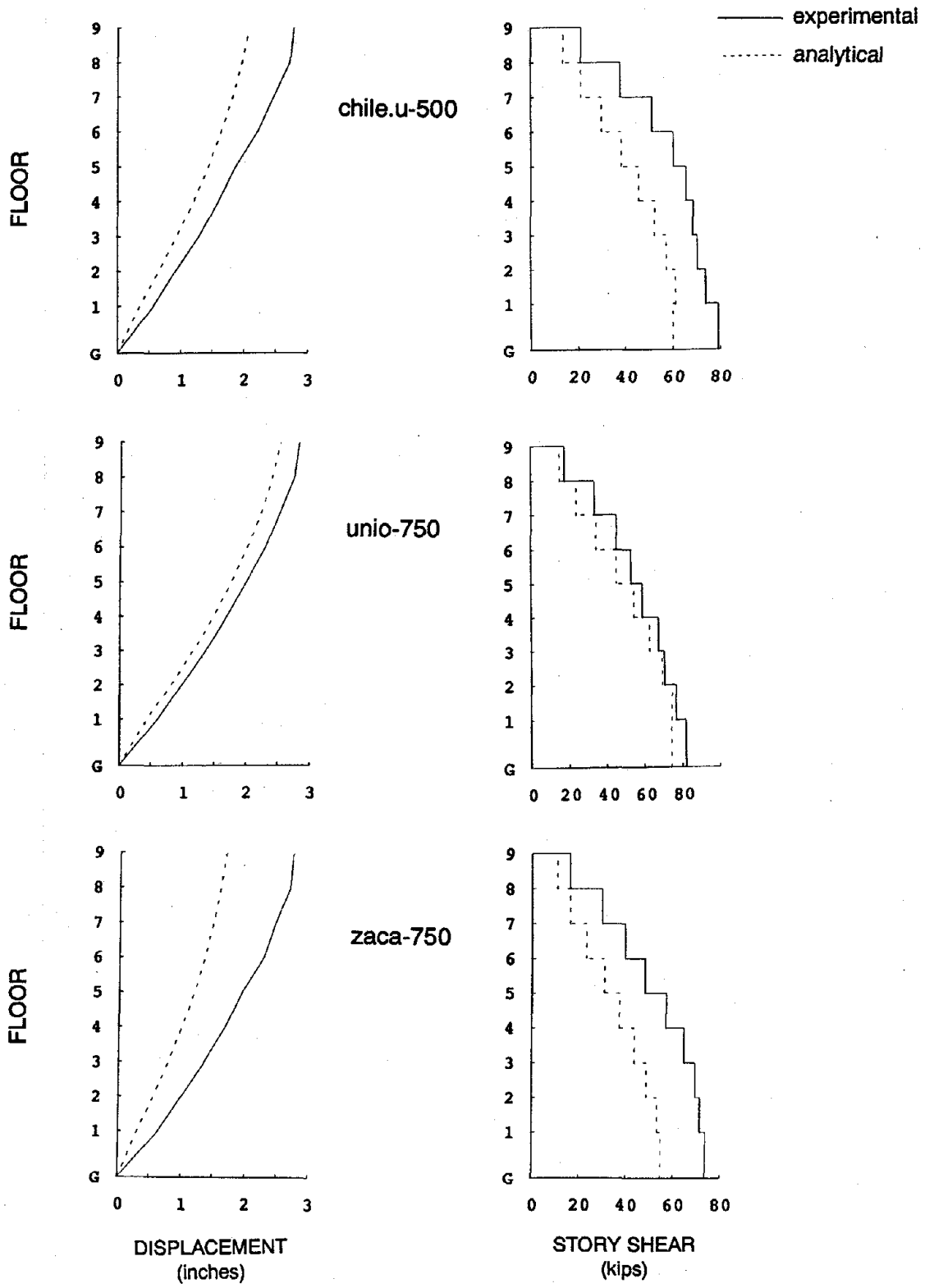
experimental
analytical
chile.u-500
unio-750
zaca-750
FLOOR
FLOOR
FLOOR
G 1 2 3 4 5 6 7 8 9
0 1 2 3
0 20 40 60 80
DISPLACEMENT
(inches)
STORY SHEAR
(kips)

Fig. 5.14 cont.

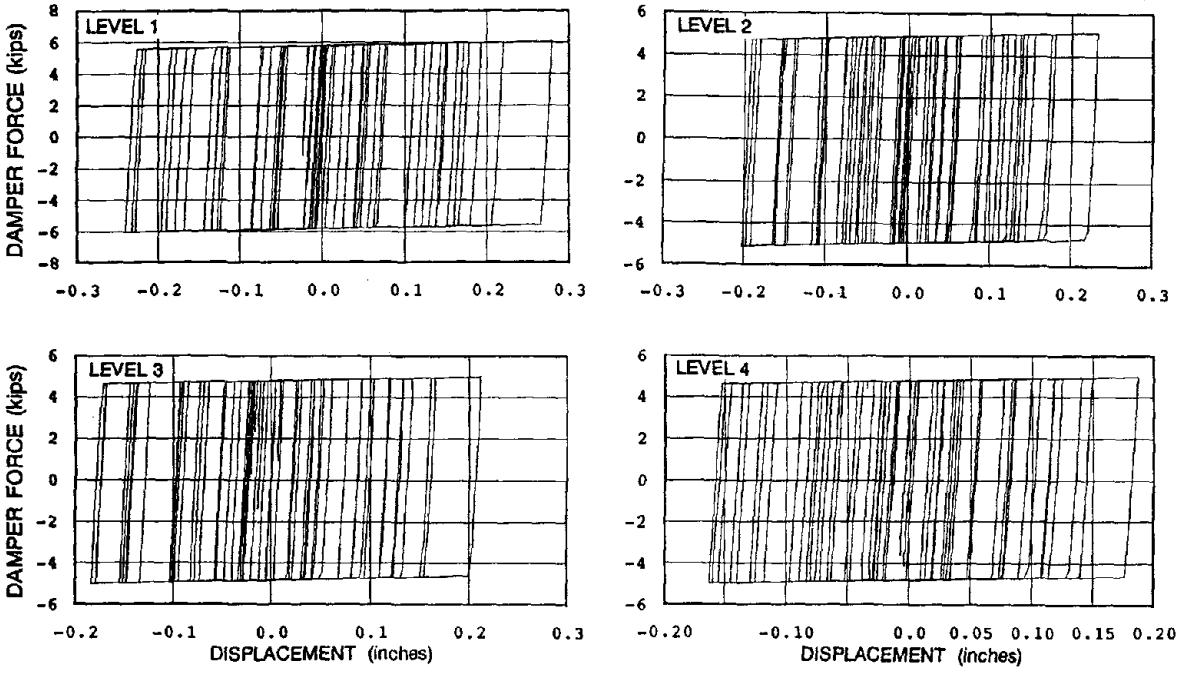

(a) Chile.u-750 Input

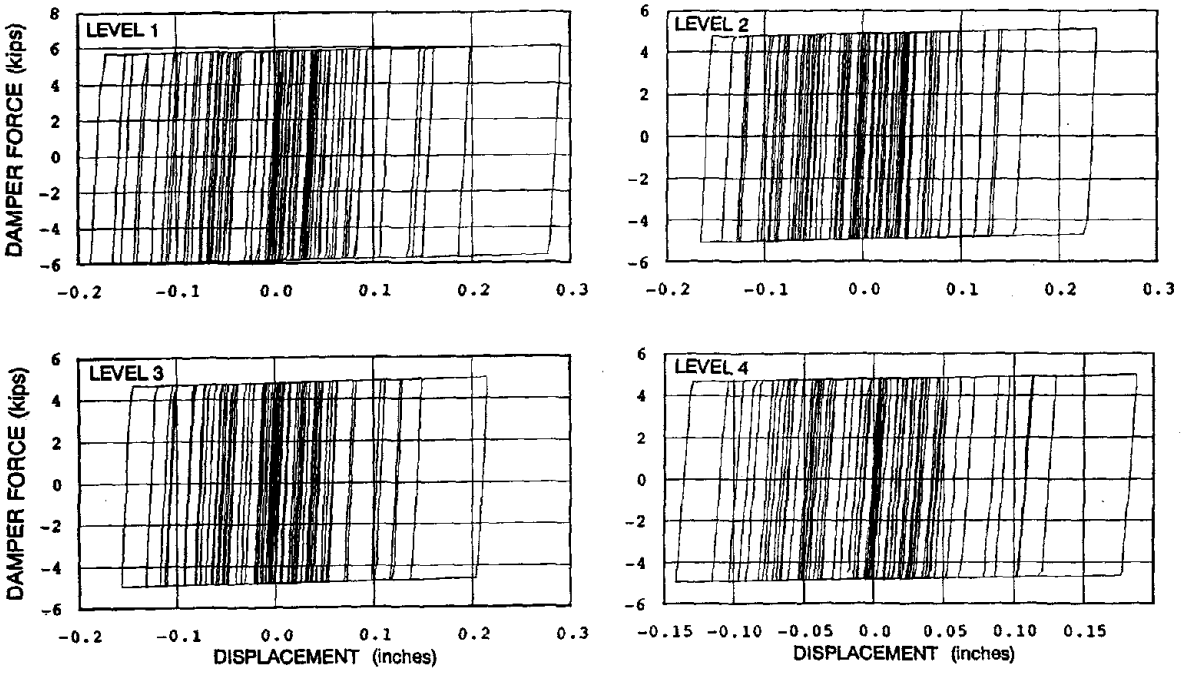

(b) Unio-750 Input

Fig. 5.15 FD Analytical Force-Displacement Plots for Friction Damper Elements, chile.u-750 and unio-750 Inputs

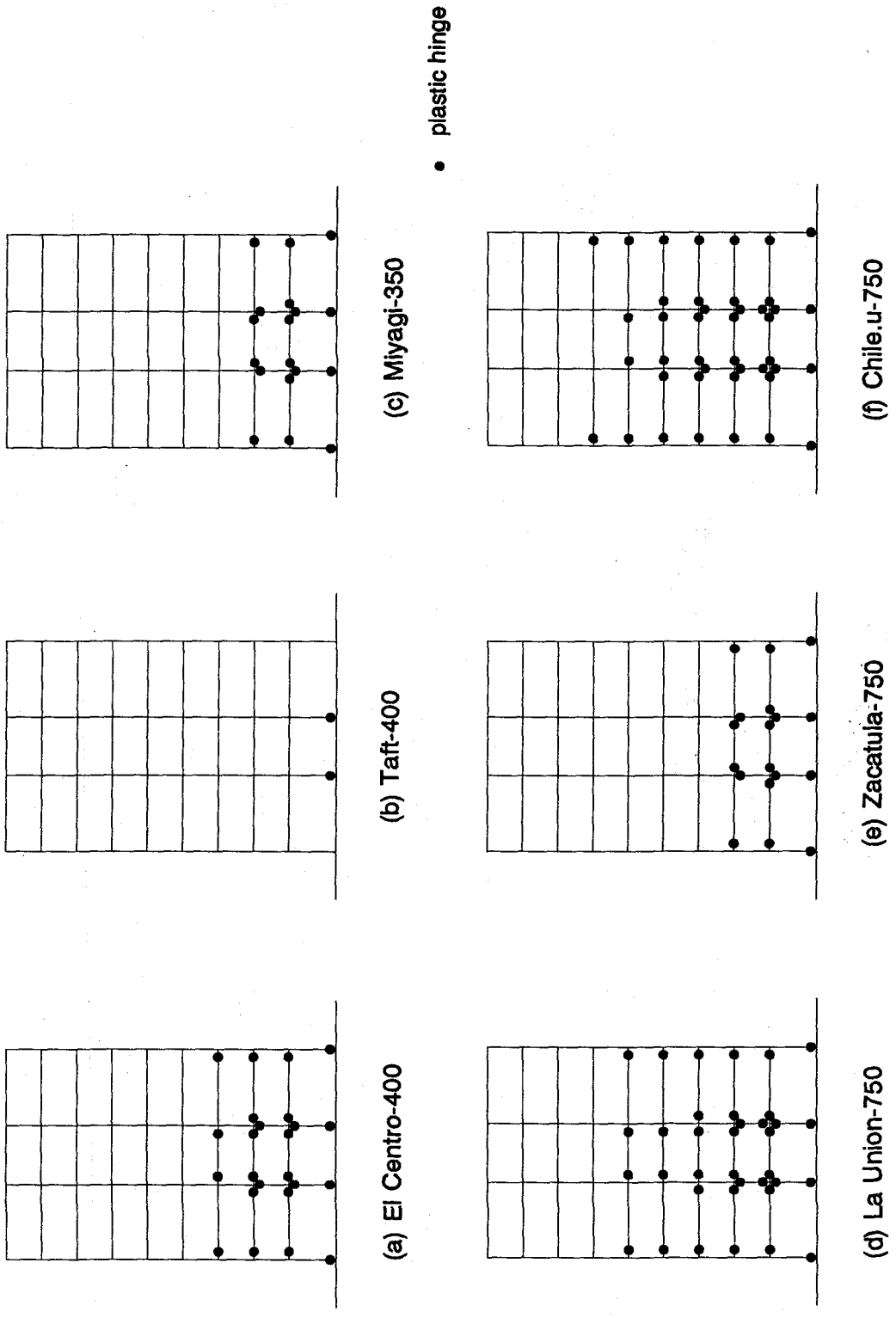

Fig. 5.16 Analytical Inelastic Demands in MRF for Various Inputs

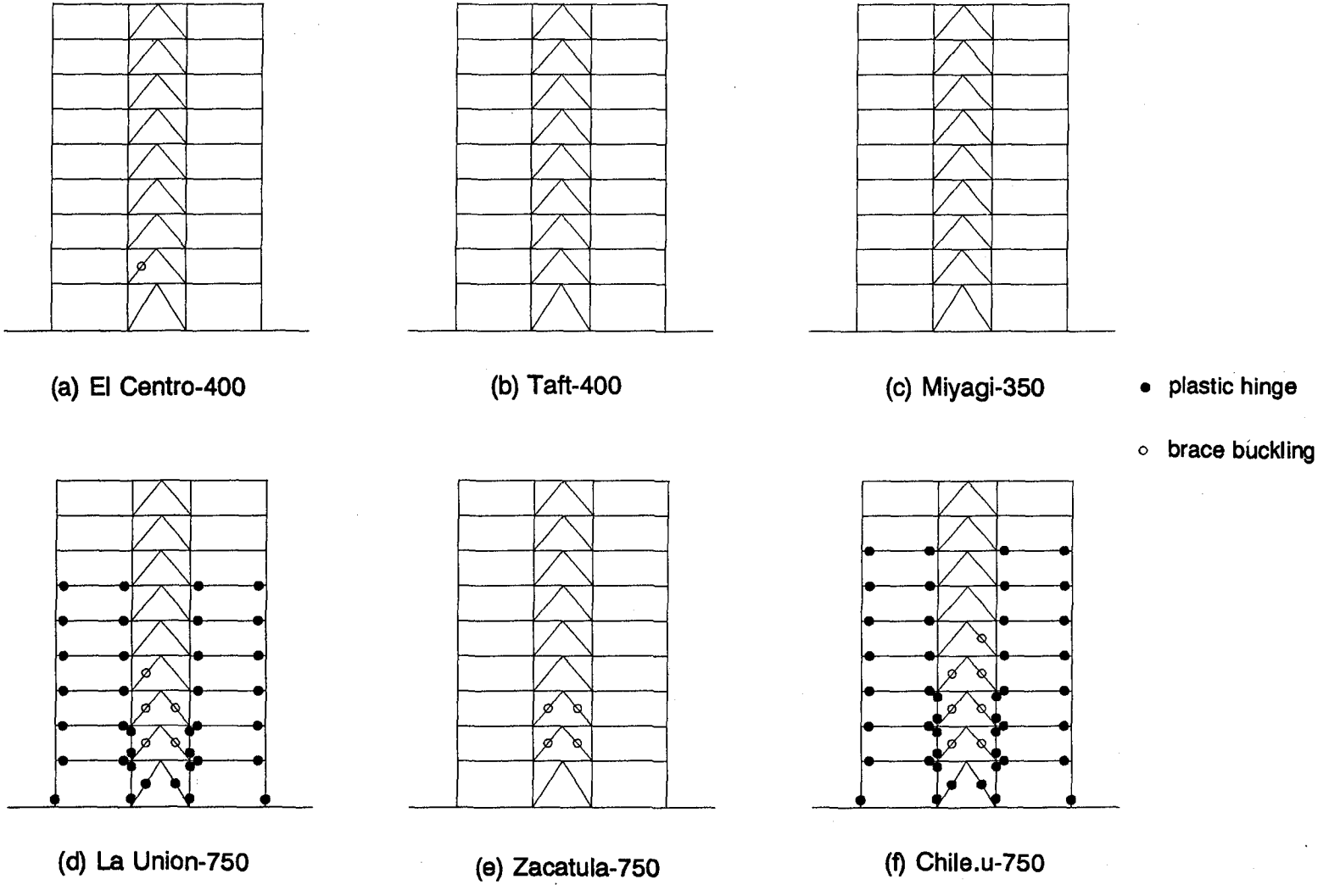

Fig. 5.17 Analytical Inelastic Demands in CBF for Various Inputs

CHAPTER 6

CONCLUSIONS

6.1 Summary and Conclusions

A combined experimental and analytical study of two different types of energy-absorbing systems for multistory structures has been presented. An existing large-scale, nine-story steel MRF was provided with viscoelastic dampers and then friction devices and subjected to an extensive program of earthquake simulator tests. The frame was also tested in moment-resisting and concentrically-braced configurations. The behavior of the dampers and their effect on the performance of the frame was studied, and a large number of comparisons between the different structural systems have been made. Analytical studies of both damped systems were performed and very good correlation with experimental results was obtained in both cases. The good experimental-analytical correlation obtained should provide the confidence necessary for future analytical parametric studies of the two types of damping systems and be a foundation for design studies and practical implementation.

The following sections summarize the important results.

Comparisons of Structural Systems

Separate comparisons of the VD and FD systems with the "undamped" MRF and CBF showed that both damped systems behaved similarly to the CBF in terms of story drifts and similarly to the MRF in terms of story accelerations and story shears. Making direct and detailed comparisons of the viscoelastic and friction-damped systems was not a primary objective of the research. However, the large number of earthquake tests performed on the two damped structural systems naturally presented some opportunity for comparison, and for a number of earthquakes global responses were compared. The VD and FD systems revealed themselves to be remarkably similar with regard to acceleration and displacement responses for

a wide selection of earthquake inputs. Peak base shears of the VD and FD models were compared for a range of input levels of the El Centro, Taft, and Miyagi signals and found to be very similar. They were approximately the same as, or less than, the MRF maximum base shears. These results were achieved while simultaneously reducing the drifts to as little as half those of the MRF for the same input. Floor response spectra were computed for the VD, FD, and MRF models and compared for a number of inputs. In almost all cases, the spectral accelerations for both damped systems were less than those of the MRF. For frequencies above about 12 Hz, the VD spectral accelerations were about half the FD accelerations. The results showed that neither type of energy absorber caused undesirable amplifications of high frequency responses.

The results are a clear example of the benefit of the energy-absorbing devices. For retrofit applications in particular, being able to reduce MRF drifts by as much as 50 %, to a level comparable with a conventionally braced structure, while not having to deal with the increased shears and foundation forces associated with the conventional bracing is a very attractive proposition. The energy absorbers also present obvious opportunities for improving the seismic performance of new construction.

Analyses

Two different methods were used for the analyses of the damped structures. In each case these were found to give particularly good correlation with experiment.

The linearity of the experimentally-observed VE damper stiffnesses over wide ranges of shear strain, combined with conclusions from other research [34] which found that viscous damping should provide an accurate analytical representation of the energy dissipation characteristics of VE dampers, were the reasons for selecting a linear elastic analysis approach for the VD model. The analytical model was given experimentally-identified values of modal damping, and brace elements with axial stiffness corresponding to the equivalent linear stiffness of the VE dampers. This approach was found to capture both the damping and stiffness charac-

teristics of the VE dampers accurately. Response spectrum analyses using a fixed value of damping and only one mode of vibration were performed for all of the earthquake tests of the VD model. These too, produced good results, with displacements and story shears typically within 10 percent of experiment, although in a few cases up to 20 percent.

Nonlinear analyses using the program DRAIN-2D were undertaken for the FD model. Existing elements were used to model the "rigid-perfectly-plastic" behavior observed for the friction devices. Good results were obtained for all of the analyses. The very stable rectangular hysteretic behavior of the Sumitomo friction dampers makes them particularly amenable to bilinear modeling. The same cannot be said of most other energy absorbers.

Design Methods

The design procedures used for the two damping systems both produced successful results. The response of the damped structures was considerably reduced from that of their "undamped" counterparts. The dampers prevented yielding of the frame under all of the earthquake motions used in the test programs. A number of observations relating to the design of the damping systems are made:

- The design of the VE dampers did not address the stiffness of the structure. In reality, however, this is likely to be an issue for both new construction and retrofit applications. For an existing structure of limited ductility, proper consideration should be given to the response of the structure incorporating the dampers, particularly with respect to likely maximum drifts. Although not necessarily a factor, drift control must be considered. The design approach of simply providing a specified level of damping to a structure at a certain displacement may well be insufficient in this regard.
- The design method used for the friction-damped system was comprehensive. Nonlinear time-history analyses were performed for a selection of earthquake motions, each at several different intensity levels. The selected distribution of damper forces was that which minimized the structure responses for the design inputs (subject to a few practical considerations).

The final test design produced good results for a wide range of earthquake inputs and intensity levels. This method, or something similar, would likely be that followed for the design of a prototype application. However, it is doubtful that structural engineers would adopt such an approach (based strongly as it is on nonlinear time-history analysis) as a routine design procedure. There is a need to investigate simplified design methods suitable for these systems. Filiatrault [56] has undertaken one such study and developed a simplified energy-based design method for one type of friction device.

Extension to Prototype — Practical Considerations

One of the obvious questions that stems from the success of the damper designs is the practicality of extending the designs to prototype conditions. In Chapter 4, the forces developed in the VE and friction dampers in the earthquake tests are studied with respect to the corresponding story shear forces. Story shears relate to the intensity of the input motion, so for the purposes of model-prototype comparisons, the ''sizes'' of the dampers are discussed in terms of the story mass associated with the damper.

The ratio of the volume of VE material in each story of the model to the corresponding story mass was 0.90 $inch^3$/kip. This was constant for all stories, with the exception of the top level. The corresponding prototype ratio is 3.60 $inch^3$/kip. This would not be an unreasonable ratio to achieve in practice. The single-diagonal brace configuration used in the experiments is only one of numerous possible installation details, and it may well be that for larger VE volume/mass ratios there will be more effective and/or economical installation configurations.

The friction damper design is considered in terms of the ratio of the total friction force per story to the corresponding story mass. This ratio varies according to the story friction forces (Fig. 2.6) from 1.05 at the bottom level to 0.44 at the top levels. This ratio scales 1:1 from the model to the prototype. The ratios at the bottom levels (1.05 and 0.88) are particularly large and it is questionable as to whether these would be economically achievable in practice. There is a cost premium associated with the outstanding performance characteristics of the

Sumitomo friction dampers, and this factor is bound to enter into the design decision-making process.

VE Dampers — Other Considerations

The damper temperatures recorded during earthquake shaking present little cause for concern. The largest temperature variations to which the dampers would be subjected are likely to be due to seasonal weather fluctuations. The actual temperature variations experienced by the dampers would be less than these, however, due to the location of the dampers in the skin of or within the building. The variation of the VE material properties that influence the energy dissipation of a damper (Eq. 2.13) decrease further the overall temperature effect. At low temperatures, G'' is low, the stiffness is high and hence γ is small. At high temperatures, G'' is low, the stiffness is low, and hence γ is large. These changes tend to offset each other and reduce the variation of energy dissipation for temperature extremes. The VE dampers can be designed for the required characteristics at a mean temperature, and checked at the temperature extremes. At most, it is likely that only small changes to the design would be necessary.

6.2 Future Research

In conclusion, the following recommendations are offered:

(i) The retrofit design of a realistic structure using both types of energy absorber should be investigated. Emphasis should be placed on determining stiffness demands to reduce drifts, and the capability of the dampers and associated bracing to provide this required stiffness.

(ii) The development of simplified design procedures for both types of energy absorbers should be pursued.

(iii) The identification of VE material properties relevant to the seismic design environment should be undertaken, and presented in material property charts or data sheets suitable for use by the designer.

(iv) The suitability of using recently-developed high damping spectra in the design of

viscoelastically-damped structures should be investigated.

(v) Studies of the long term performance of both types of dampers should be pursued. In particular, VE material property changes over long periods of time should be monitored, and friction damper performance after long durations of inactivity should be investigated. These are issues of particular interest to both prospective designers and building owners.

REFERENCES

[1] I. G. Buckle, "Development and Application of Base Isolation and Passive Energy Dissipation: A World Overview," *Proceedings of a Seminar and Workshop on Base Isolation and Passive Energy Dissipation ATC-17*, p. 153-174, Applied Technology Council, San Francisco, California, 1986.

[2] J. M. Kelly, "Progress and Prospects in Base Isolation," *Proceedings of a Seminar and Workshop on Base Isolation and Passive Energy Dissipation ATC-17*, p. 29-37, Applied Technology Council, San Francisco, California, 1986.

[3] R. I. Skinner, J. M. Kelly, and A. J. Heine, "Hysteretic Dampers for Earthquake-Resistant Structures," *International Journal of Earthquake Engineering and Structural Dynamics*, 3(3): 287-296, 1975.

[4] R. I. Skinner, R. G. Tyler, A. J. Heine, and W. H. Robinson, "Hysteretic Dampers for the Protection of Structures from Earthquakes," *Bulletin of the New Zealand National Society for Earthquake Engineering*, 13(1): 22-36, 1980.

[5] J. M. Kelly, "Base Isolation in Japan, 1988," *Report No. UCB/EERC-88/20*, Earthquake Engineering Research Center, University of California, Berkeley, December, 1988.

[6] C. W. Roeder and E. P. Popov, "Eccentrically Braced Steel Frames for Earthquakes," *Journal of the Structural Division*, 104(ST3): 391-412, American Society of Civil Engineers, March, 1978.

[7] E. P. Popov, K. Kasai, and M. D. Engelhardt, "Advances in Design of Eccentrically Braced Frames," *Earthquake Spectra*, 3(1): 43-55, February, 1987.

[8] A. S. Whittaker, C. M. Uang, and V. V. Bertero, "Earthquake Simulation Tests and Associated Studies of a 0.3-Scale Model of a Six-Story Eccentrically Braced Steel Structure," *Report No. UCB/EERC-87/02*, University of California, Berkeley, July, 1987.

[9] R. W. Henry, "Analysis of Braced Frame Energy Absorbers," *Report No. 392*,

Department of Civil Engineering, University of Auckland, Auckland, New Zealand, December, 1985.

[10] R. W. Henry, *Braced Frame Energy Absorbers: A Test Programme*, Department of Civil Engineering, University of Auckland, Auckland, New Zealand, November, 1986.

[11] R. G. Tyler, "Preliminary Tests on an Energy Absorbing Element for Braced Structures Under Earthquake Loading," *Bulletin of the New Zealand National Society for Earthquake Engineering*, 16(3): 201-212, 1983.

[12] R. G. Tyler, "Further Notes on a Steel Energy-Absorbing Element for Braced Frameworks Under Earthquake Loading," *Bulletin of the New Zealand National Society for Earthquake Engineering*, 18(3): 270-279, 1985.

[13] A. S. Whittaker, V. V. Bertero, J. L. Alonso, and C. L. Thompson, "Earthquake Simulator Testing of Steel Plate Added Damping and Stiffness Elements," *Report No. UCB/EERC-89/02*, University of California, Berkeley, 1989.

[14] R. G. Tyler, "Tapered Steel Cantilever Energy Absorbers," *Bulletin of the New Zealand National Society for Earthquake Engineering*, 11(4): 282-294, 1978.

[15] S. F. Stiemer and W. G. Godden, "Shaking Table Tests of Piping Systems with Energy-Absorbing Restrainers," *Report No. UCB/EERC-80/33*, University of California, Berkeley, 1980.

[16] S. F. Stiemer, W. G. Godden, and J. M. Kelly, "Experimental Behavior of a Spatial Piping System with Steel Energy Absorbers Subjected to Simulated Differential Seismic Input," *Report No. UCB/EERC-81/09*, University of California, Berkeley, 1981.

[17] S. F. Stiemer and F. L. Chow, "Curved Plate Energy Absorbers for Earthquake Resistant Structures," in: *Proceedings, Eighth World Conference on Earthquake Engineering*, vol. 5, p. 967-974, San Francisco, California, 1984.

[18] P. R. Boardman, B. J. Wood, and A. J. Carr, "Union House — A Cross Braced Structure With Energy Dissipators," *Bulletin of the New Zealand National Society for*

Earthquake Engineering, 16(2), June, 1983.

[19] F. Arima, M. Miyazaki, H. Tanaka, and Y. Yamazaki, "A Study on Buildings with Large Damping Using Viscous Damping Walls," in: *Proceedings, Ninth World Conference on Earthquake Engineering*, vol. 5, p. 821-826, International Association for Earthquake Engineering, Tokyo-Kyoto, Japan, 1988.

[20] A. S. Pall and C. Marsh, "Response of Friction Damped Braced Frames," *Journal of Structural Engineering*, 108(ST6): 1313-1323, American Society of Civil Engineers, June, 1982.

[21] A. S. Pall, "Energy Dissipation Devices for Aseismic Design of Buildings," in: *Proceedings of a Seminar and Workshop on Base Isolation and Passive Energy Dissipation, ATC-17*, p. 223-232, Applied Technology Council, Palo Alto, California, 1986.

[22] A. Filiatrault and S. Cherry, *Performance Evaluation of Friction Damped Braced Steel Frames Under Simulated Earthquake Loads*, Department of Civil Engineering, University of British Columbia, Vancouver, Canada, November, 1985.

[23] I. D. Aiken, J. M. Kelly, and A. S. Pall, "Experimental Study of Friction Damping for Steel Frame Structures," in: *Proceedings, ASME PVP Conference*, vol. PVP-133, p. 95-100, American Society of Mechanical Engineers, Pittsburgh, Pennsylvania, June, 1988.

[24] A. S. Pall, V. Verganelakis, and C. Marsh, "Friction Dampers for Seismic Control of Concordia University Library Building," in: *Proceedings, Fifth Canadian Conference on Earthquake Engineering*, p. 191-200, Ottawa, Canada, 1987.

[25] D. Ruiz, F. Pablo, E. D. Valle, and A. S. Pall, "Hi-Tech Repair of Escuela de Medicina, Acapulco, Mexico," in: *Proceedings, Ninth World Conference on Earthquake Engineering*, p. 828, International Association for Earthquake Engineering, Tokyo-Kyoto, Japan, 1988. Abstract Volume 1, Paper GO9-06.

[26] R. G. Tyler, "Test on a Brake-Lining Damper for Structures," *Bulletin of the New*

Zealand National Society for Earthquake Engineering, 18(3): 280-284, 1985.

[27] R. Giacchetti, A. S. Whittaker, V. V. Bertero, and H. M. Aktan, "Seismic Response of a DMRSF Retrofitted with Friction Slip Devices," in: *Proceedings, International Meeting on Base Isolation and Passive Energy Dissipation*, Assisi, Italy, June, 1989.

[28] P. J. Richter, D. K. Nims, J. M. Kelly, and R. M. Kallenbach, "The EDR-Energy Dissipating Restraint, A New Device for Mitigating Seismic Effects," in: *Proceedings, 1990 Structural Engineers Association of California Convention*, Lake Tahoe, California, September, 1990.

[29] Z. Akbay and H. M. Aktan, "Intelligent Energy Dissipation Devices," in: *Proceedings, Fourth U.S. National Conference on Earthquake Engineering*, vol. 3, p. 427-435, Earthquake Engineering Research Institute, Palm Springs, California, May, 1990.

[30] K. Roik, U. Dorka, and P. Dechent, "Vibration Control of Structures Under Earthquake Loading by Three-Stage Friction-Grip Elements," *Earthquake Engineering and Structural Dynamics*, 16: 501-521, 1988.

[31] T. E. FitzGerald, T. Anagnos, M. Goodson, and T. Zsutty, "Slotted Bolted Connections in Aseismic Design for Concentrically Braced Connections," *Earthquake Spectra*, 5(2): 383-391, Earthquake Engineering Research Institute, 1989.

[32] C. J. Keel and P. Mahmoodi, "Designing of Viscoelastic Dampers for the Columbia Center Building," *Building Motion in Wind*, p. 66-82, American Society of Civil Engineers, New York, 1986.

[33] P. Mahmoodi and C. J. Keel, "Performance of Structural Dampers for the Columbia Center Building," *Building Motion in Wind*, p. 83-106, American Society of Civil Engineers, New York, 1986.

[34] D. Bergman and R. D. Hanson, "Characteristics of Viscoelastic Damping Devices," in: *Proceedings of a Seminar and Workshop on Base Isolation and Passive Energy Dissipation, ATC-17*, p. 231-240, Applied Technology Council, Palo Alto, California,

1986.

[35] R. C. Lin, Z. Liang, T. T. Soong, and R. H. Zhang, "An Experimental Study of Seismic Structural Response with Added Viscoelastic Dampers," *Technical Report NCEER-88-0018*, National Center for Earthquake Engineering Research, State University of New York at Buffalo, Buffalo, June, 1988.

[36] A. D. Nashif, D. I. G. Jones, and J. P. Henderson, *Vibration Damping*, John Wiley & sons, 1985.

[37] P. Mahmoodi, "Structural Dampers," *Journal of Structural Engineering*, 95(ST8): 1661-1672, American Society of Civil Engineers, August, 1969.

[38] *Sumitomo Friction Damper, Dynamic Test in the University of California at Berkeley*, Sumitomo Metal Industries, Ltd., June, 1988. In-House Report.

[39] *Effect of Sumitomo Friction Dampers on 1/4-Scaled 9-Story Test Frame*, Sumitomo Metal Industries, Ltd., August, 1988. In-House Report.

[40] *Report on Tests of Sumitomo Friction Dampers for University of California Project*, Sumitomo Metal Industries, Ltd., January, 1988. Letter Report.

[41] A. A. Huckelbridge, "Earthquake Simulation Tests of a Nine Story Steel Frame with Columns Allowed to Uplift," *Report No. UCB/EERC-77/23*, University of California, Berkeley, 1977.

[42] M. S. Yang, "Seismic Behavior of an Eccentrically X-Braced Steel Structure," *Report No. UCB/EERC-82/14*, University of California, Berkeley, September, 1982.

[43] M. C. Griffith, J. M. Kelly, and I. D. Aiken, "Experimental Evaluation of Seismic Isolation of a Nine-Story Braced Steel Frame Subject to Uplift," *Report No. UCB/EERC-88/05*, Earthquake Engineering Research Center, University of California, Berkeley, May 1988.

[44] D. Rea and J. Penzien, "Dynamic Response of a 20ft by 20ft Shaking Table," *Proceedings, Fifth World Conference on Earthquake Engineering*, 2: 1447-1456, Rome,

Italy, 1974.

[45] R. A. Becker and J. M. Chambers, *S — An Interactive Environment for Data Analysis and Graphics*, Wadsworth, California, 1984.

[46] "Tentative Provisions for the Development of Seismic Regulations for Buildings," *ATC 3-06*, Applied Technology Council, 1978.

[47] C. M. Uang and V. V. Bertero, "Earthquake Simulation Tests and Associated Studies of a 0.3-Scale Model of a Six-Story Concentrically Braced Steel Structure," *Report No. UCB/EERC-86/10*, University of California, Berkeley, December, 1986.

[48] D. M. Bergman and R. D. Hanson, "Characteristics of Mechanical Dampers," in: *Proceedings, Ninth World Conference on Earthquake Engineering*, vol. 5, p. 815-820, International Association for Earthquake Engineering, Tokyo-Kyoto, Japan, 1988.

[49] E. L. Wilson and A. Habibullah, *SAP90 — A Series of Computer Programs for the Static and Dynamic Finite Element Analysis of Structures, User's Manual*, Computers and Structures, Berkeley, California, 1989.

[50] R. H. Zhang, T. T. Soong, and P. Mahmoodi, "Seismic Response of Steel Frame Structures with Added Viscoelastic Dampers," *Earthquake Engineering and Structural Dynamics*, 18: 389-396, 1989.

[51] A. E. Kannan and G. H. Powell, "General Purpose Computer Program for Inelastic Dynamic Response of Plane Structures," *Report No. UCB/EERC-73/6*, University of California, Berkeley, 1973.

[52] *Private Communication, E. L. Wilson*, University of California at Berkeley, August, 1990.

[53] J. Wu and R. D. Hanson, "Inelastic Response of Structures with High Damping Subject to Earthquake Attack," *Report No. UCME 87-9*, Department of Civil Engineering, University of Michigan, Ann Arbor, November, 1987.

[54] J. M. Nau and W. J. Hall, "Scaling Methods for Earthquake Response Spectra," *Journal of the Structural Division*, 110(7): 1533-1548, American Society of Civil Engineers, July,

1984.

[55] K. Kawashima and K. Aizawa, "Modification of Earthquake Response Spectra With Respect to Damping Ratio," in: *Proceedings, Third U.S. National Conference on Earthquake Engineering*, vol. 2, p. 1107-1116, Earthquake Engineering Research Institute, Charleston, South Carolina, August, 1986.

[56] A. Filiatrault, *Seismic Design of Friction Damped Braced Steel Plane Frames by Energy Methods*, Department of Civil Engineering, University of British Columbia, Vancouver, Canada, November, 1988. PhD. Thesis.

[57] C. M. Uang and V. V. Bertero, "Use of Energy as a Design Criterion in Earthquake-Resistant Design," *Report No. UCB/EERC-88/18*, University of California, Berkeley, November, 1988.

APPENDIX A

Terminology and Notation

A.1 Notation

The following abbreviations are used to refer to the different configurations of the test structure:

MRF = moment-resisting frame

CBF = concentrically-braced frame

FD = friction-damped

VD = viscoelastically-damped

VE = viscoelastic

A.2 Terminology

Damping is a mechanism of **energy dissipation**. In structural and earthquake engineering, the use of the word **damping** is often associated with **viscous damping**. For example, reference to damping in the context of response spectra is usually assumed to mean viscous damping. The strict association of damping with viscous damping is *not* assumed in this research. **Damping**, where used, refers in the general sense to **energy dissipation**. In this context, **dampers**, **energy dissipators**, **energy absorbers**, **energy-dissipating devices**, and **energy-absorbing devices** are assumed to all refer to some sort of mechanism or device capable of absorbing and dissipating energy input to a structure.

The phrase **supplemental damping** has seen occasional use. It is not, however, used in this research. It refers to any method of supplementing or enhancing the **damping**, that is, the **energy dissipation** (capability), of a structure subject to seismic, wind or other types of loading.

Passive energy dissipation refers to any system with unvarying characteristics that provides energy dissipation to a structure. This is in contrast to **active control** or **active energy dissipation**, which are systems that possess dynamically varying response characteristics.

APPENDIX B

EARTHQUAKE SIMULATOR SPECIFICATIONS

TABLE B.1 Earthquake Simulator Specifications

plan dimensions	20′ x 20′
model tie-down locations	2" dia. holes on 36" c/c
max. model weight	130 kips
overhead clearance	40′ to ceiling 32′ to 10 ton gantry crane
overturning resistance	3343 kip-ft
displacement	horiz. ± 5 inches vert. ± 2 inches
velocity	horiz. ± 25 in/sec vert. ± 15 in/sec
acceleration	horiz. ± 1.5g vert. ± 1.0g
frequency response bandwidth	0 to 20 Hz

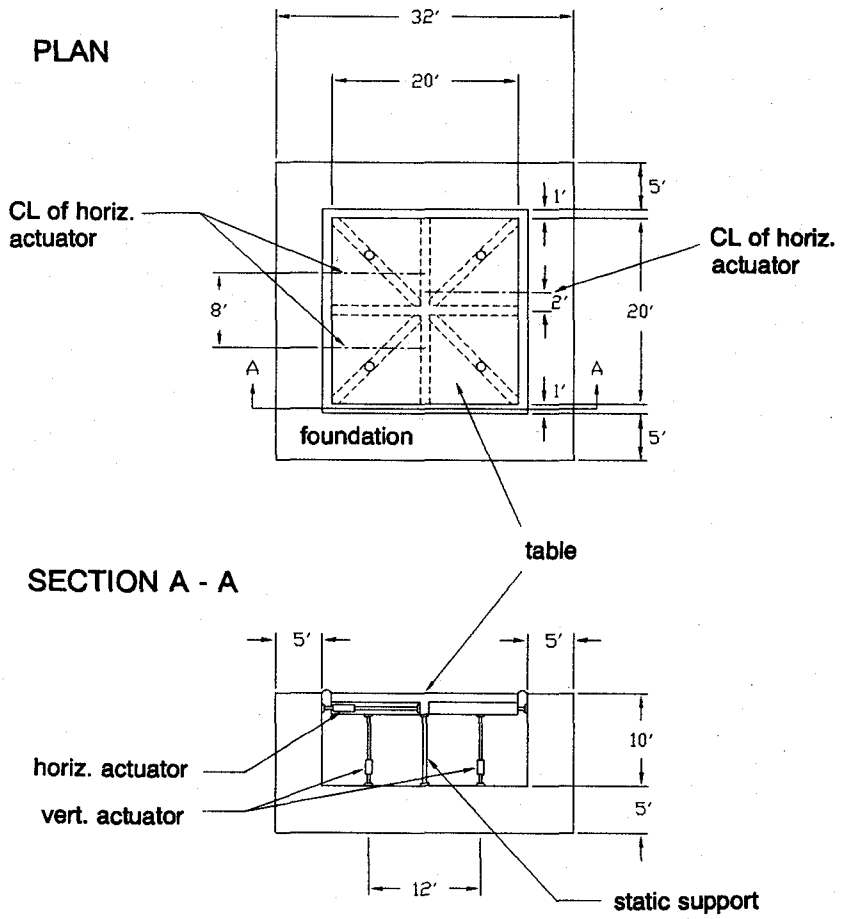

Fig. B.1 EERC Earthquake Simulator

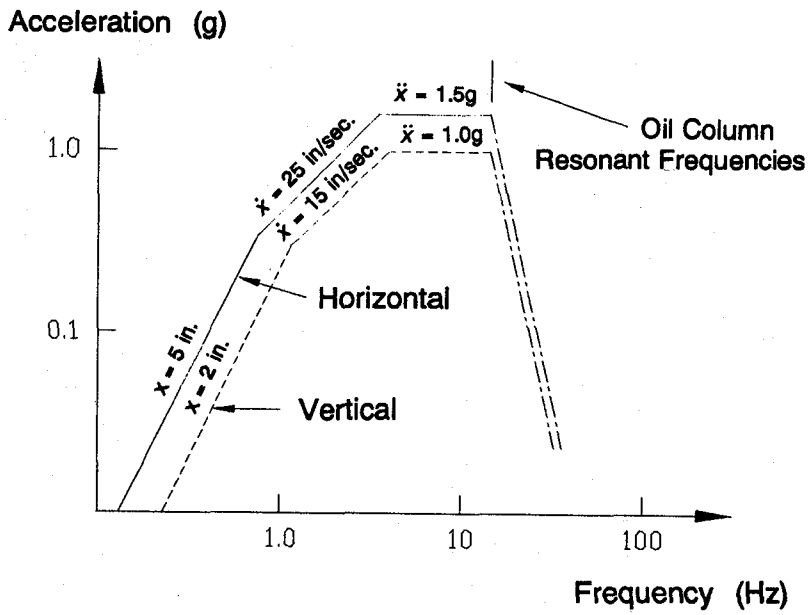

Fig. B.2 Earthquake Simulator Performance Curves (table empty)

APPENDIX C

Formulation of Energy Equation

SDOF System

The absolute energy equation for a single-degree-of-freedom system is derived from the equation of motion

$$m\ddot{v}_t + f_D + f_S = 0 \tag{C.1}$$

where m = mass
f_D = damping force
f_S = restoring force

For a linear elastic system $f_S = kv$, where k is the spring constant.

v_t = absolute displacement of m
$= v + v_g$
v_g = base displacement
v = displacement of m relative to base

Integrating Eq. C.1 with respect to v from the time of the start of the motion gives

$$\int m\ddot{v}_t dv + \int f_D dv + \int f_S dv = 0 \tag{C.2}$$

If we put $v = v_t - v_g$ in the first term of Eq. C.2, then this term can be expressed as

$$\int m\ddot{v}_t dv = \int m\ddot{v}_t (dv_t - dv_g) = \int m\ddot{v}_t dv_t - \int m\ddot{v}_t dv_g \tag{C.3}$$

Further, the first term of Eq. C.3 can be written as

$$\int m\ddot{v}_t dv_t = \int m\frac{d\dot{v}_t}{dt} dv_t = \int m\dot{v}_t d\dot{v}_t = \frac{m\dot{v}_t^2}{2} \tag{C.4}$$

Substituting the result of Eq. C.4 and the second term of Eq. C.3 back into Eq. C.2 leads to the "absolute" energy equation

$$\frac{m\dot{v}_t^2}{2} + \int f_D dv + \int f_S dv = \int m\ddot{v}_t dv_g \tag{C.5}$$

The first term of Eq. C.5 is the "absolute" kinetic energy of the system, so-called because it is formulated in terms of the *absolute* velocity, $\dot{v}_t$. The second term is the viscous-damped energy, E_ξ. The third term is the absorbed energy, E_A, and the right-hand side of Eq. C.5 is the energy input to the system, E_I. E_I is called the "absolute" input energy, because it is formulated in terms of the *absolute* acceleration, $\ddot{v}_t$. The term $m\ddot{v}_t$ represents the inertia force applied to the structure, which by Eq. C.1 is equal to the restoring force plus the damping force. This is the total force applied to the base of the structure. Thus, E_I is the work done by the total base shear through the base displacement. This is discussed further by Uang in [57] where a parallel development of the "relative" energy equation is also presented.

Using these definitions, Eq. C.5 can be rewritten in the form

$$E_I = E_K + E_\xi + E_A \tag{C.6}$$

The absorbed energy, E_A, has two components. These are the stored (recoverable) elastic strain energy, E_S, and the dissipated (irrecoverable) energy, E_D. Putting $E_A = E_S + E_D$ into Eq. C.6 gives

$$E_I = E_K + E_\xi + E_S + E_D$$

or, upon rearranging

$$E_I = E_K + E_S + E_\xi + E_D \tag{C.7}$$

where E_I = absolute input energy
E_K = absolute kinetic energy
E_S = recoverable elastic strain energy
E_ξ = viscous-damped energy
E_D = irrecoverable dissipated energy

Several points can be noted about Eq. C.7. If the terms are integrated over the entire duration of the earthquake and until the building comes to rest, then E_K and E_S are zero. In

this case, the total E_I is equated by the internal energy dissipation (damping) of the system, E_ξ and E_H. Evaluation of Eq. C.7 up to some time t (less than the earthquake duration) will yield positive values for the E_K and E_S terms, and in this case the net energy dissipation demand on the system is typically less than E_I.

MDOF System

The equivalent absolute energy equation for an MDOF system is developed below. The equation of motion for a typical n story building is

$$\underline{f}_I + \underline{f}_D + \underline{f}_S = 0$$

or

$$\underline{m}\ddot{\underline{v}}_t + \underline{f}_D + \underline{f}_S = 0 \qquad \text{(C.8)}$$

for n lateral degrees of freedom. The terms in Eq. C.8 are

$\underline{f}_I$ = inertial force vector
$\underline{f}_D$ = damping force vector
$\underline{f}_S$ = restoring force vector
$\underline{m}$ = mass matrix (diagonal)

The inertial force term is formulated using the absolute lateral displacement vector, $\underline{v}_t$, where

$\underline{v}_t = \underline{v} + \underline{r}v_g$
$\underline{v}$ = relative displacement vector
v_g = ground displacement
$\underline{r}$ = unity column vector ($n \times 1$)

Eq. C.8 applies equally for linear or nonlinear behavior. The development proceeds as for the SDOF case. Transpose Eq. C.8 and integrate with respect to $\underline{v}$ to get

$$\int \ddot{\underline{v}}_t^T \underline{m} d\underline{v} + \int \underline{f}_D^T d\underline{v} + \int \underline{f}_S^T d\underline{v} = 0 \qquad \text{(C.9)}$$

If we put $\underline{v} = \underline{v}_t - \underline{r}v_g$ then the first term of Eq. C.9 can be expressed as

$$\int \ddot{\underline{v}}_t^T \underline{m} d\underline{v} = \int \ddot{\underline{v}}_t^T \underline{m} (d\underline{v}_t - \underline{r} dv_g) = \int \frac{d\dot{\underline{v}}_t^T}{dt} \underline{m} d\underline{v}_t - \int \ddot{\underline{v}}_t \underline{m} \underline{r} dv_g$$

$$= \int d\dot{\underline{v}}_t^T \underline{m}\dot{\underline{v}}_t - \int \ddot{\underline{v}}_t^T \underline{m}\underline{r} dv_g$$

$$= \int \sum_{i=1}^{n} m_i \dot{v}_{t_i} \, d\dot{v}_{t_i} - \int \left(\sum_{i=1}^{n} m_i \ddot{v}_{t_i} \right) dv_g$$

$$= \frac{1}{2} \sum_{i=1}^{n} m_i (\ddot{v}_{t_i})^2 - \int \left(\sum_{i=1}^{n} m_i \ddot{v}_{t_i} \right) dv_g$$

$$= \frac{1}{2} \dot{\underline{v}}_t^T \underline{m}\dot{\underline{v}}_t - \int \left(\sum_{i=1}^{n} m_i \ddot{v}_{t_i} \right) dv_g \qquad \text{(C.10)}$$

Substituting the final form of Eq. C.10 into Eq. C.9 gives the ''absolute'' energy equation

$$\frac{1}{2} \dot{\underline{v}}_t^T \underline{m}\dot{\underline{v}}_t + \int \underline{f}_D^T d\underline{v} + \int \underline{f}_S^T d\underline{v} = \int \left(\sum_{i=1}^{n} m_i \ddot{v}_{t_i} \right) dv_g \qquad \text{(C.11)}$$

The first term in Eq. C.11 is the ''absolute'' kinetic energy of the MDOF system, so-called because it is formulated in terms of the *absolute* velocities, $\dot{\underline{v}}_t$. The second term is the damped energy, E_ξ, dissipated by internal structural damping mechanisms. This is usually described analytically as viscous-damped energy, but in reality the physical nature of this energy dissipation mechanism is rarely, if ever, viscous. The third term is the energy absorbed by the restoring forces, E_A, and the right-hand side of Eq. C.11 is the input energy, E_I. E_I is called the absolute input energy, because it is formulated in terms of the *absolute* accelerations, $\ddot{\underline{v}}_t$.

The energy equation C.11 can be re-written in the form

$$E_I = E_K + E_\xi + E_A \qquad \text{(C.6)}$$

as presented for the SDOF system. Putting $E_A = E_S + E_D$ gives the result of Eq. C.7

$$E_I = E_K + E_S + E_\xi + E_D \qquad \text{(C.7)}$$

where the terms are as described previously.

EARTHQUAKE ENGINEERING RESEARCH CENTER REPORT SERIES

EERC reports are available from the National Information Service for Earthquake Engineering(NISEE) and from the National Technical Information Service(NTIS). Numbers in parentheses are Accession Numbers assigned by the National Technical Information Service; these are followed by a price code. Contact NTIS, 5285 Port Royal Road, Springfield Virginia, 22161 for more information. Reports without Accession Numbers were not available from NTIS at the time of printing. For a current complete list of EERC reports (from EERC 67-1) and availablity information, please contact University of California, EERC, NISEE, 1301 South 46th Street, Richmond, California 94804.

UCB/EERC-81/01 "Control of Seismic Response of Piping Systems and Other Structures by Base Isolation," by Kelly, J.M., January 1981, (PB81 200 735)A05.

UCB/EERC-81/02 "OPTNSR- An Interactive Software System for Optimal Design of Statically and Dynamically Loaded Structures with Nonlinear Response," by Bhatti, M.A., Ciampi, V. and Pister, K.S., January 1981, (PB81 218 851)A09.

UCB/EERC-81/03 "Analysis of Local Variations in Free Field Seismic Ground Motions," by Chen, J.-C., Lysmer, J. and Seed, H.B., January 1981, (AD-A099508)A13.

UCB/EERC-81/04 "Inelastic Structural Modeling of Braced Offshore Platforms for Seismic Loading," by Zayas, V.A., Shing, P.-S.B., Mahin, S.A. and Popov, E.P., January 1981, INEL4, (PB82 138 777)A07.

UCB/EERC-81/05 "Dynamic Response of Light Equipment in Structures," by Der Kiureghian, A., Sackman, J.L. and Nour-Omid, B., April 1981, (PB81 218 497)A04.

UCB/EERC-81/06 "Preliminary Experimental Investigation of a Broad Base Liquid Storage Tank," by Bouwkamp, J.G., Kollegger, J.P. and Stephen, R.M., May 1981, (PB82 140 385)A03.

UCB/EERC-81/07 "The Seismic Resistant Design of Reinforced Concrete Coupled Structural Walls," by Aktan, A.E. and Bertero, V.V., June 1981, (PB82 113 358)A11.

UCB/EERC-81/08 "Unassigned," by Unassigned, 1981.

UCB/EERC-81/09 "Experimental Behavior of a Spatial Piping System with Steel Energy Absorbers Subjected to a Simulated Differential Seismic Input," by Stiemer, S.F., Godden, W.G. and Kelly, J.M., July 1981, (PB82 201 898)A04.

UCB/EERC-81/10 "Evaluation of Seismic Design Provisions for Masonry in the United States," by Sveinsson, B.I., Mayes, R.L. and McNiven, H.D., August 1981, (PB82 166 075)A08.

UCB/EERC-81/11 "Two-Dimensional Hybrid Modelling of Soil-Structure Interaction," by Tzong, T.-J., Gupta, S. and Penzien, J., August 1981, (PB82 142 118)A04.

UCB/EERC-81/12 "Studies on Effects of Infills in Seismic Resistant R/C Construction," by Brokken, S. and Bertero, V.V., October 1981, (PB82 166 190)A09.

UCB/EERC-81/13 "Linear Models to Predict the Nonlinear Seismic Behavior of a One-Story Steel Frame," by Valdimarsson, H., Shah, A.H. and McNiven, H.D., September 1981, (PB82 138 793)A07.

UCB/EERC-81/14 "TLUSH: A Computer Program for the Three-Dimensional Dynamic Analysis of Earth Dams," by Kagawa, T., Mejia, L.H., Seed, H.B. and Lysmer, J., September 1981, (PB82 139 940)A06.

UCB/EERC-81/15 "Three Dimensional Dynamic Response Analysis of Earth Dams," by Mejia, L.H. and Seed, H.B., September 1981, (PB82 137 274)A12.

UCB/EERC-81/16 "Experimental Study of Lead and Elastomeric Dampers for Base Isolation Systems," by Kelly, J.M. and Hodder, S.B., October 1981, (PB82 166 182)A05.

UCB/EERC-81/17 "The Influence of Base Isolation on the Seismic Response of Light Secondary Equipment," by Kelly, J.M., April 1981, (PB82 255 266)A04.

UCB/EERC-81/18 "Studies on Evaluation of Shaking Table Response Analysis Procedures." by Blondet, J. M., November 1981, (PB82 197 278)A10.

UCB/EERC-81/19 "DELIGHT.STRUCT: A Computer-Aided Design Environment for Structural Engineering," by Balling, R.J., Pister, K.S. and Polak, E., December 1981, (PB82 218 496)A07.

UCB/EERC-81/20 "Optimal Design of Seismic-Resistant Planar Steel Frames," by Balling. R.J., Ciampi, V. and Pister, K.S., December 1981, (PB82 220 179)A07.

UCB/EERC-82/01 "Dynamic Behavior of Ground for Seismic Analysis of Lifeline Systems." by Sato, T. and Der Kiureghian, A., January 1982, (PB82 218 926)A05.

UCB/EERC-82/02 "Shaking Table Tests of a Tubular Steel Frame Model," by Ghanaat, Y. and Clough, R.W., January 1982, (PB82 220 161)A07.

UCB/EERC-82/03 "Behavior of a Piping System under Seismic Excitation: Experimental Investigations of a Spatial Piping System supported by Mechanical Shock Arrestors," by Schneider, S., Lee, H.-M. and Godden, W. G., May 1982, (PB83 172 544)A09.

UCB/EERC-82/04 "New Approaches for the Dynamic Analysis of Large Structural Systems." by Wilson, E.L., June 1982, (PB83 148 080)A05.

UCB/EERC-82/05 "Model Study of Effects of Damage on the Vibration Properties of Steel Offshore Platforms," by Shahrivar, F. and Bouwkamp, J.G., June 1982, (PB83 148 742)A10.

UCB/EERC-82/06 "States of the Art and Pratice in the Optimum Seismic Design and Analytical Response Prediction of R/C Frame Wall Structures," by Aktan, A.E. and Bertero, V.V., July 1982, (PB83 147 736)A05.

UCB/EERC-82/07 "Further Study of the Earthquake Response of a Broad Cylindrical Liquid-Storage Tank Model," by Manos, G.C. and Clough, R.W., July 1982, (PB83 147 744)A11.

UCB/EERC-82/08 "An Evaluation of the Design and Analytical Seismic Response of a Seven Story Reinforced Concrete Frame," by Charney, F.A. and Bertero, V.V., July 1982, (PB83 157 628)A09.

UCB/EERC-82/09 "Fluid-Structure Interactions: Added Mass Computations for Incompressible Fluid," by Kuo, J.S.-H., August 1982, (PB83 156 281)A07.

UCB/EERC-82/10 "Joint-Opening Nonlinear Mechanism: Interface Smeared Crack Model." by Kuo, J.S.-H., August 1982, (PB83 149 195)A05.

UCB/EERC-82/11 "Dynamic Response Analysis of Techi Dam," by Clough, R.W., Stephen, R.M. and Kuo, J.S.-H., August 1982, (PB83 147 496)A06.

UCB/EERC-82/12 "Prediction of the Seismic Response of R/C Frame-Coupled Wall Structures," by Aktan, A.E., Bertero, V.V. and Piazzo, M., August 1982, (PB83 149 203)A09.

UCB/EERC-82/13 "Preliminary Report on the Smart 1 Strong Motion Array in Taiwan," by Bolt, B.A., Loh, C.H., Penzien, J. and Tsai, Y.B., August 1982, (PB83 159 400)A10.

UCB/EERC-82/14 "Seismic Behavior of an Eccentrically X-Braced Steel Structure," by Yang, M.S., September 1982, (PB83 260 778)A12.

UCB/EERC-82/15 "The Performance of Stairways in Earthquakes," by Roha, C., Axley, J.W. and Bertero, V.V., September 1982, (PB83 157 693)A07.

UCB/EERC-82/16 "The Behavior of Submerged Multiple Bodies in Earthquakes," by Liao, W.-G., September 1982, (PB83 158 709)A07.

UCB/EERC-82/17 "Effects of Concrete Types and Loading Conditions on Local Bond-Slip Relationships," by Cowell, A.D., Popov, E.P. and Bertero, V.V., September 1982, (PB83 153 577)A04.

UCB/EERC-82/18 "Mechanical Behavior of Shear Wall Vertical Boundary Members: An Experimental Investigation," by Wagner, M.T. and Bertero, V.V., October 1982, (PB83 159 764)A05.

UCB/EERC-82/19 "Experimental Studies of Multi-support Seismic Loading on Piping Systems," by Kelly, J.M. and Cowell, A.D., November 1982, (PB90 262 684)A07.

UCB/EERC-82/20 "Generalized Plastic Hinge Concepts for 3D Beam-Column Elements," by Chen, P. F.-S. and Powell, G.H., November 1982, (PB83 247 981)A13.

UCB/EERC-82/21 "ANSR-II: General Computer Program for Nonlinear Structural Analysis," by Oughourlian, C.V. and Powell, G.H., November 1982, (PB83 251 330)A12.

UCB/EERC-82/22 "Solution Strategies for Statically Loaded Nonlinear Structures," by Simons, J.W. and Powell, G.H., November 1982, (PB83 197 970)A06.

UCB/EERC-82/23 "Analytical Model of Deformed Bar Anchorages under Generalized Excitations," by Ciampi, V., Eligehausen, R., Bertero, V.V. and Popov, E.P., November 1982, (PB83 169 532)A06.

UCB/EERC-82/24 "A Mathematical Model for the Response of Masonry Walls to Dynamic Excitations," by Sucuoglu, H., Mengi, Y. and McNiven, H.D., November 1982, (PB83 169 011)A07.

UCB/EERC-82/25 "Earthquake Response Considerations of Broad Liquid Storage Tanks," by Cambra, F.J., November 1982, (PB83 251 215)A09.

UCB/EERC-82/26 "Computational Models for Cyclic Plasticity, Rate Dependence and Creep," by Mosaddad, B. and Powell, G.H., November 1982, (PB83 245 829)A08.

UCB/EERC-82/27 "Inelastic Analysis of Piping and Tubular Structures," by Mahasuverachai, M. and Powell, G.H., November 1982, (PB83 249 987)A07.

UCB/EERC-83/01 "The Economic Feasibility of Seismic Rehabilitation of Buildings by Base Isolation," by Kelly, J.M., January 1983, (PB83 197 988)A05.

UCB/EERC-83/02 "Seismic Moment Connections for Moment-Resisting Steel Frames.," by Popov, E.P., January 1983, (PB83 195 412)A04.

UCB/EERC-83/03 "Design of Links and Beam-to-Column Connections for Eccentrically Braced Steel Frames," by Popov, E.P. and Malley, J.O., January 1983, (PB83 194 811)A04.

UCB/EERC-83/04 "Numerical Techniques for the Evaluation of Soil-Structure Interaction Effects in the Time Domain," by Bayo, E. and Wilson, E.L., February 1983, (PB83 245 605)A09.

UCB/EERC-83/05 "A Transducer for Measuring the Internal Forces in the Columns of a Frame-Wall Reinforced Concrete Structure," by Sause, R. and Bertero, V.V., May 1983, (PB84 119 494)A06.

UCB/EERC-83/06 "Dynamic Interactions Between Floating Ice and Offshore Structures," by Croteau, P., May 1983, (PB84 119 486)A16.

UCB/EERC-83/07 "Dynamic Analysis of Multiply Tuned and Arbitrarily Supported Secondary Systems," by Igusa, T. and Der Kiureghian, A., July 1983, (PB84 118 272)A11.

UCB/EERC-83/08 "A Laboratory Study of Submerged Multi-body Systems in Earthquakes," by Ansari, G.R., June 1983, (PB83 261 842)A17.

UCB/EERC-83/09 "Effects of Transient Foundation Uplift on Earthquake Response of Structures," by Yim, C.-S. and Chopra, A.K., June 1983, (PB83 261 396)A07.

UCB/EERC-83/10 "Optimal Design of Friction-Braced Frames under Seismic Loading," by Austin, M.A. and Pister, K.S., June 1983, (PB84 119 288)A06.

UCB/EERC-83/11 "Shaking Table Study of Single-Story Masonry Houses: Dynamic Performance under Three Component Seismic Input and Recommendations," by Manos, G.C., Clough, R.W. and Mayes, R.L., July 1983, (UCB/EERC-83/11)A08.

UCB/EERC-83/12 "Experimental Error Propagation in Pseudodynamic Testing," by Shiing, P.B. and Mahin, S.A., June 1983, (PB84 119 270)A09.

UCB/EERC-83/13 "Experimental and Analytical Predictions of the Mechanical Characteristics of a 1/5-scale Model of a 7-story R/C Frame-Wall Building Structure," by Aktan, A.E., Bertero, V.V., Chowdhury, A.A. and Nagashima, T., June 1983, (PB84 119 213)A07.

UCB/EERC-83/14 "Shaking Table Tests of Large-Panel Precast Concrete Building System Assemblages," by Oliva, M.G. and Clough, R.W., June 1983, (PB86 110 210/AS)A11.

UCB/EERC-83/15 "Seismic Behavior of Active Beam Links in Eccentrically Braced Frames," by Hjelmstad, K.D. and Popov, E.P., July 1983, (PB84 119 676)A09.

UCB/EERC-83/16 "System Identification of Structures with Joint Rotation," by Dimsdale, J.S., July 1983, (PB84 192 210)A06.

UCB/EERC-83/17 "Construction of Inelastic Response Spectra for Single-Degree-of-Freedom Systems," by Mahin, S. and Lin, J., June 1983, (PB84 208 834)A05.

UCB/EERC-83/18 "Interactive Computer Analysis Methods for Predicting the Inelastic Cyclic Behaviour of Structural Sections," by Kaba, S. and Mahin, S., July 1983, (PB84 192 012)A06.

UCB/EERC-83/19 "Effects of Bond Deterioration on Hysteretic Behavior of Reinforced Concrete Joints," by Filippou, F.C., Popov, E.P. and Bertero, V.V., August 1983, (PB84 192 020)A10.

UCB/EERC-83/20 "Correlation of Analytical and Experimental Responses of Large-Panel Precast Building Systems," by Oliva, M.G., Clough, R.W., Velkov, M. and Gavrilovic, P., May 1988, (PB90 262 692)A06.

UCB/EERC-83/21 "Mechanical Characteristics of Materials Used in a 1/5 Scale Model of a 7-Story Reinforced Concrete Test Structure," by Bertero, V.V., Aktan, A.E., Harris, H.G. and Chowdhury, A.A., October 1983, (PB84 193 697)A05.

UCB/EERC-83/22 "Hybrid Modelling of Soil-Structure Interaction in Layered Media," by Tzong, T.-J. and Penzien, J., October 1983, (PB84 192 178)A08.

UCB/EERC-83/23 "Local Bond Stress-Slip Relationships of Deformed Bars under Generalized Excitations," by Eligehausen, R., Popov, E.P. and Bertero, V.V., October 1983, (PB84 192 848)A09.

UCB/EERC-83/24 "Design Considerations for Shear Links in Eccentrically Braced Frames," by Malley, J.O. and Popov, E.P., November 1983, (PB84 192 186)A07.

UCB/EERC-84/01 "Pseudodynamic Test Method for Seismic Performance Evaluation: Theory and Implementation," by Shing, P.-S.B. and Mahin, S.A., January 1984, (PB84 190 644)A08.

UCB/EERC-84/02 "Dynamic Response Behavior of Kiang Hong Dian Dam," by Clough, R.W., Chang, K.-T., Chen, H.-Q. and Stephen, R.M., April 1984, (PB84 209 402)A08.

UCB/EERC-84/03 "Refined Modelling of Reinforced Concrete Columns for Seismic Analysis," by Kaba, S.A. and Mahin, S.A., April 1984, (PB84 234 384)A06.

UCB/EERC-84/04 "A New Floor Response Spectrum Method for Seismic Analysis of Multiply Supported Secondary Systems," by Asfura, A. and Der Kiureghian, A., June 1984, (PB84 239 417)A06.

UCB/EERC-84/05 "Earthquake Simulation Tests and Associated Studies of a 1/5th-scale Model of a 7-Story R/C Frame-Wall Test Structure," by Bertero, V.V., Aktan, A.E., Charney, F.A. and Sause, R., June 1984, (PB84 239 409)A09.

UCB/EERC-84/06 "R/C Structural Walls: Seismic Design for Shear," by Aktan, A.E. and Bertero, V.V., 1984.

UCB/EERC-84/07 "Behavior of Interior and Exterior Flat-Plate Connections subjected to Inelastic Load Reversals," by Zee, H.L. and Moehle, J.P., August 1984, (PB86 117 629/AS)A07.

UCB/EERC-84/08 "Experimental Study of the Seismic Behavior of a Two-Story Flat-Plate Structure," by Moehle, J.P. and Diebold, J.W., August 1984, (PB86 122 553/AS)A12.

UCB/EERC-84/09 "Phenomenological Modeling of Steel Braces under Cyclic Loading," by Ikeda, K., Mahin, S.A. and Dermitzakis, S.N., May 1984, (PB86 132 198/AS)A08.

UCB/EERC-84/10 "Earthquake Analysis and Response of Concrete Gravity Dams," by Fenves, G. and Chopra, A.K., August 1984, (PB85 193 902/AS)A11.

UCB/EERC-84/11 "EAGD-84: A Computer Program for Earthquake Analysis of Concrete Gravity Dams," by Fenves, G. and Chopra, A.K., August 1984, (PB85 193 613/AS)A05.

UCB/EERC-84/12 "A Refined Physical Theory Model for Predicting the Seismic Behavior of Braced Steel Frames," by Ikeda, K. and Mahin, S.A., July 1984, (PB85 191 450/AS)A09.

UCB/EERC-84/13 "Earthquake Engineering Research at Berkeley - 1984," by , August 1984, (PB85 197 341/AS)A10.

UCB/EERC-84/14 "Moduli and Damping Factors for Dynamic Analyses of Cohesionless Soils," by Seed, H.B., Wong, R.T., Idriss, I.M. and Tokimatsu, K., September 1984, (PB85 191 468/AS)A04.

UCB/EERC-84/15 "The Influence of SPT Procedures in Soil Liquefaction Resistance Evaluations," by Seed, H.B., Tokimatsu, K., Harder, L.F. and Chung, R.M., October 1984, (PB85 191 732/AS)A04.

UCB/EERC-84/16 "Simplified Procedures for the Evaluation of Settlements in Sands Due to Earthquake Shaking," by Tokimatsu, K. and Seed, H.B., October 1984, (PB85 197 887/AS)A03.

UCB/EERC-84/17 "Evaluation of Energy Absorption Characteristics of Highway Bridges Under Seismic Conditions - Volume I (PB90 262 627)A16 and Volume II (Appendices) (PB90 262 635)A13," by Imbsen, R.A. and Penzien, J., September 1986.

UCB/EERC-84/18 "Structure-Foundation Interactions under Dynamic Loads," by Liu, W.D. and Penzien, J., November 1984, (PB87 124 889/AS)A11.

UCB/EERC-84/19 "Seismic Modelling of Deep Foundations," by Chen, C.-H. and Penzien, J., November 1984, (PB87 124 798/AS)A07.

UCB/EERC-84/20 "Dynamic Response Behavior of Quan Shui Dam," by Clough, R.W., Chang, K.-T., Chen, H.-Q., Stephen, R.M., Ghanaat, Y. and Qi, J.-H., November 1984, (PB86 115177/AS)A07.

UCB/EERC-85/01 "Simplified Methods of Analysis for Earthquake Resistant Design of Buildings," by Cruz, E.F. and Chopra, A.K., February 1985, (PB86 112299/AS)A12.

UCB/EERC-85/02 "Estimation of Seismic Wave Coherency and Rupture Velocity using the SMART 1 Strong-Motion Array Recordings," by Abrahamson, N.A., March 1985, (PB86 214 343)A07.

UCB/EERC-85/03 "Dynamic Properties of a Thirty Story Condominium Tower Building," by Stephen, R.M., Wilson, E.L. and Stander, N., April 1985, (PB86 118965/AS)A06.

UCB/EERC-85/04 "Development of Substructuring Techniques for On-Line Computer Controlled Seismic Performance Testing," by Dermitzakis, S. and Mahin, S., February 1985, (PB86 132941/AS)A08.

UCB/EERC-85/05 "A Simple Model for Reinforcing Bar Anchorages under Cyclic Excitations," by Filippou, F.C., March 1985, (PB86 112 919/AS)A05.

UCB/EERC-85/06 "Racking Behavior of Wood-framed Gypsum Panels under Dynamic Load," by Oliva, M.G., June 1985, (PB90 262 643)A04.

UCB/EERC-85/07 "Earthquake Analysis and Response of Concrete Arch Dams," by Fok, K.-L. and Chopra, A.K., June 1985, (PB86 139672/AS)A10.

UCB/EERC-85/08 "Effect of Inelastic Behavior on the Analysis and Design of Earthquake Resistant Structures," by Lin, J.P. and Mahin, S.A., June 1985, (PB86 135340/AS)A08.

UCB/EERC-85/09 "Earthquake Simulator Testing of a Base-Isolated Bridge Deck," by Kelly, J.M., Buckle, I.G. and Tsai, H.-C., January 1986, (PB87 124 152/AS)A06.

UCB/EERC-85/10 "Simplified Analysis for Earthquake Resistant Design of Concrete Gravity Dams," by Fenves, G. and Chopra, A.K., June 1986, (PB87 124 160/AS)A08.

UCB/EERC-85/11 "Dynamic Interaction Effects in Arch Dams," by Clough, R.W., Chang, K.-T., Chen, H.-Q. and Ghanaat, Y., October 1985, (PB86 135027/AS)A05.

UCB/EERC-85/12 "Dynamic Response of Long Valley Dam in the Mammoth Lake Earthquake Series of May 25-27, 1980," by Lai, S. and Seed, H.B., November 1985, (PB86 142304/AS)A05.

UCB/EERC-85/13 "A Methodology for Computer-Aided Design of Earthquake-Resistant Steel Structures," by Austin, M.A., Pister, K.S. and Mahin, S.A., December 1985, (PB86 159480/AS)A10 .

UCB/EERC-85/14 "Response of Tension-Leg Platforms to Vertical Seismic Excitations," by Liou, G.-S., Penzien, J. and Yeung, R.W., December 1985, (PB87 124 871/AS)A08.

UCB/EERC-85/15 "Cyclic Loading Tests of Masonry Single Piers: Volume 4 - Additional Tests with Height to Width Ratio of 1," by Sveinsson, B., McNiven, H.D. and Sucuoglu, H., December 1985.

UCB/EERC-85/16 "An Experimental Program for Studying the Dynamic Response of a Steel Frame with a Variety of Infill Partitions," by Yanev, B. and McNiven, H.D., December 1985, (PB90 262 676)A05.

UCB/EERC-86/01 "A Study of Seismically Resistant Eccentrically Braced Steel Frame Systems," by Kasai, K. and Popov, E.P., January 1986, (PB87 124 178/AS)A14.

UCB/EERC-86/02 "Design Problems in Soil Liquefaction," by Seed, H.B., February 1986, (PB87 124 186/AS)A03.

UCB/EERC-86/03 "Implications of Recent Earthquakes and Research on Earthquake-Resistant Design and Construction of Buildings," by Bertero, V.V., March 1986, (PB87 124 194/AS)A05.

UCB/EERC-86/04 "The Use of Load Dependent Vectors for Dynamic and Earthquake Analyses," by Leger, P., Wilson, E.L. and Clough, R.W., March 1986, (PB87 124 202/AS)A12.

UCB/EERC-86/05 "Two Beam-To-Column Web Connections," by Tsai, K.-C. and Popov, E.P., April 1986, (PB87 124 301/AS)A04.

UCB/EERC-86/06 "Determination of Penetration Resistance for Coarse-Grained Soils using the Becker Hammer Drill," by Harder, L.F. and Seed, H.B., May 1986, (PB87 124 210/AS)A07.

UCB/EERC-86/07 "A Mathematical Model for Predicting the Nonlinear Response of Unreinforced Masonry Walls to In-Plane Earthquake Excitations," by Mengi, Y. and McNiven, H.D., May 1986, (PB87 124 780/AS)A06.

UCB/EERC-86/08 "The 19 September 1985 Mexico Earthquake: Building Behavior," by Bertero, V.V., July 1986.

UCB/EERC-86/09 "EACD-3D: A Computer Program for Three-Dimensional Earthquake Analysis of Concrete Dams," by Fok, K.-L., Hall, J.F. and Chopra, A.K., July 1986, (PB87 124 228/AS)A08.

UCB/EERC-86/10 "Earthquake Simulation Tests and Associated Studies of a 0.3-Scale Model of a Six-Story Concentrically Braced Steel Structure," by Uang, C.-M. and Bertero, V.V., December 1986, (PB87 163 564/AS)A17.

UCB/EERC-86/11 "Mechanical Characteristics of Base Isolation Bearings for a Bridge Deck Model Test," by Kelly, J.M., Buckle, I.G. and Koh, C.-G., November 1987, (PB90 262 668)A04.

UCB/EERC-86/12 "Effects of Axial Load on Elastomeric Isolation Bearings," by Koh, C.-G. and Kelly, J.M., November 1987.

UCB/EERC-87/01 "The FPS Earthquake Resisting System: Experimental Report," by Zayas, V.A., Low, S.S. and Mahin, S.A., June 1987.

UCB/EERC-87/02 "Earthquake Simulator Tests and Associated Studies of a 0.3-Scale Model of a Six-Story Eccentrically Braced Steel Structure," by Whittaker, A., Uang, C.-M. and Bertero, V.V., July 1987.

UCB/EERC-87/03 "A Displacement Control and Uplift Restraint Device for Base-Isolated Structures," by Kelly, J.M., Griffith, M.C. and Aiken, I.D., April 1987.

UCB/EERC-87/04 "Earthquake Simulator Testing of a Combined Sliding Bearing and Rubber Bearing Isolation System," by Kelly, J.M. and Chalhoub, M.S., 1987.

UCB/EERC-87/05 "Three-Dimensional Inelastic Analysis of Reinforced Concrete Frame-Wall Structures," by Moazzami, S. and Bertero, V.V., May 1987.

UCB/EERC-87/06 "Experiments on Eccentrically Braced Frames with Composite Floors," by Ricles, J. and Popov, E., June 1987.

UCB/EERC-87/07 "Dynamic Analysis of Seismically Resistant Eccentrically Braced Frames," by Ricles, J. and Popov, E., June 1987.

UCB/EERC-87/08 "Undrained Cyclic Triaxial Testing of Gravels-The Effect of Membrane Compliance," by Evans, M.D. and Seed, H.B., July 1987.

UCB/EERC-87/09 "Hybrid Solution Techniques for Generalized Pseudo-Dynamic Testing," by Thewalt, C. and Mahin, S.A., July 1987.

UCB/EERC-87/10 "Ultimate Behavior of Butt Welded Splices in Heavy Rolled Steel Sections," by Bruneau, M., Mahin, S.A. and Popov, E.P., September 1987.

UCB/EERC-87/11 "Residual Strength of Sand from Dam Failures in the Chilean Earthquake of March 3, 1985," by De Alba, P., Seed, H.B., Retamal, E. and Seed, R.B., September 1987.

UCB/EERC-87/12 "Inelastic Seismic Response of Structures with Mass or Stiffness Eccentricities in Plan," by Bruneau, M. and Mahin, S.A., September 1987, (PB90 262 650)A14.

UCB/EERC-87/13 "CSTRUCT: An Interactive Computer Environment for the Design and Analysis of Earthquake Resistant Steel Structures," by Austin, M.A., Mahin, S.A. and Pister, K.S., September 1987.

UCB/EERC-87/14 "Experimental Study of Reinforced Concrete Columns Subjected to Multi-Axial Loading," by Low, S.S. and Moehle, J.P., September 1987.

UCB/EERC-87/15 "Relationships between Soil Conditions and Earthquake Ground Motions in Mexico City in the Earthquake of Sept. 19, 1985," by Seed, H.B., Romo, M.P., Sun, J., Jaime, A. and Lysmer, J., October 1987.

UCB/EERC-87/16 "Experimental Study of Seismic Response of R. C. Setback Buildings," by Shahrooz, B.M. and Moehle, J.P., October 1987.

UCB/EERC-87/17 "The Effect of Slabs on the Flexural Behavior of Beams," by Pantazopoulou, S.J. and Moehle, J.P., October 1987, (PB90 262 700)A07.

UCB/EERC-87/18 "Design Procedure for R-FBI Bearings," by Mostaghel, N. and Kelly, J.M., November 1987, (PB90 262 718)A04.

UCB/EERC-87/19 "Analytical Models for Predicting the Lateral Response of R C Shear Walls: Evaluation of their Reliability," by Vulcano, A. and Bertero, V.V., November 1987.

UCB/EERC-87/20 "Earthquake Response of Torsionally-Coupled Buildings," by Hejal, R. and Chopra, A.K., December 1987.

UCB/EERC-87/21 "Dynamic Reservoir Interaction with Monticello Dam," by Clough, R.W., Ghanaat, Y. and Qiu, X-F., December 1987.

UCB/EERC-87/22 "Strength Evaluation of Coarse-Grained Soils," by Siddiqi, F.H., Seed, R.B., Chan, C.K., Seed, H.B. and Pyke, R.M., December 1987.

UCB/EERC-88/01 "Seismic Behavior of Concentrically Braced Steel Frames," by Khatib, I., Mahin, S.A. and Pister, K.S., January 1988.

UCB/EERC-88/02 "Experimental Evaluation of Seismic Isolation of Medium-Rise Structures Subject to Uplift," by Griffith, M.C., Kelly, J.M., Coveney, V.A. and Koh, C.G., January 1988.

UCB/EERC-88/03 "Cyclic Behavior of Steel Double Angle Connections," by Astaneh-Asl, A. and Nader, M.N., January 1988.

UCB/EERC-88/04 "Re-evaluation of the Slide in the Lower San Fernando Dam in the Earthquake of Feb. 9, 1971," by Seed, H.B., Seed, R.B., Harder, L.F. and Jong, H.-L., April 1988.

UCB/EERC-88/05 "Experimental Evaluation of Seismic Isolation of a Nine-Story Braced Steel Frame Subject to Uplift," by Griffith, M.C., Kelly, J.M. and Aiken, I.D., May 1988.

UCB/EERC-88/06 "DRAIN-2DX User Guide.," by Allahabadi, R. and Powell, G.H., March 1988.

UCB/EERC-88/07 "Cylindrical Fluid Containers in Base-Isolated Structures," by Chalhoub, M.S. and Kelly, J.M. , April 1988.

UCB/EERC-88/08 "Analysis of Near-Source Waves: Separation of Wave Types using Strong Motion Array Recordings," by Darragh, R.B., June 1988.

UCB/EERC-88/09 "Alternatives to Standard Mode Superposition for Analysis of Non-Classically Damped Systems," by Kusainov, A.A. and Clough, R.W., June 1988.

UCB/EERC-88/10 "The Landslide at the Port of Nice on October 16, 1979," by Seed, H.B., Seed, R.B., Schlosser, F., Blondeau, F. and Juran, I., June 1988.

UCB/EERC-88/11 "Liquefaction Potential of Sand Deposits Under Low Levels of Excitation," by Carter, D.P. and Seed, H.B., August 1988.

UCB/EERC-88/12 "Nonlinear Analysis of Reinforced Concrete Frames Under Cyclic Load Reversals," by Filippou, F.C. and Issa, A., September 1988.

UCB/EERC-88/13 "Implications of Recorded Earthquake Ground Motions on Seismic Design of Building Structures," by Uang, C.-M. and Bertero, V.V., November 1988.

UCB/EERC-88/14 "An Experimental Study of the Behavior of Dual Steel Systems," by Whittaker, A.S. , Uang, C.-M. and Bertero, V.V., September 1988.

UCB/EERC-88/15 "Dynamic Moduli and Damping Ratios for Cohesive Soils," by Sun, J.I., Golesorkhi, R. and Seed, H.B., August 1988.

UCB/EERC-88/16 "Reinforced Concrete Flat Plates Under Lateral Load: An Experimental Study Including Biaxial Effects," by Pan, A. and Moehle, J., October 1988.

UCB/EERC-88/17 "Earthquake Engineering Research at Berkeley - 1988," by EERC, November 1988.

UCB/EERC-88/18 "Use of Energy as a Design Criterion in Earthquake-Resistant Design," by Uang, C.-M. and Bertero, V.V., November 1988.

UCB/EERC-88/19 "Steel Beam-Column Joints in Seismic Moment Resisting Frames," by Tsai, K.-C. and Popov, E.P., November 1988.

UCB/EERC-88/20 "Base Isolation in Japan, 1988," by Kelly, J.M., December 1988.

UCB/EERC-89/01 "Behavior of Long Links in Eccentrically Braced Frames," by Engelhardt, M.D. and Popov, E.P., January 1989.

UCB/EERC-89/02 "Earthquake Simulator Testing of Steel Plate Added Damping and Stiffness Elements," by Whittaker, A., Bertero, V.V., Alonso, J. and Thompson, C., January 1989.

UCB/EERC-89/03 "Implications of Site Effects in the Mexico City Earthquake of Sept. 19, 1985 for Earthquake-Resistant Design Criteria in the San Francisco Bay Area of California," by Seed, H.B. and Sun, J.I., March 1989.

UCB/EERC-89/04 "Earthquake Analysis and Response of Intake-Outlet Towers," by Goyal, A. and Chopra, A.K., July 1989.

UCB/EERC-89/05 "The 1985 Chile Earthquake: An Evaluation of Structural Requirements for Bearing Wall Buildings," by Wallace, J.W. and Moehle, J.P., July 1989.

UCB/EERC-89/06 "Effects of Spatial Variation of Ground Motions on Large Multiply-Supported Structures," by Hao, H., July 1989.

UCB/EERC-89/07 "EADAP - Enhanced Arch Dam Analysis Program: Users's Manual," by Ghanaat, Y. and Clough, R.W., August 1989.

UCB/EERC-89/08 "Seismic Performance of Steel Moment Frames Plastically Designed by Least Squares Stress Fields," by Ohi, K. and Mahin, S.A., August 1989.

UCB/EERC-89/09 "Feasibility and Performance Studies on Improving the Earthquake Resistance of New and Existing Buildings Using the Friction Pendulum System," by Zayas, V., Low, S., Mahin, S.A. and Bozzo, L., July 1989.

UCB/EERC-89/10 "Measurement and Elimination of Membrane Compliance Effects in Undrained Triaxial Testing," by Nicholson, P.G., Seed, R.B. and Anwar, H., September 1989.

UCB/EERC-89/11 "Static Tilt Behavior of Unanchored Cylindrical Tanks," by Lau, D.T. and Clough, R.W., September 1989.

UCB/EERC-89/12 "ADAP-88: A Computer Program for Nonlinear Earthquake Analysis of Concrete Arch Dams," by Fenves, G.L., Mojtahedi, S. and Reimer, R.B., September 1989.

UCB/EERC-89/13 "Mechanics of Low Shape Factor Elastomeric Seismic Isolation Bearings," by Aiken, I.D., Kelly, J.M. and Tajirian, F., December 1989.

UCB/EERC-89/14 "Preliminary Report on the Seismological and Engineering Aspects of the October 17, 1989 Santa Cruz (Loma Prieta) Earthquake," by EERC, October 1989.

UCB/EERC-89/15 "Experimental Studies of a Single Story Steel Structure Tested with Fixed, Semi-Rigid and Flexible Connections," by Nader, M.N. and Astaneh-Asl, A., August 1989.

UCB/EERC-89/16 "Collapse of the Cypress Street Viaduct as a Result of the Loma Prieta Earthquake," by Nims, D.K., Miranda, E., Aiken, I.D., Whittaker, A.S. and Bertero, V.V., November 1989.

UCB/EERC-90/01 "Mechanics of High-Shape Factor Elastomeric Seismic Isolation Bearings," by Kelly, J.M., Aiken, I.D. and Tajirian, F.F., March 1990.

UCB/EERC-90/02 "Javid's Paradox: The Influence of Preform on the Modes of Vibrating Beams," by Kelly, J.M., Sackman, J.L. and Javid, A., May 1990.

UCB/EERC-90/03 "Earthquake Simulator Testing and Analytical Studies of Two Energy-Absorbing Systems for Multistory Structures," by Aiken, I.D. and Kelly, J.M., October 1990.